Kanwal Majeed Farooqi
*Editor*

# Rapid Prototyping in Cardiac Disease

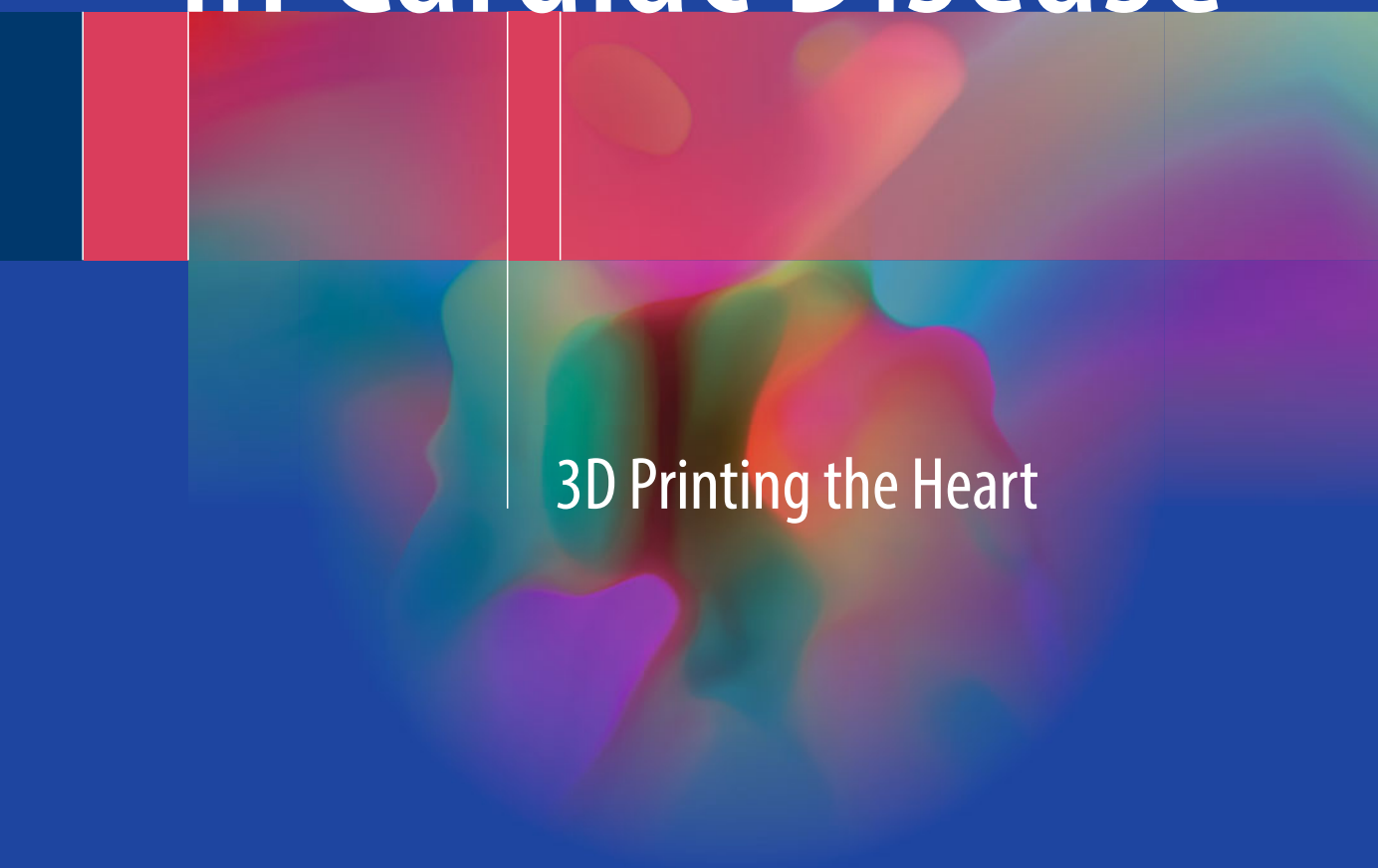

## 3D Printing the Heart

Springer

# Rapid Prototyping in Cardiac Disease

Kanwal Majeed Farooqi, MD
Editor

# Rapid Prototyping in Cardiac Disease

## 3D Printing the Heart

Springer

*Editor*
Kanwal Majeed Farooqi, MD
Assistant Professor of Pediatrics
Division of Pediatric Cardiology
Rutgers, New Jersey Medical School
Newark, NJ, USA

Adjunct Assistant Professor of Pediatrics
Division of Pediatric Cardiology
Icahn School of Medicine at Mount Sinai
New York, NY, USA

ISBN 978-3-319-53522-7 ISBN 978-3-319-53523-4 (eBook)
DOI 10.1007/978-3-319-53523-4

Library of Congress Control Number: 2017932770



Printed on acid-free paper

This Springer imprint is published by Springer Nature
The registered company is Springer International Publishing AG
The registered company address is: Gewerbestrasse 11, 6330 Cham, Switzerland

*This book is dedicated to my family.*

*My parents, Abdul Majeed Farooqi and Farkhanda Farooqi (née Siddiqui), the two most selfless people I know. Thank you for a beautiful childhood despite challenging times, unrestricted moral support and all the love we could ever ask for.*

*My darling sisters Sumble and Saadia Farooqi, who always manage to steer me right because they know of all my inner workings.*

*My husband Omar Saeed, who never misses an opportunity to praise me for an accomplishment and offers the utmost support and love.*

*And to my son, Feroz Farooqi Saeed…you have taught us to love in a whole new dimension.*

# Preface

*It ain't what you don't know that gets you into trouble. It's what you know for sure that just ain't so.*

Mark Twain

True and accurate comprehension of cardiac anatomy in a patient with complex congenital heart disease is essential for appropriate presurgical planning. Although this concept is clearly not a point of debate, the discussion of whether or not one can truly grasp a patients three-dimensional (3D) anatomy from two-dimensional (2D) imaging data may be a point of contention. The current mainstay of diagnosing congenital heart disease and eliciting the details of intracardiac spatial relationships is 2D echocardiography. The evolution of echocardiography over the last 50 years has been tremendous, progressing from M-mode, to 2D echocardiography, color Doppler imaging, and 3D echocardiography. Pediatric cardiology trainees are taught to deduce anatomic relationships in space, as did their predecessors, using sweeps of the transducer from different positions on a patient's chest. In patients with complex congenital heart disease, such as double-outlet right ventricle, the path of a potential left ventricle to aortic baffle is primarily determined based on careful examination of a sweep in the subcostal view. The theoretical path is deduced on 2D images from posterior and inferior structures to those which are anterior and superior. While these images are presented in surgical conference, the assumption is that the audience, which consists of pediatric cardiologists, not all of whom are trained in imaging, surgeons, fellows, and echocardiography technologists are all recreating the same virtual cardiac anatomy in their mind. Given the lack of true 3D representation, it is difficult to imagine that this assumption would be accurate, especially given that people vary in their ability to translate 2D data into 3D. In cases for which further anatomic data are needed, cardiac computed tomography or magnetic resonance imaging is often applied. Although these modalities certainly offer the advantage of providing clear whole-heart datasets, we are again faced with the challenge of translating 2D imaging data or 3D renderings presented on a 2D screen. The advent of 3D printing technology allows for creation of 3D physical models using the method of stacking thin layers on top of one another to create a height, width, and length. When performed in a precisely defined pattern, a complex 3D structure can be printed. Using imaging datasets that possess 3D cardiac

spatial information, a virtual cardiac model can be used to create a physical model on a 3D printer. Given the significant time commitment needed to arrive at the final product, these models do not necessarily provide vital anatomic information for all patients with congenital heart disease. Those with the most severe anatomic abnormalities benefit the most at this time.

With the application of this technology within the realm of cardiac disease growing rapidly, I am confident that this text will serve as an informative reference guide. The topics covered speak to a diverse audience including pediatric and adult cardiologists, cardiothoracic surgeons, radiologists, biomedical engineers, and imaging technologists, many of whom may play a role in the workflow of 3D printing cardiac models. The wide range of expertise of the authors who contributed to this work serves to enhance the experience of the reader, offering insights ranging from the history of 3D printing and details of different additive manufacturing techniques to its applications in specific disease states and potential for utility in printing live tissue. I am hopeful that the enthusiasm of each contributor for this technology comes across to the reader, so that it strengthens the fervor of those who support it and persuades those who remain skeptical regarding its applications and substantial presence in the future of advanced cardiac imaging.

I would like to express gratitude to all the contributors who worked so hard toward putting this text together. We are thankful to Springer, for agreeing to publish this book and all the Springer staff, especially Tracy Marton, who helped in its production. I am indebted to my numerous mentors who each had a hand in uniquely shaping my career, most of all Dr. Robert Pass who has wholeheartedly supported me from the beginning.

Kanwal Majeed Farooqi, MD
Newark, NJ, USA

# Contents

# Contributors

**Shafkat Anwar, MD** Division of Cardiology, Department of Pediatrics, Washington University in St. Louis School of Medicine, St. Louis, MO, USA

**Eleonora Avenatti, MD** Department of Cardiology, Houston Methodist DeBakey Heart and Vascular Center, Houston, TX, USA

**Peter Backeris, ME** Department of Biomedical Engineering, Icahn School of Medicine at Mount Sinai, Mount Sinai Institute of Technology, New York, NY, USA

**Joseph J. Billadello, MD** Division of Cardiovascular Medicine, Department of Internal Medicine, Washington University in St. Louis School of Medicine, St. Louis, MO, USA

**Joseph Borrello, BE** Department of Biomedical Engineering, Icahn School of Medicine at Mount Sinai, Mount Sinai Institute of Technology, Graduate School of Biomedical Sciences, New York, NY, USA

**Matthew Bramlet, MD** Advanced Imaging and Modeling, Jump Trading Simulation and Education Center, Children's Hospital of Illinois, University of Illinois College of Medicine, Peoria, IL, USA

**Anjali Chelliah, MD** Division of Pediatric Cardiology, Columbia University Medical Center, New York, NY, USA

**Yoav Dori, MD, PhD** Department of Cardiology, The Children's Hospital of Philadelphia, Philadelphia, PA, USA

**Bin Duan, PhD** Mary & Dick Holland Regenerative Medicine Program, University of Nebraska Medical Center, Omaha, NE, USA; Division of Cardiology, Department of Internal Medicine, University of Nebraska Medical Center, Omaha, NE, USA; Department of Surgery, College of Medicine, University of Nebraska Medical Center, Omaha, NE, USA

**Pirooz Eghtesady, MD, PhD** Division of Cardiothoracic Surgery, Department of Surgery, Washington University in St. Louis School of Medicine, St. Louis, MO, USA

**Kanwal Majeed Farooqi, MD** Division of Pediatric Cardiology, Rutgers New Jersey Medical School, Newark, NJ, USA; Division of Pediatric Cardiology, Icahn School of Medicine at Mount Sinai, New York, NY, USA

**Jordan M. Gosnell, BS, RDCS** Congenital Heart Center, Helen DeVos Children's Hospital of Spectrum Heath, Grand Rapids, MI, USA

**Kevin A. Gralewski, MSE** Department of Cardiology, The Children's Hospital of Philadelphia, Philadelphia, PA, USA

**Jelliffe Jeganathan, MBBS** Department of Anesthesia, Critical Care and Pain Medicine, Beth Israel Deaconess Medical Center, Harvard Medical School, Boston, MA, USA

**Ulrich P. Jorde, MD** Department of Medicine, Division of Cardiology, Montefiore Medical Center, Albert Einstein College of Medicine, New York, NY, USA

**Harikrishnan K.N. Kurup, MBBS, MD** Congenital Heart Center, Helen DeVos Children's Hospital of Spectrum Heath, Grand Rapids, MI, USA

**Mitchell Kuss, BS** Mary & Dick Holland Regenerative Medicine Program, University of Nebraska Medical Center, Omaha, NE, USA; Division of Cardiology, Department of Internal Medicine, University of Nebraska Medical Center, Omaha, NE, USA

**Carlos A. Gonzalez Lengua, MD** Department of Medicine—Cardiology, Icahn School of Medicine at Mount Sinai, Mount Sinai St. Luke and Bronx Lebanon Hospital, New York, NY, USA

**Stephen H. Little, MD, FRCPC, FACC, FASE** Department of Cardiology, Houston Methodist DeBakey Heart and Vascular Center, Houston, TX, USA

**Leo Lopez, MD** Nicklaus Children's Hospital, The Heart Program, Miami, FL, USA

**Feroze Mahmood, MD, FASE** Department of Anesthesia, Critical Care and Pain Medicine, Beth Israel Deaconess Medical Center, Harvard Medical School, Boston, MA, USA

**Meghan Coakley McCarthy, MS, PhD** Bioinformatics and Computational Biosciences Branch, Office of Cyber Infrastructure and Computational Biology, National Institute of Allergy and Infectious Diseases, National Institutes of Health, Bethesda, MD, USA

**Mario Montealegre-Gallegos, MD** Department of Anesthesia, Critical Care and Pain Medicine, Beth Israel Deaconess Medical Center, Harvard Medical School, Boston, MA, USA

**Ryan A. Moore, MD** The Heart Institute, Cincinnati Children's Hospital Medical Center, Cincinnati, OH, USA

**Juan-Carlos G. Muñiz, MD** Division of Cardiology, Nicklaus Children's Hospital, Miami, FL, USA; Department of Pediatrics, Herbert Wertheim College of Medicine, Florida International University, Miami, FL, USA

**Khanh Nguyen, MD** Department of Cardiovascular Surgery, Mount Sinai Hospital, New York, NY, USA

**James C. Nielsen, MD** Department of Pediatrics and Radiology, Stony Brook University School of Medicine, Stony Brook, NY, USA

**Laura J. Olivieri, MD** George Washington University School of Medicine, Division of Cardiology, Children's National Medical Center, Washington DC, WA, USA

**Orlando Petrucci, MD** Division of Cardiothoracic Surgery, Department of Surgery, Washington University in St. Louis School of Medicine, St. Louis, MO, USA

**Alistair B.M. Phillips, MD** Cedars Sinai Medical Center, Los Angeles, CA, USA

**Stephen Pophal, MD** Department of Cardiology, Phoenix Children's Hospital, Phoenix, USA

**Justin Ryan, PhD** Department of Cardiology, Phoenix Children's Hospital, Phoenix, USA

**Omar Saeed, MD** Department of Medicine, Division of Cardiology, Montefiore Medical Center, Albert Einstein College of Medicine, New York, NY, USA

**Javier Sanz, MD** Cardiovascular Institute, Mount Sinai Hospital, New York, NY, USA

**Bennett P. Samuel, MHA, BSN, RN** Congenital Heart Center, Helen DeVos Children's Hospital of Spectrum Heath, Grand Rapids, MI, USA

**Gautam K. Singh, MD** Division of Cardiology, Department of Pediatrics, Washington University in St. Louis School of Medicine, St. Louis, MO, USA

**Shubhika Srivastava, MBBS** Department of Pediatric Cardiology, Mount Sinai Medical Center, New York, NY, USA

**Michael D. Taylor, MD, PhD** The Heart Institute, Cincinnati Children's Hospital Medical Center, Cincinnati, OH, USA

**Joseph J. Vettukattil, MBBS, MD, DNB, CCST, FRCPCH, FRSM, FRCP** Congenital Heart Center, Helen DeVos Children's Hospital of Spectrum Heath, Grand Rapids, MI, USA; College of Human Medicine, Michigan State University, Grand Rapids, MI, USA

**Marija Vukicevic, PhD** Department of Cardiology, Houston Methodist DeBakey Heart and Vascular Center, Houston, TX, USA

**Kevin K. Whitehead, MD, PhD** Department of Cardiology, The Children's Hospital of Philadelphia, Philadelphia, PA, USA

**Pamela K. Woodard, MD** Mallinckrodt Institute of Radiology, Washington University in St. Louis School of Medicine, St. Louis, MO, USA

**Evan M. Zahn, MD** Cedars Sinai Medical Center, Los Angeles, CA, USA

# Part I

# Introduction

# History of Rapid Prototyping

1

Carlos A. Gonzalez Lengua, MD

## History of Rapid Prototyping

The field of 3D printing or rapid prototyping as we know it today is relative young. Its major developments were in the early 1980s but it gained more visibility a decade later. Much of the initial work was done by two pioneers in the field, Professor Hideo Kodama from Japan who is considered the first to develop a method of rapid prototyping and Charles Hull from California who invented the stereolithography apparatus (SLA) [1, 2].

In 1997, a report on rapid prototyping in Europe and Japan, sponsored by the US government and administered by the Japan Technology Evaluation Center/World Technology Evaluation Center (JTEC/WTEC), and lead by Friedrich B. Prinz from Stanford University, focused on the advances of rapid prototyping in the USA compared to Europe and Japan. The panel focused its investigation on a technology of rapid prototyping called solid freeform fabrication (SFF) [3]. In the report, the authors claimed that the idea of creating a 3D object in layered fashion was not in fact new at all and could be traced back to the ancient civilizations in Egypt, including layered manufacturing of the pyramids. In the nineteenth century, two other techniques were developed which are considered to have formed the foundation of rapid prototyping. These two methods include creation of 3D maps in topography and the photosculpture [3].

## Topography

At the end of the nineteenth century, J. E. Blanther patented a method to create 3D maps using topographical contour lines on a series of wax plates. This involved cutting, staking, and smoothing them to produce 3D surfaces that corresponded to the terrain surface variation [4]. Similar techniques were developed later in the twentieth century, starting with Kenji Matusubara in Japan who invented a topographical process that resembles the modern process of rapid prototyping. While working at Mitsubishi Motors, he developed a process using photopolymer resins coated in refractory particles. The resins were sprayed in layers onto a surface and a mercury vapor lamp caused them to harden. The unhardened portion was dissolved with a solvent and finally, the layers were stacked together [3]. Two years later Paul L. DiMatteo started to apply the same technique to fabricate items such as propellers and air foils. Finally, in 1979 at the University of Tokyo, Professor Takeo Nakagawa began to use this lamination process to fabricate devices such as press forming tools, blanking tools, and injection tools that are key in the modern manufacturing industry [3].

C.A.G. Lengua (✉)
Department of Medicine—Cardiology, Icahn School of Medicine at Mount Sinai, Mount Sinai St. Luke and Bronx Lebanon Hospital, New York, NY, USA
e-mail: carlos.gonzalezlengua@mountsinai.org


K.M. Farooqi (ed.), *Rapid Prototyping in Cardiac Disease*,
DOI 10.1007/978-3-319-53523-4_1

## Photosculpture

Photosculpture was invented in 1859 by French painter, sculptor and photographer François Willeme. The goal of this technique was to create a 3D object out of multiple photographs that were taking simultaneously. The object or person to be recreated was placed in the middle of a circular room. Twenty-four cameras were placed surrounding the object, each separated by 15°, and a photo was taking simultaneously from these different angles. To create the actual 3D object, each image was projected onto a screen. Using a pantograph attached to a cutter, he translated the image into the movement that would be required to create each individual layer. Willeme traced each profile with one end of the pantograph while a blade simultaneously cut a sheet of wood with the exact same movement to recreate the traced profile. Once each layer had been recreated, the layers of wood were assembled to create the photosculpture (Figs. 1.1 and 1.2) [5]. Photosculpture enjoyed brief success but the technique was soon abandoned due to it being a very labor intensive process. Different versions of this technique were later designed in an attempt to make the process less laborious by Carlo Baese in 1904 and later by Isao Morioka in Japan.

More recently, the development of modern techniques was influenced by the work of two men, Otto John Munz and Wyn Kelly Swainson. Otto John Munz was born in Czechoslovakia, moved to Canada in the late 1930s and later settled in Alexandria, Virginia in the 1940s. He was an inventor and patent lawyer. He patented a system called Photo-Glyph Recording, which consisted of creating multiple layers of a photo emulsion to replicate a 3D structure that came from a scanned object. Using a piston in a cylinder, the photo emulsions were added to create a 3D object. Subsequently, this object could be manually or photochemically carved to create the final 3D object [6].

**Fig. 1.1** Interior of Willeme's studio with pantograph, lantern projector and example of photosculpture including photosculpture of Willeme himself ca. 1865. Reproduced with permission from George Eastman House museum

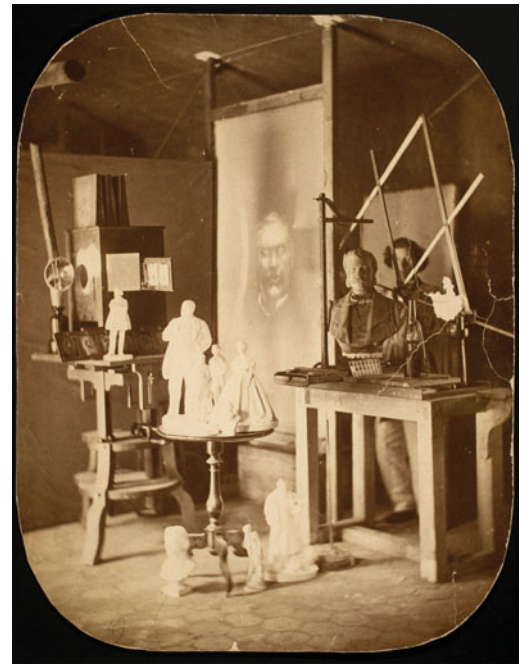

**Fig. 1.2** Admiral Farragut seated on a dais, posing for a photosculpture ca. 1862. Reproduced with permission from George Eastman House museum

The other pioneer was Wyn Kelly Swainson from California. In 1968, he proposed the "Method, Medium and Apparatus for Producing Three Dimensional Figure Product". This method consisted of creating a 3D figure in a volume of medium which includes an intimate mixture of at least two components selectively sensitive to dissimilar parameters of electromagnetic radiation. The medium was then exposed to two beams of radiation guided in response to an image description and having dissimilar electromagnetic parameters matched to the medium. In this manner, the path of the first beam with a specific parameter of activation resulted in the first component being formed. The path of a second beam with a second parameter of activation resulted in another part of the object being completed [7].

As was mentioned at the beginning of the chapter, Hideo Kodama and Charles Hull are considered the fathers of "modern" rapid prototyping. In 1981, while working in the Nagoya municipal industrial research institute in Japan, Professor Kodama published a paper on a photopolymer rapid prototyping system entitled "Automatic Method for Fabricating Cubic Shapes," as a 3D information display method. In his method, Kodama described a way to fabricate solid models by building layers using a 3D plastic model with photo-hardening polymer [1]. A 2 story house piling up 27 layers of 2 mm thick layers of resin was built using this method and is likely the first ever 3D printed object in history (Fig. 1.3). Professor Kodama presented his work in national and international meetings. However, he was unsuccessful to get the attention of the scientific community causing him to abandon the project. He started to file a patent but never completed the application. His work therefore remained unrecognized for several years, until 1995, when he was awarded the Rank Prize, a privately funded British award for outstanding inventors. He shared the prize with Charles Hull.

Charles Hull was born 1939 in Clifton, Colorado. He received a Bachelor of Science degree in engineering physics in 1961 from the University of Colorado. In 1984, he invented a system for generating a 3D object using successive, adjacent, cross-sectional laminae of the object. A fluid medium capable of altering its physical state in response to appropriate synergistic stimulation was used to create the layers. Each successive lamina was automatically integrated onto the previous ones to recreate the desired 3D object. He called this method stereolithography apparatus (SLA) [2]. He filed and obtained a patent in 1987 for this innovative method, similar to the one described by Kodama. Hull founded a company called 3D systems in Valencia California and sold the first SLA in 1988. The company continued to grow, and Hull remains the chief technology officer. He has been recognized internationally as great inventor and was included in the hall of fame for inventors in 2014. Figure 1.4 shows the first SLA and the first object printed using the machine, a cup that took months to finish. (Photo courtesy of 3D system, Inc.).

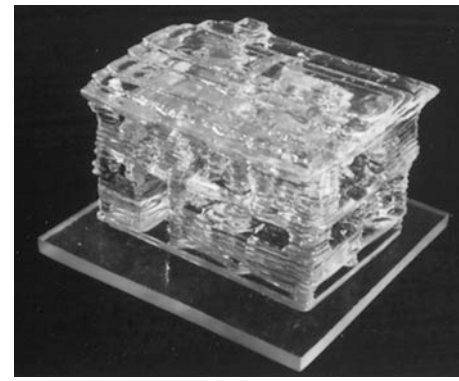

**Fig. 1.3** First object printed by Kodama using the automatic method for fabricating a three-dimensional plastic model with photo-hardening polymer

Around the same time, in the late 1980s, Carl Deckard at the University of Texas was in his freshman year of college and sought to develop an automated process to create casting patterns out of computer-aided design (CAD) models to fabricate machinery parts [8]. After a few years of working on the project, under the guidance of professor Joseph Beaman, he was able to create a new method. His method consisted of using a directed energy beam (such as a laser or electron beam) to melt particles of powder together to

**Fig. 1.4** First SLA machine build by Charles Hull in 1983, and the first object printed in that machine a cup that took months to finish. Courtesy of 3D System, Inc

make a part or object. Deckard called this method selective laser sintering (SLS). With a budget of $30,000 he and his team built the first SLS machine, called Betsy [8]. This same technology was later bought by 3D systems [8].

Around the same time Scott Crump and his wife invented a method called fused deposition modeling (FDM) after experimenting with mixing wax and plastic in the family kitchen. FDM consists of building an object by depositing multiple layers of a material in a fluid state onto a base. The material is selected on the basis that it has the ability to liquefy at a specific temperature and then solidifies instantaneously upon extrusion. Crump and his wife founded the company, Stratasys. Their company along with 3D system and EOS are the world leaders in rapid prototyping [9].

In 1989, Dr. Hans J. Langer and Dr. Hans Steinbichler founded Electro Optical System (EOS) in Gräfelfing near Munich, Germany. They were commissioned by German car maker Bayerische Motoren Werke (BMW) to develop a stereolithography machine to help the company with its innovation projects. They built their first 3D printer, the Stereo 400, that worked using an argon laser and epoxy as the print material. Their real success came later in 1992 when they developed the laser sintering technology (LST) that worked with powder material. In the years that followed, the company focus evolved from using resins to metals [10]. EOS is currently one of the leading suppliers of equipment, materials, and solutions in the field of LST.

In 2005, Adrian Bowyer at the University of Bath in the United Kingdom, founded the RepRap project. The project was created with the goal of making an affordable 3D printer that could print its own components. This involved creating an open source method of rapid prototyping called fused filament fabrication (FFF). The technique was very similar to FDM invented by Scott Crump. The RepRap project is now an international project with hundreds of people contributing to it. The first four official 3D printing machines of the RepRap project were "Darwin", released in March 2007, "Mendel", released in October 2009, and "Prusa Mendel" and "Huxley" released in 2010 [11].

By end of 2009 the concept of more affordable desktop 3D printers started to gain popularity. 3D systems created the BfB RapMan 3D printer built with a similar concept as the RepRap. Another company, Makerbot, also began marketing relatively low cost desktop printers. Makerbot was later bought by Stratasys. These two were the first companies to offer low cost desktop 3D printers. Currently, Makerbot

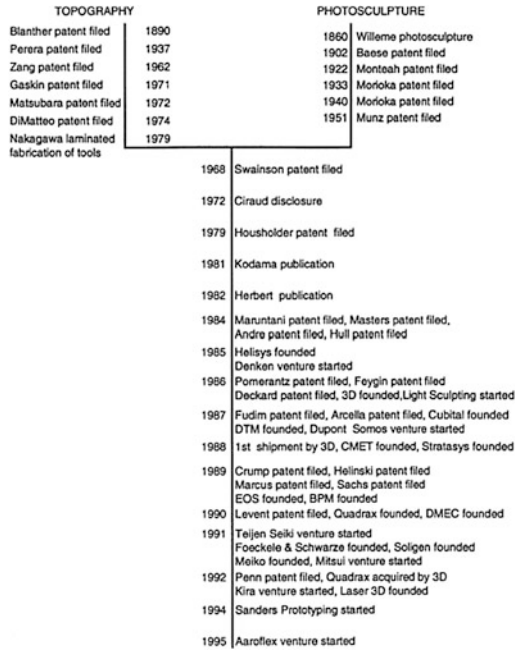


**Fig. 1.5** History of rapid prototyping. "Solid freeform fabrication chronology". Reproduced from Ref. [13]

offers a great variety of desktop printers starting at $1375. These printers use a polylactic acid (PLA) filament made of corn that comes in a variety of colors [12].

The technology of rapid prototyping has come a long way (Fig. 1.5) and is considered of crucial importance as a tool to decrease duration of the product development cycle and decreasing time from an initial design to the final physical product. The process has proven to be effective regardless of complexity of the geometry of the object suggesting that its future applications are limitless.

## References


1. Kodama H. Automatic method for fabricating a three-dimensional plastic model with photohardening polymer. Rev Sci Instrum. 1981;1770–73.
2. Hull C. Apparatus for production of three-dimensional objects by stereolithography. US Patent #4575330 A. 1984.
3. Prinz FB, et al. JTEC/WTEC panel on rapid prototyping in Europe and Japan. Baltimore, MD: Rapid Prototyping Association of the Society of Manufacturing Engineers in cooperation with International Technology Research Institute. 1997. http://www.wtec.org/loyola/rp/toc.htm. Accessed 16 Nov 2015.
4. Blanther JE. Manufacture of contour relief maps. US Patent #473,901. 1892.
5. Bogart M. Photosculpture. Art Hist. 1981;4:1–54 doi: 10.1111/j.1467-8365.1981.tb00696.
6. Munz OJ. Photo-glyph recording. US Patent #2,775,758. 1956.
7. Swainson WK. Method, medium and apparatus for producing three-dimensional figure product. US Patent #4,041,476. 1977.
8. Lindstrom A. Selective laser sintering, birth of an industry. http://www.me.utexas.edu/news/news/selective-laser-sintering-birth-of-an-industry. Accessed 16 Nov 2015.
9. Crump SS. Apparatus and method for creating three-dimensional objects. US Patent #5121329. 1992.
10. EOS e-Manufacturing Solutions. http://www.eos.info/about_eos/history. Accessed 16 Nov 2015.
11. RepRap. http://reprap.org. Accessed 16 Nov 2015.
12. MakerBot® 3D Printers. http://www.makerbot.com. Accessed 16 Nov 2015.
13. Beaman JJ, et al. Solid freeform fabrication: a new direction in manufacturing. © Springer Science +Business Media: New York; 1997.

# Creation of a 3D Printed Model: From Virtual to Physical

2

Joseph J. Vettukattil, MBBS, MD, DNB, CCST, FRCPCH, FRSM, FRCP, Bennett P. Samuel, MHA, BSN, RN, Jordan M. Gosnell, BS, RDCS and Harikrishnan K.N. Kurup, MBBS, MD

## Introduction

The complexity of congenital heart disease has led cardiologists and cardiothoracic surgeons to search for innovative methods to understand the spatial relationships in malformed hearts. The treatment of congenital heart disease requires an in-depth understanding of the three-dimensional (3D) relationships of cardiovascular structures. In the last several years, there have been significant advancements in transcatheter interventions in congenital and structural heart diseases [1]. However, the comprehension of abnormal cardiac morphology is dependent on quality imaging, namely cardiac computed tomography (CT), cardiac magnetic resonance (CMR), and 3D transthoracic (TTE) or transesophageal (TEE) echocardiography. In addition, the information gained from post-processed imaging datasets continues to be limiting as the 3D renderings are visualized on a two-dimensional (2D) screen. Interpretation of these images requires assumptions, where aspects of spatial relationships are left to the imagination without a tangible model. In this context, rapid prototyping, the technique where 3D computerized models of anatomical structures are converted into physical models, plays a significant role in filling this gap in cardiac medicine [1–7].

The management of congenital heart disease relies heavily on accurate imaging of the morphology and interrelationships between cardiac structures. Virtual preoperative models of congenital heart disease were first created from CMR datasets in 1988. Surface reconstruction software, originally developed for craniofacial and orthopedic surgical planning, was adapted for post-processing of preoperative CMR datasets. The reconstructions were consistent with echocardiography, cineangiography, 2D CMR, and intraoperative findings. However, they were not readily adopted for clinical use due to low-resolution images and lack of computing power [8].

3D echocardiography began to develop in the 1960s, and the first 3D scan of the heart was reported in 1974 [9]. Over the next two decades, improvements in resolution and computing power transformed the visualization of congenital heart disease. Although multiple options for 3D imaging became available, the representation of the 3D images on a 2D screen left depth and spatial relationships to the imagination. Research

J.J. Vettukattil (✉) · B.P. Samuel · J.M. Gosnell
H.K.N. Kurup
Congenital Heart Center, Helen DeVos Children's Hospital of Spectrum Heath, Grand Rapids, MI, USA
e-mail: Joseph.Vettukattil@helendevoschildrens.org

B.P. Samuel
e-mail: Bennett.Samuel@helendevoschildrens.org

J.M. Gosnell
e-mail: Jordan.Gosnell@spectrumhealth.org

H.K.N. Kurup
e-mail: drhari.kurup@gmail.com

J.J. Vettukattil
College of Human Medicine, Michigan State University, Grand Rapids, MI, USA


K.M. Farooqi (ed.), *Rapid Prototyping in Cardiac Disease*,
DOI 10.1007/978-3-319-53523-4_2

into the ability of individuals to deduce spatial relationships, and mental rotation reveals vast intra-observer and inter-observer variability in interpreting 3D data [1–7, 10]. Rapid prototyping leaves no aspect of the spatial relationships to the imagination, which can be invaluable in children and adults with complex congenital heart disease [3].

Rapid prototyping was introduced in the early 1980s and applied by the manufacturing industry to design components for various products including aircrafts, computers, and vehicles [1, 11]. For these industrial applications, rapid prototyping has been utilized to assess the ease of future product assembly and evaluate the feasibility of developing newly designed products prior to mass production [11]. In medicine, 3D printing from radiological images to replicate anatomical structures was initially used in orthopedic and plastic surgery [1, 7]. The software was later adapted to accommodate CT and CMR datasets for rapid prototyping of cardiovascular structures. More recently, high-resolution cardiac imaging has ushered in an era where rapid prototyping or 3D printing of congenital heart disease is more feasible [8]. Within one complex congenital heart diagnosis, patients may have varied morphology and prognosis depending on the specific anatomy or associated comorbidities. 3D printed cardiac models can enhance the management of patients by improving interventional and surgical planning and perhaps lead to individualized device deployment targeting specific cardiac defects [6–11].

Typically, high-resolution cross-sectional CT and CMR are used as the source datasets to derive whole heart 3D printed models [10, 11]. 3D printing derived from 3D echocardiographic imaging is also feasible and accurately reflects cardiac morphology, albeit focusing on one part of the anatomy (Figs. 2.1, 2.2, 2.3, and 2.4) [12, 13]. The integration of multiple imaging modalities for hybrid 3D printing is an additional technique which can be used when one modality is insufficient to give a complete picture of the pathology [9, 14]. This technique utilizes the strength of each imaging modality to be incorporated separately into one model improving the accuracy of the hybrid 3D printedheart model.

A 3D printed heart model may be used to teach patients and their family members about the congenital heart defect and plan for repair. Currently, a 2D representation, such as a drawing on a piece of paper or whiteboard, is used to explain the procedure to patients and their family members. The visual and tactile feedback provided by 3D printed heart models markedly improves the understanding of complex structural heart defects and may be beneficial to teach medical students, residents, nurses, and other

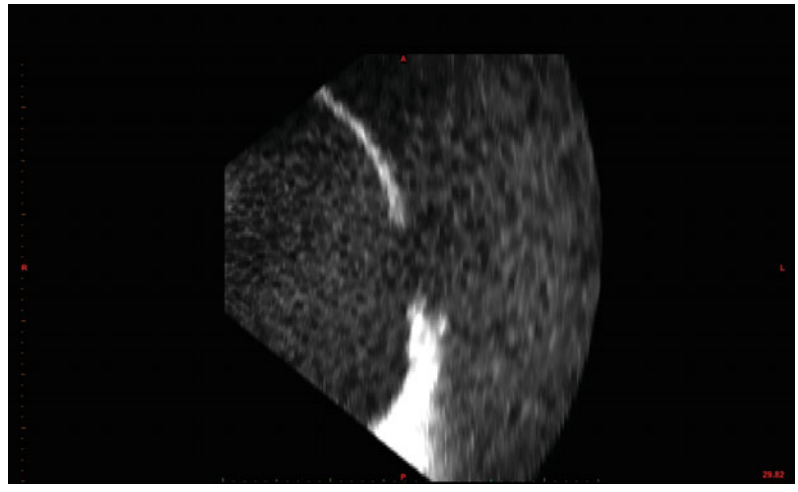

**Fig. 2.1** Imported image from a 3D echocardiography dataset for 3D printing performed for evaluation of an atrial septal defect

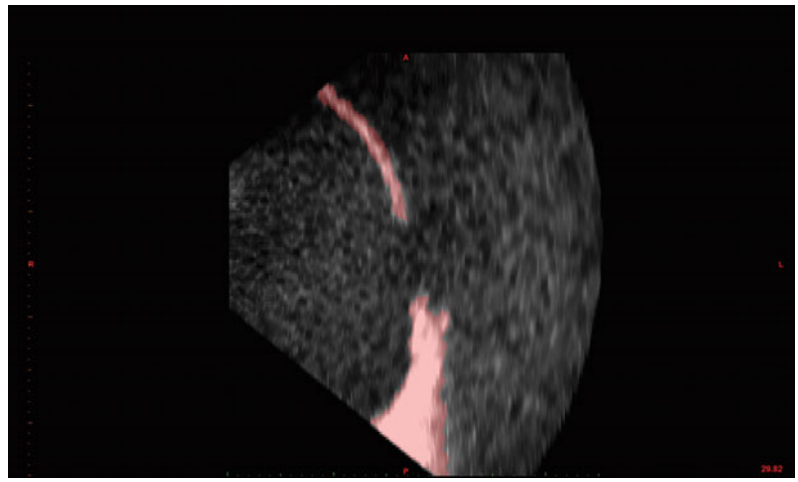

**Fig. 2.2** The atrial septum was segmented using Materialise Mimics® Innovation Suite

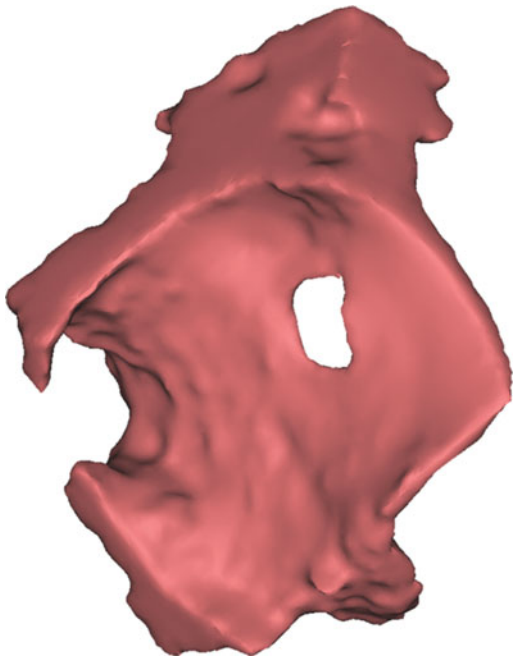

**Fig. 2.3** Mimics® Innovation Suite was used to reconstruct a 3D rendering of the atrial septum, which is shown with the visible atrial septal defect

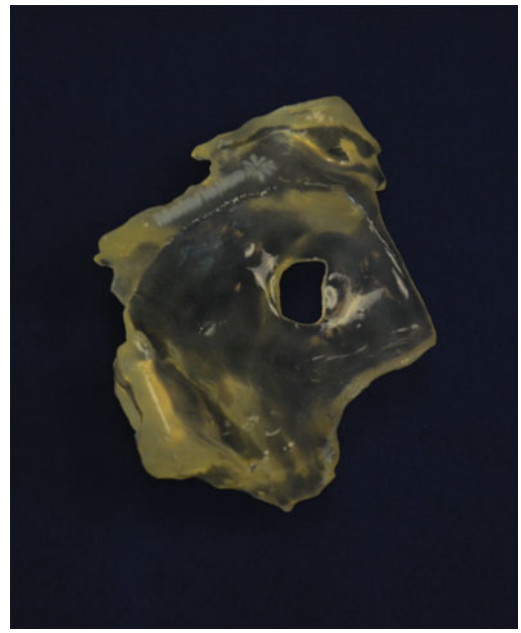

**Fig. 2.4** Materialise Heart Print® Flex 3D printed model of an atrial septal defect from 3D echocardiography

medical professionals about specific congenital heart defects [1, 6–9, 11–16]. The 3D printed heart model is expected to enhance professional training, enable practicing procedures before performing them, and help design precise prostheses prior to an interventional or surgical procedure. In complex anatomical repairs where expert opinion is required, the 3D virtual and printed models can be shared rather than inconveniencing the patient to travel long distances.

The cost and time needed to create 3D printed models may vary widely depending on the complexity of the lesion and quality of the material used for printing. As a result, it is important to consider the indications or degree of complexity of congenital heart defects for 3D

printing to maximize its utility and reduce commercial misuse [9].

## Patient Selection and Image Acquisition

The field of congenital heart disease has undergone major treatment improvisations over the last 4 decades. For example, the arterial switch operation has been the treatment of choice for transposition of the great arteries for the past 30 years [17]. This congenital defect was previously managed by the Mustard or Senning procedure, which could functionally correct the altered hemodynamics. The Fontan operation as the final procedure in the common single ventricle pathway has also undergone major revisions in the past 40 years [18]. However, these patients who underwent palliative procedures in the past are now presenting with cardiac complications and require advanced imaging to help form a complete picture of their clinical status. It may be difficult for cardiologists and surgeons new to the field, or who are not trained in imaging, to interpret the cardiovascular images obtained by conventional modalities in these patients. 3D printing of such complex repaired defects facilitates the understanding of the anatomical substrate. 3D printed models help in planning the appropriate interventions well in advance, which can improve the interventionalists' or the surgeons' preparation for the procedure. The utility of 3D printing in planning catheter intervention in pulmonary venous baffle obstruction in Mustard repair has recently been demonstrated [11]. The size of devices, size, and shape of conduits or patches, and the accessory equipment required during the intervention can also be planned, contributing to the procedure going smoothly. This may reduce procedure time and risk of radiation exposure and aid in the prevention of inadvertent complications. Some of the specific congenital heart defects for which 3D printing can make significant differences in the management are described below.

Determining the morphology of the superior and inferior bridging leaflets as well as identifying any imbalance of the valve opening into the ventricles is critical in determining the suitability for biventricular repair in atrioventricular septal defects (AVSD) [19]. Ventricular size can be underestimated due to foreshortening on conventional imaging modalities. Visualization of AVSDs by hybrid 3D printing can provide insight into the actual ventricular volumes, the relationship of the bridging leaflets to the ventricles, presence of straddling leaflets, and associated anomalies. The size of the patch required and strategies to repair the left-sided cleft valve to prevent later regurgitation can also be planned [20]. 3D hybrid segmentation and printing is especially relevant in this setting given that valvular structures are best re-created using 3D echocardiographic images.

Double-chambered right ventricle (RV) is another congenital heart defect for which 3D printing may be useful. It occurs due to muscle bundles separating the RV inlet and outlet (pulmonary artery) from the body of the RV [21]. This malformation is found in up to 10% of patients with ventricular septal defects (VSD) on long-term follow-up. The RV is difficult to image and quantify because it does not conform to the geometric assumptions made for the left ventricle. The cardiothoracic surgeon requires vital information regarding how much extra volume may be added to the RV once the muscle bundles are resected, especially in patients with corrected complex congenital heart disease or 1½ ventricular repair. The tangibility offered by 3D printed models provides the surgeon with a hands-on experience of the actual muscle resection prior to the procedure. This can have far-reaching implications such as choosing between 1½ ventricular repair versus biventricular repair (Fig. 2.5a–e) [22].

Corrective surgery in double outlet right ventricle (DORV) may involve baffling of the VSD to the aorta or performing an arterial switch operation. One of the factors that influence the approach is the proximity of the ventricular septal margin to the aorta. However, DORV with subpulmonary VSD (Taussig-Bing anomaly) requires baffling of the VSD to the pulmonary artery followed by an arterial switch procedure.

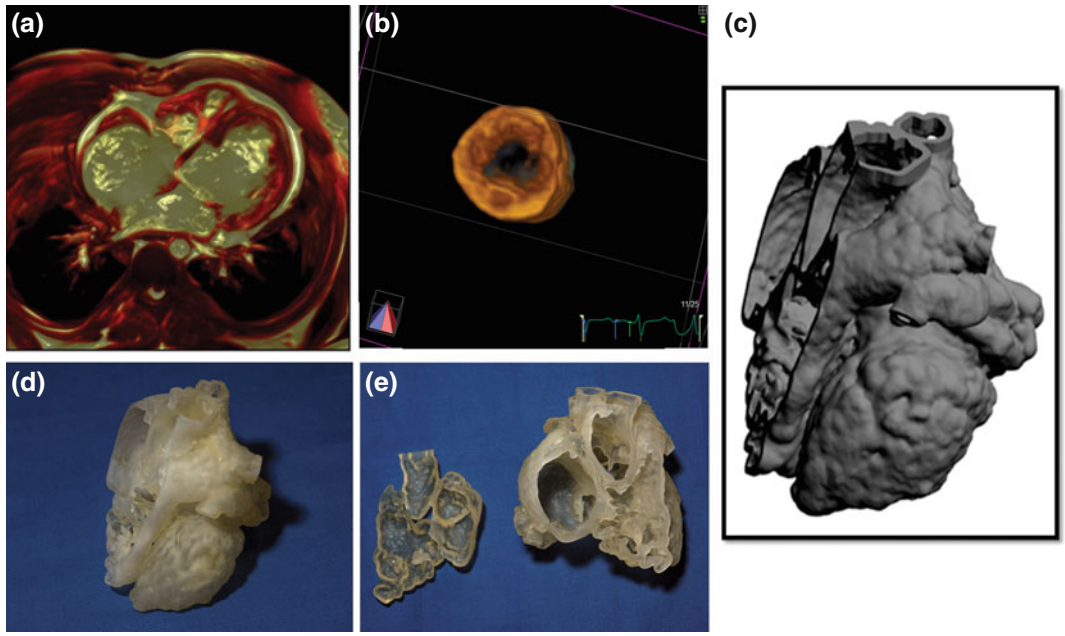


**Fig. 2.5** **a** A 4-chamber view from CMR showing muscle bundles in the mid-right ventricle in a patient with pulmonary atresia intact ventricular septum palliated with a bidirectional Glenn anastomosis. **b** A 3D TEE showing the tricuspid valve. **c** A 3D rendering of the integrated CMR and 3D TEE datasets. **d** A hybrid 3D printed model showing the LV and the obstructing muscle bundles in the RV. **e** A hybrid 3D printed model corresponding to an echocardiographic apical 4-chamber view

Commitment of the VSD to one of the great vessels (pulmonary artery or aorta) is mandatory for successful biventricular repair. 3D printed models of the heart provide accurate visualization of the relationship of the VSD to the outflow tracts so that treatment decisions regarding routability can be made [23].

Considering the complications and late failure of the Fontan procedure, Fontan conversion or takedown may be considered in some cases [24]. Hybrid 3D printed models of these complex hearts provide excellent representation of the size and relationship of the chambers and the valvular anatomy. There are recent reports of the utility of 3D printed models of the RV outflow tract in the accurate selection of patients for pulmonary valve implantation [25]. It is critical to evaluate the size and orientation of the outflow tract and possibly test out the surgical intervention on a 3D printed model prior to undertaking such complex interventions. 3D printed models of the heart and the great vessels have been found to be useful in preoperative and pre-interventional planning of stent sizes in coarctation of aorta, branch pulmonary artery stenosis, and caval valve implantation techniques [16, 26]. Custom-sized patent ductus arteriosus stents in hybrid procedures for hypoplastic left heart syndrome may also be a potential application of 3D printing.

It is important to have proper guidelines for the effective use of this technology when it is integrated into routine clinical practice. The time and risk involved in obtaining the necessary images, performing segmentation, and the cost for printing must be taken into account. Patients with simple heart defects wherein the routine imaging modalities provide a straightforward diagnosis, and appropriate treatment strategies do not require 3D printed heart models, although models of these defects may still be useful for educational purposes. These include simple atrial and ventricular septal defects, tetralogy of Fallot without associated defects, and simple transposition of the great arteries.

Image acquisition is the most important step in the process of creating a virtual model to be used to print a physical model. A significant determinant in patient selection for 3D printing is the availability of high-quality images. Currently, the imaging modalities used to derive 3D printed models include cardiac CT, CMR, and both 3D TEE and TTE. Each imaging modality has different strengths and weaknesses that impact the quality and accuracy of the 3D printed model [9]. The visualization of extracardiac anatomy and "blood pool" imaging is enhanced by CT [27]. However, nephrotoxic intravenous contrast is often required for acquisition of cardiac CT imaging datasets and exposes patients to ionizing radiation. Cumulative medical radiation is of concern and can have important health implications for young patients [28, 29]. CMR is superior to other imaging modalities for the quantification of ventricular volumes and myocardial architecture [4]. For CMR, intubation and general anesthesia are often necessary in pediatric patients. Gadolinium-based contrast may also be required for acquisition of high-resolution imaging datasets. Scanning is not possible in patients with implanted devices that are incompatible with CMR. In contrast, 3D echocardiography is a bedside tool, which is safe for severely ill patients as they do not require transportation or positioning in a scanner. Intubation and sedation are also not required except when 3D TEE is utilized or if the patient's age makes it difficult for them to lie still for a prolonged period of time [30]. The best visualization of cardiac valve morphology is provided by 3D echocardiography when compared to other imaging modalities [31]. However, there are several limiting factors that may affect valve visualization by 3D echocardiography. Image acquisition focuses on one aspect of the anatomy, and a whole heart image dataset cannot be acquired. Technical settings including frame rate, gain, compression, and depth must be set by the echocardiographer to clearly define the blood–tissue border and to distinguish valve anatomy from artifact. Furthermore, hardware and software limitations in current ultrasound systems, specifically those affecting temporal and spatial resolutions, may not provide sufficient image quality for a 3D printed model. These limitations affect both 3D TTE and 3D TEE imaging. Availability of appropriate sized probes for TEE may be a limiting factor in young patients with complex congenital heart disease. However, 3D TEE has better image resolution and frame rates [20] and is preferable as a source dataset for 3D printing. Image acquisition is discussed in detail in subsequent chapters.

## Post-processing to Virtual Model

A factor that significantly impacts the accuracy of 3D printed models is post-processing, the quality of which may vary among cardiologists and sonographers [20]. For this reason, there is a need for a unified protocol. The images from cardiac CT, CMR, and 3D ultrasound are usually acquired in the Cartesian digital imaging and communications in medicine (DICOM) format. As traditional 3D echocardiogram post-processing elements cannot be exported from segmentation software, image acquisition settings play an important role in determining the quality of ultrasound datasets. A frame rate of 30 frames per second (fps) is more than adequate for 3D echocardiography datasets. If there is no fusion artifact, 4 cardiac cycles provide optimal data for post-processing. The gain and compression settings must be optimized to get adequate visualization of the tissue–blood separation point. Visualization of the blood-tissue interface is also dependent on the patient's size and the frequency setting of the ultrasound probe. A frequency of 5–7 MHz is usually adequate for acquisition of 3D TTE datasets for 3D printing in children.

After assessing the data for quality and clarity and filtering for noise reduction, it is imported into the segmentation software. We utilized Mimics® Innovation Suite and 3-matic® (Materialise, Leuven, Belgium), a commercially available post-processing software. Thresholding and other interactive editing operations are then performed using automatic, semiautomatic, and hand segmentation methods. Thresholding is used to isolate tissue with a specific signal

intensity in different regions of the image dataset to create anatomy-specific masks. In ultrasound datasets, thresholding helps to identify the blood–tissue border based on the intensity of the cardiac structures' echogenicity (echodensity). For CMR and CT data, segmentation is used to create a mask of the blood pool which is subsequently hollowed out to represent the intracardiac anatomy and orientation. For example, a 2–4 mm thickness may be provided to the model at all blood–tissue interfaces to depict cardiac/vessel walls in the rendered model.

For all three modalities, there are varying degrees of manual editing required for proper representation of cardiac morphology. Thin-walled structures such as the interatrial septum may result in "dropout" on a CT scan when other imaging datasets do not support the presence of a hole or defect. Careful attention must also be given to artifacts in ultrasound datasets to reduce similar errors in being represented in the 3D printed models. We have not yet reached the state of technological advancement required for fully automated segmentation. A sound knowledge of normal and abnormal intracardiac anatomy is essential for appropriate segmentation and accurate reproduction in the printed model. It is recommended that the caregivers managing the patient be involved in the segmentation process and be familiar with all available imaging information.

Upon the completion of segmentation, a 3D digital replica of the heart is rendered for visualization and measurements. The segmentation software is then utilized to prepare the digital model for printing and exporting in stereolithography (STL) format. Prior to conversion into STL file format, the 3D rendering is smoothed to reduce pixilation and improve the 3D file quality. The surface of the STL file is then prepped for printing by creating a surface mesh model (Fig. 2.6a, b). The STL file can then be printed on any 3D printer depending on the choice of model material and detail needed [9, 12, 13]. Prior to 3D printing, the reconstructed model can be dissected to display the region of specific interest [9–14]. This step also relies heavily on the contributions of the interventionalist or surgeon so that maximum information for procedure planning can be obtained from the model.

For hybrid 3D printing from two or more imaging modalities, the 3D rendering must be imported into dedicated post-processing software for additive manufacturing such as 3-matic® (Materialise). The datasets are imported into segmentation software and integrated after individual imaging segmentation has been performed. It is important to identify the targeted cardiac phases for rapid prototyping and ensure that each imaging modality is in the same phase prior to integration [9, 14]. After completion of segmentation of the individual imaging modalities as described above, the datasets can be merged manually in 3-matic by superimposing the datasets to create a composite mask (Fig. 2.7a–c). After confirming that the measurements of the virtual file correlate with the original dataset, the merged dataset is exported back into Mimics® Innovation Suite for optimization. The 3D rendering is (Fig. 2.7d) then converted to STL format for hybrid 3D printing (Fig. 2.7e–g).

More recently, CT and CMR data segmentation has become less labor-intensive due to automation of the segmentation function within the 3D segmentation software. Comparatively, 3D ultrasound data segmentation continues to be a long, manual editing process even for experienced individuals. The ideal personnel for processing data for 3D printing must be familiar with both the segmentation software and congenital heart disease. For hybrid 3D printing, additional time and experience is required for proper alignment of modality datasets. Ideally, anatomical markers such as a valve annulus can be identified on each modality to assist with hybrid model reconstruction.

## Limitations of 3D Printing

A limitation of a 3D printed cardiac model is that it is a static model of a dynamic organ, making it difficult to deduce from it any hemodynamic information. The various changes that occur during the cardiac cycle are frozen in time and

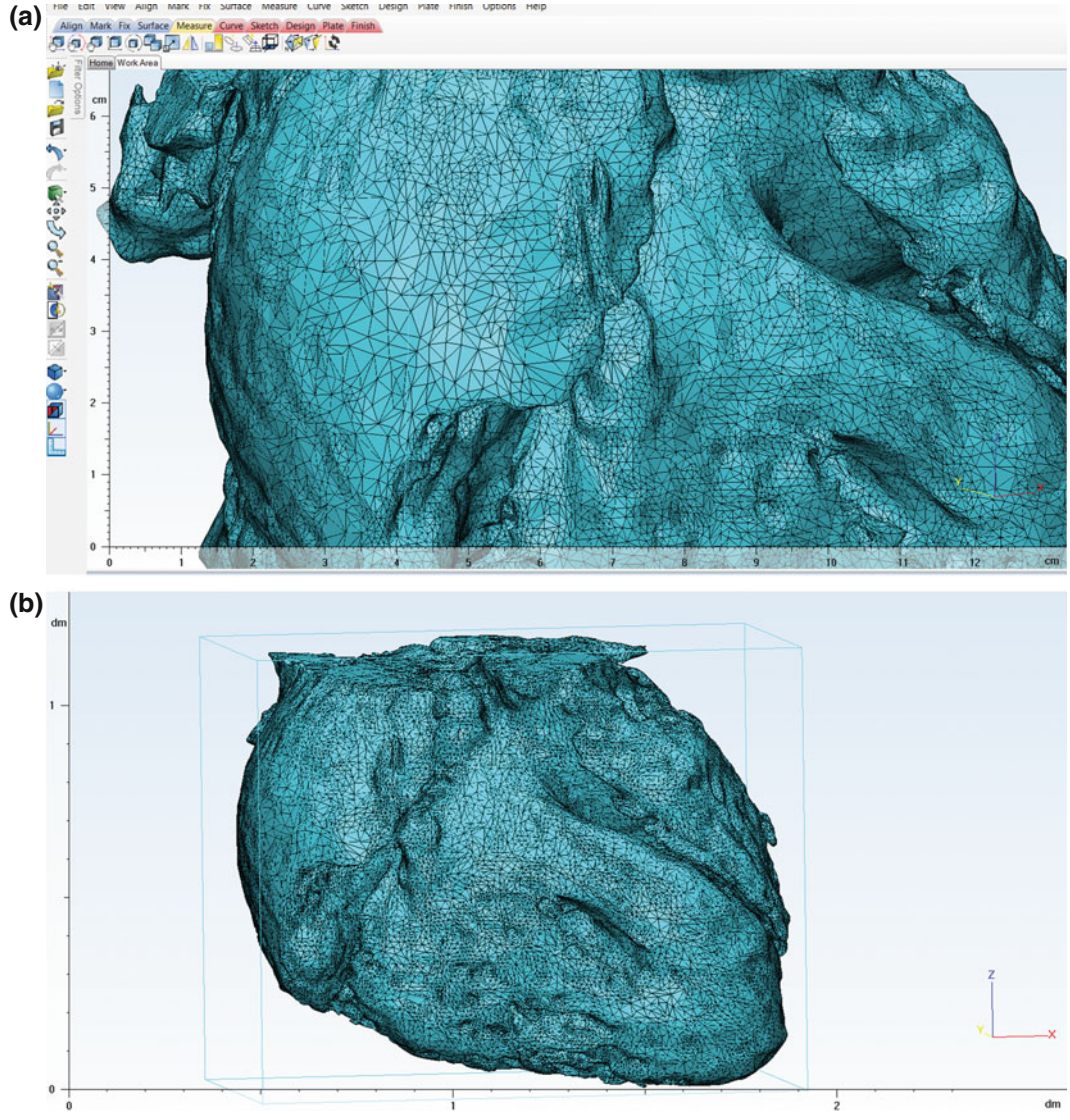


**Fig. 2.6** **a**, **b** The surface mesh model utilized to fill in any signal dropouts or gaps in the 3D virtual model in preparation for 3D printing

**Fig. 2.7** **a–c** The integration of CT and 3D TEE in a patient with congenitally corrected transposition of the great arteries for hybrid 3D printing. **d** A 3D rendering produced from integration of CT and 3D TEE in a patient with congenitally corrected transposition of the great arteries for hybrid 3D printing. **e** The HeartPrint® Flex hybrid 3D printed model. The translucent material depicts the extracardiac structures and the cardiac contour derived from CT with the right (*green*) and left (*pink*) atrioventricular valve morphology derived from 3D TEE. **f** The right (*green*) and left (*pink*) atrioventricular valve morphology derived from 3D TEE. The leaflets of the systemic atrioventricular valve (*pink*) are clearly defined; however, the mitral valve (*green*) was less accurate due to the data acquisition being affected by interference from pacing wires. **g** The Amplatzer septal occluder device visualized in the atrial septum on the 3D printed model ►

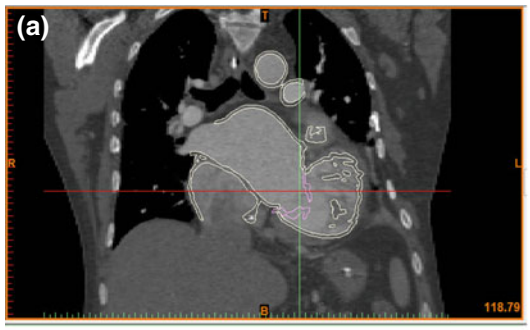
(a)
T
R
L
B
118.79

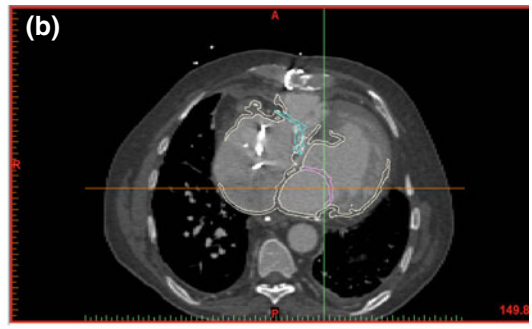
(b)
A
R
P

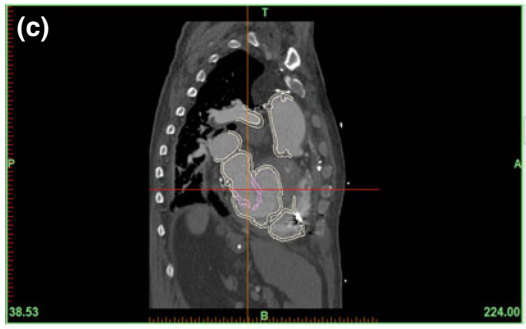
(c)
T
P
A
38.53
B
224.00

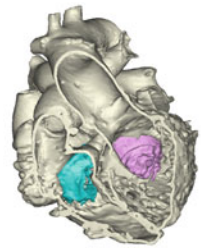
(d)


(e)


(f)


(g)

space, lacking the function and hemodynamic changes related to the functional morphology of the heart.

## Conclusion: Personalized Medicine in Congenital Heart Disease

A 3D printed model that would be able to replicate the anatomical and physiological changes that occur during the cardiac cycle would be invaluable for diagnosis and management of children and adults with complex congenital heart disease. Further advancements in cardiac imaging and computing power combined with miniaturization of processors promise a new era in advanced cardiac imaging. Visualization of 3D images in 3D media with augmented reality will define the future of personalized cardiac medicine.

## References


1. Laschinger JC, Vannier MW, Gutierrez E, et al. Preoperative three-dimensional reconstruction of the heart and great vessels in patients with congenital heart disease. Technique and initial results. J Thorac Cardiovasc Surg. 1988;96(3):464–73.
2. Dekker DL, Piziali RL, Dong E Jr. A system for ultrasonically imaging the human heart in three dimensions. Comput Biomed Res. 1974;7(6):544–53. doi:10.1016/0010-4809(74)90031-7.
3. Farooqi KM, Sengupta PP. Echocardiography and three-dimensional printing: sound ideas to touch a heart. J Am Soc Echocardiogr. 2015;28(4):398–403. doi:10.1016/j.echo.2015.02.005.
4. Luijnenburg SE, Robbers-Visser D, Moekler A, et al. Intra-observer and interobserver variability of biventricular function, volumes and mass in patients with congenital heart disease measure by CMR imaging. Int J Cardiovasc Imaging. 2010;26(1):57–64. doi:10.1007/s10554-009-9501-y.
5. Guillot A, Champely S, Batier C, et al. Relationship between spatial abilities, mental rotation, and functional anatomy learning. Adv Health Sci Educ Theor Pract. 2007;12(4):491–507. doi:10.1007/s10459-006-9021-7.
6. Hoyek N, Collect C, Rastello O, et al. Enhancement of mental rotation abilities and its effect on anatomy learning. Teach Learn Med. 2009;21(3):201–6. doi:10.1080/10401330903014178.
7. Estevez ME, Lindgren KA, Bergethon PR. A novel three-dimensional tool for teaching human neuroanatomy. Anat Sci Edu. 2010;3(6):309–17. doi:10.1002/ase.186.
8. Greil GF, Wolf I, Kuettner A, et al. Stereolithographic reproduction of complex cardiac morphology based on high resolution imaging. Clin Res Cardiol. 2007;96(3):176–85. doi:10.1007/s00392-007-0482-3.
9. Kurup HKN, Samuel BP, Vettukattil JJ. Hybrid 3D printing: a game-changer in personalized cardiac medicine? Expert Rev Cardiovasc Ther. 2015. doi:10.1586/14779072.2015.1100076
10. Jacobs S, Grunert R, Mohr FW, et al. 3D-Imaging of cardiac structures using 3D heart models for planning in heart surgery: a preliminary study. Interact CardioVasc Thorac Surg. 2008;7(1):6–9. doi:10.1510/icvts.2007.156588.
11. Olivieri L, Krieger A, Chen MY, et al. 3D heart model guides complex stent angioplasty of pulmonary venous baffle obstruction in a mustard repair of D-TGA. Int J Cardiol. 2014;172(2):e297–8. doi:10.1016/j.ijcard.2013.12.192.
12. Samuel BP, Pinto C, Pietila T, et al. Ultrasound-derived three-dimensional printing in congenital heart disease. J Digit Imaging. 2015;28(4):459–61. doi:10.1007/s10278-014-9761-5.
13. Olivieri LJ, Krieger A, Loke YH. Three-dimensional printing of intracardiac defects from three-dimensional echocardiographic images: feasibility and relative accuracy. J Am Soc Echocardiogr. 2015;28(4):392–7. doi:10.1016/j.echo.2014.12.016.
14. Gosnell J, Pietila T, Samuel BP, et al. Integration of computed tomography and three-dimensional echocardiography for hybrid three-dimensional printing in congenital heart disease. J Digit Imaging. 2016. doi:10.1007/s10278-016-9879-8.
15. Kim MS, Hansgen AR, Wink O, et al. Rapid prototyping: a new tool in understanding and treating structural heart disease. Circulation. 2008;117(18):2388–94. doi:10.1161/CIRCULATIONAHA.107.740977.
16. Valverde I, Gomez G, Coserria JF, et al. 3D printed models for planning endovascular stenting in transverse aortic arch hypoplasia. Catheter Cardiovasc Interv. 2015;85(6):1006–12. doi:10.1002/ccd.25810.
17. Villafane J, Lantin-Hermoso MR, Bhatt AB, Tweddell JS, Geva T, Nathan M, et al. D-transposition of the great arteries: the current era of the arterial switch operation. J Am Coll Cardiol. 2014;64(5):498–511.
18. John AS. Fontan repair of single ventricle physiology: consequences of a unique physiology and possible treatment options. Cardiol Clin. 2015;33(4):559–69.
19. Anderson RH, Wessels A, Vettukattil JJ. Morphology and morphogenesis of atrioventricular septal defect with common atrioventricular junction. World J Pediatr Congenit Heart Surg. 2010;1(1):59–67.

20. Cohen MS, Spray TL. Surgical management of unbalanced atrioventricular canal defect. Semin Thorac Cardiovasc Surg Pediatr Card Surg Annu. 2005:135–44.
21. Loukas M, Housman B, Blaak C, Kralovic S, Tubbs RS, Anderson RH. Double-chambered right ventricle: a review. Cardiovasc Pathol. 2013;22(6): 417–23.
22. Haw MP, Gosnell JM, Samuel BP, Kurup H, Baliulis G, Hillman ND, Lacina SL, Vettukattil JJ. 147: hybrid 3D printing in congenital heart disease. Select abstracts from cardiology 2016: The 19th annual update on pediatric and congenital cardiovascular disease, Orlando, Florida, 24–28 Feb 2016. World J Pediatr Congenit Heart Surg. 2016;7(2):274–5. doi:10.1177/2150135115626922.
23. Farooqi KM, Uppu SC, Nguyen K, Srivastava S, Ko HH, Choueiter N, et al. Application of virtual three-dimensional models for simultaneous visualization of intracardiac anatomic relationships in double outlet right ventricle. Pediatr Cardiol. 2015.
24. Kottayil BP, Sunil GS, Kappanayil M, Mohanty SH, Francis E, Vaidyanathan B, et al. Two-ventricle repair for complex congenital heart defects palliated towards single-ventricle repair. Interact CardioVasc Thorac Surg. 2014;18(3):266–71.
25. Schievano S, Migliavacca F, Coats L, Khambadkone S, Carminati M, Wilson N, et al. Percutaneous pulmonary valve implantation based on rapid prototyping of right ventricular outflow tract and pulmonary trunk from MR data. Radiology. 2007;242(2): 490–7.
26. O'Neill B, Wang DD, Pantelic M, Song T, Guerrero M, Greenbaum A, et al. Transcatheter caval valve implantation using multimodality imaging: roles of TEE, CT, and 3D printing. JACC Cardiovasc Imaging. 2015;8(2):221–5.
27. Goitein O, Salem Y, Jacobson J, et al. The role of cardiac computed tomography in infants with congenital heart disease. Isr Med Assoc J. 2014;16(3): 147–52.
28. Glatz AC, Purrington KS, Klinger A, et al. Cumulative exposure to medical radiation for children requiring surgery for congenital heart disease.
29. Hoffman A, Engelfriet P, Mulder B. Radiation exposure during follow-up of adults with congenital heart disease. Int J Cardiol. 2007;118(2):151–3. doi:10.1016/j.ijcard.2006.07.012.
30. Vettukattil JJ. Three dimensional echocardiography in congenital heart disease. Heart 2012;98:79–88. doi:10.1136/heartjnl-2011-300488.
31. Black D, Vettukattil J. Advanced echocardiographic imaging of the congenitally malformed heart. Curr Cardiol Rev. 2013;9(3):241–52. doi:10.2174/1573403x11309030008.

# Image Acquisition for Creation of a 3D Model: CT, CMR, and Echocardiography

3

Javier Sanz, MD, Kanwal Majeed Farooqi, MD, James C. Nielsen, MD and Shubhika Srivastava, MBBS

## Introduction

The quality of a 3D printed model is highly dependent on the quality of the source 3D image dataset. Although meticulous post-processing of the 3D object created from a dataset can certainly improve the appearance of a model, focus on the image acquisition technique results in a dataset that will result in a more accurate model with less post-processing needed. The images used to create a model can be 3D datasets from cardiac magnetic resonance (CMR) imaging, computed tomography (CT), or echocardiography. Each of these modalities varies in its advantages, disadvantages, and applicability in different clinical scenarios. In this chapter, we will describe the techniques by which images can be acquired to create good quality 3D printed cardiac models with acquisition considerations specific to each modality.

J. Sanz, MD
Cardiovascular Institute, Mount Sinai Hospital, New York, NY, USA
e-mail: Javier.sanz@mountsinai.org

K.M. Farooqi, MD
Division of Pediatric Cardiology, Rutgers, New Jersey Medical School, Newark, NJ, USA
e-mail: kanwal.farooqi@rutgers.edu

J.C. Nielsen, MD (✉)
Department of Pediatrics and Radiology, Stony Brook University School of Medicine, Stony Brook, NY, USA
e-mail: james.nielsen@stonybrookmedicine.edu

S. Srivastava, MBBS
Department of Pediatric Cardiology, Mount Sinai Medical Center, New York, NY, USA
e-mail: shubhika.srivastava@mssm.edu

## Cardiac CT

### Computed Tomography Angiography

Contrast-enhanced computed tomography angiography (CTA) can provide very good quality 3D datasets for rapid prototyping (RPT) and has indeed been used for this purpose [1–3]. Advantages over ultrasound include ability to depict vascular and non-vascular extracardiac structures and coronary anatomy with high tissue contrast between lumen and myocardium/vessel wall. CTA also offers superior spatial resolution to MRI, is more widely available, and can be acquired in shorter imaging times. However, CTA has lower temporal resolution, requires contrast administration, and, importantly, involves ionizing radiation exposure, a special concern in the typical age range of patients with congenital heart disease (CHD). Therefore, while CTA is typically considered a third-line test in the evaluation of CHD [4], it may be considered first line in pediatric patients with CHD (or in adults with structural heart disease) if 3D printing is intended. Typically, only one single CTA dataset is acquired that must contain all necessary information; thus, it is vital for successful imaging that communication exists between the referring clinician and the cardiac imager regarding specific anatomy,


K.M. Farooqi (ed.), *Rapid Prototyping in Cardiac Disease*,
DOI 10.1007/978-3-319-53523-4_3

shunts, prior repair, etc., so that the protocol can be tailored to the individual patent. While extracardiac vascular structures can be adequately depicted with older generation technology, today 64-slice or higher scanners are recommended for cardiac CTA [5].

## Patient Preparation

Intravenous (i.v.) access is required for contrast injection. While for most non-CHD applications the location of the i.v. is of limited relevance, in patients with CHD it may need to be placed on a specific side (left vs. right) or extremity (lower vs. upper) depending on the presence of venous obstructions, abnormal connections, or other anatomic variants.

For patients who can cooperate, images are typically obtained during an end-expiratory breath-hold. If unfeasible (i.e., younger children), most acquisitions can be performed during shallow breathing, with or without sedation, resulting in sufficient image quality. The exception would be depiction of the coronary arteries, for which apnea is usually recommended and which may require general anesthesia and suspended respiration [6]. For coronary evaluation, image quality is inversely related to heart rate so, in the absence of contraindications, beta-blockers and/or sublingual nitroglycerine are often administered to decrease heart rate to less than 80 beats per minute and increase coronary lumen [7]. In patients with pacemakers or defibrillators, device reprogramming to ensure regular heart rate during the examination may help improve image quality [6].

## Contrast Protocol

Low- or iso-osmolar iodinated contrast agents are the current standard for CTA. The contrast injection protocol is dependent on the size of the i.v. access, the target structure to be depicted/printed, and the individual anatomy. The dose is typically 1–2 ml/kg with an additional 0.5–1 ml/kg of saline flush if this is used. The injection rate is determined by the desired duration of the contrast bolus, the peripheral i.v. gauge, and the pressure limits deemed to be safe for that gauge (Table 3.1). Injection through central lines can be safely performed as long as the position of the catheter tip in relation to the vessel wall and myocardium is checked before injection and manufacturer-specific pressure limit recommendations are followed [8]. Alternatively, a hand injection can be performed.

As shown in Fig. 3.1, different combinations of contrast and saline can be used depending on the specific clinical scenario [6]. For most cases of

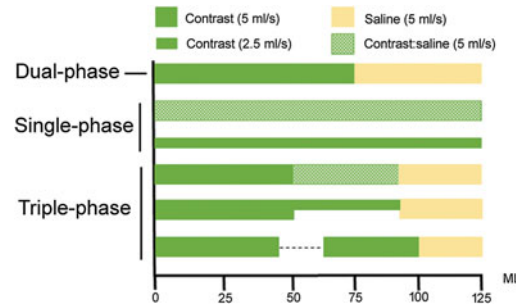


**Fig. 3.1** Schematic representation of different contrast injection protocols. The variation in contrast injection protocols is depicted, with relative volumes of contrast versus saline specified

**Table 3.1** Recommended contrast injection rates and pressure limits according to different peripheral i.v. sizes

| Gauge | Injection rate (ml/s) | Pressure limits (psi) |
|---|---|---|
| 24 | $\leq 2$ | $\leq 100$ |
| 22 | $\leq 3$ | $\leq 300$ |
| 20 | $\leq 4$ | |
| 18 | $\leq 5$ | |

Modified from Ref. [6]. *psi* pressure per square inch

simple CHD (i.e., evaluation of systemic or pulmonary vessels in the absence of shunts) or adult structural heart disease, a relatively compact bolus of contrast followed by a saline chaser (dual-phase protocol) is normally used (Fig. 3.2a). For many CHD cases where simultaneous opacification of both left and right cardiovascular structures is desired, a triple-phase protocol can be used (Fig. 3.2b). This typically comprises a faster initial injection of contrast, followed by a second slower injection and a saline chaser; alternatively, contrast injection can be followed for a mixture of contrast and saline (i.e., 60:40) at the same rate plus saline. These typically result in lower although sufficient attenuation of the pulmonary chambers compared to the systemic ones. Alternatively, a prolonged injection either of contrast alone at slower rates or contrast:saline mixture at standard rates (single-phase protocols) can result in similar although overall lower biventricular opacification. For cases where simultaneous arterial and venous evaluation is intended, an initial injection of contrast can be administered, and after a 30–60 s pause, a standard dual-phase protocol is performed, with the goal of obtaining sufficient attenuation within the arteries from the second injection and in the veins from the initial contrast bolus (triple-phase venous protocol).

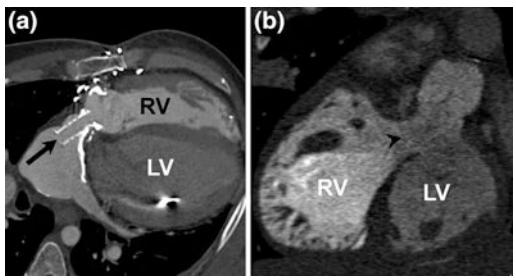


**Fig. 3.2** Examples of CTA in CHD. **a** 35-yo male with dextrotransposition of the great arteries and prior Mustard repair complicated with baffle stenosis treated percutaneously. The CTA demonstrates a widely patent stent between the left atrium and RV (*arrow*). **b** 2-yo female with double-outlet RV. The *arrowhead* indicates the ventricular septal defect. *LV* Left ventricle; *RV* right ventricle

## Image Acquisition

Timing of acquisition is determined by the arrival of the contrast to the structure(s) of interest. In most cases, a region of interest (ROI) is placed in the target chamber and acquisition begins automatically when attenuation within the ROI raises above a certain threshold (automatic bolus tracking). In cases when the path of the contrast cannot be predicted because of unknown anatomy, a test bolus with a small contrast dose can be first performed to determine the delay to its arrival to the target structure, and subsequent CTA is timed accordingly. Alternatively, contrast can be tracked real time and acquisition initiated manually when the contrast arrives to the anatomic region of interest.

Although in the past images were often obtained without electrocardiographic (ECG) synchronization because ECG gating was associated with markedly increased radiation dose, today there are several ECG-synchronized scanning modes that allow for comparable or even lower doses [9]. Thus, we routinely perform cardiac CTA with ECG gating because it reduces motion artifact and improves image quality [9]. ECG-gated acquisition can be helical (spiral) or axial [10]. In the former, the table moves continuously during acquisition, while in the latter the table is stationary during imaging and moves in between acquisitions. Four types of ECG-gated CTA are currently available [10]:

- Retrospective ECG-gated helical scan: In this scanning mode, radiation is given throughout the cardiac cycle and images are retrospectively reconstructed in the desired cardiac phase of the cardiac cycle. It has the advantages of allowing visualization of cardiac motion (cine imaging) and being more robust to arrhythmias; however, it requires higher radiation dose.
- Prospective ECG-triggered axial scan: Images are acquired in a single phase of the cardiac cycle (at a time delay from the prior QRS complex) over several heartbeats. It significantly reduces radiation exposure since X-rays are delivered in only one phase, but it

**Table 3.2** Dose reduction tools

| | |
|---|---|
| All scans | Limit scan length |
| | Reduce FOV |
| | Decrease mA |
| | Decrease kV |
| | Use iterative reconstruction |
| | Use anatomic-based current modulation (if possible) |
| | Use thicker slice collimation (if possible) |
| Retrospective helical scanning | Use ECG-based current modulation |
| Prospective axial scanning | Narrow acquisition window |

*ECG* Electrocardiogram; *FOV* field of view; *kV* kilovolts; *mA* milliamperes

is susceptible to arrhythmias and tachycardia. When used for RPT, which phase of the cardiac cycle is preferable should be determined in advance.

- Prospective ECG-triggered scan with a wide detector array (volumetric target scan mode): With a wide enough detector array (typically 320 detectors), the heart can be covered in one single heartbeat. Similarly, to the previous mode, the cardiac phase needs to be predetermined and quality is best with slow, regular heart rates.
- Prospective ECG-triggered helical scan: In scanners with two X-ray tubes, detection of the QRS can trigger a high-pitch helical scan that allows covering large anatomic areas in a short time. This technique also requires slow, steady heart rates.

Volumetric and prospective helical scans afford the lowest radiation doses and should be used whenever possible; however, both scanning modes exist only in specific scanners. Prospective axial scanning, which is available in most modern scanners, is the alternative of choice. Retrospective gating is generally avoided unless quantification of cardiac function or valvular evaluation is desired.

## Radiation Reduction

When performing cardiac CTA in general, and in infants or children in particular, it is imperative to aggressively reduce radiation exposure. As summarized in Table 3.2, a number of tools are available, and ideally as many of them in combination should be employed whenever possible [11]. Today, it is feasible to routinely perform sub-millisievert (mSv) scans in children and few mSv in adults [4, 11].

The main determinants of radiation exposure are scanned length and X-ray tube output. As a general principle, scanning should be limited to the region of interest. Some scanners allow additional dose savings if the field of view in the transverse plane is reduced. Both tube current (milliamperes or mA) and voltage (kilovolts or kV) should be adjusted to body size for every acquisition, including localizers and contrast tracking sequences. Reducing kV is the most effective way of decreasing radiation dose, and the minimum value that affords diagnostic signal-to-noise ratio should be used: This is typically 70–80 kV for neonates, infants, and young children, and 80–100 kV for older children and most adults. Milliamperes should be also minimized according to body size. Many scanners currently provide anatomic-based current modulation, by which mA, and in some scanners kV [12], are automatically increased or decreased based on the patient's specific anatomic information collected from the initial localizers; however, this implementation may not be available in ECG-gated studies. As mentioned before, volumetric [13] or prospective helical scanning [7] should be used whenever feasible. If prospective axial scanning is employed [14],

scanning window should be as narrow as possible. Retrospective ECG gating should ideally be avoided; otherwise, ECG-based tube current modulation (an implementation that only gives maximal dose during a certain phase of the cardiac cycle and minimizes it during the remaining) should be employed [7]. Newer iterative reconstruction algorithms result in significant noise reduction and allow additional reduction in tube settings [15]. Finally, while thinner slice collimations are preferred when imaging neonates or smaller structures such as valves or coronary arteries, other structures can be evaluated with thicker slices that result in reduced noise and similarly enable further dose savings. The details of considerations relevant to the performance of pediatric scans are covered in a later chapter.

## Magnetic Resonance Imaging

### Patient Selection and Preparation

When deciding whether CMR is the appropriate image modality to be utilized, MRI compatibility must be assessed of any implants, i.e., cardiac pacemakers and implanted cardiac defibrillators, or presence of metallic or ferromagnetic foreign bodies that can be subject to both thermal and mechanical forces during the scan. Other metallic devices such as stents, coils, or sternal wires may not be a contraindication to performance of the CMR, but may cause significant image artifact, rendering the dataset unusable to create a 3D virtual model. In patients such as infants or young children who are unable to breath-hold for a good quality MRA image dataset, i.v. placement with general anesthesia and intubation can be utilized. In working with the anesthesia team, an adequate breath-hold is used to allow lack of movement artifact during image acquisition. Patients who have acutely deteriorating renal function, have had nephrogenic systemic fibrosis or a previous anaphylactic reaction to a Gadolinium based contrast agent are not candidates to receive Gadolinium contrast and other imaging modalities must be considered.

### CMR Technique and Image Analysis

The ability to create 3D cardiac models from CMR allows direct visualization of complex anatomy prior to entering the operating room [16–18]. Compared to cardiac CT, CMR offers the advantages of lack of radiation exposure, better temporal resolution, and good blood to myocardium differentiation without the necessary use of intravenous contrast. Both 3D balanced steady-state free precession (bSSFP) and magnetic resonance angiography (MRA) are commonly utilized CMR 3D sequences and either may be used to create a 3D model. Our group compared the quality of models created by these sequences, given that there was no published data on the optimal CMR sequence for 3D printed cardiac models [19].

The image datasets used for this study were retrospectively collected. The settings used for both MRA and post-contrast bSSFP at our institution are detailed. CMR was performed on a 1.5-tesla General Electric scanner (GE Signa HD®, GE Medical Systems, Waukesha, Wisconsin). Gadolinium-enhanced MRA was performed during respiratory suspension after administration of 0.2 mmol/kg Magnevist® (Berlex, Montville, New Jersey) at an injection rate of 1.5–2.0 ml/s followed by a 10–20 ml saline flush. Two acquisitions were performed using a non-electrocardiogram (ECG)-gated, 3D spoiled fast gradient-echo sequence, also known as fast low-angle shot (FLASH), with the following parameters: echo time (TE) 1–2 ms, repetition time (TR) 3–5 ms, flip angle 40°, receiver bandwidth 62.5 kHz/s, rectangular field of view, coronal orientation, acquired slice thickness 2.4–3.0 mm interpolated to 1.2–1.5 mm, and matrix size adjusted to produce near-isotropic voxels with spatial resolution of ~1.6–2.8 mm. The typical breath-hold time was 15–30 s. The image acquisition was done after a delay of approximately 10 s after contrast injection, with the goal of having the contrast present in both sides of the heart.

After the contrast-enhanced MRA, ECG-gated and respiratory navigated isotropic 3D bSSFP

images were acquired in the following manner: sagittal acquisition, 224 − 192 × 224 − 192 (frequency × phase) matrix, slice thickness 2.4–3.0 mm interpolated to 1.2–1.5 mm, frequency field of view 240–300 mm with 100% FOV in the phase direction, TE 1.09–1.69 ms, TR 3.14–3.6 ms, flip angle 60°, and receiver bandwidth 125 kHz/s. Acquisition was triggered to mid-diastole, and temporal resolution was adjusted for faster heart rates. The navigator was set to acquire during end-expiration, with a tracker length of 5–10 cm and an acceptance window of 1–2 cm.

## Comparison of Models by Image Acquisition Sequence

Both blood pool and myocardial segmentation were used to create a 3D model in each of our patients from each set of either bSSFP or MRA source images resulting in 76 models categorized in four groups: Group 1—bSSFP/MS, Group 2—bSSFP/BP, Group 3—MRA/MS, and Group 4—MRA/BP (Fig. 3.3). In BP segmentation, a 1-mm-thick layer was created onto the 3D object which represented the blood pool. The 3D object was then "hollowed" internally, excluding the 1-mm layer, allowing for the intracardiac anatomy to be represented. For MS, the threshold cutoffs of gray values were set to isolate the myocardium. Once the models were created, the quality of the models using bSSFP and MRA was compared.

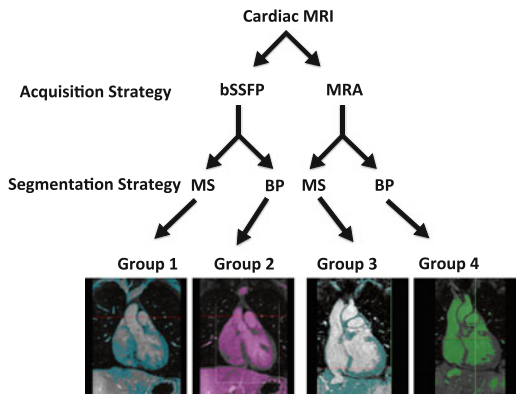


**Fig. 3.3** Variations in acquisition and segmentation strategy result in 4 virtual model groups. Magnetic resonance imaging (*MRI*), balanced steady-state free precession (*bSSFP*), magnetic resonance angiography (*MRA*), myocardial segmentation (*MS*), and blood pool segmentation (*BP*)

The overall quality of a model refers to the ability to easily recognize cardiac anatomic landmarks as well as lack of artifact. The lowest rating of 1 (Poor) was given to a model with difficult identification of heart borders and unclear origins of great arteries and venous structures. The highest rating of 3 (Excellent) was given to a model with easily identifiable borders of the heart and clearly recognizable origins of the great arteries, venous structures and ventricles. The rating of 2 (Good) was given to models with a quality that was intermediate between these two. The number of visualized vessels could range from 1 to 5 based on whether the superior vena cava, inferior vena cava, main pulmonary artery, ascending aorta, and at least one pulmonary vein could be identified (Fig. 3.4).

The overall quality rating of the models was statistically higher for those models created using BP segmentation with datasets from either contrast-enhanced MRA or post-contrast 3D bSSFP sequences. Overall, the average number of vessels visualized was also greatest using BP segmentation (Fig. 3.5).

This was a retrospective study, and as such, there was some variability in the imaging protocols used in different patients. Although the interpolated slice thickness for the datasets we used was 1.2–1.5 mm, and many of the models were of reasonable quality, the goal is to acquire images with the highest spatial resolution while maintaining adequate signal-to-noise and imaging (breath-holding) times. Some protocols recommend a slice thickness as thin as 0.3 mm for model creation. We only included two sequences commonly used in clinical practice: non-ECG-gated MRA and ECG-gated and respiratory navigated bSSFP. We did not find significant differences between these 2 techniques for image quality or vessel visualization, which may be related to sample size limitations. In theory, bSSFP should be advantageous to use since acquisition is typically ECG gated; therefore,

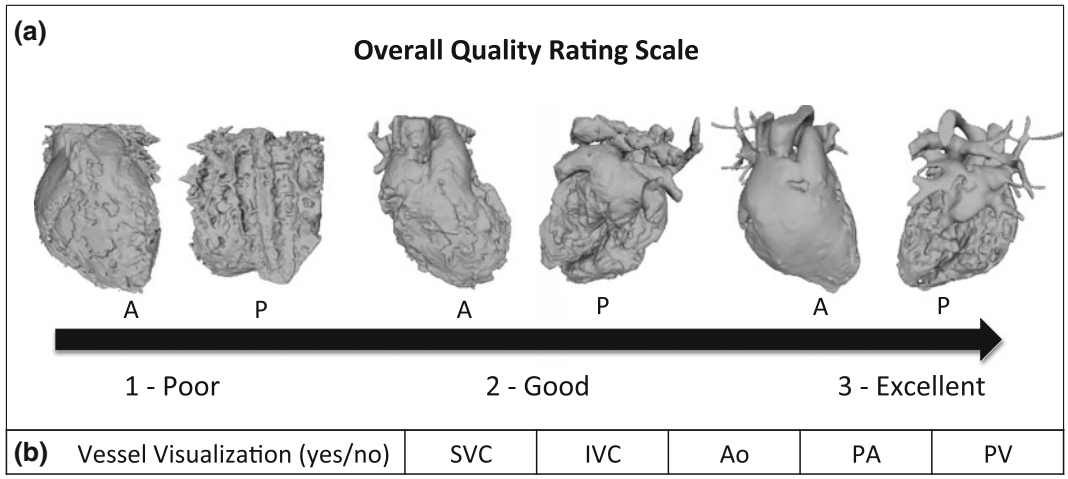


**Fig. 3.4** Examples of models assigned to each rating category for overall quality. **a** A sample model is shown for each rating category with the quality increasing *from left to right*, as viewed anteriorly (*A*) and posteriorly (*P*). **b** The type of vessels evaluated for visualization is listed

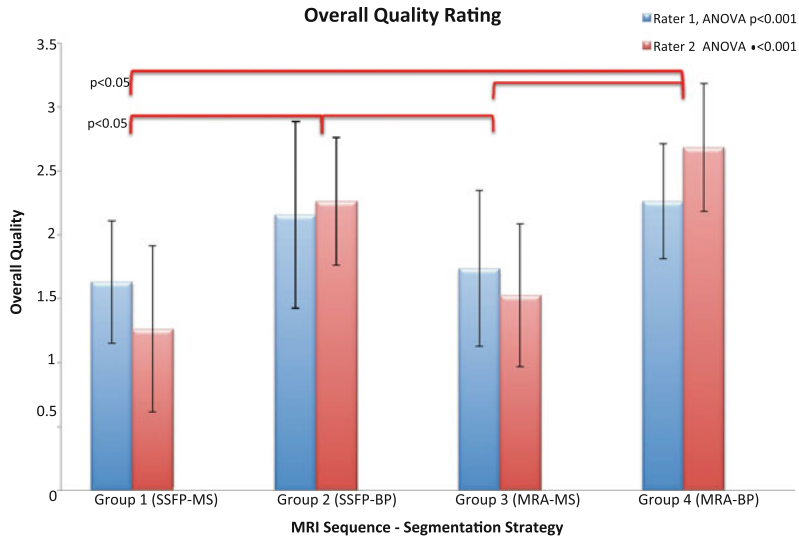


**Fig. 3.5** The results for ratings for overall quality and vessels visualized are graphically demonstrated. Groups with statistically significant differences in rating are indicated with the red brackets. **a** The overall quality rating for both Rater 1 (*blue*) and Rater 2 (*red*) is demonstrated. The BP Groups (2 and 4) had highest overall quality ($p < 0.05$). **b** The BP Groups (2 and 4) had had the highest numbers of vessels visualized ($p < 0.05$)

intracardiac anatomy is more sharply depicted. However, MRA may be better suited to depict extracardiac structures given its inherent higher contrast-to-noise ratio. Moreover, we cannot extrapolate these findings to ECG-gated MRA techniques [20] or to pre-contrast bSSFP sequences that would be expected to have lower blood contrast-to-noise ratio [21].

We excluded patients that had severe artifacts, as high-quality source datasets remain mandatory

for successful segmentation. Finally, most of our patients were cooperative adults with relatively simple disease. The ability of CMR datasets to generate successful 3D models in infants or small children with complex disease has yet to be fully explored and is a critical, active area of research.

Given these findings, it is reasonable to use either post-contrast bSSFP or MRA as source datasets for model creation in patients for whom CMR is an appropriate study to perform. Spatial resolution should be as high as is attainable with consideration being given to signal-to-noise and image acquisition time, with isotropic or near-isotropic voxels. Whenever possible, it is advisable to run both sequences allowing for there to be options available to choose the dataset of better quality for post-processing.

## Echocardiography

3D echocardiography became a reality after the year 2000 with the advent of matrix array transducers [22]. Since then, its utilization has become more routine in many practices. It is being used for a wide range of applications, including congenital cardiac abnormalities, assessment of atrioventricular valves, septal defects, and complex intraventricular baffles [23, 24]. Advantages to use of this technology have been reported in the assessment of chamber size, volume, segmental and global function, morphology of valves, and valve function when used in conjunction with color Doppler. Although 3D echocardiography allows some assessment of spatial relationships, the images are limited in that they are displayed in two dimensions with the perception of depth created using various color scale alterations [24–26]. Applying 3D printing technology to 3D echocardiographic images offers visualization of cardiac anatomy in true 3D [27, 28]. The steps involved in creating a 3D printed model from a 3D echocardiography dataset are as follows:

1. Define details of the cardiac anatomy using two-dimensional echocardiography.
2. Optimize the imaging window to negate any artifacts and to get the best resolution image of the region of interest.
3. Acquire a high-resolution 3D volume dataset of the structure of interest incorporating an adjacent anatomic localizer (example: aortic valve with the ventricular septum).
4. The 3D image data at a single time point (mid-systole or end diastole) can then be further analyzed by converting to DICOM format.
5. Image segmentation software is used to create a 3D virtual cardiac model by highlighting the region of interest [28–31].
6. The virtual file can then be exported in a 3D file format, such as .STL, for printing.

### Patient Preparation

Ensuring that the patient is calm and comfortable are key in establishing minimal variations in heart rate and respiratory motion. In an intubated patient, imaging data can be optimized by suspending respiration thereby minimizing translational motion of the heart as well as beat-to-beat variability in cardiac cycle length. Younger patients may require sedation to allow for good quality image acquisition.

### Image Acquisition

A high-resolution 3D dataset requires the data to be captured over multiple cardiac cycles and minimization of stitch artifact. Single-beat volume acquisitions can also be performed, albeit at the expense of frame rate and resolution. Data from transesophageal versus transthoracic windows have an advantage of minimal artifact and acoustic interference from chest wall and lungs. Transthoracic 3D acquisition can be performed from the window (apical, parasternal, and sub-xiphoid) that provides the best far-field resolution and minimal near-field noise and eliminates artifacts. Transesophageal echocardiography, if and when

available, provides excellent resolution for mitral and aortic valve imaging but is limited in its field of view.

3D echocardiography at our center is routinely performed using a Philips system and appropriate 3D transthoracic (X5-1 and X7-2) or transesophageal (X7-2t) transducers (Philips Medical Systems, Andover, MA). 3D transesophageal imaging is limited to those with body weight more than 20 kg. Identifying the specific anatomy of interest is paramount prior to image acquisition so that the correct structural details can be elicited. Imaging the heart as a full-volume dataset will result in a lower frame rate and temporal resolution. Optimizing temporal resolution and not sacrificing spatial resolution is key to obtaining a usable dataset. As described in the publication by Olivieri et al. [27], a full-volume acquisition of the heart yielded 4–5 frame rates of data. In cases where the goal is to obtain images of a valve and the valve apparatus, one can increase the temporal resolution (volumes per second) by minimizing depth with focus on the region of interest, optimizing sector width (narrow angle) and elevation, and then doing a full-volume multiple beat acquisition. The disadvantage of a multiple beat full-volume acquisition is the artifact produced by respiratory and heart rate variations. Images should be examined after acquisition for such artifacts. In cases in which they are unavoidable, a single-beat or a live 3D volume dataset will need to be acquired. Adjusting the loop to a specific segment of the cardiac cycle (i.e., diastole) will also increase the temporal resolution.

After the structure that needs to be imaged for 3D printing is in view, optimizing the window and adjusting the gray scale with the 2D image should be a priority. The goal is to make the blood pool as dark as possible to contrast with the bright myocardium. This can be done with manipulation of the dynamic range or compression (between 40 and 50 dB). Adjusting the overall 2D gain will allow distant background structures to have a blue tint and near-field structures to be in well-defined chrome. Care should be taken not to be overly aggressive about increasing the tissue 2D contrast as one can lose definition of fine chordal structures and boundaries of septal defects. Atrial and ventricular septal anatomy as well as complex intracardiac anatomy can be imaged using the i-crop mode with full-volume acquisition or with narrow sector 3D live or zoom mode on the Philips systems. Once an acceptable 3D dataset has been stored, it should be exported in Cartesian DICOM format and can then be imported into post-processing software for virtual model creation.

## References


1. Shiraishi I, Yamagishi M, Hamaoka K, Fukuzawa M, Yagihara T. Simulative operation on congenital heart disease using rubber-like urethane stereolithographic biomodels based on 3D datasets of multislice computed tomography. Eur J Cardiothorac Surg. 2010;37(2):302.
2. Greil GF, Wolf I, Kuettner A, et al. Stereolithographic reproduction of complex cardiac morphology based on high spatial resolution imaging. Clin Res Cardiol. 2007;96(3):176.
3. Maragiannis D, Jackson MS, Igo SR, et al. Replicating patient-specific severe aortic valve stenosis with functional 3D modeling. Circ Cardiovasc Imaging. 2015;8(10):e003626.
4. Han BK, Rigsby CK, Hlavacek A, et al. Computed tomography imaging in patients with congenital heart disease part I: rationale and utility. An expert consensus document of the society of Cardiovascular Computed Tomography (SCCT): endorsed by the Society of Pediatric Radiology (SPR) and the north American Society of Cardiac Imaging (NASCI). J Cardiovasc Comput Tomogr. 2015;9(6):475.
5. American College of Cardiology Foundation Task Force on Expert Consensus D, Hundley WG, Bluemke DA et al. ACCF/ACR/AHA/NASCI/SCMR 2010 expert consensus document on cardiovascular magnetic resonance: a report of the American College of Cardiology Foundation task force on expert consensus documents. J Am Coll Cardiol. 2010;55(23):2614.
6. Han BK, Rigsby CK, Leipsic J, et al. Computed tomography imaging in patients with congenital heart disease, part 2: technical recommendations. An expert consensus document of the society of Cardiovascular Computed Tomography (SCCT): Endorsed by the Society of Pediatric Radiology (SPR) and the North American Society of Cardiac Imaging (NASCI). J Cardiovasc Comput Tomogr. 2015;9(6):493.
7. Han BK, Lindberg J, Overman D, et al. Safety and accuracy of dual-source coronary computed

tomography angiography in the pediatric population. J Cardiovasc Comput Tomogr. 2012;6(4):252.
8. Rigsby CK, Gasber E, Seshadri R, et al. Safety and efficacy of pressure-limited power injection of iodinated contrast medium through central lines in children. AJR Am J Roentgenol. 2007;188(3):726.
9. Shuman WP, Leipsic JA, Busey JM, et al. Prospectively ECG gated CT pulmonary angiography versus helical ungated CT pulmonary angiography: impact on cardiac related motion artifacts and patient radiation dose. Eur J Radiol. 2012;81(9):2444.
10. Halliburton S, Arbab-Zadeh A, Dey D, et al. State-of-the-art in CT hardware and scan modes for cardiovascular CT. J Cardiovasc Comput Tomogr. 2012;6(3):154.
11. Halliburton SS, Abbara S, Chen MY, et al. SCCT guidelines on radiation dose and dose-optimization strategies in cardiovascular CT. J Cardiovasc Comput Tomogr. 2011;5(4):198.
12. Siegel MJ, Hildebolt C, Bradley D. Effects of automated kilovoltage selection technology on contrast-enhanced pediatric CT and CT angiography. Radiology. 2013;268(2):538.
13. Jadhav SP, Golriz F, Atweh LA, Zhang W, Krishnamurthy R. CT angiography of neonates and infants: comparison of radiation dose and image quality of target mode prospectively ECG-gated 320-MDCT and ungated helical 64-MDCT. AJR Am J Roentgenol. 2015;204(2):W184.
14. Huang MP, Liang CH, Zhao ZJ, et al. Evaluation of image quality and radiation dose at prospective ECG-triggered axial 256-slice multi-detector CT in infants with congenital heart disease. Pediatr Radiol. 2011;41(7):858.
15. Son SS, Choo KS, Jeon UB, et al. Image quality of CT angiography with model-based iterative reconstruction in young children with congenital heart disease: comparison with filtered back projection and adaptive statistical iterative reconstruction. Int J Cardiovasc Imaging. 2015;31(Suppl 1):31.
16. Mottl-Link S, Hübler M, Kühne T, Rietdorf U, Krueger JJ, Schnackenburg B, et al. Physical models aiding in complex congenital heart surgery. Ann Thorac Surg. 2008;86(1):273–7.
17. Vranicar M, Gregory W, Douglas WI, Di Sessa P, Di Sessa TG. The use of stereolithographic hand held models for evaluation of congenital anomalies of the great arteries. Stud Health Technol Inform. 2008;132:538–43.
18. Farooqi KM, Nielsen JC, Uppu SC, Srivastava S, Parness I, Sanz J, Nguyen K. Use of 3D printing to demonstrate complex intra-cardiac relationships in double outlet right ventricle for surgical planning. Circ Cardiovasc Imaging. 2015;8(5):e003043.
19. Farooqi KM, Gonzalez-Lengua C, Weinberg AD, Nielsen JC, Sanz J. Blood pool segmentation results in superior virtual cardiac models than myocardial segmentation for 3D printing. Pediatr Cardiol. 2016.
20. Groves EM, Bireley W, Dill K, Carroll TJ, Carr JC. Quantitative analysis of ECG-gated high-resolution contrast-enhanced MR angiography of the thoracic aorta. AJR Am J Roentgenol. 2007;188(2):522–8.
21. Foo TK, Ho VB, Marcos HB, Hood MN, Choyke PL. MR angiography using steady-state free precession. Magn Reson Med. 2002;48(4):699–706.
22. Lang RM, Badano LP, Tsang W, Adams DH, Agricola E, Buck T, et al. EAE/ASE recommendations for image acquisition and display using three-dimensional echocardiography. Eur Heart J Cardiovasc Imaging. 2012;13(1):1–46.
23. Roberson DA, Cui W, Patel D, Tsang W, Sugeng L, Weinert L, et al. Three-dimensional transesophageal echocardiography of atrial septal defect: a qualitative and quantitative anatomic study. J Am Soc Echocardiogr. 2011;24(6):600–10.
24. Pushparajah K, Miller OI, Simpson JM. 3D echocardiography of the atrial septum: anatomical features and landmarks for the echocardiographer. JACC Cardiovasc Imaging. 2010;3(9):981–4.
25. Simpson JM, Miller O. Three-dimensional echocardiography in congenital heart disease. Arch Cardiovasc Dis. 2011;104(1):45–56.
26. Lang RM, Badano LP, Tsang W, Adams DH, Agricola E, Buck T, et al. EAE/ASE recommendations for image acquisition and display using three-dimensional echocardiography. J Am Soc Echocardiogr. 2012;25(1):3–46.
27. Olivieri LJ, Krieger A, Loke YH, Nath DS, Kim PC, Sable CA. Three-dimensional printing of intracardiac defects from three-dimensional echocardiographic images: feasibility and relative accuracy. J Am Soc Echocardiogr. 2015;28(4):392–7.
28. Witschey WR, Pouch AM, McGarvey JR, Ikeuchi K, Contijoch F, Levack MM, et al. Three-dimensional ultrasound-derived physical mitral valve modeling. Ann Thorac Surg. 2014;98(2):691–4.
29. Pouch AM, Yushkevich PA, Jackson BM, Jassar AS, Vergnat M, Gorman JH, et al. Development of a semi-automated method for mitral valve modeling with medial axis representation using 3D ultrasound. Med Phys. 2012;39(2):933–50.
30. Pouch AM, Wang H, Takabe M, Jackson BM, Gorman JH 3rd, Gorman RC, et al. Fully automatic segmentation of the mitral leaflets in 3D transesophageal echocardiographic images using multi-atlas joint label fusion and deformable medial modeling. Med Image Anal. 2014;18(1):118–29.
31. Pouch AM, Xu C, Yushkevich PA, Jassar AS, Vergnat M, Gorman JH 3rd, et al. Semi-automated mitral valve morphometry and computational stress analysis using 3D ultrasound. J Biomech. 2012;45(5):903–7.

# Postprocessing: Software and Technique Options

4

Juan-Carlos G. Muñiz, MD

## Image Characteristics

3D models can be created from nearly any medical imaging modality that produces volumetric datasets. The most common modalities used to make 3D heart models are computed tomography (CT) and magnetic resonance imaging (MRI). Less frequently used are echocardiographic (ultrasound, or US) images. All of these modalities can be used for clinical imaging in even the smallest and youngest of patients with congenital heart defects (Fig. 4.1) [1, 2].

Modern digital imaging systems store images primarily in DICOM format. Regardless of modality, digital images are displayed as a matrix of pixels. Pixels are two-dimensional (2D) boxes that vary in brightness or attenuation based on the characteristics of the tissue they represent. The intensity of a particular tissue depends on the imaging modality used. For example, blood is bright on contrast-enhanced CT images, dark on echo images, and on MRI varies by the type of sequence used.

2D image slices are stacked in order to form a 3D volumetric dataset. 3D pixels are known as voxels. Isotropic voxels have equal or nearly equal size in the $x$, $y$, and $z$ dimensions. The cubical nature of isotropic or near-isotropic voxels allows for the image to be reconstructed in any plane, including oblique views, without distortion.

## Cardiac Imaging Modalities

Computed Tomography

Contemporary multidetector-row CT scanners acquire stacks of thin axial slices with isotropic resolution. CT angiography (CTA) employs intravenously administered contrast to improve visualization of blood-filled structures. CTA images obtained on modern high-pitch scanners allow for excellent visualization of cardiac tissue, vasculature, and extracardiac structures. CT has the advantage of high spatial and temporal resolution. Scan time is very short, resulting in increased availability and the ability to scan younger patients with minimal or no sedation. Two main disadvantages of CT are radiation exposure and the use of iodinated contrast, which has important nephrotoxic and allergic side effects [3].

Magnetic Resonance Imaging

Cardiac MRI examinations employ a wide variety of imaging sequences. Most sequences are obtained as bright-blood cine or black blood still images in specific cardiac planes. These images are typically non-isotropic and vary in thickness from 3 to 10 mm. However, high-resolution electrocardiogram (ECG)-gated 3D balanced steady-state free precession

J.-C.G. Muñiz (✉)
Division of Cardiology, Nicklaus Children's Hospital, Miami, FL, USA
e-mail: juan.muniz@mch.org

J.-C.G. Muñiz
Department of Pediatrics, Herbert Wertheim College of Medicine, Florida International University, Miami, FL, USA


K.M. Farooqi (ed.), *Rapid Prototyping in Cardiac Disease*,
DOI 10.1007/978-3-319-53523-4_4

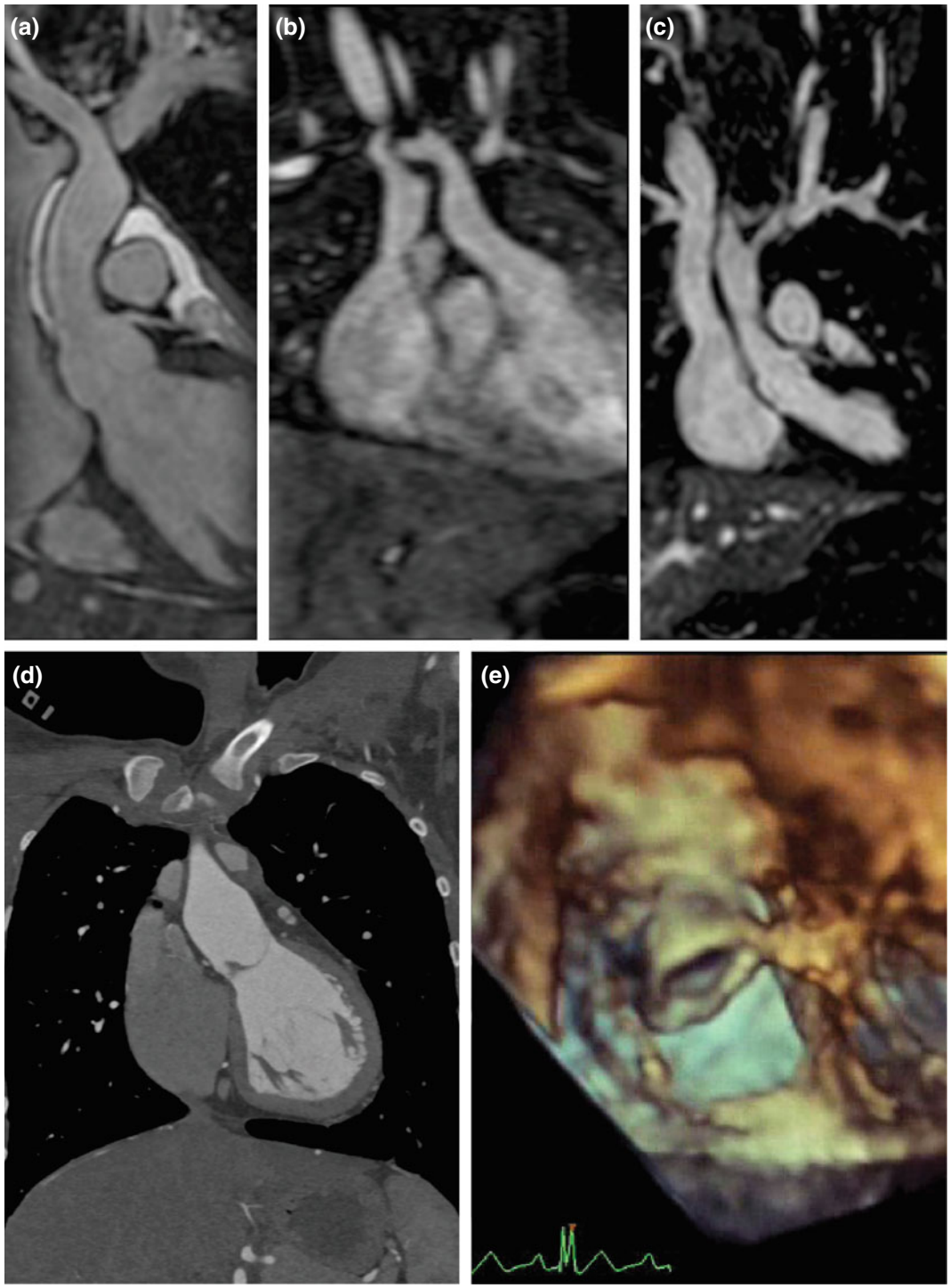


**Fig. 4.1** Image types used for 3D modeling. **a** MRI 3D-SSFP. **b** MRA. **c** MRI 3D-IR. **d** CTA. **e** 3D echo

(3D-SSFP) and 3D inversion recovery (3D-IR) sequences can be obtained isotropically. Like CT, 3D-SSFP and 3D-IR datasets allow for high-resolution visualization of cardiac tissue and vasculature. Contrast-enhanced 3D magnetic resonance angiogram (MRA) sequences can also be reconstructed isotropically and tend to produce superior vascular imaging compared to 3D-SSFP and 3D-IR sequences. They do, however, suffer in delineation of intracardiac anatomy due to lack of ECG gating. Compared to CT, MRI does not employ ionizing radiation, not all sequences require contrast, and the contrast used has a lower rate of idiosyncratic reactions. MRI suffers from decreased spatial resolution compared to CT. Imaging takes longer and often requires sedation and general anesthesia in younger patients. Images are also susceptible to ferromagnetic and flow-related artifacts [4].

3D Echocardiography

Modern commercial echocardiographic equipment now routinely has the capability to obtain 3D volumetric datasets using both transthoracic and transesophageal probes. Images can be acquired in real time or can be stitched together over multiple heartbeats to increase temporal resolution and the size of the image volume. In general, US has high temporal and spatial resolution that allows for excellent visualization of intracardiac anatomy, particularly in pediatric patients. In particular, imaging of heart valves is superior, and imaging of extracardiac vascular structures inferior, to CT and MRI. US suffers from limitations due to poor acoustic windows, limited penetration, and a relatively small field of view. Compared to CT and MRI, US is low-cost, portable, widely available, does not require radiation or contrast, and does not always require sedation in young patients. [5–7]

Traditionally, images from a single modality have been used in preparing individual models. More recently, groups have begun to describe hybrid models making use of CT or MRI data for the bulk of intracardiac anatomy, combined US data focused on the heart valves [8].

Regardless of modality, images used for 3D modeling should be isotropic or near-isotropic and high-resolution. Accurate and efficient modeling is also dependent on uniform and clear image contrast. Thinner slices generally allow for higher spatial resolution and decreased partial volume effects; however, they may suffer from decreased signal-to-noise ratio and also take longer to process.

## Basic Principles of Segmentation

In order to create a 3D model, image data to be used in the final model must be separated from extraneous data. This is achieved through the process of segmentation. Segmentation involves assigning labels to individual pixels within a DICOM image. Pixels representing a particular tissue (e.g., blood pool, myocardium) can be grouped together into masks, thus separating them from pixels representing tissue that is not of interest (e.g., bone, lung).

Successful segmentation relies on images with high spatial and contrast resolution. Contrast resolution is the ability to differentiate between different tissue types. Blood pool must be differentiated from cardiac tissues, and cardiac tissues from adjacent structures such as thymus, chest wall, lung, diaphragm, and liver. Image contrast differs between imaging modalities, and within modalities based on imaging technique and sequence. For example, CTA may yield higher blood–myocardium contrast than 3D-SSFP, yet 3D-SSFP may have higher myocardium–liver contrast. Individual CTA examinations may differ in myocardium–blood contrast due to differences in technical factors such as radiation dose, as well as timing, and density of contrast administration.

Several approaches to segmentation exist and vary based on the intended purpose of the model (Fig. 4.2). Vascular only models tend to be the easiest and most efficient to produce, as they only require segmentation of the vascular lumen. Segmentation here is simplified by the relatively high contrast between blood and extravascular tissue, particularly on CTA, 3D-SSFP, 3D-IR, and MRA sequences.

The generation of models depicting intracardiac anatomy poses a different set of challenges.

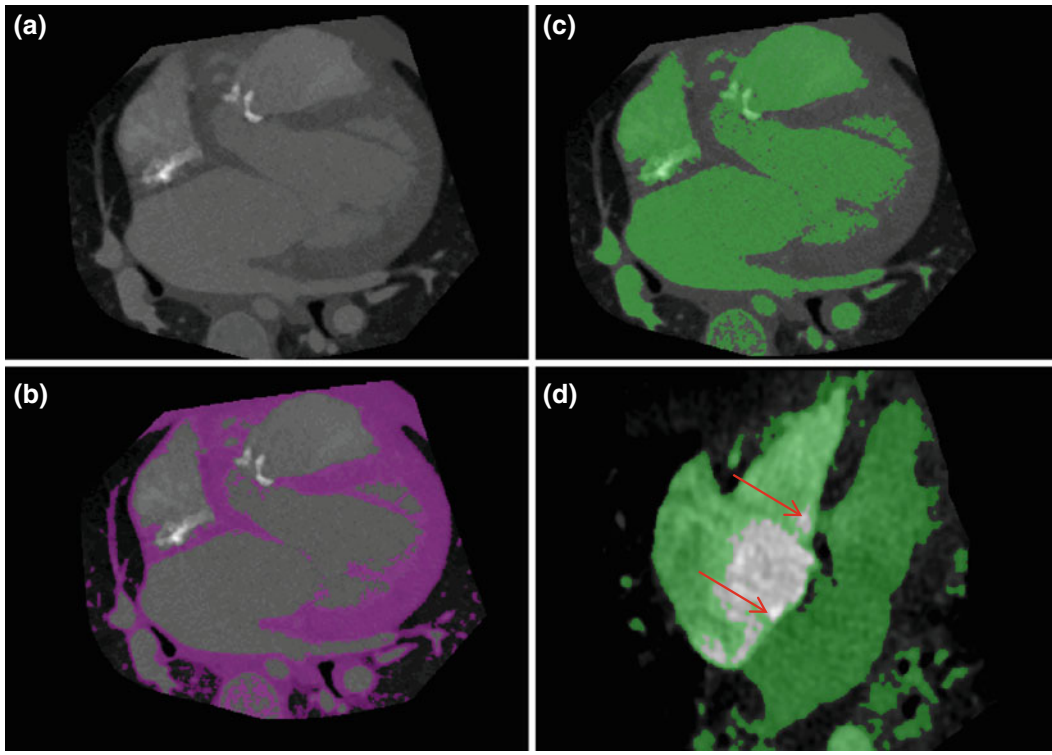


**Fig. 4.2** Segmentation techniques. **a** Source image, axial CTA. **b** Myocardial segmentation. Note how with myocardial segmentation the border between the epicardium and extracardiac tissue is difficult to distinguish, particularly anteriorly and posteriorly. **c** Blood pool segmentation. **d** Errors in segmentation. *Arrows* point to unmasked areas of atrial and ventricular septum. Once modeled, these "bridges" will appear as septal defects

Segmentation of cardiac tissue and myocardium is possible but can be difficult and time-consuming, primarily due to lack of contrast between myocardium and adjacent epicardial structures. This finding is true for both CT and MR images.

One commonly employed method to circumvent this problem is the "hollow shell" method, which relies on blood pool segmentation rather than myocardial segmentation (Fig. 4.3). This method is based on the principle that the outer contour of an intracardiac blood pool mask is the negative impression of the endocardial surface, much in the same way that a cast is an impression of the inner surface of the mold. If a shell (or "mold") is created around the outer surface of the blood pool ("cast"), then the inner surface of the shell will replicate the endocardial surface. The blood pool mask is then removed to reveal this surface. It is important to note that because the thickness of the shell is applied arbitrarily and uniformly, it does not provide a true representation of the actual wall of the heart and the vessels. However, the general shape of the heart and vessel wall is maintained, and this creates an aesthetically pleasing representation of the surface of the heart.

## Postprocessing Software

Software functionalities required for postprocessing and creation of 3D models are DICOM viewing, DICOM editing, DICOM segmentation, STL file creation, and STL file editing. Image viewing is the ability to display and manipulate DICOM images, and is an essential component of all software packages mentioned. Image editing is the ability to alter DICOM images. The most common editing task is the

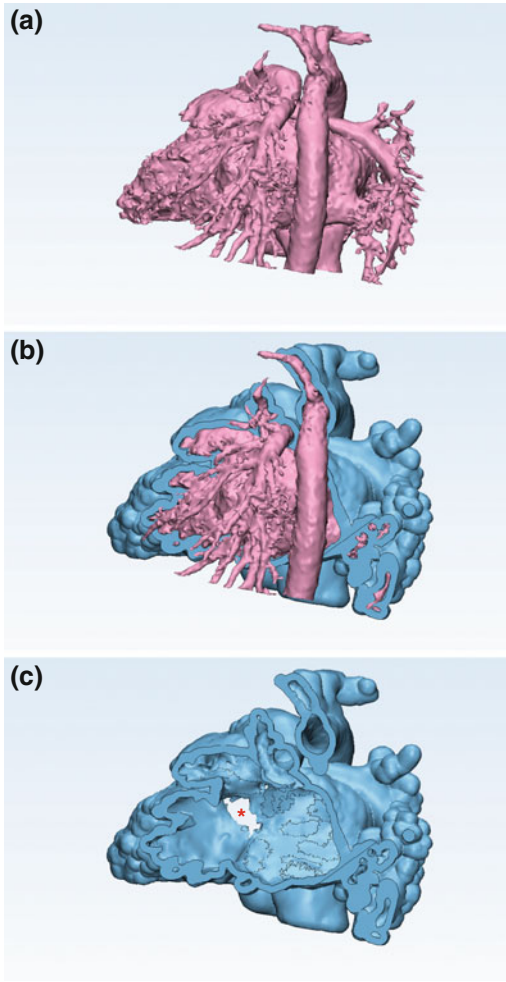


**Fig. 4.3** "Hollow shell" intracardiac segmentation method. **a** STL model of the blood pool mask in a patient with TGA and VSD. The blood pool is viewed from a posterior angle. **b** A shell of arbitrary thickness is applied to the outer surface of the blood pool. **c** The blood pool mask is removed. The inner surface of the shell represents the endocardial surface, note the VSD*. Also note that the exterior surface of the shell does not represent the true epicardial surface

removal of unwanted portions of the image in order to simplify segmentation. Segmentation creates masks that are exported as 3D models in STL format. The STL model may be further edited and optimized for printing or visualization using computer-aided design (CAD) software.

These processes may be performed using a variety of commercial and open-source software packages. The most common programs reported in the scientific literature are Mimics and 3-Matic, Windows-based commercial software made by Materialise (Leuven, Belgium) [9]. Mimics has advanced manual, automated, and semiautomated segmentation functions and the ability to export STL files. 3-Matic is a CAD software that performs advanced STL editing.

Other freeware and open-source software solutions exist. Osirix (Pixmeo, Geneva, Switzerland) is a freeware, a Mac-based open-source image processing software. It performs advanced DICOM viewing and editing functions. It can also perform basic segmentation and has the ability to export STL files. ITK-SNAP (www.itksnap.org), 3D slicer (www.slicer.org), and Seg3D (www.sci.utah.edu/cibc-software/seg3d.html) are free open-source multiplatform solutions for segmentation of medical images and STL creation. Meshlab (meshlab.sourceforge.net) and Netfabb Basic (www.netfabb.com) are free open-source multiplatform solutions for STL editing.

## Postprocessing Technique

The following section describes a sample process based mainly on the use of Osirix and Materialise software. As mentioned above, many other software options exist that provide similar functionality.

### Initial Image Preparation

The original DICOM data is first displayed in a multiformat display that can show standard orthogonal (axial, sagittal, coronal) or oblique planes as well as a maximum intensity projection (MIP) and 3D virtual reconstructions (3D VR). The task of image segmentation can be made simpler and more efficient by employing basic editing tools to remove large portions of unwanted pixels from the medical image

(Fig. 4.4). This simplifies the segmentation process by confining less efficient advanced tools to the area of interest. Depending on the software used, edited data are either deleted entirely from the source image, or kept and excluded from further processing.

## Cropping

Cropping is a basic task that removes the outer portions of an image. Cropping can be applied selectively in standard orthogonal planes to easily remove unwanted structures in bulk from edges of

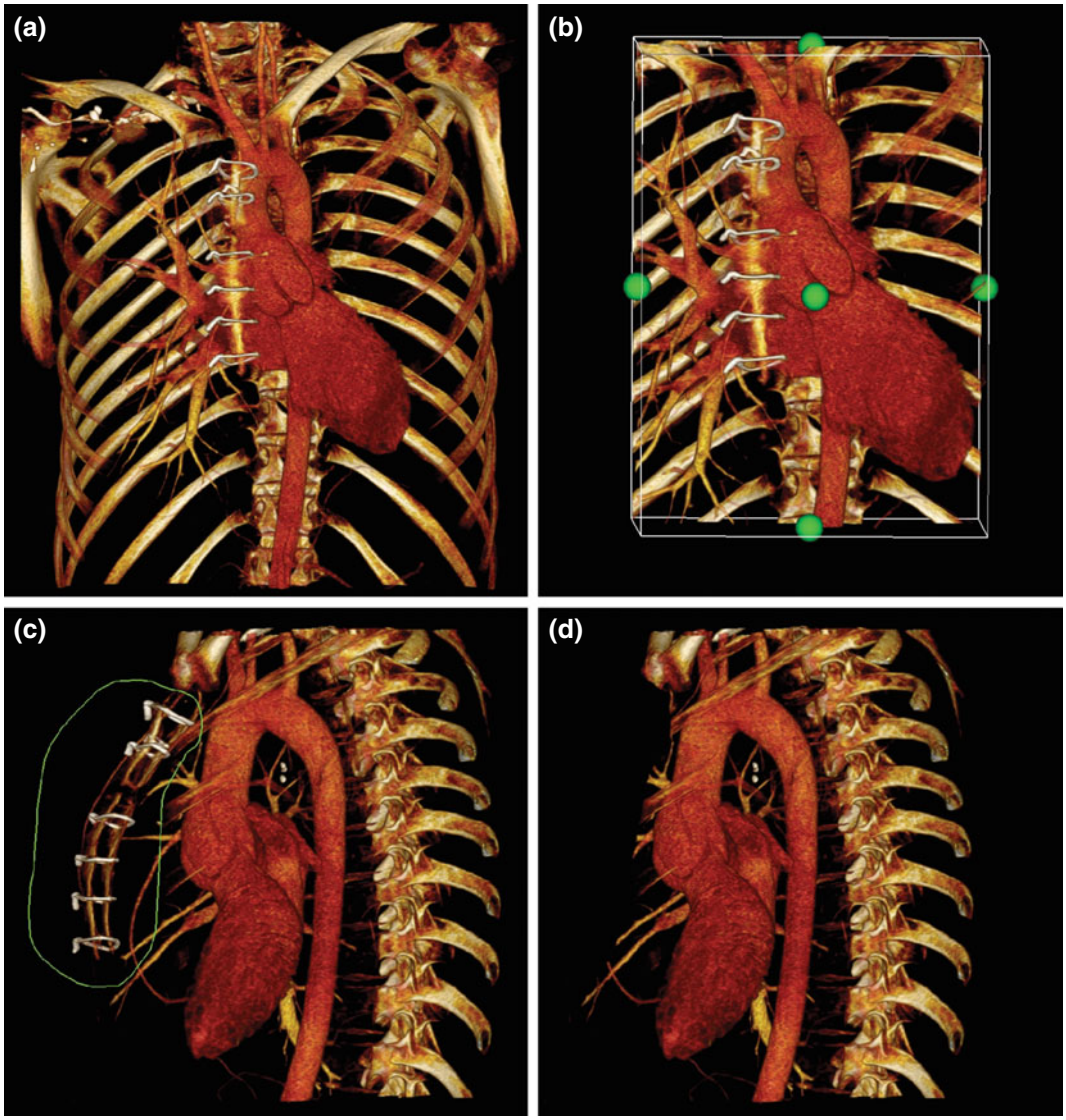


**Fig. 4.4** Image preparation, **a** 3D Virtual reconstruction. **b** Cropping applied laterally and supero-inferiorly. **c** Sculpting of sternum. **d** After sculpting of sternum

the image. For example, lateral cropping is useful for removing arms, rib cage, and peripheral vasculature. Antero-posterior cropping can remove spine, sternum, and sternal wires. Supero-inferior cropping can remove neck and abdomen. Care must be taken to scroll through the entire region of interest before applying cropping, as cardiac structures may cross into the crop plane at different levels. Cropping can be performed in both the 2D image space or on 3D VRs.

### Sculpting

One limitation of cropping is that data removal occurs in a linear fashion along the main anatomical planes. Invariably, unwanted structures that exist in the same plane as cardiac and vascular structures cannot be removed using this technique. Sculpting is a tool that allows for wholesale removal of portions of the image using user-defined regions of interest (ROIs) that can encompass more complex and irregular shapes. 3D sculpting is performed on a 3D VR and extends the ROI removal through the entire volume of the image, making the process less labor-intensive than performing sculpting on individual 2D slices.

### Bone Removal

Bone displays very brightly (high Hounsfield units) on CT images due to its high radiodensity. Many commonly used postprocessing software solutions allow for automatic bone removal based on this property. Vascular structures dense with contrast may have similar Hounsfield values to bone, and care must be taken to not inadvertently remove these structures when performing automated bone removal. In this case, bone should be removed using sculpting techniques mentioned above.

### Segmentation

Once the bulk of unwanted tissue is removed from the original image, the process of segmentation may proceed. As described previously, segmentation is the process of assigning labels to individual pixels within a DICOM image. Pixels representing a particular tissue (e.g., blood pool, myocardium) can be lumped together into groups called masks. Individual masks may be combined with other masks or split arbitrarily. For example, all pixels representing blood on a CT angiogram can be labeled in a large mask called "blood pool." This "blood pool" mask can be further subdivided into smaller individual masks such as "right atrium," "right ventricle," "pulmonary artery," "left atrium," "left ventricle," and "aorta." Conversely, individual masks such as "left atrium" and "left ventricle" can be arbitrarily combined into larger masks such as "left heart."

### Thresholding

Thresholding is usually the first step employed in the process of image segmentation. This process creates a mask that contains all the pixels in the image within an adjustable range of intensity (Hounsfield unit range). Thresholding is most commonly applied in a range that selects either blood pool or myocardial tissue (Fig. 4.5). A limitation of this technique occurs when there is low tissue contrast resulting in overlap between different tissues such as myocardium and thymus, blood pool and bone, or blood pool and myocardium. The upper and the lower limits of the threshold range can be manually adjusted to remove such overlap. Usually, compromises must be made in these adjustments. Broadening the threshold range includes all target tissue at the expense of including unwanted tissue.

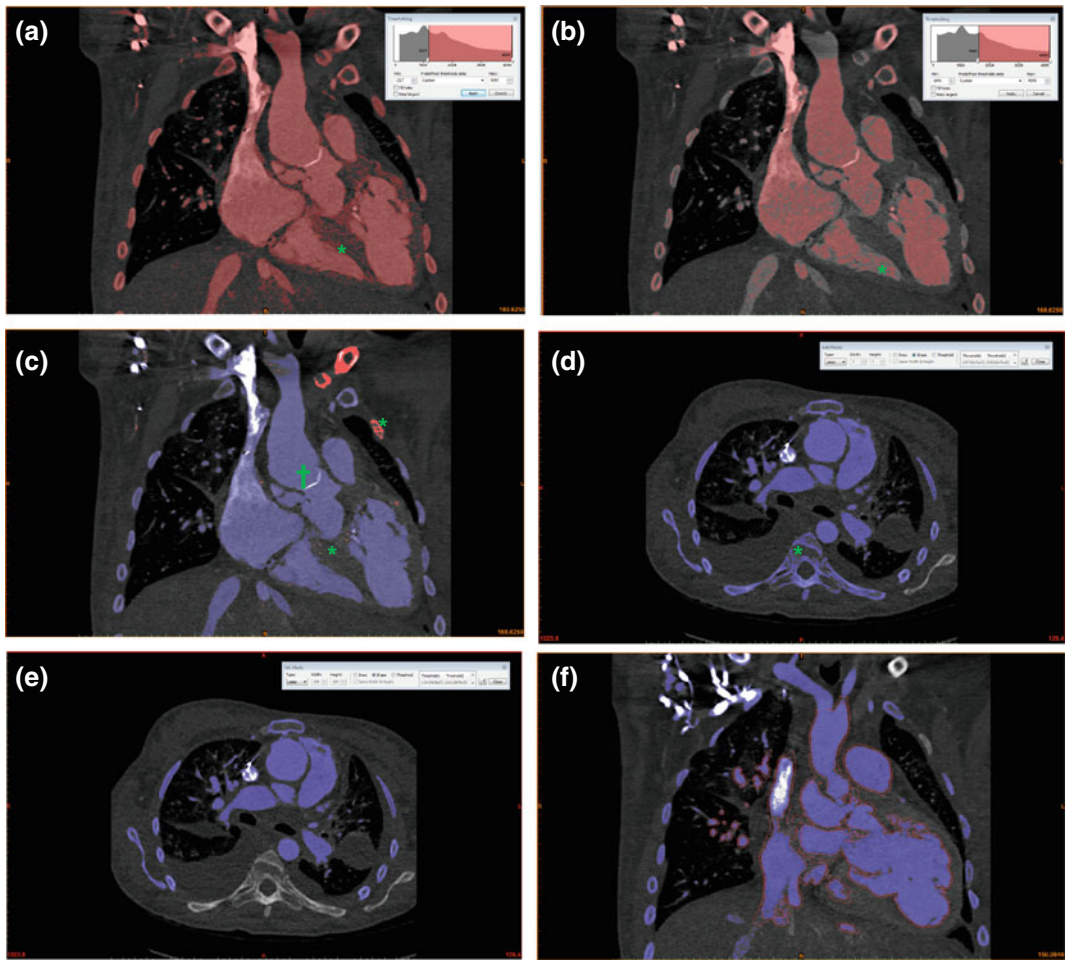


**Fig. 4.5** Segmentation techniques. **a** Thresholding the blood pool. If the range is set too broadly, then myocardium and bone (*asterisk*) will be selected along with blood pool. **b** If the range is set too narrow, then myocardium is excluded at the expense of also excluding portions of blood pool (*asterisk*). **c** Region growing helps to exclude portions of the mask that are not in continuity with the area of interest. In this case region growing of the blood pool has helped to exclude some bony structures and myocardial tissue (*asterisk*). Note also that the prosthetic aortic valve (*dagger*) is now also correctly excluded from the blood pool. Areas that cannot be removed using automated techniques must be removed manually. **d**, **e** A vertebral body (*asterisk*) is removed using mask editing tools. **f** Once the STL file (represented by the red contour) is created and edited, it should be checked against the source image to ensure accuracy

Conversely, narrowing will help exclude all unwanted tissue at the expense of also excluding portions of wanted tissue. In most cases, further refinement of the mask is required, involving techniques such as region growing, and manual and semiautomated editing of masks.

## Region Growing

When thresholding is applied to an image, it will select all in-range pixels regardless of whether they are in continuity with the tissue of interest or not. Region growing tools allow for refinement of

a threshold mask. A seed point is selected, and only those parts of the mask in continuity with the seed point are selected. "Floating" pixels and non-continuous objects are thus excluded from the segment mask. Non-continuous objects may include sternum and ribs that share intensity values that overlap with the blood pool on CT images.

### Editing Masks

Once thresholding and region growing have been performed, further refinement of the mask often involves manual and semiautomated editing. Manual segmentation at its most basic involves using cursors of different sizes and shapes as "paintbrushes" or "erasers" to either directly add or remove pixels from a mask. More sophisticated techniques add thresholding functions to these cursors, i.e., unmasked pixels with intensity within the specified range, will be added, and masked pixels outside of the threshold range will be removed.

Manual segmentation is often required for very thin structures that are not recognized by automated thresholding techniques. Such thin structures may include the atrial septum, membranous ventricular septum, valvar tissue, and tissues surrounding areas of strong artifact such as calcium. Limitations of spatial resolution and partial voluming effects give these tissues intermediate intensity between myocardium and blood pool, leading to errors in segmentation. For example, a thin portion of atrial or ventricular septum erroneously included in the blood pool mask will appear as a septal defect (continuity of blood pool between left and right chambers) upon modeling (Fig. 4.2d).

Another situation where manual segmentation is useful arises when the blood pool mask needs to be divided into separate anatomical regions, such as separating pulmonary arterial from pulmonary venous vasculature. Because of limitations in spatial resolution, vessels in very close proximity to each other will have connected voxels, limiting the utility of region growing. Manual removal of segmented voxels in areas of continuity allows region growing to be applied to separate regions.

### Multiple Slice Edit

Manual segmentation of individual slices can be tedious and labor-intensive, particularly on high-resolution image sets where the area to be edited spans multiple slices. Multiple slice editing allows single slice edits to be propagated over multiple adjacent slices, thus reducing editing time. Edits can be propagated without alteration to adjacent slices, or interpolated in a semiautomated fashion. In this feature, edits are made manually on two non-contiguous slices, and the software creates smart edits on the slices in between the manually created slices.

### Edit Mask in 3D

Manual segmentation can also be applied to a 3D rendering of the segment mask, in a manner analogous to 3D sculpting. This allows for more efficient cropping of complex shapes over large areas, but in general, it is only useful for editing the outside border of the mask rather than portions within it.

## Exporting Segment Masks to CAD Software

Once the desired mask has been created and refined, it is exported as a 3D virtual model in an STL file for printing or visualization. An STL file contains a digital representation of a 3D object. The 3D object is represented as a "mesh" composed of multiple triangular faces. The mesh solely describes the geometry of the 3D object and does not contain information about color or texture. The STL models produced by segmentation software may be printed or visualized as-is; however, they usually benefit from further editing using (CAD) software. Among many functions, CAD software allows for the following: editing or cropping of unwanted areas of the model, aesthetic refinement and smoothing of the model surface, removal of imperfections in the model surface, creation of "hollow shell" intracardiac models, partitioning of models into multiple pieces in order to allow visualization of the inside of the heart, creation of hybrid models

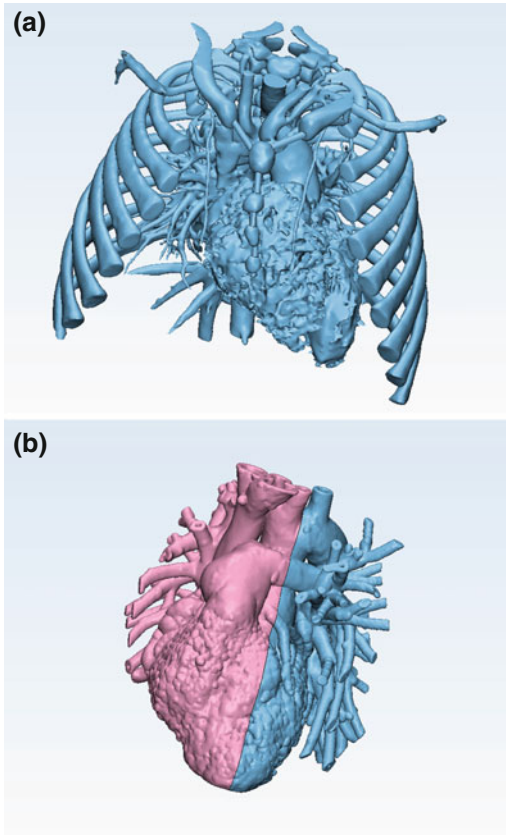


**Fig. 4.6** Examples of uses of CAD STL editing. **a** STL model of heart, thoracic vessels, and bony structures of the chest wall. Supports have been placed to keep the sternum attached to the model. **b** STL model of a heart after TGA repair. The model has been split in two halves, which can be separated in order to view the intracardiac anatomy

by fusing meshes created from different modalities (e.g., CT and US), creation of support structures to connect model pieces together (e.g., keep trachea and aorta together), and annotation of text onto the model (Fig. 4.6).

## Final STL Confirmation

Once the STL has been edited and refined, a useful last step is to reimport the STL into the segmentation software. The contours of the STL mesh can be superimposed on the original image data in order to confirm that the model is anatomically accurate (Fig. 4.5f). The model is now ready for 3D printing or visualization.

## References

1. Matsumoto JS, Morris JM, Foley TA, Williamson EE, Nesberg LE, Vrtiska TJ. Three-dimensional physical modeling : applications and experience at Mayo Clinic 1. 2015.
2. Mitsouras D, Liacouras P, Imanzadeh A, Giannopoulos AA, Cai T, Kumamaru KK, et al. Medical 3D printing for the radiologist. Radiographics [Internet]. 2015;35:1965–88.
3. Han BK, Rigsby CK, Hlavacek A, Leipsic J, Nicol ED, Siegel MJ, et al. Computed tomography imaging in patients with congenital heart disease part I: rationale and utility. An expert consensus document of the society of cardiovascular computed tomography (SCCT): endorsed by the society of pediatric radiology (SPR). Nor J Cardiovasc Comput Tomogr [Internet]. Elsevier Ltd.; 2015;9:475–92.
4. Fratz S, Chung T, Greil GF, Samyn MM, Taylor AM, Valsangiacomo Buechel ER, et al. Guidelines and protocols for cardiovascular magnetic resonance in children and adults with congenital heart disease: SCMR expert consensus group on congenital heart disease. J Cardiovasc Magn Reson [Internet]. 2013;15:51.
5. Simpson JM, Miller O. Three-dimensional echocardiography in congenital heart disease. Arch Cardiovasc Dis. 2011;104:45–56.
6. Olivieri LJ, Krieger A, Loke YH, Nath DS, Kim PCW, Sable CA. Three-dimensional printing of intracardiac defects from three-dimensional echocardiographic images: feasibility and relative accuracy. J Am Soc Echocardiogr [Internet]. Elsevier Inc.; 2015;28:392–7.
7. Samuel BP, Pinto C, Pietila T, Vettukattil JJ. Ultrasound-derived three-dimensional printing in congenital heart disease. J Digit Imag [Internet]. 2014;459–61.
8. Kurup HK, Samuel BP, Vettukattil JJ. Hybrid 3D printing: a game-changer in personalized cardiac medicine? Exp Rev Cardiovasc Ther [Internet]. 2015;9072:1–4.
9. Byrne N, Velasco Forte M, Tandon A, Valverde I, Hussain T. A systematic review of image segmentation methodology, used in the additive manufacture of patient-specific 3D printed models of the cardiovascular system. JRSM Cardiovasc Dis [Internet]. 2016;5:1–9.

# Rapid Prototyping Technologies

5

Joseph Borrello, BE and Peter Backeris, ME

## Overview

Many people have only recently become familiar with the concept of 3D printing, despite the fact that 3D printers have been available for nearly three decades. This fabrication method was started by two companies in the late 1980s/early 1990s that are still the largest 3D printer companies today: 3D Systems and Stratasys [1]. Each developed different ways of additive manufacturing, a term that describes the principle behind 3D printing. Rather than subtracting (or cutting away) from a block of a raw material, additive manufacturing starts with an empty platform and adds material layer by layer to form the printed part. This enables more intricate geometries to be produced than would be possible with traditional subtractive or injection molding processes, and without the need for custom tooling or complex machining instructions.

Both 3D Systems and Stratasys had patents on their respective 3D printing technologies that prevented competition for many years. The early printers were cost-prohibitive and only viable for industrial clients, with price tags over $100 K and costly materials to match.

In the late 1990s and early 2000s, the expiration of these patents and several other factors led to a rise in 3D printing to the commercial, and more recently, the consumer markets [2, 3]. Improved and more accessible computer-aided design (CAD) software has allowed a wider base of desigers to create complex 3D models quickly and accurately—another factor that enabled 3D printing to take a stronger hold in other markets. The growth of the "Maker Movement", its open-source community, and the growth of crowd-sourcing were especially helpful to further their adoption and the improvements in their design [4].

There are now many variations of 3D printing technology available, and several of the major 3D printing technologies (Fig. 5.1) are reviewed here. Hundreds of 3D printers in several of these classes now fall in the under $5 K price range and the number continue to grow [5]. These printers are also constantly improving and are capable of printing ever more sophisticated models including accurate 3D models of organs from medical imaging data. Different 3D printing technologies hold various advantages for printing these organs depending on the nature of the model and the intended application. These technologies are reviewed below, followed by considerations for deciding which type of printer is appropriate for cardiac disease modeling.

P. Backeris (✉)
Department of Biomedical Engineering, Icahn School of Medicine at Mount Sinai, Mount Sinai Institute of Technology, New York, NY, USA
e-mail: peter.backeris@mssm.edu

J. Borrello
Department of Biomedical Engineering, Icahn School of Medicine at Mount Sinai, Mount Sinai Institute of Technology, Graduate School of Biomedical Sciences, New York, NY, USA
e-mail: joseph.borrello@mssm.edu


K.M. Farooqi (ed.), *Rapid Prototyping in Cardiac Disease*,
DOI 10.1007/978-3-319-53523-4_5

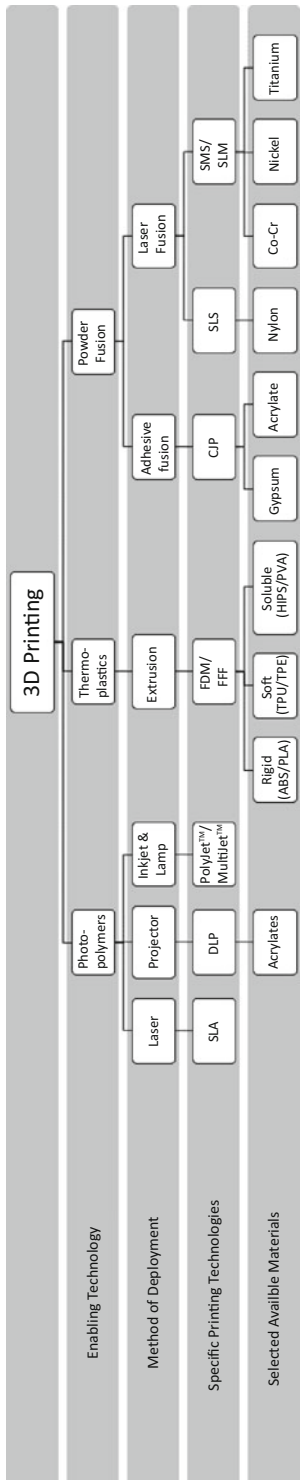


**Fig. 5.1** The major 3D printing technologies reviewed in this chapter, organized hierarchically by enabling technology, delivery system and available materials for each system

## Fused Deposition Modeling (FDM)

Fused deposition modeling—also known as fused filament fabrication (FFF) and plastic jet printing (PJP)—was first developed in the early 1990s by Crump [6], who went on to found the 3D printing company Stratasys. While Stratasys still technically trademarks the abbreviation for fused deposition modeling (FDM) over the past decade, it has come to be ubiquitously associated with a class of 3D printers that produce objects through the successive layering of a thermoplastic, and we will use that abbreviation for this chapter.

## Thermoplastics—Enabling Technology of FDM

Thermoplastic materials are at the heart of FDM technology. These materials are capable of being repeatedly melted and re-solidified by the exposure and removal of heat [7]. FDM takes advantage of this property by feeding a thin (typically 1.5–3 mm in diameter) filament of thermoplastic into a heated nozzle (or printer head) from which the melted plastic is then extruded through an opening a few hundred microns in diameter (most are 100–500 microns) (Fig. 5.2a). Upon extrusion, the thermoplastic material quickly returns to a solid state, which allows FDM printers to achieve layer-resolutions (layer heights) on the order of tens of microns. Such a rapid transition from solid to liquid (or semisolid) and back to solid is enabled by keeping the temperature of the nozzle at or close to the glass transition temperature of the material being extruded. At this temperature, the thermoplastic is heated enough to flow through the printer head of an FDM printer in a semi-liquid manner, but also cool enough to rapidly return to solid state temperatures once it is no longer in direct contact with the heated extrusion assembly.

In order to actually print with this method, the printer head is attached to a mechanical chassis comprised of motors that use belt and/or lead screw systems to move the extrusion assembly in a 3-dimensional, Cartesian system (i.e. X-, Y-,

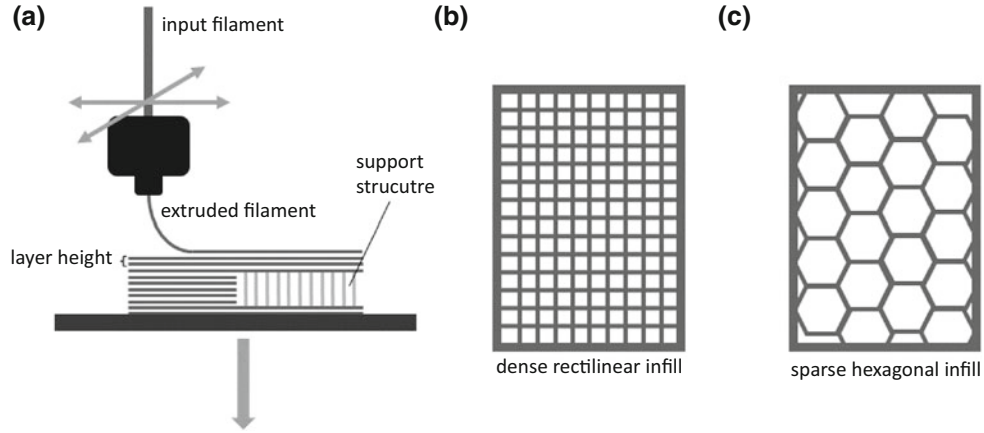


**Fig. 5.2** **a** A diagrammatic representation of the FDM printing process, showing the extruder, print head and print head motion, as well as the layering method used by FMD and a schematic representation of a part that includes overhang and supports. b, c Two examples of the trabecular-structured infill used by FDM 3D printers. **b** shows a dense, rectilinear infill pattern while **c** shows a sparser, hexagonal infill pattern

and Z-axes). In addition to the three Cartesian motors, a fourth motor is used to advance thermoplastic filament into the printer's heated nozzle. Coordinated control of these four motors (typically abbreviated as X, Y, Z, and E) by a computer allows the printer head to rapidly move through 3D space while continuously extruding melted filament (Fig. 5.2a).

## FDM Method of Printing and Design/Manufacturing Considerations

While an FDM printer head is capable of simultaneously moving in X, Y, and Z, these printers only print in two-dimensional layers at a time. To produce a three-dimensional model, FDM printers print successive layers of thermoplastic that can be thought of as two-dimensional cross-sections of the whole three-dimensional model. The first layer of an FDM print is deposited onto the bed of the 3D printer—which is typically made of metal, ceramic, or hard plastic—and each successive layer is deposited on top of the printed layer beneath it. Thus, at any given time, an FDM 3D printer is usually printing only a 2D layer on the X/Y plane for some Z height, only briefly pausing extrusion to advance one-step up to the next Z height to print that layer's 2D cross-section.

An important manufacturing contingency for this method of successive layering requires that the material deposited on each layer has something to rest upon beneath it, be that the printer bed or a previous layer of material. If a significant portion of a subsequent layer has no material to rest upon from the previous layer, typically referred to as "overhang," that portion of extruded thermoplastic will be unable to maintain its intended structure and instead "droop" downwards. Since, by design, some 3D models must include overhanging structural features, FDM printers are capable of additionally printing struts of material beneath these features for support, as depicted by the lighter colored, vertical bars in Fig. 5.2a. These struts, known as "supports," can be printed from the same material as the model and then removed after printing using cutting tools and brute force. They can also be printed from a soluble thermoplastic that is deposited by a second extruder during the print, if present, allowing the supports to be dissolved in a particular solvent while leaving the model intact.

## FDM Output Considerations—Layers and Infill

Overhang and supports are two of several manufacturing considerations that are involved in the determination of how to print a 3D model using FDM (and other types of 3D printers as well). Two other important output parameters include the height of each layer and the amount of infill material printed on each layer.

Layer height directly translates to the amount of distance the Z-axis motor will move the head upwards per cross-sectional layer of the model. For example, a layer height of 0.2 mm means that after printing each 2D section, the printer head will move up 0.2 mm and then begin printing the next layer of the model. Layer height can also be thought of—and is often easier to translate back to a 3D model—as the spacing between the planes that will slice the 3D model into its respective 2D cross-sections. As one might expect, the larger the layer height, the lesser the printed model can capture small changes in the profile of a model. A 3D model with a sinusoidal profile will be smoother when printed with a layer height of 0.1 mm versus that same model when printed with a layer height of 0.3 mm, since more points along the sinusoid can be captured if the model is printed in increasing increments of 0.1 mm versus increasing increments of 0.3 mm. In exchange for a loss of resolution, however, a model will take less time to print using a larger layer height compared to that same model on a smaller layer height, since the printer head will have to make fewer passes in order to complete the total height of the model. In several other forms of 3D printing discussed later on in this chapter, layer height is also a printing parameter than can be adjusted for each printing job. As is the case with FDM, there is a degree of tradeoff between time and model accuracy that accompanies a given layer height.

FDM printing also provides users with the capability to adjust how a printer will pattern each layer of a model. Since the material from which the model is constructed is only deposited from the printer head, a 3D model does not need to be made out of solid thermoplastic. Rather, a semi-hollow, trabecular structure (Fig. 5.2b, c) is often used in FDM in order to reduce the weight of the part and the amount of material needed to produce it while also maintaining strength and form. The density of that trabecular thermoplastic structure (infill) can be adjusted by the user depending on the function and performance of the printed model. With the exception of the first few and last few layers, which are printed as solid thermoplastic, all other layers of an FDM printed model are produced by first tracing out the perimeter of that layer and then filling in the space enclosed by that perimeter with an alternating pattern of material and space. The most common patterns used by FDM printers are hexagons (Fig. 5.2c), rectangles, and parallel lines (Fig. 5.2b), but more playful internal patterns, such as cat outlines [8], can also be produced (if desired). As layer height corresponds to model resolution, infill density corresponds, generally, to model strength—a model printed with an infill density of 100% (effectively solid) will be able to withstand more mechanical stress than that same model printed with an infill density of only 10% (90% of the internal space of the model is empty).

## FDM Materials

FDM is one of the most versatile forms of 3D printing, with respect to materials selection. Unlike other forms of 3D printing, which are limited to a single class of polymeric compound, the exclusively physical phase changes associated with FDM materials allow the technology to make use of a wide array of materials with vastly different properties with minimal adjustment to the 3D printer. Fundamentally, any thermoplastic is a candidate material for FDM (of which there are about a dozen available) including poly-lactic acid (PLA), acrylonitrile butadiene styrene (ABS), polycarbonate (PC), thermoplastic urethane (TPU), and polystyrene. For the purposes of descriptive modeling where material properties are less important than model geometry, the

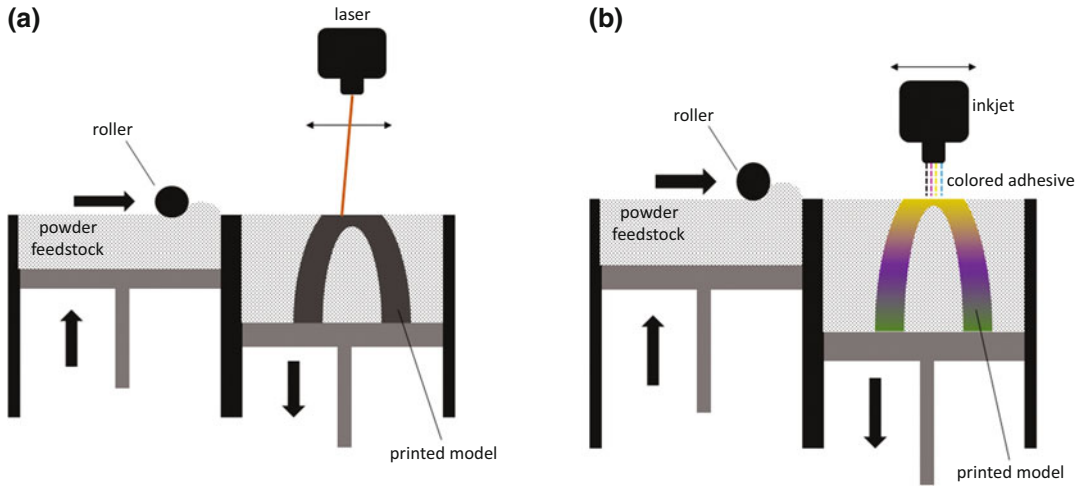


**Fig. 5.3** **a** A diagrammatic representation of the laser sintering method of additive manufacturing primarily employed for SLS. The diagram shows how the powder is spread by a roller from a containing chamber into the build chamber and is then selectively fused by a laser tracing 2D cross-sections of the model. **b** In ColorJet printing, or CJP, an adhesive—typically cyanoacrylate-based—is used to glue together very fine particles of gypsum and, recently, acrylate-based powders. Just as an inkjet printer is capable of printing color images by combining cyan, magenta, yellow, and black—ColorJet printers are capable of printing full-color models by including dyes of those same colors in the adhesive material

most common materials such as ABS and PLA will usually be sufficient.[1]

## Final Thoughts on FDM

Although it cannot offer the high resolutions or mechanical complexity that other 3D printing methods can produce, FDM is advantageous for being a relatively quick and cheap form of 3D printing with a wide selection of materials available for users. Within the scope of printing out models for structural reference, as is often the case for presurgical planning, the most commonly available thermoplastics—primarily ABS and PLA—are usually sufficient. In certain cases, particularly those involving highly intricate or complex structures, FDM may only be adequate as a preliminary print to a model produced by higher-resolution printing technologies (to be discussed next), or may not be suitable at all. In many cases, though, the output of an FDM printer is more than sufficient to convey the information needed by clinicians and surgeons to inform interventional approaches and methods.

## Powder-Based Printing

One of the largest and most varied 3D printing methods works by selectively fusing very fine particulates of material, deposited in thin layers within a print bed (Fig. 5.3a, b). This fusion is achieved through a variety of means, and current methods make use of adhesives, aqueous sugar solutions, or high-power lasers. While the

[1]It is worth pointing out that, while the elastic moduli of many tissues in the body range from kPa in magnitude to MPa, materials currently available for 3D printing—both FDM and otherwise—typically range from a few dozen MPa to several GPa in elastic modulus. As a result, the average 3D printed part, even in the softest available material, can be about 100–1000 times more rigid than the tissue or organs being studied. For this reason, it is not currently practical to expect a 3D printed model of a soft-tissue organ to accurately mimic the mechanical properties of the organ. Models consisting of several different materials with different material properties can be printed for illustrative purposes, but a truly meaningful mechanical characterization will not be possible.

means of fusing the powder particulates varies widely between these technologies, the method of depositing the layers of powder remains similar. In all cases, the powder material is deposited onto the print bed in thin ($\sim$100 μm) layers. As each layer of powder is deposited, a fusing agent—be it adhesive, laser, water, or another catalyst—traces out each layer of the model, fusing only those particles that will make up that layer. All remaining unfused particles act as the supporting structure for the printed part, allowing highly complex structures to be printed with very little need to consider specific geometric orientations and their impact on the manufacture of the part. Furthermore, because this supporting powder is left unfused and is made of the same material as the model, it is capable of being reused by the printer once a print is finished. As such, powder printers include vacuum systems to recycle the material —making this form of 3D printing among the most efficient and sustainable, at least in terms of material consumption.

## Selective Laser Sintering (SLS)

SLS was the first powder-based 3D printing technology developed and patented in the late 1980s to mid-1990s by Deckard and Beaman [9]. It uses a highly focused infrared laser to sinter powder granules together at high resolution (Fig. 5.3a). Since it is fusing the powder together through a sintering process, no additional binding chemicals are required in the process. SLS materials are typically nylon or nylon composites with superior mechanical properties over other printing methods.

## ColorJet Printing (CJP)

Shortly after SLS was developed, another form of powder printing was invented that used a very similar method of laying down material layers, but a disparate method of fusing those particles together. Commonly referred to as ColorJet printing, or CJP, this form of powder printing was created several years after SLS. In this method, an adhesive—typically cyanoacrylate-based—is used to glue together very fine particles of gypsum and, recently, acrylate-based powders. To achieve very precise deposition of the adhesive, standard 2D inkjet printing systems were repurposed to print adhesive onto powder the same way a typical inkjet would deposit ink onto a piece of paper. Additionally, just as an inkjet printer is capable of printing color images by combining cyan, magenta, yellow, and black —ColorJet printers are capable of printing full-color models by including dyes of those same colors in the adhesive material (Fig. 5.3b). It is important to note, though, that only certain file types and 3D modeling software are capable of producing models that will properly encode color for a ColorJet 3D printer.

## Photopolymerization-Based Printers

Photopolymers are light-curable resins that are liquid at room temperature and harden almost instantaneously when exposed to light of a certain intensity and wavelength (normally in the UV range), making them ideal for applications such as dental composites, medical adhesives, and 3D printing. The advantage of photopolymer-based 3D printing is primarily two-fold: higher resolution without sacrificing speed (and in some cases being faster) and thermoset plastics (which do not melt). Essentially, a photopolymer is a mixture of three components: an oligomer/monomer compound, a cross-linker, and a photoinitiator, each component lending a property to the final, printed material [10]. The oligomer, which is usually some form of acrylate molecule, provides the bulk material properties, including optical transmission, color, and reactivity. The cross-linker provides the mechanical structure that holds together the long chains of polymerized molecules; varying its concentration in the resin mixture allows modulation between hard and soft printed polymers. Photoinitiator molecules, while not directly responsible for the properties of the printed polymer, are the components that actually make 3D printing with these materials possible. Incident light of the proper wavelength band (usually in the UV spectrum) will

cause the photoinitiator molecules to catalyze both the lengthening of polymer chains from oligomer/monomer precursors, as well as the perpendicular attachment of cross-linker molecules. Of the three components of this "recipe," only the levels of photoinitiator must be kept steady to assure the proper rate of polymerization. The levels of oligomer and cross-linker (relative to each other) can be adjusted to produce a polymer with variable mechanical strength and stiffness.

## SLA-Based 3D Printers

Stereolithography (SLA) is considered to be the first 3D printing technology, developed in the mid-1980s by Chuck Hull [11] who went on to found 3D Systems. Despite its age, SLA is still one of the gold standards of additive manufacturing and is still used today in a wide range of printers at both consumer and industrial-grade levels. The process works by selectively curing successive layers of resin with a highly-focused UV laser. There are three main components to SLA printers: a vat of photopolymer resin, a build platform to which the printed part adheres, and a laser scanner (Fig. 5.4a). The build platform starts at the top or bottom of the vat, and the laser emits from the opposing end. The 3D model to be printed is sliced in software to form a stack of cross-sections, which are scanned in sequence by the laser. Each time a single layer is scanned; the platform moves a distance equal to the layer height, allowing the next layer to be scanned and fused to the previous layer. Support structures in the form of thin pillars, similar to the struts in FDM printers, are added to provide support to overhanging features in the model, which are removed during post-processing.

One disadvantage of SLA is the inability to combine multiple materials, which limits the complexity of printable geometries, although it is also known for its exceptional surface smoothness compared to other 3D printing modalities.

## DLP-SLA

DLP-SLA 3D printers are a new type of photopolymer 3D printers that work similarly to SLA printers but replace the laser scanning light source with a UV lamp (using either a custom UV-LED assembly, or by integrating an off-the-shelf projector into the system) that

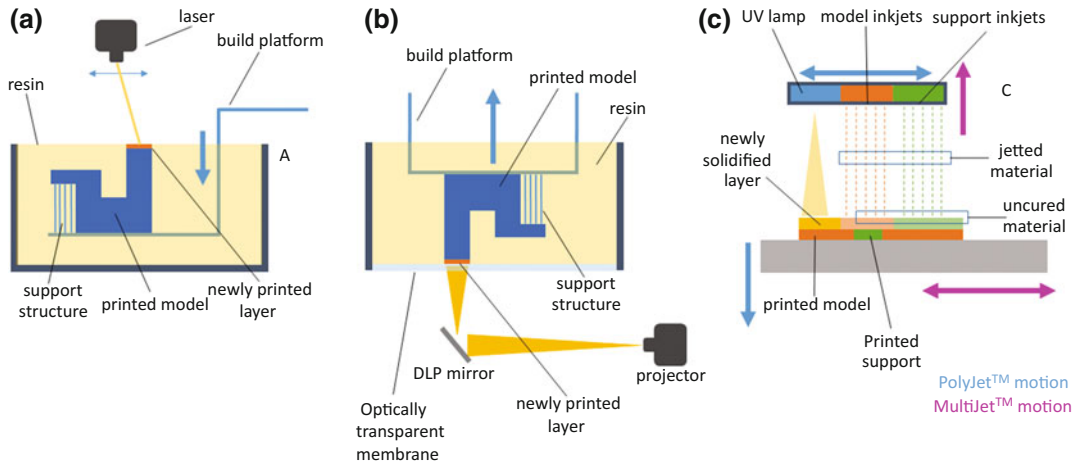


**Fig. 5.4** **a** There are three main components to SLA printers: a vat of photopolymer resin, a build platform to which the printed part adheres, and a laser scanner. **b** DLP-SLA 3D printers work similarly to SLA printers but replaced the laser scanning light source with a UV lamp—using either a custom UV-LED assembly—or by integrating an off-the-shelf projector into the system—that reflects light off a DLP chip and focuses it onto the build platform. **c** PolyJet™ and MultiJet™ printers make use of inkjet technology to deposit a large array of model material and/or build material, which is then cured by a UV lamp in order to build models layer by layer. The primary difference between these two printing technologies is the movement of the print head and build platform, represented by the *two colors of arrows* in the diagram

directs light into a DLP module that reflects and focuses it onto the build platform (Fig. 5.4b). In this way, an entire layer is cured simultaneously, increasing print speed. The DLP module contain a chip comprised of an array of tiny mirrors, representing the pixels of an image that are switched on or off to create an image pattern that can be focused onto the build platform. This system has advantages of being lower cost, with printers in the sub-$5 K range, but is currently limited by its smaller build area.

## Photopolymer Inkjet (PolyJet™/ MultiJet™)

Photopolymer inkjet 3D printers utilize piezoelectric inkjet technology to dispense tiny droplets of photopolymer onto a bed, creating a thin layer that is cured after each layer is deposited. The terms PolyJet™ (trademarked by Stratasys) and MultiJet™ (used by 3D Systems) refer to similar processes of depositing two materials simultaneously: a photopolymer build material that comprises the model and a photo-curable gel (Stratasys) or wax (3D Systems) that acts as a removable support material that enables diverse and complex features to be printed (Fig. 5.4c). The printers can print at resolutions similar to SLA but with rougher surface finish. The addition of support material to the printed model allows for virtually any solid volume of any geometry to be printed, including moving assemblies. There are a variety of build materials that can be printed with this technology, with some printers able to print more than one type simultaneously, and with the ability to mix two different resins together at controllable ratios to provide tunable stiffness.

## Considerations for Cardiac Printing

The majority of 3D printing technologies, especially those discussed here, are suitable for printing heart models from clinical image data if properly processed for the particular printer. However, depending on the purpose or application of the printed heart, one printer technology may be more appropriate than another may. It is important to consider several factors when deciding on which type of printer to purchase or print from to create the best models for a particular application. These factors include printer and material costs, minimum feature size, overhang support, speed, etc. FDM printers, although having larger minimum feature sizes, have lower costs for both materials and printers on average and are capable of printing perfectly suitable models for many presurgical planning applications. SLA, while having much smaller minimum feature sizes and higher resolution—has higher costs and limited ability to print complex or extended overhanging features that may be present in a heart model. It would, however, provide options for optically translucent parts that may be useful for certain applications. PolyJet™/MultiJet™ printers from Stratasys or 3D Systems preserve the feature resolution of SLA and allow the most complex internal structures to be produced. However, the printer and material costs are much higher, with entry-level printers starting at 50 K and going upwards toward $500 K, and materials costing over $300 per kg. These printers may be necessary when printing a 1:1 scale model of a heart with small, thin features of interest that would not be possible with SLA or FDM.

Powder printers of the ColorJet printing technology provide for some interesting applications where the researcher or physician may wish to highlight any number of features on the model in color. This could be to highlight a surgical cut path, the anatomy of arteries and veins, congenital defects, infarct regions, or any other area of interest in the model that can be colored in software prior to printing.

This overview serves only as introduction to the wide variety of 3D printing technologies now available. The pace by which these printers are improving across many categories including costs, ease-of-use, print quality, and material options is accelerating and will enable the creation and scaling of existing and new applications of 3D printing for cardiac disease modeling.

## References


1. 3D printing history: the free beginner's guide [Internet]. 3D Printing Industry. (cited 21 Nov 2015). Available from: http://3dprintingindustry.com/3d-printing-basics-free-beginners-guide/history/.
2. Mims C. Get ready: 3D printing will explode next year, when key patents expire. The Atlantic [Internet]. 22 Jul 2013 (cited 21 Nov 2015). Available from: http://www.theatlantic.com/technology/archive/2013/07/get-ready-3d-printing-will-explode-next-year-when-key-patents-expire/278008/.
3. Print the legend. Directed by Lopez L, Tweel JC. Audax Films; 2014. Netflix. Web. 24 Nov 2015. http://www.netflix.com/watch/80005444?trackId=13752289&tctx=0%2C0%2C43848ddb-2844-4678-ab37-9ac8ff9a4202-250647.
4. Anderson C. Makers: The New Industrial Revolution. New York: Crown Business; 2014. 272 pp.
5. Price compare—3D printers [Internet]. 3Ders.org. 2015. Available from: http://www.3ders.org/pricecompare/3dprinters/.
6. Crump SS. Apparatus and method for creating three-dimensional objects [Internet]. US5121329 A. 1992 (cited 21 Nov 2015). Available from: http://www.google.com/patents/US5121329.
7. Baeurle SA, Hotta A, Gusev AA. On the glassy state of multiphase and pure polymer materials. Polymer. 2006;47(17):6243–53.
8. MakerWare 2.2.0 | Release [Internet]. MakerBot (cited 21 Nov 2015). Available from: http://www.makerbot.com/blog/2013/06/12/makerware-2-2-0-preview.
9. Deckard CR, Beaman JJ, Darrah JF. Method for selective laser sintering with layerwise cross-scanning [Internet]. US5155324 A. 1992 (cited 21 Nov 2015). Available from: http://www.google.com/patents/US5155324.
10. Odian G. Principles of polymerization. In: Principles of polymerization [Internet]. Wiley; 2004 (cited 21 Nov 2015). p. i–xxiv. Available from: http://onlinelibrary.wiley.com/doi/10.1002/047147875X.fmatter/summary.
11. Hull CW. Apparatus for production of three-dimensional objects by stereolithography [Internet]. US4575330 A. 1986 (cited 21 Nov 2015). Available from: http://www.google.com/patents/US4575330.

# Part II
# Congenital Heart Disease

# Imaging Considerations and Challenges in Pediatrics

6

Anjali Chelliah, MD

## Introduction

Rapid prototyping of cardiac models relies upon the acquisition and segmentation of 3-dimensional, isotropic digital imaging and communications in medicine (DICOM) source images. Standard 2-dimensional echocardiography, the mainstay of congenital cardiac imaging, is not sufficient to generate these datasets. Instead, more advanced imaging modalities, including magnetic resonance imaging (MRI), computed tomography (CT), and more recently, 3D echocardiography are typically used to generate 3D printed heart models.

Utilizing these more advanced imaging modalities can be challenging in the pediatric population. Compared to adults, children have faster heart rates, smaller anatomic structures, and, depending on their developmental stage, can have difficulty limiting their motion and suspending their breathing in order to acquire images of diagnostic quality. Sedation is often required in younger children to avoid motion artifact, which can be of particular risk in children with unrepaired or partially palliated congenital heart disease (CHD). And exposure to radiation during CTs or contrast agents during MRIs and CTs remains a particular risk to children.

One of the most difficult decisions for the clinician obtaining an anatomical dataset for rapid prototyping can be weighing the benefits and risks of these imaging modalities to choose the most appropriate study for a given patient. Once an imaging modality is chosen, it is equally important to then perform the test using the most appropriate technique to minimize the risk of harm to the patient. This chapter outlines some of the technical considerations and unique challenges involved in performing cardiac MRIs, CTs, and 3D echocardiograms to create 3D heart models in children.

## Cardiovascular MRI

The use of cardiac magnetic resonance imaging to evaluate complex congenital heart defects has grown rapidly over the past two decades and has increasingly supplanted the use of invasive catheterization-based angiography [1, 2]. Its non-invasive, radiation-free images provide not only detailed volumetric and anatomic information, but also functional and hemodynamic data that may be of complementary use to surgeons planning complex intracardiac repairs in patients undergoing rapid prototyping. For example, in deciding whether to pursue a single- or two-ventricle repair, cardiac MRI can provide data on ventricular volumes, quantify systemic and pulmonary blood flows, and assess atrioventricular valve regurgitation [3]. It is MR angiography, however, either contrast-enhanced (CE-MRA) or non-contrast respiratory-navigated

A. Chelliah (✉)
Division of Pediatric Cardiology, Columbia University Medical Center, New York, NY, USA
e-mail: ac2967@columbia.edu


K.M. Farooqi (ed.), *Rapid Prototyping in Cardiac Disease*,
DOI 10.1007/978-3-319-53523-4_6

3D steady-state free precession (SSFP), that is used as the source data for 3D printing.

CE-MRA is a typically non-ECG-gated, T1-weighted sequence that is obtained after administration of a gadolinium-based intravenous contrast agent [4]. Gadolinium, a paramagnetic compound, shortens T1 relaxation time by disrupting spin-lattice interactions between protons, thereby enhancing the contrast between myocardium and blood pool [5]. By imaging the contrast-enhanced blood pool as it fills the cardiac chambers and vessels, CE-MRA creates an isotropic 3D dataset of the entire cardiac vasculature. This DICOM dataset can then be processed and segmented into a stereolithography file. The entire acquisition typically lasts under 30 s, particularly when parallel imaging techniques such as Array coil Spatial Sensitivity Encoding (ASSET) or Sensitivity Encoding (SENSE) are used [6].

Unlike CE-MRA, non-contrast volumetric datasets can be obtained without the use of gadolinium-based contrast using 3D SSFP, which has been reported by some groups as a preferred source dataset for rapid prototyping [7]. 3D SSFP, a T2-weighted sequence, is ideal for use in the pediatric population because it does not require the use of contrast, placement of an IV catheter, or breath-holding. It is both ECG-gated, acquiring images during a specified rest period of the heart (which may be in end-systole for patients with rapid heart rates), and respiratory-gated through the use of a navigator beam that tracks diaphragm motion and obtains images at end-expiration [4]. Preferred spatial resolution of these sequences for 3D printing purposes should be approximately 1.5 mm slice thickness or less.

A number of practical and safety considerations must be addressed in order to obtain adequate CE-MRA or 3D SSFP data for 3D cardiac modeling, though any well-equipped pediatric cardiac MR facility should be able to ensure that these needs are met. 1.5 Tesla MRI scanners are the mainstay of pediatric cardiac MR and are available at most pediatric centers. Some centers have begun to adopt the use of 3 Tesla (3T) MRI for clinical scanning in children. The higher signal-to-noise ratio of 3T imaging and more rapid acquisition times are ideal for contrast angiography in young children, but increased field inhomogeneity in 3T imaging, especially at the high heart rates seen in children, can worsen artifacts, particularly those related to devices [4, 8, 9]. Markl and colleagues have reported using 3T cardiac MR angiography to generate a rapid prototype of the thoracic aorta in an adult patient, but 3T-based 3D cardiac printing has not yet been reported in children [10].

The process of setting up a patient in the MRI scanner can pose unique challenges in the pediatric population. MRI scanners require a cool and low-humidity environment to function optimally, which can make it difficult for children, particularly neonates and infants, to maintain an adequate body temperature. Attention must be paid to completing the scan efficiently while monitoring patients for hypothermia [11]. It may also be difficult to position ECG monitoring leads on small children to ensure a sufficient signal. Also, respiratory bellows may not adequately detect the shallow breathing of infants and toddlers. Imaging coils must be appropriately sized and placed to optimize the signal-to-noise ratio over the thorax. For small infants, cardiac coils may be too large or heavy, and adult-sized head or knee coils are often used instead. At the other end of the pediatric size spectrum, it may occasionally be difficult for obese teenagers and young adults to comfortably fit into a standard 60 cm MRI scanner bore, though the use of wider bore scanners is growing among the pediatric population.

Another major consideration in pediatric cardiac MRI is ensuring that children can remain motionless and comply with breath hold instructions during long scans. Many children under the age of 7 years or older children with developmental delays or significant claustrophobia require sedation. This often involves general endotracheal anesthesia with neuromuscular blockade and suspending ventilation to minimize motion and respiratory artifact, particularly during contrast angiography, to ensure that images are of adequate quality for 3D printing [12]. Unfortunately, in recent years, safety concerns

have arisen about deleterious long-term effects of general anesthesia on neurocognitive function in the developing brain [13, 14]. More acutely, children with congenital heart disease are at increased risk of cardiac arrest during general anesthesia and also have higher arrest-associated mortality than in children without CHD [15]. One solution used in very young infants to avoid anesthesia is the "feed and wrap" technique, in which young infants are fed just prior to being placed in the scanner and swaddled to induce a deep sleep. This method is generally most successful in infants under two months of age, though it has been reported in infants up to 6 months old [16]. However, this technique does not control for respiratory motion, which is not ideal for images used in rapid prototyping. Sedation can also be avoided in some young school-aged children who might otherwise require anesthesia by utilizing child life therapists to help prepare patients emotionally for the MRI scan [17]. A more recently introduced technology using MRI-compatible audiovisual systems to show movies for distraction has been shown to decrease the need for sedation in children [18].

Many children with complex CHD referred for MRI may also have implanted devices from previous surgeries and catheter-based interventions. These may include pacemakers, implantable defibrillators, stents, coils, and non-cardiac devices such as cochlear implants or orthopedic rods. Newer pacemakers and implantable cardioverter defibrillators have been introduced that are considered to be conditionally MRI safe, but even implanted devices considered safe, i.e., not ferromagnetic, may cause significant susceptibility artifact [12].

One of the most significant considerations in performing cardiac MR angiography for 3D printing in children is the use of intravenous contrast agents. Gadolinium-based contrast agents, though considered "off-label" for pediatric MRI use in the USA, have been used for several decades now for CE-MRA. Gadolinium contrast has also been noted to be of use in 3D SSFP imaging, as it helps to increase blood pool to myocardial contrast. Newer blood pool contrast agents that remain in the intravascular space instead of distributing through extracellular fluid, such a gadofosveset trisodium (Ablavar), have been popular especially for use in small children. These agents will remain in the bloodstream for up to an hour of imaging, limiting the risk of uninterpretable images [19, 20]. Gadolinium remains associated with a risk of developing nephrogenic systemic fibrosis (NSF), a widespread progressive tissue fibrosis seen mostly in the skin of patients with severely reduced renal function and a glomerular filtration rate <30 ml/min/1.73 $m^2$ [21, 22]. Fortunately, NSF is quite rare in the pediatric population and has been reported fewer than 20 times in children as of 2010 [4]. Other acute adverse events from gadolinium such as anaphylaxis are exceedingly rare, occurring at an approximate rate of 0.001% [23].

Recently, new concerns have been raised about possible neurotoxicity from repeated use of gadolinium. Multiple reports have described the deposition of gadolinium in the brains of patients who had received greater than four doses of intravenous gadolinium contrast, despite normal renal function and an intact blood–brain barrier [24]. This finding has been of particular concern given that cardiac MRI typically requires double dosing of gadolinium contrast. Other studies have found differences in deposition by kinetic stability of various gadolinium-based contrast agents, with the lowest deposition in more stable versions of gadolinium (such as gadoteridol and gadobutrol) that may be slower to dissociate into the bloodstream [25, 26]. Although the long-term clinical effects of these findings are not yet well characterized, these findings raised enough concern to prompt the US Food and Drug Administration to issue a formal safety warning in 2015 advising clinicians to minimize their use of gadolinium contrast [27].

## Cardiovascular CT

With growing concerns about the neurodevelopmental effects of general anesthesia and gadolinium toxicity in children undergoing

cardiac MRI, and rapid advances in CT technology that have dramatically reduced radiation exposure, cardiac CT has become an increasingly popular choice for acquiring 3D datasets. Unlike cardiac MRI, cardiac CT provides a static anatomic image without incurring significant radiation exposure, albeit one with superior spatial resolution compared to MRI. Modern multidetector row CT scanners are capable of isotropic submillimeter slice thickness. Advantages of CT include the fairly short acquisition time, lack of artifact caused by implants such as stents or coils, clear assessment of extracardiac structures such as the airway and lungs, and that it may be performed without sedation in compliant patients.

The most important consideration in using cardiac CT for 3D printing, particularly in pediatric patients, is exposure to ionizing radiation. Older CT scanner technology traditionally required significant amounts of radiation, with effective doses often upwards of 10 millisieverts (mSv) per study [28]. By comparison, a routine PA and lateral chest X-ray generally exposes patients to approximately 0.1 mSv of radiation, equivalent to about 10 days' of exposure to natural environmental background radiation in the USA, or atmospheric radiation exposure from two round-trip flights from New York to Los Angeles [29]. Despite the significant radiation exposure from these older scanners, utilization of CT in the pediatric population has skyrocketed in recent decades. In 2000, it was estimated that children under the age of 16 years accounted for over 11% of CT utilization in the USA, and radiation from CTs accounted for 67% of the pediatric population's radiation exposure that year [29]. This increase in radiation exposure is of particular concern in children, who compared to adults are inherently more radiosensitive and also have more years of remaining life during which a malignancy may develop [30].

Children with CHD are subjected to repeated radiation exposures in the form, not only of cardiac CT, but also X-rays, cardiac catheterizations, lung perfusion testing, and nuclear stress tests. Johnson and colleagues recently reported on cumulative radiation exposure in a cohort of children aged six years and under at their center who had undergone surgical repair of a major cardiac lesion. They found even at this young age, a median radiation exposure of 2.7 mSv, with a range of up to nearly 77 mSv and an estimated lifetime attributable risk of cancer of up to 6.5% [31]. A similar study at a large CHD center reported that over 5% of young patients were exposed to more than 20 mSv/year of medical radiation during treatment for cardiac defects [32].

Fortunately, in recent years the medical community has placed increased emphasis on minimizing radiation in children. Efforts like Image Gently, an international campaign funded by multiple pediatric and radiology organizations, have promoted the radiation safety concept of "ALARA," or "As low as reasonably achievable," as a guiding principle in performing pediatric imaging studies like cardiac CT [33, 34]. These efforts have been supported by rapid developments in cardiac CT scanning in recent years. One technique that has made a significant contribution to the efforts of radiation dose reduction has been the introduction of prospective ECG gating. This technique involves the X-ray beam being turned on only during quiescent parts of the cardiac cycle, typically end-diastole, though end-systole is often used in patients with high heart rates, rather than throughout the cardiac cycle. This technique has been reported to reduce radiation exposure during cardiac CT by as much as 77%, compared to retrospective gating, without affecting image quality [35]. Additional technologic advances, such as use of multidetector technology, faster gantry rotation speeds (lowering exposure time), higher pitch (table distance traveled in one gantry rotation), and more recently, dual-source ("flash") CT scanners simultaneously employing two X-ray tubes, have also impressively decreased radiation by decreasing acquisition time and increasing temporal resolution [36, 37]. Other techniques such as iterative reconstruction algorithms that improve image quality in post-processing have allowed the use of lower X-ray beam energy (kVp) and tube current (mA) without significantly sacrificing scan quality [38]. Many groups are also aggressively

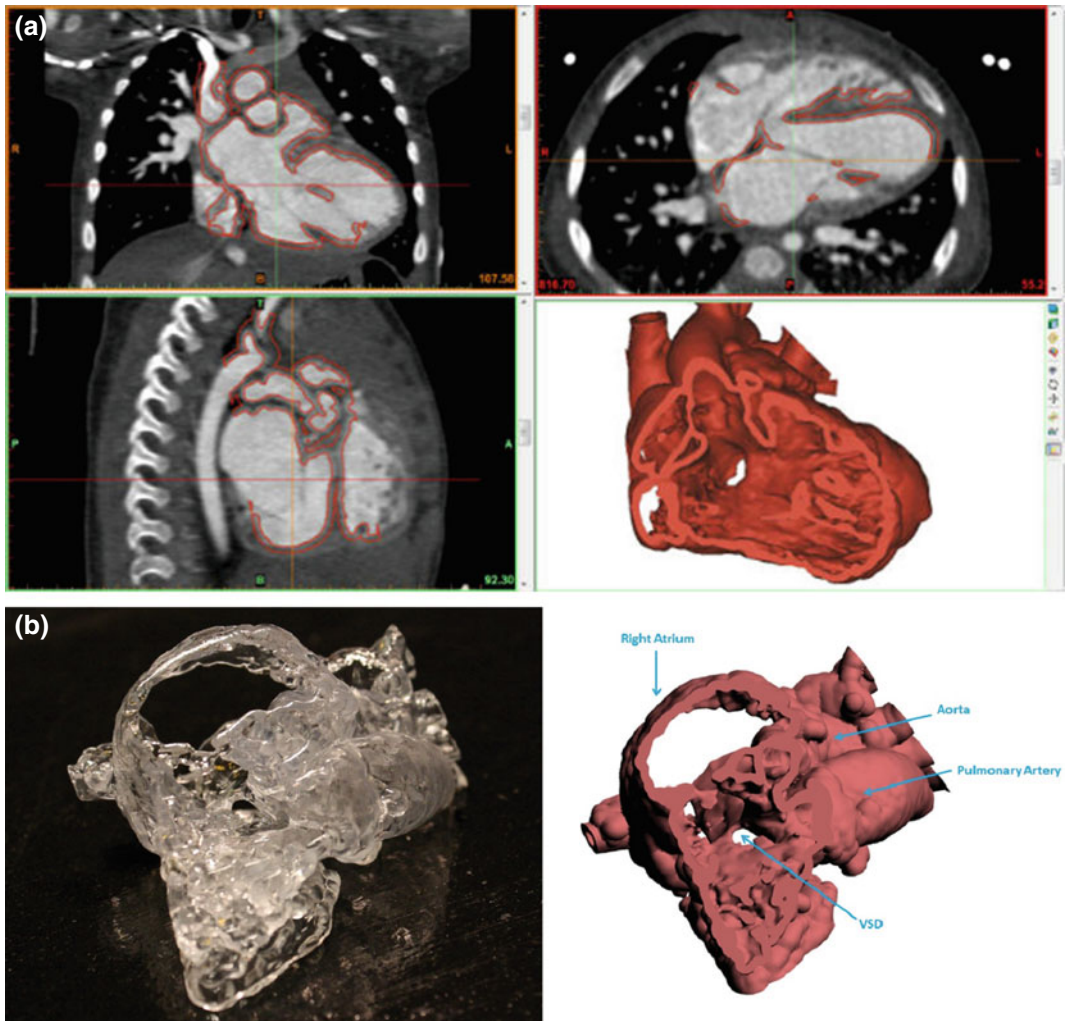


**Fig. 6.1** **a** Segmentation of a 1-day-old infant prenatally diagnosed with complex DORV, uncommitted VSD, d-malposed great vessels, and coarctation. CT was obtained with 0.2 mSv radiation dose. **b** 3D digital rendering and printed cardiac model (performed using Mimics software, Materialise NV, Plymouth, MI)

moving to limiting scan coverage in the z-axis to the area of interest rather than the whole heart or chest [39]. While there is wide variation in clinical practice and therefore in pediatric cardiac CT dosing, many groups have reported average radiation doses of less than 1 mSv in children with CHD [40–42]. At our center, using a 64-slice scanner with prospective ECG gating, an 80 kVp protocol with aggressive mA reduction and iterative reconstruction algorithms, we typically achieve 0.625 cm slice thickness images with dose-length-products less than 15 mGy-cm and, multiplying by a conversion factor of 0.03, effective radiation doses of less than 0.5 mSv. An example is shown in Fig. 6.1.

Aside from radiation, other unique considerations, both risks and benefits, are involved in performing cardiac CTs on pediatric patients. A major benefit of the increased temporal resolution of cardiac CT is that the need for sedation is minimized. Children over the age of 3 years can usually remain still for the brief time needed for CT acquisition. Breath-holding may not be required for volumetric or high-pitch scanners, though it is still needed for imaging acquired over several heartbeats or coronary artery imaging [39, 43]. At our institution, for

3D printing purposes, we typically administer at least moderate sedation to patients under 3 years to avoid blurring from motion and minimize stair-step artifact on our step-and-shoot CT scanner. In neonates, in whom anatomic structures are small and spatial resolution is important, we will consider intubation, paralysis, and suspending ventilation to acquire very high-quality datasets for prototyping. Often, neonates facing the prospect of complex surgical repair requiring 3D modeling are critically ill and may be already intubated in the neonatal intensive care unit.

As previously mentioned, cardiac CT does not require the use of gadolinium, but does require intravenous injection of iodinated contrast at doses of about 1–2 mL/kg. Though not associated with neurotoxicity, CT contrast can induce nephropathy in patients with decreased renal function. This is often a concern in children with CHD and pediatric patients who have undergone a heart transplant. Patients may benefit from pre-hydration and treatment with protective agents like n-acetyl cysteine [44, 45]. Contrast extravasations are rare, even when using a power injector in a 24-gauge IV in a neonate [46]. Risk of iodinated contrast allergy is higher than that of gadolinium-based agents but is typically less than 0.5% in children [47, 48]. In patients with aortopulmonary shunts or a Fontan palliation, it is particularly important to tailor contrast injection protocols to a patient's specific anatomy and circulation pathways. When imaging a patient after Fontan palliation, some groups suggest simultaneous contrast administration through upper and lower extremity intravenous lines to opacify the entire pathway, though delaying imaging after contrast injection may also achieve the same effect [49, 50].

Other benefits of cardiac CT include its ability to simultaneously image extracardiac structures such as the airway and lung parenchyma with high-spatial resolution. It is also ideal for patients with metallic devices such as pacemakers or stents that are either contraindicated in MRI or may cause significant artifact. CT is optimal for critically ill patients, who may not be stable enough to undergo long MRI examinations [37]. The relatively high heart rates of pediatric patients are not a significant limitation to obtaining high-quality CT images unless coronary imaging is a critical component of a 3D model. If coronary imaging is needed, beta blockers or calcium channel blockers may be administered when indicated in order to reduce the heart rate to less than 70, and ideally less than 60, beats per minute to achieve adequate image quality. Our group recently reported that using an intravenous phenylephrine infusion in conjunction with these medications can further decrease heart rates even in young children by supporting blood pressure as well as causing reflex bradycardia [51]. Such low heart rates may not be safely achievable in very young patients, however [39].

## 3D Echocardiography

Regardless of the increasing popularity of cardiac MRI and CT, echocardiography remains the first-line bedside imaging modality in children with CHD. It is less resource-intensive, typically does not require sedation, and does not involve exposure to ionizing radiation or intravenous contrast agents. Recent advances in 3D echocardiography have improved our ability to obtain 3D echo images in young children and have made it increasingly possible to obtain volumetric DICOM datasets that can be used for rapid prototyping.

While 3D echo technology has been in use for several decades, more advanced real-time 3D echo systems have become commercially available in recent years, and smaller, high-frequency 3D echo probes that can be used in pediatric patients have been introduced [52]. 3D transesophageal echocardiography has also been introduced; however, the large size of the 3D TEE probe generally limits its use to children weighing at least 20 kg [53]. 3D echo has been shown to be particularly useful for delineating atrioventricular valve morphology and function, details of atrial and ventricular septal defects, and complex intracardiac relationships such as the ones often highlighted by 3D printing [54].

Obtaining high-quality 3D echocardiographic datasets is more operator-dependent than cardiac MRI or CT and can present some challenges in the pediatric population. Movement artifact can pose

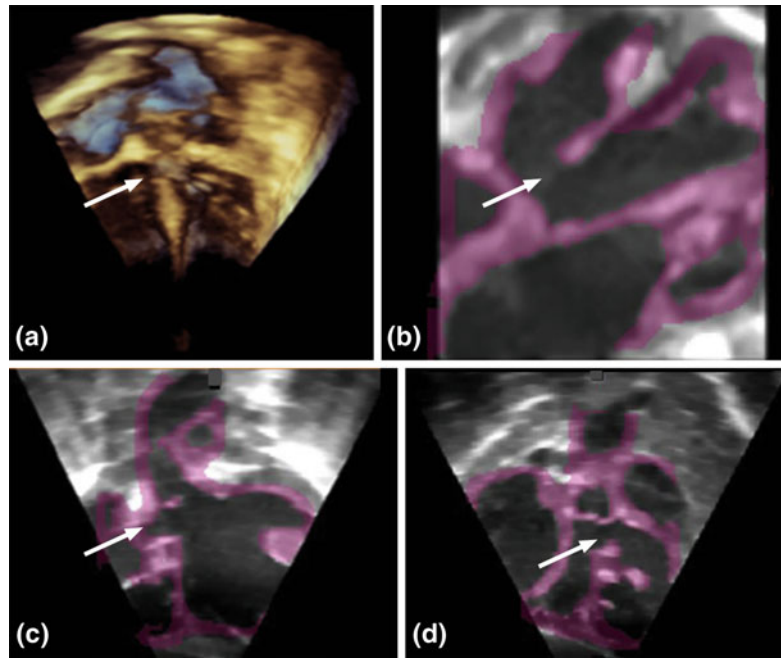


**Fig. 6.2** Segmentation of 3D echocardiogram depicting a membranous ventricular septal defect; reproduced with permission of the publisher from *J Am Soc Echocardiogr.* 2015 Apr;28(4):392–7

an issue in young children, and sedation may be required in some patients. Highspatial resolution and frame rates are also needed, which can be difficult to achieve in children with small cardiac structures and high heart rates [54]. Using live 3D imaging can overcome this limitation by providing true real-time imaging, though it limits the size of the field of view that can be acquired. Alternatively, a full volume acquisition can be obtained that provides a considerably larger imaging field but requires imaging over multiple heartbeats and may therefore results in "stitch artifact" from combining information from multiple cardiac cycles [55].

Olivieri and colleagues recently reported successfully 3D printing accurate cardiac models of patients with ventricular septal defect and periprosthetic aortic valve leaks based on 3D echocardiographic datasets [56]. The group noted that image acquisition was optimized by using a high-frequency 3D transducer, minimizing image depth, acquiring images only in diastole, and minimizing image gains to decrease blood pool noise. They also applied noise reduction filters to the imaging data in order to further minimize the blood pool and emphasize anatomic details prior to segmentation. This technique produced high-quality, highly accurate defect depictions (Fig. 6.2). However, as the authors noted, their methodology may not be as applicable to segmenting 3D echo images of valves and other cardiac structures involving tissue rather than spaces created by defects.

More recently, Vettukatil et al. have also reported using 3D echocardiography to create 3D printed models of atrial septal defects, as well as cardiac models based upon hybrid 3D echo and cross-sectional MRI or CT datasets. Their methods are described in an earlier chapter of this text [57, 58].

## Which Imaging Modality Should Be Used?

As technologic advances provide us with more options for sourcing 3D datasets for rapid cardiac prototyping, it can be difficult to choose the most appropriate option for one's patient. Careful consideration must be made in order to choose the optimal study for the patient and perform it optimally. Patient age and size, developmental

**Table 6.1** Comparative benefits of cardiac imaging modalities used in children to create 3D heart models

| Cardiac MRI | Cardiac CT | 3D Echocardiography |
|---|---|---|
| • Ideal for patients who do not require sedation and can tolerate a 1+ h study<br>• Avoids radiation exposure<br>• Provides additional ventricular function, volume, and/or flow data<br>• CT contrast allergy<br>• Poor echocardiography windows | • Submillimeter spatial resolution needed (e.g., in small infants)<br>• Coronary artery imaging needed<br>• Implanted metallic devices that may preclude or limit MRI imaging<br>• Only anatomic imaging needed<br>• Avoids general anesthesia (e.g., age <7 years, increased risk of anesthesia complications)<br>• Poor echocardiography windows<br>• Patient unable to fit in MRI due to morbid obesity or claustrophobia | • Rapid, easily accessible bedside imaging needed<br>• Detailed cardiac valve imaging needed<br>• Renal insufficiency, contrast allergy, or other contraindication to intravenous contrast agents<br>• Avoids IV placement<br>• Avoids sedation and radiation<br>• Patient unable to fit in MRI due to morbid obesity or claustrophobia |

stage, clinical indication, comorbidities, available technology, ensuring patient safety, and the overall goals of 3D printing must be taken into account. At our institution, for example, low-radiation cardiac CT is preferred to maximize spatial resolution in small infants and avoid the need for general anesthesia needed for MRI in young children. Table 6.1 summarizes some of the benefits and optimal uses of cardiac MRI, CT, and 3D echocardiography, respectively, in pediatric patients with CHD.

## References


1. Heathfield E, Hussain T, Qureshi S, Valverde I, Witter T, Douiri A, et al. Cardiovascular magnetic resonance imaging in congenital heart disease as an alternative to diagnostic invasive cardiac catheterization: a single center experience. Congenit Heart Dis. 2013;8(4):322–7.
2. Ntsinjana HN, Hughes ML, Taylor AM. The role of cardiovascular magnetic resonance in pediatric congenital heart disease. J Cardiovasc Magn Reson. 2011;13:51.
3. Krishnamurthy RCT. Principles and practice of cardiac magnetic resonance in congenital heart disease: form, function, and flow (Fogel MA, editor). Chichester, West Sussex, UK; Hoboken, NJ: Wiley-Blackwell; 2010. xii, 464 p.
4. Fratz S, Chung T, Greil GF, Samyn MM, Taylor AM, Valsangiacomo Buechel ER, et al. Guidelines and protocols for cardiovascular magnetic resonance in children and adults with congenital heart disease: SCMR expert consensus group on congenital heart disease. J Cardiovasc Magn Reson. 2013;15:51.
5. Sharma P, Socolow J, Patel S, Pettigrew RI, Oshinski JN. Effect of Gd-DTPA-BMA on blood and myocardial T1 at 1.5T and 3T in humans. J Magn Reson Imaging. 2006;23(3):323–30.
6. Hartung MP, Grist TM, Francois CJ. Magnetic resonance angiography: current status and future directions. J Cardiovasc Magn Reson. 2011;13:19.
7. Bramlet M, Wang K, Clemons A, Speidel NC, Lavalle SM, Kesavadas T. Virtual reality visualization of patient specific heart model. J Cardiovasc Magn Reson. 2016;18(1):1–2.
8. Ditchfield M. 3T MRI in paediatrics: challenges and clinical applications. Eur J Radiol. 2008;68(2):309–19.
9. Nguyen KL, Khan SN, Moriarty JM, Mohajer K, Renella P, Satou G, et al. High-field MR imaging in pediatric congenital heart disease: initial results. Pediatr Radiol. 2015;45(1):42–54.
10. Markl M, Schumacher R, Kuffer J, Bley TA, Hennig J. Rapid vessel prototyping: vascular modeling using 3T magnetic resonance angiography and rapid prototyping technology. MAGMA. 2005;18(6):288–92.
11. Odegard KC, DiNardo JA, Tsai-Goodman B, Powell AJ, Geva T, Laussen PC. Anaesthesia considerations for cardiac MRI in infants and small children. Paediatr Anaesth. 2004;14(6):471–6.
12. Mitchell FM, Prasad SK, Greil GF, Drivas P, Vassiliou VS, Raphael CE. Cardiovascular magnetic resonance: diagnostic utility and specific considerations in the pediatric population. World J Clin Pediatr. 2016;5(1):1–15.
13. Loepke AW, Soriano SG. An assessment of the effects of general anesthetics on developing brain structure and neurocognitive function. Anesth Analg. 2008;106(6):1681–707.
14. Wilder RT, Flick RP, Sprung J, Katusic SK, Barbaresi WJ, Mickelson C, et al. Early exposure to anesthesia and learning disabilities in a population-based birth cohort. Anesthesiology. 2009;110(4):796–804.
15. Ramamoorthy C, Haberkern CM, Bhananker SM, Domino KB, Posner KL, Campos JS, et al. Anesthesia-related cardiac arrest in children with

heart disease: data from the pediatric perioperative cardiac arrest (POCA) registry. Anesth Analg. 2010;110(5):1376–82.
16. Windram J, Grosse-Wortmann L, Shariat M, Greer ML, Crawford MW, Yoo SJ. Cardiovascular MRI without sedation or general anesthesia using a feed-and-sleep technique in neonates and infants. Pediatr Radiol. 2012;42(2):183–7.
17. Durand DJ, Young M, Nagy P, Tekes A, Huisman TA. Mandatory child life consultation and its impact on pediatric MRI workflow in an academic medical center. J Am Coll Radiol. 2015;12(6):594–8.
18. Lemaire C, Moran GR, Swan H. Impact of audio/visual systems on pediatric sedation in magnetic resonance imaging. J Magn Reson Imaging. 2009;30(3):649–55.
19. Naehle CP, Kaestner M, Muller A, Willinek WW, Gieseke J, Schild HH, et al. First-pass and steady-state MR angiography of thoracic vasculature in children and adolescents. JACC Cardiovasc Imaging. 2010;3(5):504–13.
20. Rigsby CK, Popescu AR, Nelson P, Orr RJ, Boylan EE, Schoeneman S, et al. Safety of blood pool contrast agent administration in children and young adults. AJR Am J Roentgenol. 2015;205(5):1114–20.
21. Marckmann P, Skov L, Rossen K, Dupont A, Damholt MB, Heaf JG, et al. Nephrogenic systemic fibrosis: suspected causative role of gadodiamide used for contrast-enhanced magnetic resonance imaging. J Am Soc Nephrol. 2006;17(9):2359–62.
22. Kribben A, Witzke O, Hillen U, Barkhausen J, Daul AE, Erbel R. Nephrogenic systemic fibrosis: pathogenesis, diagnosis, and therapy. J Am Coll Cardiol. 2009;53(18):1621–8.
23. Dillman JR, Ellis JH, Cohan RH, Strouse PJ, Jan SC. Frequency and severity of acute allergic-like reactions to gadolinium-containing i.v. contrast media in children and adults. AJR Am J Roentgenol. 2007;189(6):1533–8.
24. McDonald RJ, McDonald JS, Kallmes DF, Jentoft ME, Murray DL, Thielen KR, et al. Intracranial gadolinium deposition after contrast-enhanced MR imaging. Radiology. 2015;275(3):772–82.
25. Ramalho J, Semelka RC, Ramalho M, Nunes RH, AlObaidy M, Castillo M. Gadolinium-based contrast agent accumulation and toxicity: an update. AJNR Am J Neuroradiol. 2015.
26. Radbruch A, Weberling LD, Kieslich PJ, Eidel O, Burth S, Kickingereder P, et al. Gadolinium retention in the dentate nucleus and globus pallidus is dependent on the class of contrast agent. Radiology. 2015;275(3):783–91.
27. Administration USFaD. FDA drug safety communication: FDA evaluating the risk of brain deposits with repeated use of gadolinium-based contrast agents for magnetic resonance imaging (MRI). 2015.
28. Hollingsworth CL, Yoshizumi TT, Frush DP, Chan FP, Toncheva G, Nguyen G, et al. Pediatric cardiac-gated CT angiography: assessment of radiation dose. AJR Am J Roentgenol. 2007;189(1):12–8.
29. Lin EC. Radiation risk from medical imaging. Mayo Clin Proc. 2010;85(12):1142–6; quiz 6.
30. Miglioretti DL, Johnson E, Williams A, Greenlee RT, Weinmann S, Solberg LI, et al. The use of computed tomography in pediatrics and the associated radiation exposure and estimated cancer risk. JAMA Pediatr. 2013;167(8):700–7.
31. Johnson JN, Hornik CP, Li JS, Benjamin DK Jr, Yoshizumi TT, Reiman RE, et al. Cumulative radiation exposure and cancer risk estimation in children with heart disease. Circulation. 2014;130(2):161–7.
32. Glatz AC, Purrington KS, Klinger A, King AR, Hellinger J, Zhu X, et al. Cumulative exposure to medical radiation for children requiring surgery for congenital heart disease. J Pediatr. 2014;164(4):789–94 e10.
33. Frush DP, Donnelly LF, Rosen NS. Computed tomography and radiation risks: what pediatric health care providers should know. Pediatrics. 2003;112(4):951–7.
34. Goske MJ, Applegate KE, Boylan J, Butler PF, Callahan MJ, Coley BD, et al. The Image Gently campaign: working together to change practice. AJR Am J Roentgenol. 2008;190(2):273–4.
35. Shuman WP, Branch KR, May JM, Mitsumori LM, Lockhart DW, Dubinsky TJ, et al. Prospective versus retrospective ECG gating for 64-detector CT of the coronary arteries: comparison of image quality and patient radiation dose. Radiology. 2008;248(2):431–7.
36. Lell MM, May M, Deak P, Alibek S, Kuefner M, Kuettner A, et al. High-pitch spiral computed tomography: effect on image quality and radiation dose in pediatric chest computed tomography. Invest Radiol. 2011;46(2):116–23.
37. Hlavacek AM. Imaging of congenital cardiovascular disease: the case for computed tomography. J Thorac Imaging. 2010;25(3):247–55.
38. Zacharias C, Alessio AM, Otto RK, Iyer RS, Philips GS, Swanson JO, et al. Pediatric CT: strategies to lower radiation dose. AJR Am J Roentgenol. 2013;200(5):950–6.
39. Han BK, Rigsby CK, Leipsic J, Bardo D, Abbara S, Ghoshhajra B, et al. Computed tomography imaging in patients with congenital heart disease, part 2: technical recommendations. an expert consensus document of the society of cardiovascular computed tomography (SCCT): endorsed by the society of pediatric radiology (SPR) and the North American Society of Cardiac Imaging (NASCI). J Cardiovasc Comput Tomogr. 2015;9(6):493–513.
40. Goo HW. State-of-the-art CT imaging techniques for congenital heart disease. Korean J Radiol. 2010;11(1):4–18.
41. Jin KN, Park EA, Shin CI, Lee W, Chung JW, Park JH. Retrospective versus prospective ECG-gated dual-source CT in pediatric patients with congenital heart diseases: comparison of image quality and radiation dose. Int J Cardiovasc Imaging. 2010;26(Suppl 1):63–73.

42. Paul JF, Rohnean A, Elfassy E, Sigal-Cinqualbre A. Radiation dose for thoracic and coronary step-and-shoot CT using a 128-slice dual-source machine in infants and small children with congenital heart disease. Pediatr Radiol. 2011;41(2):244–9.
43. Han BK, Overman DM, Grant K, Rosenthal K, Rutten-Ramos S, Cook D, et al. Non-sedated, free breathing cardiac CT for evaluation of complex congenital heart disease in neonates. J Cardiovasc Comput Tomogr. 2013;7(6):354–60.
44. Han BK, Rigsby CK, Hlavacek A, Leipsic J, Nicol ED, Siegel MJ, et al. Computed tomography imaging in patients with congenital heart disease part i: rationale and utility. an expert consensus document of the society of cardiovascular computed tomography (SCCT): endorsed by the society of pediatric radiology (SPR) and the North American Society of Cardiac Imaging (NASCI). J Cardiovasc Comput Tomogr. 2015;9(6):475–92.
45. Alonso A, Lau J, Jaber BL, Weintraub A, Sarnak MJ. Prevention of radiocontrast nephropathy with N-acetylcysteine in patients with chronic kidney disease: a meta-analysis of randomized, controlled trials. Am J Kidney Dis. 2004;43(1):1–9.
46. Amaral JG, Traubici J, BenDavid G, Reintamm G, Daneman A. Safety of power injector use in children as measured by incidence of extravasation. AJR Am J Roentgenol. 2006;187(2):580–3.
47. Callahan MJ, Poznauskis L, Zurakowski D, Taylor GA. Nonionic iodinated intravenous contrast material-related reactions: incidence in large urban children's hospital–retrospective analysis of data in 12,494 patients. Radiology. 2009;250(3):674–81.
48. Dillman JR, Strouse PJ, Ellis JH, Cohan RH, Jan SC. Incidence and severity of acute allergic-like reactions to i.v. nonionic iodinated contrast material in children. AJR Am J Roentgenol. 2007;188(6):1643–7.
49. Dillman JR, Hernandez RJ. Role of CT in the evaluation of congenital cardiovascular disease in children. AJR Am J Roentgenol. 2009;192(5):1219–31.
50. Sandler KL, Markham LW, Mah ML, Byrum EP, Williams JR. Optimizing CT angiography in patients with Fontan physiology: single-center experience of dual-site power injection. Clin Radiol. 2014;69(12):e562–7.
51. Chelliah A, Kubacki T, Julien HM, Einstein AJ. Pediatric coronary CTA using phenylephrine to lower heart rate. J Cardiovasc Comput Tomogr. 2016;10(4):339–40.
52. Simpson JM. Real-time three-dimensional echocardiography of congenital heart disease using a high frequency paediatric matrix transducer. Eur J Echocardiogr. 2008;9(2):222–4.
53. Shirali GS. Three-dimensional echocardiography in congenital heart disease. Echocardiography. 2012;29(2):242–8.
54. Simpson JM, Miller O. Three-dimensional echocardiography in congenital heart disease. Arch Cardiovasc Dis. 2011;104(1):45–56.
55. Simpson JM, Miller O. Congenital heart disease in children. In: Buck T, Franke A, Monaghan MJ, editors. Three-dimensional echocardiography. Berlin, New York: Springer; 2011.
56. Olivieri LJ, Krieger A, Loke YH, Nath DS, Kim PC, Sable CA. Three-dimensional printing of intracardiac defects from three-dimensional echocardiographic images: feasibility and relative accuracy. J Am Soc Echocardiogr. 2015;28(4):392–7.
57. Gosnell J, Pietila T, Samuel BP, Kurup HK, Haw MP, Vettukattil JJ. Integration of computed tomography and three-dimensional echocardiography for hybrid three-dimensional printing in congenital heart disease. J Digit Imaging; 2016.
58. Samuel BP, Pinto C, Pietila T, Vettukattil JJ. Ultrasound-derived three-dimensional printing in congenital heart disease. J Digit Imaging. 2015;28(4):459–61.

# Septal Defects

7

Laura J. Olivieri, MD

## Introduction

The diagnosis and management of congenital heart defects, including septal defects, is driven by cardiovascular imaging. As imaging advances, so does the depth of our understanding of the subtle features of heart defects, which in turn informs clinical management. Septal defects are the most common type of congenital heart defects, with a prevalence of 1/1500 live births for atrial septal defects, 1/1000 live births for ventricular septal defects, and 1/2500 live births for all forms of atrioventricular septal defect (AVSD). Within each of these three categories of septal defect is a wide variety of defect location, type, and size. Clinical management of these defects is largely driven by their appearance on imaging; thus, imaging and display of the imaging data is of particular importance in the management of these patients. In complex septal defects, or septal defects associated with other lesions, three-dimensional (3D) cardiac models can add value, particularly when procedures will be planned to manage the defects. The optimal 3D imaging dataset is the one that will adequate spatial and temporal resolutions to show the subtleties of the defect without cardiorespiratory motion blur, and with adequate signal intensity differentiation between the blood pool and the myocardium, so that the septal defects are clearly visible and easily segmentable.

L.J. Olivieri (✉)
George Washington University School of Medicine, Division of Cardiology, Children's National Medical Center, 111 Michigan Avenue NW, W3-200, Washington DC, WA 20010, USA
e-mail: lolivier@childrensnational.org


K.M. Farooqi (ed.), *Rapid Prototyping in Cardiac Disease*,
DOI 10.1007/978-3-319-53523-4_7

## ASD

Atrial septal defects (ASD) have a prevalence of 1/1500 live births (excluding patent foramen ovalae). There are four general types of atrial septal defects—primum defects, secundum defects, coronary sinus defects, and sinus venosus defects [1]. In each of these types of defects, it is imperative to note the atrial situs, pulmonary and systemic venous anatomy, and estimate right-sided volume overload through the assessment of right atrial and right ventricular enlargement.

### Current Imaging of ASDs

Currently, the majority of imaging of the interatrial septum is undertaken by transthoracic echocardiography with 3D echo acquisitions, particularly in babies and children. Subcostal views, in particular the subcostal short axis, will give unparalleled views of the interatrial septum. In the case of more complex atrial septal defects, cardiovascular magnetic resonance (CMR) imaging with contrast may be used to create a 3D reconstruction highlighting venous connections and often demonstrates larger defects, although smaller central defects are sometimes poorly seen

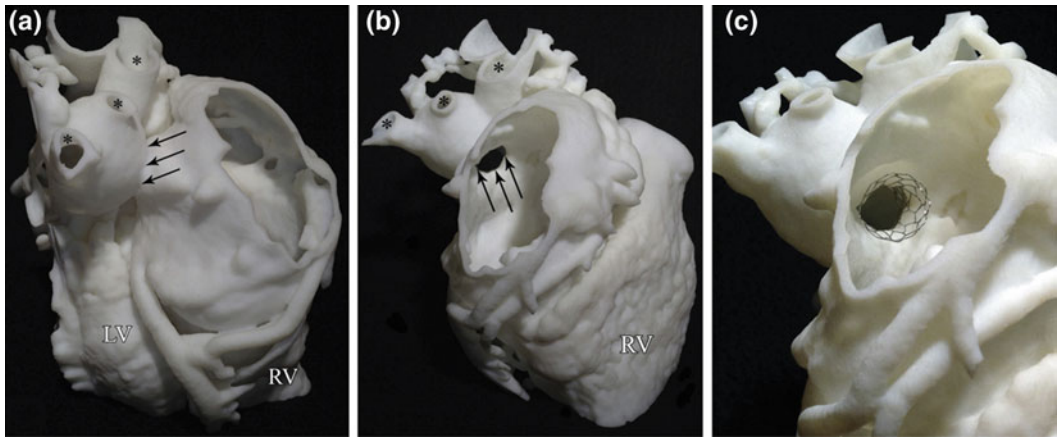


**Fig. 7.1** Photograph of a 3D model of D-transposition of the great arteries status post-Mustard atrial switch with pulmonary venous baffle obstruction. **a** View of the model from the patient's right side. Three right pulmonary veins (*asterisks*) are seen entering the pulmonary venous atrium posteriorly. The stenosis (*arrows*) sits between the dilated posterior pulmonary venous atrium (to *left*) and the much larger anterior atrial chamber (to *right*). **b** View of the stenotic orifice (*arrows*) as seen through a cutaway in the anterior atrial wall. The 3 right pulmonary veins (*asterisks*) can be seen entering the posterior atrial chamber. **c** View of the stent in the stenotic orifice as seen through a cutaway in the anterior atrial wall. Adapted with permission from International Journal of Cardiology

using CMR [2]. In adults, 3D transesophageal echocardiogram is frequently used for the assessment of the interatrial septum and venous structures, although this does require sedation. Other imaging modalities, such as CMR or multi-detector cardiac computed tomography (MD-CCT), can make beautiful 3D reconstructions of the heart, highlighting both the ASD and any associated anomalies [3]. Finally, in both children and adults, intracardiac echocardiography (ICE) or transesophageal echo with 3D imaging are frequently utilized to confirm atrial septal defect anatomy and guide device closure during a procedure in the cardiac catheterization laboratory [4].

## Value Added by 3D Cardiac Model of ASD

Uncomplicated secundum atrial septal defects rarely require additional imaging prior to management decisions. Before undertaking management of unusual types of septal defects, however, more advanced imaging can be useful. Such defects include common atrium with heterotaxy syndrome and venous anomalies, atrial septal defects that involve more than one portion of the interatrial septum, post-surgical septal defects such as Mustard/Senning baffle leaks [5] or lateral tunnel Fontan baffle leaks. In patients with these types of septal defects, a 3D model can be extremely helpful in visualizing complex 3D relationships of the defect to its surrounding structures (see Fig. 7.1).

## ASD Model Creation and Post-processing

In such cases, where 3D models will be created to guide the management of complex atrial septal defects, source images for the model may come from any of the three imaging modalities; 3D echo, cardiac magnetic resonance or cardiac computed tomography. For source images derived from 3D echo, the goal is to set the field of view as large as possible to mitigate disorientation from a narrow imaging field. Setting the gains to create little noise in the blood pool helps to make post-processing of the model easier. Obtaining late systolic or early diastolic imaging datasets is best, so that the defect is viewed when the atria and the interatrial septum are at their

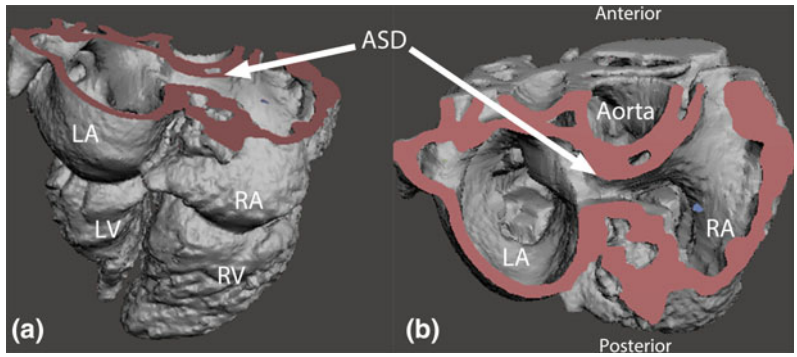


**Fig. 7.2** Digital 3D cardiac model of a moderate, retroaortic secundum atrial septal defect derived from multi-detector cardiac computed tomography (MD-CCT) data. **a** shows an anterior–posterior view, **b** shows a superior–inferior view, looking into the atria from above. In this case, a model was created to help guide decision-making about the appropriateness of device closure with minimal retroaortic septal rim. *ASD* atrial septal defect, *RA* right atrium, *RV* right ventricle, *LA* left atrium, *LV* left ventricle

largest. Finally, if an interventional procedure is being planned, the model may need to show systemic venous connections, so that an approach to the defect can be fully visualized. If a complex surgical procedure is being planned, again, the pulmonary and systemic veins should be segmented and included in the model.

For source images derived from CT or MR, these datasets should be segmented, paying particular attention to the region of the septal defect (see Fig. 7.2). Typically, a segmentation of the blood pool is created, and then the inside is subtracted so that a thin (1–2 mm) layer at the blood pool–myocardial border is left for optimal display of the defect. Again, systemic and pulmonary venous information should be included in the model whenever relevant to the repair.

## VSD

Ventricular septal defects (VSDs) are the most common congenital heart defects, with a prevalence of 1/700 live births for muscular defects to 1/1300 live births for perimembranous defects [1]. There are generally four types of VSDs according to the Society of Thoracic Surgeons (STS) classification—muscular, perimembranous, inlet-type (or atrioventricular canal VSDs), and outlet-type (or conoseptal hypoplasia/supracristal defects) [6]. VSDs can also be associated with a malaligned conal septum and are frequently seen in conjunction with conotruncal defects, such as double outlet right ventricular or transposition of the great arteries. For the purposes of this chapter, we will consider isolated VSDs and allow for discussion of more complex defects in other chapters.

### Current Imaging of VSD

Similar to ASDs, the majority of imaging of uncomplicated VSDs is currently carried out by transthoracic echocardiogram in children with both 2D and 3D imaging [7]. Occasionally, CMR may be used to create a 3D reconstruction, particularly if an intervention is being planned in the management of the defect, or if views are limited from the transthoracic echo [8]. Finally, when multiple or complex defects are seen, MD-CCT is occasionally used in adults to delineate VSDs, particularly in post-myocardial infarction defects where patients may be too sick to undergo CMR or transesophageal echocardiography. In each of these defects, it is important to note the extent of the defect and which regions of the interventricular septum are involved.

## Value Added by 3D Cardiac Model of VSD

Uncomplicated perimembranous VSDs rarely require additional imaging beyond standard transthoracic echocardiography prior to management decision-making. However, before undertaking the management of unusual types of VSDs such as large or multiple muscular defects, malalignment VSDs, or post-infarction VSDs [9], a 3D model can be helpful in visualizing complex anatomic relationships of the defect to its surrounding structures (Figs. 7.3 and 7.4).

## VSD Model Creation and Post-processing

In cases where 3D models will be useful to guide management of complex ventricular septal defects, source images for the model may come from any of the three modalities. For source

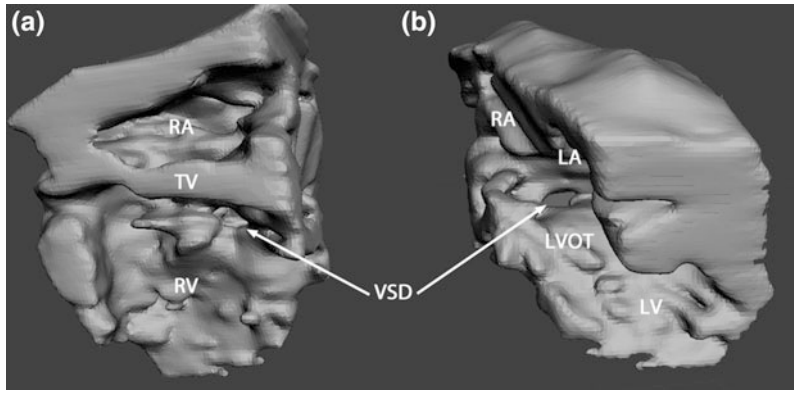


**Fig. 7.3** Digital 3D cardiac model of a perimembranous ventricular septal defect derived from 3D echo data from a 5-month-old infant. **a** is a view from the right ventricular side of the dataset, with the VSD indicated by a *white arrow*. **b** is a view from the left ventricular side of the dataset. The VSD is indicated by the *white arrow*. *RA* right atrium, *RV* right ventricle, *LA* left atrium, *LV* left ventricle

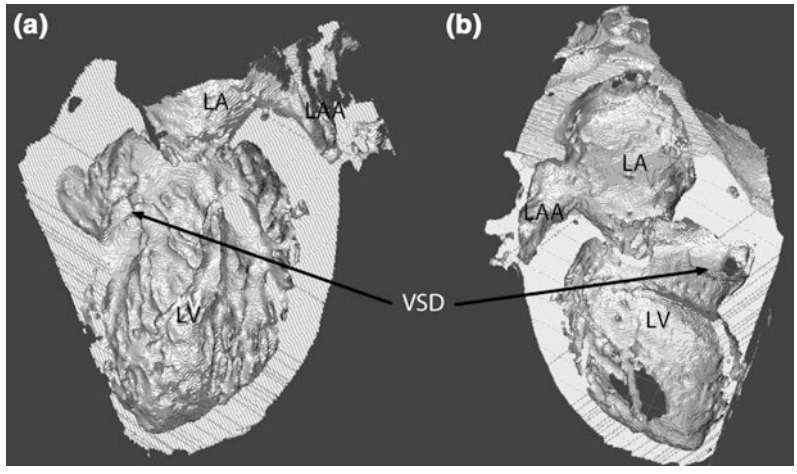


**Fig. 7.4** Digital 3D cardiac model of a post-infarction ventricular septal defect derived from multi-detector cardiac computed tomography data. The VSD in this case is located very inferiorly within the basal portion of the interventricular septum. **a** is a view from the "four chamber view," with the VSD indicated by a *black arrow*. **b** is a view from the "two chamber view." *LA* left atrium, *LV* left ventricle, *LAA* left atrial appendage

images derived from 3D echo, the margins of the defect should be completely within the field of view of the echo probe as well as major associated structures such as the septal leaflet of the tricuspid valve and the right ventricular moderator band [10]. Adjusting gains to minimize blood pool noise is helpful in post-processing the images for segmentation. Finally, obtaining end-diastolic imaging datasets will show the defect in its full size, without distortion during systole. If an interventional procedure is being planned, the model may need to show the moderator band, septal band, and the tricuspid and aortic valves, so that device placement can be planned to minimize the risk of valve disruption and conduction problems. If a complex surgical procedure is being planned, the pulmonary and systemic outflows should be segmented and included in the model.

Models derived from CT or MR source images favor an approach where the blood pool is segmented and expanded circumferentially, following by a subtraction of the blood pool so that a thin (1–2 mm) layer at the blood pool–myocardial border is left for optimal display of the defect, and associated structures. Systemic and pulmonary outflow information should be included in the model whenever relevant to the repair.

## AVSD

Atrioventricular septal defect (AVSD) or AV canal defects are a rarer type of septal defect with a prevalence of 1/2500 live births. Embryologically, this lesion is comprised of a primum-type atrial septal defect, an inlet-type ventricular septal defect, with a common atrioventricular valve. There is a spectrum of severity of these defects, ranging from a partial AVSD which consists of a large primum ASD with a cleft mitral valve to a transitional AVSD with a primum ASD with a common atrioventricular valve, and either an intact or nearly intact ventricular septum [1]. AVSD can be associated with other congenital heart defects, such as tetralogy of Fallot or pulmonary venous anomalies. They can also be unbalanced, where the atrioventricular valve directs the flow preferentially into one ventricle as compared to the other. Finally, the common atrioventricular valve can be poorly formed and dysfunctional, causing a significantly increased volume load on the heart. All forms of AVSD generally require operative repair, and the timing of repair is usually in early childhood, depending on the growth and overall well-being of the child.

### Current Imaging of AVSD

Currently, the majority of imaging of uncomplicated AVSD is by transthoracic echocardiogram in children, with both 2D and 3D imaging [7]. Occasionally, CMR or MD-CCT may be used to create a 3D reconstruction, particularly if there is concern about unbalance of the valve. However, it is difficult to visualize AV valve leaflets on CMR, so if there is a concern about the anatomy of the valve itself, this would not be a recommended imaging modality from which to segment the valve.

### Value Added by 3D Cardiac Model of AVSD

Straightforward AVSDs rarely require imaging beyond transthoracic echocardiogram prior to undertaking surgical repair. However, before undertaking the management of unbalanced AVSD, AVSD with a common valve that leaks a significant amount, or AVSD with complex venous anomalies, a 3D model may be helpful in visualizing the relationship of the atrioventricular valve to the interatrial septum and interventricular septum.

### AVSD Model Creation and Post-processing

In cases, where 3D models will be created to guide the management of AVSD, source images for the model may come from any of the three

modalities. For source images derived from 3D echo, the most important information to focus on will be the atrioventricular valve itself. Turning gains down to show the valve leaflets and subvalvar apparatus will aid the segmentation process. Ideally, segmenting the valve *en face,* from the surgeon's view, will be the most helpful to surgeons looking to repair a common valve as part of an AVSD repair. Obtaining early systolic imaging datasets will show any clefts or coaptation defects in the atrioventricular valve and will still allow visualization of the relationship of the valve to the ASD and VSD. For models derived from CT source images, it may be useful to consider segmenting lower signal intensity structures (myocardium and papillary muscles) to achieve a targeted segmentation of the atrioventricular valve. To segment the AV valves, 3D echo is the best type of imaging dataset given the blood pool–valve leaflet difference in signal intensity.

## References


1. Kruszka P, Olivieri L. Cardiovascular malformations (Chap. 20). In: Human malformation and related anomalies. 4th ed. Oxford: Oxford University Press; 2015.
2. Ganigara M, Tanous D, Celermajer D, Puranik R. The role of cardiac MRI in the diagnosis and management of sinus venosus atrial septal defect. Ann Pediatr Cardiol. 2014;7(2):160–2.
3. Kong D, Cheng L, Dong L, Pan C, Yao H, Zhou D, et al. Three-dimensional echocardiography in the evaluation of right ventricular global and regional systolic function in patients with atrial septal defect before and after percutaneous closure. Echocardiography. 2015 Dec 15.
4. Silvestry FE, Kadakia MB, Willhide J, Herrmann HC. Initial experience with a novel real-time three-dimensional intracardiac ultrasound system to guide percutaneous cardiac structural interventions: a phase 1 feasibility study of volume intracardiac echocardiography in the assessment of patients with structural heart disease undergoing percutaneous transcatheter therapy. J Am Soc Echocardiogr Off Publ Am Soc Echocardiogr. 2014;27(9):978–83.
5. Olivieri L, Krieger A, Chen MY, Kim P, Kanter JP. 3D heart model guides complex stent angioplasty of pulmonary venous baffle obstruction in a Mustard repair of D-TGA. Int J Cardiol. 2014 Jan 8.
6. Jacobs JP, Burke RP, Quintessenza JA, Mavroudis C. Congenital heart surgery nomenclature and database project: ventricular septal defect. Ann Thorac Surg. 2000;69(4 Suppl):S25–35.
7. Simpson JM, Miller O. Three-dimensional echocardiography in congenital heart disease. Arch Cardiovasc Dis. 2011;104(1):45–56.
8. Fratz S, Chung T, Greil GF, Samyn MM, Taylor AM, Valsangiacomo Buechel ER, et al. Guidelines and protocols for cardiovascular magnetic resonance in children and adults with congenital heart disease: SCMR expert consensus group on congenital heart disease. J Cardiovasc Magn Reson Off J Soc Cardiovasc Magn Reson. 2013;15:51.
9. Lazkani M, Bashir F, Brady K, Pophal S, Morris M, Pershad A. Postinfarct VSD management using 3D computer printing assisted percutaneous closure. Indian Heart J. 2015;67(6):581–5.
10. Olivieri LJ, Krieger A, Loke Y-H, Nath DS, Kim PCW, Sable CA. Three-dimensional printing of intracardiac defects from three-dimensional echocardiographic images: feasibility and relative accuracy. J Am Soc Echocardiogr Off Publ Am Soc Echocardiogr. 2015;28(4):392–7.

# Tetralogy of Fallot with Major Aortopulmonary Collateral Arteries

8

Justin Ryan, PhD and Stephen Pophal, MD

## Definition

Tetralogy of Fallot (TOF) is a defect of the heart with four characteristic components: (1) a stenosed, obstructed, or atretic pulmonary artery; (2) an overriding aorta; (3) a ventricular septal defect (VSD); and (4) a hypertrophied right ventricle [1]. Additional malformations can complicate this lesion, including highly stenotic, hypoplastic, discontinuous, or absent pulmonary arteries. The obstructed pulmonary artery can lead to the dependence on the patent ductus arteriosus and/or major aortopulmonary collateral arteries (MAPCAs) to ensure pulmonary flow to the lungs [1, 2].

## Description

TOF is one of the most common cyanotic congenital heart diseases (CHDs) with an incidence of 28 per every 100,000 live births and accounts for 2.6% of all CHDs [3]. MAPCAs are present in 30–65% of patients with TOF with pulmonary atresia and provide partial or complete pulmonary blood flow [1, 4]. Common variations of TOF/MAPCA include pulmonary atresia in 7% of patients [1, 5] and a common origin of the left anterior descending and right coronary arteries arising from the right sinus of Valsalva [1, 6]. Additional VSDs can be present in up to 5% of TOF patients, further complicating interventional or surgical repair [2, 7].

In TOF with pulmonary atresia, it is common for pulmonary blood flow to be diverted through MAPCAs instead of native pulmonary arteries. These MAPCAs lead to further stenosis or lack of growth of native vessels by circumventing blood flow through the native pulmonary arteries. Current literature supports embolization and removal of these vessels if there is competitive or dual supply in order to stimulate the development of the patient's native pulmonary vessels [1, 2, 8–10]. To help in their evaluation, 3D reconstruction and 3D-printed models can be used to differentiate the native and collateral vessels by locating vessel origin and destination (Fig. 8.1).

We will not review the various methods (and controversies) of unifocalization, one-stage or multistage approach, or the benefits/deficits of a transatrial or transventricular approach as a better option for repair. This chapter will investigate the role of 3D modeling and 3D printing as a means to support an institutions' approach to TOF/MAPCA repair.

## Current Imaging Modalities

### Overview

For diagnostic evaluation, 3D modeling, and presurgical planning, accurate clinical images are important to understanding the cardiac morphology of patients with TOF and MAPCAs.

J. Ryan, PhD (✉) · S. Pophal, MD
Department of Cardiology, Phoenix Children's Hospital, Phoenix, USA
e-mail: jryan1@phoenixchildrens.com


K.M. Farooqi (ed.), *Rapid Prototyping in Cardiac Disease*,
DOI 10.1007/978-3-319-53523-4_8

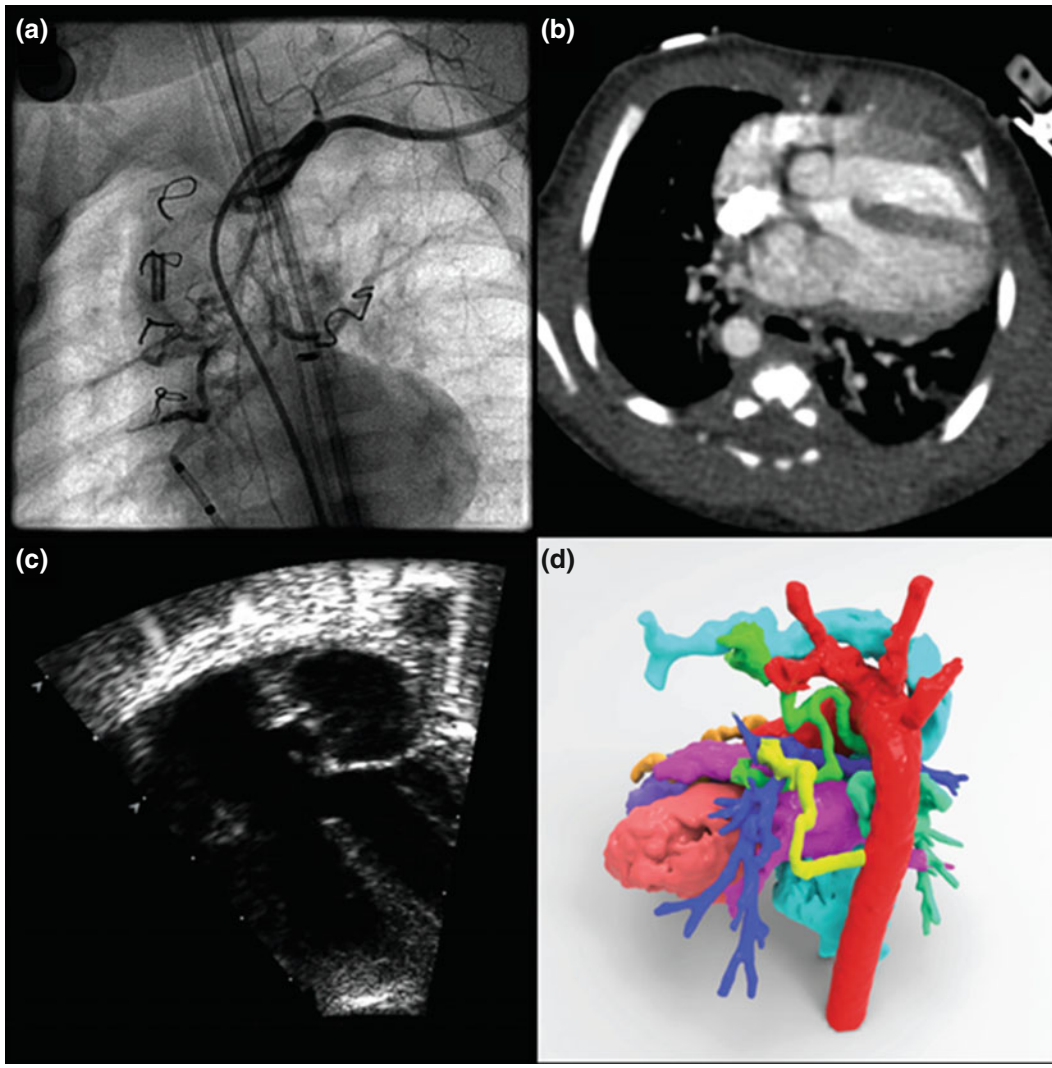


**Fig. 8.1** **a** CCA illustrating MAPCAs in situ. **b** Axial CT image illustrating overriding aorta, hypertrophied right ventricle, and MAPCAs. **c** 2D echo illustrating overriding aorta. **d** 3D reconstruction of CT dataset from a posterior angle. MAPCAs are colored various shades of green; see Table 8.1 for full color explanation. Cardiac catheterization angiography (*CCA*), major aortopulmonary collateral arteries (*MAPCAs*), computed tomography (*CT*), three-dimensional (*3D*)

Here, we discuss the different common imaging modalities as they relate to 3D modeling and 3D printing of TOF/MAPCA anatomy.

## 2D and 3D Echocardiography

Two-dimensional (2D) echocardiogram (echo) is typically sufficient in defining most structures important for surgical repair of TOF. Echo is particularly well suited to noninvasively locate and define the shape of the anterior malalignment VSD and any additional VSDs. Noting the size and location of these VSDs can be important to surgical success [11]. It is also useful to note the presence of an anomalous left anterior descending from the right coronary artery across the infundibulum of the right ventricle for

preoperative planning of a ventriculotomy. Due to the relatively small diameter of pulmonary vessels and MAPCAs, 2D echo may not be an ideal tool for observing the size, course, and tortuosity of the collateral vessels, especially when they course through the parenchyma.

With regard to 3D printing, 2D echo is largely insufficient and lacks significant image processing algorithms needed for anatomical reconstruction. 3D echo provides opportunities for reconstructing TOF anatomy, although it too has its limitations. Similar to 2D echo, 3D echo can accurately capture large defects such as the malaligned VSD and may illustrate eccentricity of pulmonary stenosis, but discontinuous vessels in the lung's parenchyma may be lost. In addition, the field of view for 3D echo is insufficient in capturing the entire cardiac anatomy, and its low signal-to-noise ratio for small structures, pulmonary vessels, and MAPCAs make it less appealing for anatomical reconstruction and 3D printing. However, a multimodal approach where 3D echo data is coregistered with computed tomography (CT) or magnetic resonance (MR) angiography dataset holds some promise of bringing 3D echo's strengths to clinical 3D printing [12]. In fact, the shape and location of the malaligned VSD may best be described by this multimodality approach to 3D printing. Additional image processing technology will need to be developed to improve the signal-to-noise ratio of 3D echo in addition to improve coregistering techniques with other image modalities.

## Cardiac Catheterization Angiography

Traditionally, cardiac catheterization angiography (CCA) is considered the gold standard for the identification of muscular VSDs, true pulmonary arteries, and MAPCAs in TOF/MAPCA patients. CCA procedures are well suited for identifying MAPCAs and their paths, especially in hemodynamically complex cases such as in the presence of aortopulmonary shunts [13]. This is in part due to the interventionalists' control of where and how much contrast is deployed during the procedure.

Although certainly useful for defining the morphology of a TOF lesion or identifying MAPCAs, CCA has drawbacks in regard to patient safety. While minimally invasive, CCA does have inherent risks associated with any catheterization procedure including bleeding, arrhythmia, vessel damage, and infections [14]. In addition, CCA procedures involve radiation exposure and serial investigations can exacerbate the radiation dose [13, 15, 16]. Median effective radiation doses in comparative studies showed an increase of 1400% from CCA as compared to CT with some simulations putting potential dose increases as high as 7100% greater than minimal radiation CT [13, 17–19]. Further, compounding the issue of radiation exposure is the lowered rates of mortality for the TOF population [20, 21]. While surgical and interventional procedures are enabling longer lives for patients with TOF, higher accumulative radiation exposure may lead to secondary complications.

Direct 3D modeling or 3D printing solely from CCA images is a challenge due to the 2D image acquisition. Multiple perspectives or rotational techniques in conjunction with image processing would be needed to create a 3D print. However, these techniques are seldom used due to lack of spatial (volumetric) resolution, that is, resolution defining a volumetric feature. CCA images can be used to compliment the segmentation and anatomical reconstruction of CT or MR images as they provide supplementary information regarding the morphology and course of the MAPCAs and other key TOF structures.

## Computed Tomography

CT has traditionally been used as a support tool for CCA as it can help to identify the number and location of MAPCAs [22]. The intended utility is to reduce the amount of time under CCA, thereby decreasing radiation exposure. CT also allows visualization of the pulmonary parenchymal

anatomy. Emerging CT technologies have enhanced the acquisition of images so that they offer clarity comparable to CCA. In fact, studies support that CT is as accurate for MAPCA measurement as traditional CCA-based measuring schemes [13]. In the past, the decision of whether to perform a complete, two-ventricle repair with closure of the VSD was based on linear measurements of the pulmonary arteries from CCA. These metrics are known as the Nakata (pulmonary artery) index and the McGoon ratio [23, 24]. CT and MR imaging afford the capabilities to reassess these criteria with volumetric measurements of the pulmonary arteries. The volumetric nature of CT images yields well to the creation of 3D models (Fig. 8.1). These CT-based models are well described in the literature [25, 26].

### Magnetic Resonance Imaging

Magnetic resonance imaging (MRI) is presently in a state of rapid advancement and evolution. Current generation technologies can provide an enormous amount of both structural and functional information. Volumetric 3D MR angiography can be used to identify key structures such as the pulmonary arteries and MAPCAs as accurately as CT methods [15, 27]. However, current MR technologies do not have the spatial resolution offered by CT, resulting in a loss of fidelity of minute structures. MR angiography has made great strides in the recent past and may soon overcome CT technologies with regard to volumetric datasets. In addition, less contraindications for MR angiography and the lack of radiation make MR angiography an appealing alternative for TOF/MAPCA diagnosis and surgical planning.

## 3D Modeling and Printing

### Overview

3D visualization and 3D printing are well suited to aid in the understanding of morphologically complex CHD lesions. Anatomic reconstruction and visualization begin with image acquisition. For the remainder of the chapter, we will focus on current and emerging technologies and how they impact TOF/MAPCA evaluation and surgical/interventional planning.

### 3D Reconstruction

Following image acquisition, medical images are brought into a medical image software suite featuring segmentation tools. Segmentation is the image processing technique where an image, or image dataset in the case of volumetric patient data, is separated into discrete parts (Fig. 8.2). Segmentation is performed largely based on two concepts: discontinuity and/or similarity of intensity values. In discontinuity segmentation, an image is partitioned based on abrupt changes in intensity, such as edges in an image [28]. In similarity segmentation, an image is partitioned based on intensity criteria such as thresholding, region growing, and Boolean operations [28].

Specific challenges to TOF reconstruction include segmentation of all distal pulmonary vessels and MAPCAs. As MAPCAs typically travel through the lung parenchyma, CT or MR identification can be difficult. Even in cases where MAPCAs are identifiable, pixel intensity value for these vessels may be effectively similar to the intensity value of soft tissue. Global thresholding techniques are not as useful as local thresholding techniques or more advanced image processing techniques such as marching boxes.

Care should be taken in the reconstruction of the pulmonary arteries, pulmonary veins, MAPCAs, right ventricular outflow tract (RVOT), and the coronary arteries. An aberrant origin of the left anterior descending coronary artery from the right coronary sinus in TOF is ideal to model in cases for surgical preparation. Surgical interventions such as the creation of a right ventricle to pulmonary artery conduit may compress the aberrant coronary artery that crosses the RVOT. A 3D model can accurately display the course of these coronaries and their relationships to surrounding, critical structures.

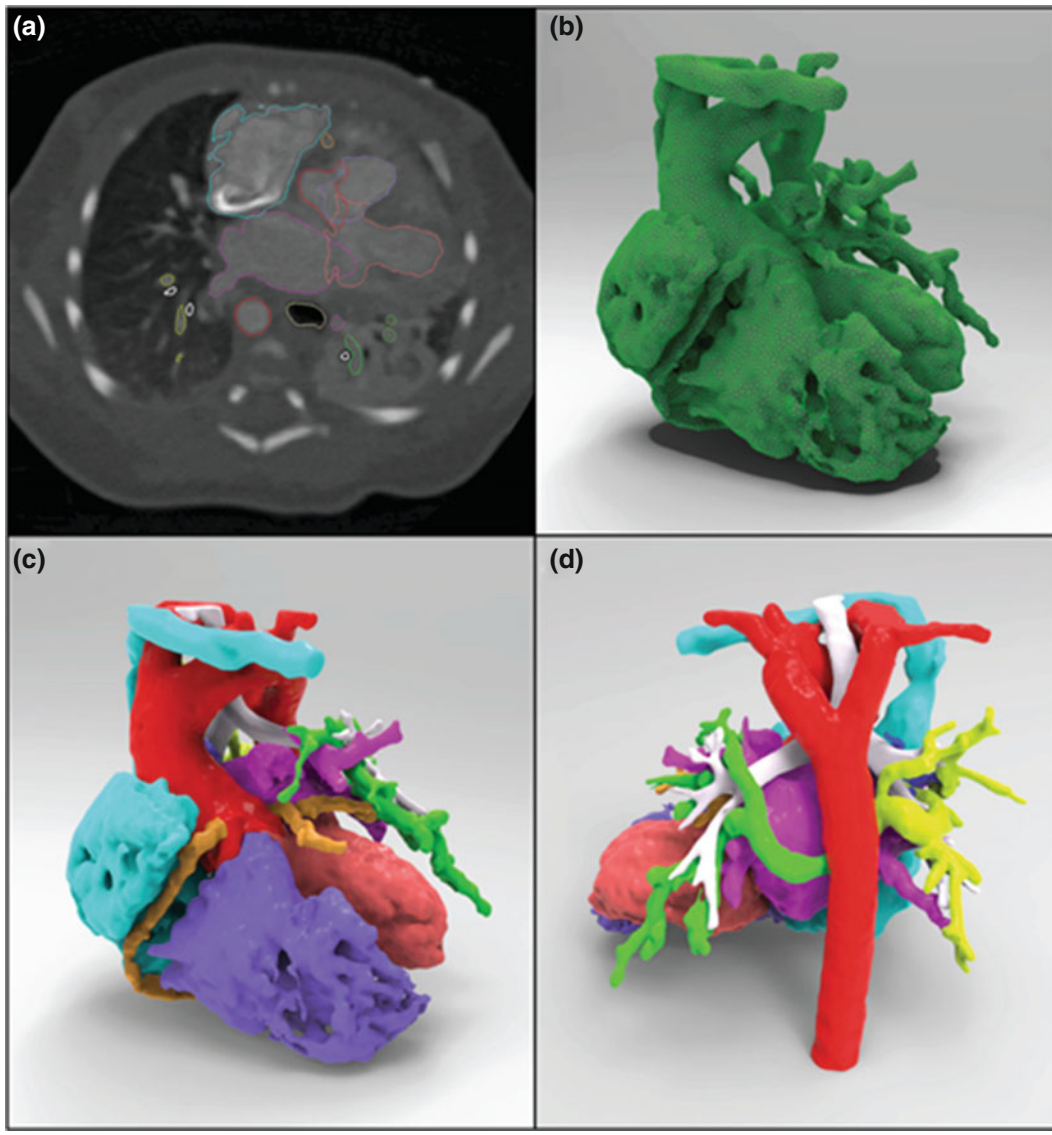


**Fig. 8.2** **a** Segmented mask (multicolor) of the cardiac blood volume. **b** Polygonal reconstruction from the blood volume mask. **c**, **d** Full colored 3D reconstruction from CT dataset. Computed tomography (*CT*)

## Fused Filament Modeling

Fused filament modeling (FFF), also commonly known as the trademarked fused deposition modeling (FDM, Stratasys), is currently the most cost effective form of 3D printing. FFF 3D printers can currently be purchased under $300 at consumer electronic stores. This 3D printing technology entails the use of a plastic filament that is heated past its glass transition temperature and extruded onto a build platform. The 3D printer extrudes each layer of the intended model with the near-molten plastic. Common materials for this process include acrylonitrile butadiene styrene (ABS), polylactic acid (PLA), and nylon [29, 30]. Material properties for this 3D printing technology include high durability and low elasticity. Advantages in using this technique include low cost for printer and materials, durability, and post processing applications.

Limitations of this technology include comparatively low-resolution capabilities, limited color palette, and limited non-rigid options.

While FFF technology may be more affordable than other printing methods, its printing resolution limitations and support generation make the technology less than ideal when 3D modeling TOF/MAPCA and its small, delicate features. Due to these limitations, we recommend utilizing FFF technology for macrostructures such as the shape of the overriding aorta or the hypertrophied right ventricle.

## Powder Bed/Inkjet Printing

Inkjet printing technology entails the use of a binding agent ejected through a printhead onto a bed of powder media such as gypsum or acrylic. Depending on the technology, the binding agent acts either as an adhesive, forming a resin, or as a plastic binding agent, fusing the plastic powder media. A 3D object is printed through the many depositions of this binding agent onto the powder bed until the object is complete [29, 30]. Until recently, inkjet printing was the only method of achieving full color 3D prints.

The role of color in informing clinicians and the patient's family about a patient's CHD cannot be understated. In an educational environment, the utility of color-coded 3D-printed heart models led to statistically significant higher responses to questions probing CHD lesions and morphology (Table 8.1) [26]. The application of color can also assist clinicians in evaluating and differentiating the heart's true pulmonary arteries from MAPCAs. In addition, serial CT or MR studies in conjunction with color 3D prints can enable a clinician to designate pulmonary vessels with unique colors (Fig. 8.3). The unique colors of an earlier time point when compared to a later time point may aid in understanding the development of the patient's true pulmonary arteries.

Inkjet technology is now largely considered a prosumer class 3D print technology, with printers starting at $35,000. As such, this technology is attractive to community hospitals and hospitals looking to start a pilot 3D print program. Deficits

**Table 8.1** Color-coding scheme for 3D-printed blood volumes as developed by Richardson et al. [26]

| Anatomical Structure(s) | Color |
|---|---|
| Aorta | Red |
| Left Atrium | Fuchsia |
| Left Ventricle | Light Red |
| Pulmonary Arteries | Blue |
| Right Atrium & Vena Cava | Turquoise |
| Right Ventricle | Lavender |
| MAPCAs | Green(s) |
| Coronaries | Light Orange |
| Conduit | White |

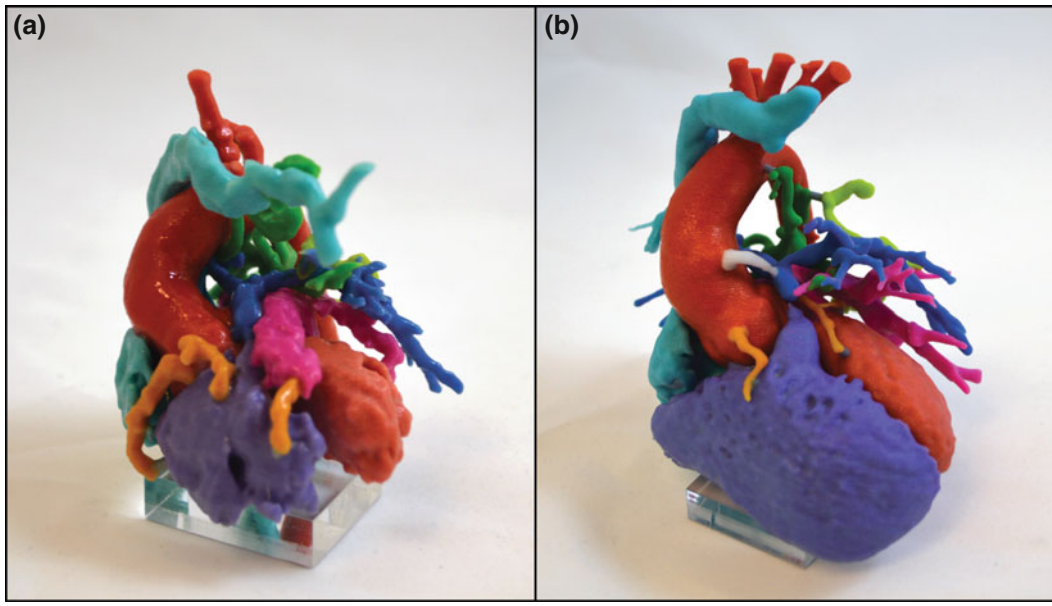


**Fig. 8.3** **a** 3D print of TOF/MAPCAs (>5) and pulmonary atresia patient at one day of life 1. **b** 3D print of same patient at a year follow-up following the placement of central aortopulmonary shunt. Note focal left pulmonary artery stenosis and only 2 residual MAPCAs. Tetralogy of Fallot (*TOF*), major aortopulmonary collateral arteries (*MAPCAs*), three-dimensional (*3D*)

of this technology are largely due to the build material. Gypsum-based inkjet technology produces brittle models. The lack of durability is especially notable in unsupported and delicate structures such as the pulmonary vessels, coronary arteries, and MAPCAs. Newer generation inkjet technologies utilize more durable materials such as an acrylic-based powder media. These technologies greatly increase the tensile strength of the material as well as lower its elastic modulus, further increasing the models' overall durability.

## Stereolithography

Stereolithography (SLA) is a 3D process where an ultraviolet light source selectively illuminates a vat of photopolymer resin. Wherever the resin is exposed to the UV light, the material solidifies and forms a layer of the intended 3D object [29, 30]. This process is repeated for each layer until the 3D object is complete.

SLA's strengths include its high-resolution capabilities in addition to unique material properties such as transparency. SLA technology can accurately represent the complex morphology of a TOF/MAPCA patient. Support media may need to be generated to aid in the printing of delicate features, but these support structures can be removed in a postprocessing step.

Limitations of this technology include the inability to print in multiple colors (except through novel processes of overcuring parts of the resin). The printing material used for SLA, while unique, also has some drawbacks. Over time, ultraviolet exposure to these 3D prints causes breakdown of the model. Long-term exposure will either embrittle or deform the model, negating its patient specificity and accuracy. While the accuracy and unique material properties still make this technology attractive for the creation of patient-specific models, it may be a challenge for many institutions to adopt due to the higher National Fire Protection Association's health ratings for the resin material.

## Jet Photopolymerization

Jet photopolymerization (3DJP) is very similar to SLA technology in that an ultraviolet-sensitive resin is used to construct a 3D model. 3DJP utilizes printheads to jet the photosensitive material onto a build platform and subsequently cure the printed media [29, 30]. This higher level of control allows for discrete printheads to contribute to the printing process, thus enabling multicolor media. In addition, 3DJP enables a wider array of material properties such as rigid, flexible, opaque, and translucent media in the same print.

For the evaluation and planning of TOF/MAPCA repair, a multicolor model with flexible vessel walls can enable a surgeon to practice an entire repair prior to entering the surgical suite. This enhanced form of surgical simulation is well described in current literature and can be easily translated to TOF/MAPCA technology. Drawbacks of this technology include its high cost. The printers utilizing the multicolor and multimaterial media currently range from $150,000 to $350,000. Until 3D printing can be reimbursed through insurance companies, the acquisition of this technology may be prohibitive for many midsized and smaller hospitals.

## Case Studies

### Case Study 1

A patient with TOF with pulmonary atresia was prenatally diagnosed. Cardiac CT at 1 day of age revealed dual pulmonary blood supply to the lungs, confirming the presence of MAPCAs. The native pulmonary arteries were hypoplastic but confluent and appeared distributed to all major lung segments. 3D reconstruction and 3D printing were performed to illustrate the anatomic location of the aortopulmonary collaterals, including those with dual supply (Fig. 8.3). The imaging and 3D reconstructions were used to guide successful placement of a central aortopulmonary shunt and used as a map for subsequent embolization of redundant collateral vessels. Additionally, the 3D print model was available in the cardiac intensive care unit, presurgical conference, the operating room, and the cardiac catheterization laboratory during percutaneous coiling of aortopulmonary collaterals. This process helped focus catheter-based intervention and reduced the amount of fluoroscopy time and contrast exposure. The central, confluent pulmonary arteries grew, and the patient underwent central shunt takedown and complete repair.

This case illustrates that 3D printing of CT datasets may provide significant advantages in preoperative and preprocedural planning. It is the impression of the interventionalist and the medical team that the 3D model facilitated reduction in cumulative radiation exposure, fluoroscopy time, and cardiopulmonary bypass time. The 3D print was also used as a didactic tool in explaining to the patients' parents about the congenital lesion and surgery prior to operation. A year following the surgical repair, the patient received a follow-up CT scan. Again, the CT scan was reconstructed for the interventional team for angioplasty of stenotic pulmonary arteries. The interventionalists compared the new 3D print with the previous 3D print in order to isolate and embolize all dual-supply MAPCAs and therefore enable the growth of the native pulmonary arteries.

### Case Study 2

A cyanotic patient was diagnosed at birth with TOF/MAPCAs featuring a diminutive, patent RVOT and confluent pulmonary arteries. Initially, the decision was made to create a right ventricular to pulmonary artery conduit. A cardiac CT was acquired of the patient, which revealed an anomalous coronary artery. Subsequently, a 3D reconstruction and 3D print were completed and delivered to the surgical team during consultation (Fig. 8.4). Due to the course of the coronary and the surrounding outflow tract, central shunt placement

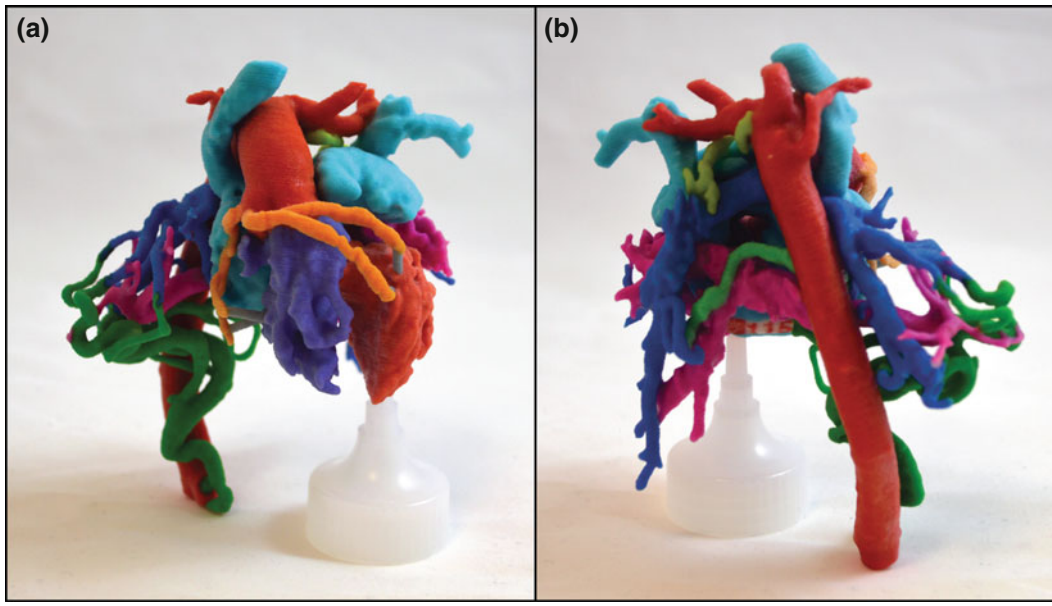


**Fig. 8.4** **a** Anterior perspective on TOF/MAPCAs patient with anomalous left anterior descending coronary artery from the right coronary artery. **b** Posterior perspective of the same patient, illustrating tortuous MAPCAs with distal connections to native pulmonary arteries (dual supply). Tetralogy of Fallot (*TOF*) and major aortopulmonary collateral arteries (*MAPCAs*)

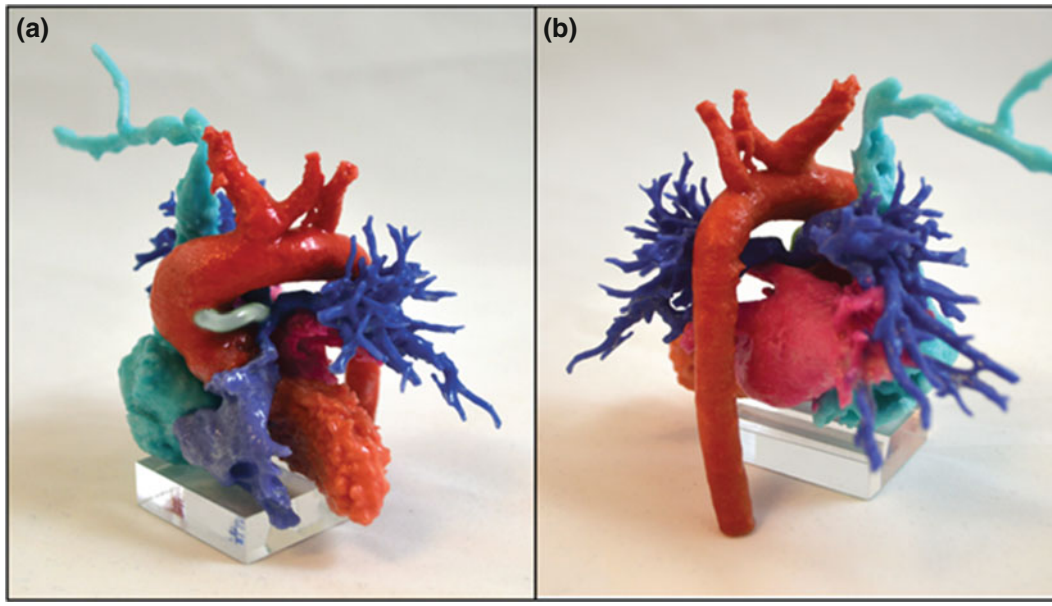


**Fig. 8.5** **a**, **b** Initial 3D print following the placement of a central aortopulmonary shunt. Note focal left pulmonary artery stenosis. Three-dimensional (*3D*)

and coil occlusion of MAPCAs with dual supply were chosen as initial palliations. Full repair was delayed due to the complexity of the RVOT.

## Case Study 3

A one-month-old female was referred from an outside institution for management of TOF with MAPCAs and severely hypoplastic native pulmonary arteries. Serial cardiac CT studies with 3D reconstruction and printing were performed (Fig. 8.5). The information gained from the 3D print along with CCA and surgery allowed embolization of MAPCAs with dual supply and therefore significant growth of native PAs. The patient has residual branch right pulmonary artery stenosis and focal left pulmonary artery stenosis awaiting reintervention. The left pulmonary artery has grown significantly more than the right pulmonary artery and is compressing the left bronchus causing intermittent respiratory issues. Further CT studies and 3D printing will be utilized to assess the development of the native pulmonary vessels prior to surgical intervention.

## Conclusions

TOF and MAPCAs with pulmonary atresia are one of the most severe forms of TOF and challenging for surgeons and interventionalists. MAPCAs are highly variable with unpredictable morphologies. The diverse nature of this cardiac disease is difficult to image with echo and CCA alone. Cardiac CT and MRI with 3D visualization and segmentation allow for clearer definition of vascular and surrounding structures and help differentiate native pulmonary arteries from MAPCAs. 3D printing is an emerging technology that offers potentially improved personalized strategies for patients with TOF/MAPCAs. Different 3D printing technologies have advantages and disadvantages when it comes to surgical planning aids (Table 8.2). Some technologies such as FFF and SLA with lower cost may be better suited for medical education or family consultation where absolute accuracy is not as necessary. Inkjet technologies effectively balance cost and accuracy although they often require additional personnel for postprocessing. 3DJP, while the most expensive technology, yields the greatest accuracy and can achieve the widest

**Table 8.2** Summary of technological capabilities and their advantages/disadvantages with regard to 3D printing for TOF/MAPCA surgical and interventional planning

| Technology | Potential advantages | Potential disadvantages |
|---|---|---|
| Fused filament modeling | • Inexpensive<br>• Able to capture macrostructures in TOF | • Technological constraints for small structures and vessels<br>• Limitations on printing complex features such as MAPCAs |
| Inkjet printing | • Full color<br>• Support material enables complex features | • Brittle<br>• Limited to rigid materials |
| Stereolithography | • Inexpensive desktop versions are available<br>• Able to render complex features<br>• Wider material choices such as transparent media | • Safety concerns for materials |
| Jet polymerization | • Multicolor<br>• Material with variable flexibility<br>• Able to practice surgical scenarios such as unifocalization of MAPCAs | • Expensive |

Tetralogy of Fallot (*TOF*), major aortopulmonary collateral arteries (*MAPCAs*), and three-dimensional (*3D*)

range of material properties. Emerging technologies may supplant current processes with respect to accuracy, material properties, and even cost. No matter the technology used, 3D printing has significant utility in assisting surgical and interventional planning and may lead to better outcomes, with reduced morbidity and mortality as is being investigated in coming clinical trials.

## References


1. Mavroudis C, Backer C, Idriss RF. Pediatric cardiac surgery. 4th ed. Hoboken, NJ: Wiley-Blackwell; 2012 958 p.
2. Jonas RA. Comprehensive surgical management of congenital heart disease. 2nd ed. Boca Raton, FL: CRC Press; 2014 706 p.
3. Egbe A, Uppu S, Stroustrup A, Lee S, Ho D, Srivastava S. Incidences and sociodemographics of specific congenital heart diseases in the United States of America: an evaluation of hospital discharge diagnoses. Pediatr Cardiol. 2014;35(6):975–82.
4. Shimazaki Y, Maehara T, Blackstone EH, Kirklin JW, Bargeron LM. The structure of the pulmonary circulation in tetralogy of Fallot with pulmonary atresia. A quantitative cineangiographic study. J Thorac Cardiovasc Surg. 1988;95(6): 1048–58.
5. Chiariello L, Meyer J, Wukasch DC, Hallman GL, Cooley DA. Intracardiac repair of tetralogy of Fallot. Five-year review of 403 patients. J Thorac Cardiovasc Surg. 1975;70(3):529–35.
6. van Son JA. Repair of tetralogy of Fallot with anomalous origin of left anterior descending coronary artery. J Thorac Cardiovasc Surg. 1995;110 (2):561–2.
7. Dickinson DF, Wilkinson JL, Smith A, Hamilton DI, Anderson RH. Variations in the morphology of the ventricular septal defect and disposition of the atrioventricular conduction tissues in tetralogy of Fallot. Thorac Cardiovasc Surg. 1982;30(5):243–9.
8. Fouilloux V, Bonello B, Kammache I, Fraisse A, Macé L, Kreitmann B. Management of patients with pulmonary atresia, ventricular septal defect, hypoplastic pulmonary arteries and major aorto-pulmonary collaterals: focus on the strategy of rehabilitation of the native pulmonary arteries. Arch Cardiovasc Dis. 2012;105(12):666–75.
9. Zhang Y, Hua Z, Yang K, Zhang H, Yan J, Wang X, et al. Outcomes of the rehabilitative procedure for patients with pulmonary atresia, ventricular septal defect and hypoplastic pulmonary arteries beyond the infant period. Eur J Cardiothorac Surg. 2014;46 (2):297–303.
10. Murthy K, Reddy P, Nagarajan R, Goutami V, Cherian K. Management of ventricular septal defect with pulmonary atresia and major aorto pulmonary collateral arteries: challenges and controversies. Ann Pediatr Cardiol. 2010;3(2):127.
11. Spevak PJ, Mandell VS, Colan SD, Van Der Velde ME, Jonas RA, Lock JE, et al. Reliability of Doppler color flow mapping in the identification and localization of multiple ventricular septal defects. Echocardiogr Mt Kisco N. 1993;10(6):573–81.
12. Olivieri LJ, Krieger A, Loke Y-H, Nath DS, Kim PCW, Sable CA. Three-dimensional printing of intracardiac defects from three-dimensional echocardiographic images: feasibility and relative accuracy. J Am Soc Echocardiogr Off Publ Am Soc Echocardiogr. 2015;28(4):392–7.
13. Meinel FG, Huda W, Schoepf UJ, Rao AG, Cho YJ, Baker GH, et al. Diagnostic accuracy of CT angiography in infants with tetralogy of Fallot with pulmonary atresia and major aortopulmonary collateral arteries. J Cardiovasc Comput Tomogr. 2013;7 (6):367–75.
14. Chambers CE, Eisenhauer MD, McNicol LB, Block PC, Phillips WJ, Dehmer GJ, et al. Infection control guidelines for the cardiac catheterization laboratory: society guidelines revisited. Catheter Cardiovasc Interv Off J Soc Card Angiogr Interv. 2006;67(1):78–86.
15. Prasad SK. Role of magnetic resonance angiography in the diagnosis of major aortopulmonary collateral arteries and partial anomalous pulmonary venous drainage. Circulation. 2004;109(2):207–14.
16. Alpert JS, Sloss LJ, Cohn PF, Grossman W. The diagnostic accuracy of combined clinical and noninvasive cardiac evaluation: comparison with findings at cardiac catheterization. Cathet Cardiovasc Diagn. 1980;6(4):359–70.
17. Garg N, Walia R, Neyaz Z, Kumar S. Computed tomographic versus catheterization angiography in tetralogy of Fallot. Asian Cardiovasc Thorac Ann. 2015;23(2):164–75.
18. Yakoumakis EN, Gialousis GI, Papadopoulou D, Makri T, Pappouli Z, Yakoumakis N, et al. Estimation of children's radiation dose from cardiac catheterisations, performed for the diagnosis or the treatment of a congenital heart disease using TLD dosimetry and Monte Carlo simulation. J Radiol Prot Off J Soc Radiol Prot. 2009;29(2):251–61.
19. Karambatsakidou A, Sahlgren B, Hansson B, Lidegran M, Fransson A. Effective dose conversion factors in paediatric interventional cardiology. Br J Radiol. 2009;82(981):748–55.
20. Pigula FA, Khalil PN, Mayer JE, Nido PJ del, Jonas RA. Repair of tetralogy of fallot in neonates and young infants. Circulation. 1999;100(suppl 2): II-57–Ii-161.
21. Kirklin JW, Blackstone EH, Shimazaki Y, Maehara T, Pacifico AD, Kirklin JK, et al. Survival,

functional status, and reoperations after repair of tetralogy of Fallot with pulmonary atresia. J Thorac Cardiovasc Surg. 1988;96(1):102–16.
22. Tann OR, Muthurangu V, Young C, Owens CM. Cardiovascular CT imaging in congenital heart disease. Prog Pediatr Cardiol. 2010;28(1–2):21–7.
23. Nakata S, Imai Y, Takanashi Y, Kurosawa H, Tezuka K, Nakazawa M, et al. A new method for the quantitative standardization of cross-sectional areas of the pulmonary arteries in congenital heart diseases with decreased pulmonary blood flow. J Thorac Cardiovasc Surg. 1984;88(4):610–9.
24. Piehler JM, Danielson GK, McGoon DC, Wallace RB, Fulton RE, Mair DD. Management of pulmonary atresia with ventricular septal defect and hypoplastic pulmonary arteries by right ventricular outflow construction. J Thorac Cardiovasc Surg. 1980;80(4):552–67.
25. Ryan JR, Moe TG, Richardson R, Frakes DH, Nigro JJ, Pophal S. A novel approach to neonatal management of tetralogy of Fallot, with pulmonary atresia, and multiple aortopulmonary collaterals. JACC Cardiovasc Imaging. 2015;8(1):103–4.
26. Ejaz F, Ryan J, Henriksen M, Stomski L, Feith M, Osborn M, et al. Color-coded patient-specific physical models of congenital heart disease. Rapid Prototyp J. 2014;20(4):336–43.
27. Rao UV, Vanajakshamma V, Rajasekhar D, Lakshmi AY, Reddy RN. Magnetic resonance angiography vs. angiography in tetralogy of Fallot. Asian Cardiovasc Thorac Ann. 2013;21(4):418–25.
28. Gonzalez RC, Woods RE. Digital image processing. 2nd ed. Upper Saddle River, N.J: Prentice Hall; 2002 793 p.
29. Gibson I, Rosen D, Stucker B. Additive manufacturing technologies [Internet]. New York, NY: Springer; 2015 [cited 2015 Dec 7]. Available from: http://link.springer.com/10.1007/978-1-4939-2113-3.
30. Bogue Robert. 3D printing: the dawn of a new era in manufacturing? Assem Autom. 2013;33(4):307–11.

# Double Outlet Right Ventricle

9

Kanwal Majeed Farooqi, MD and Leo Lopez, MD

## Double Outlet Right Ventricle

### Definition

Double outlet right ventricle (DORV) falls under the umbrella of congenital heart defects known as conotruncal defects [1]. The conotruncus refers to the segment of the cardiac tube in embryonic development that forms the conus, the space beneath the semilunar valves, and the great arteries. Aberration in conotruncal development results in anomalies involving ventricular outflow tracts and the great arteries. Examples of conotruncal defects include DORV, transposition of the great arteries, and truncus arteriosus.

### Variations in Anatomy

As the name suggests, DORV consists of both "outlets" or great arteries arising from the right ventricle. The anatomic variations of DORV can be classified in a number of different ways. Categorization by the position of the ventricular septal defect (VSD) in relation to the great arteries results in four descriptive groups: subaortic, subpulmonary, doubly committed, or remote. DORV with subaortic VSD is the most common variant and results in left ventricular blood being directed primarily to the aorta resulting in physiology similar to that of patients with a VSD and associated pulmonary overcirculation. An additional component of pulmonary stenosis in this group results in physiology that resembles patients with tetralogy of Fallot and associated restrictive pulmonary blood flow. When the VSD is closer to the pulmonary valve, oxygenated blood is directed from the left ventricle to the pulmonary artery leading to a physiology much like transposition of the great arteries with cyanosis. When the VSD is either related to both (doubly committed) or neither great arteries (remote), the clinical picture can be anywhere in between these scenarios.

In planning surgical repair for a DORV, it must be determined whether a patient is a candidate for biventricular repair or will be unable to sustain a two-ventricle circulation, thereby requiring a single-ventricle or Fontan palliation. Multiple factors contribute to making this decision, including adequacy of biventricular size, atrioventricular valve tissue obstructing a pathway from the left ventricle to a great artery, and size and position of the VSD relative to the great arteries. If an unobstructed baffle pathway from the left ventricle to the aorta or pulmonary artery is present in the setting of two adequate-sized ventricles, a biventricular repair is a viable

K.M. Farooqi (✉)
Division of Pediatric Cardiology, Rutgers,
New Jersey Medical School, Newark, NJ, USA
e-mail: kanwal.farooqi@rutgers.edu

K.M. Farooqi
Division of Pediatric Cardiology, Icahn School
of Medicine at Mount Sinai, New York, NY, USA

L. Lopez
Nicklaus Children's Hospital, The Heart Program,
Miami, FL, USA
e-mail: leolopezmd@gmail.com


K.M. Farooqi (ed.), *Rapid Prototyping in Cardiac Disease*,
DOI 10.1007/978-3-319-53523-4_9

option. In the absence of these factors, however, a patient will have to undergo two- or three-stage palliative surgery, culminating in the single-ventricle "Fontan" circulation [2].

The mainstay of assessing a patient for congenital heart disease is two-dimensional (2D) echocardiography [3]. Using 2D imaging with sweeps through planes, the three-dimensional (3D) anatomic relationships are inferred. A subcostal long-axis sweep from the abdomen, for example, starts from the inferior and posterior aspect of the heart. The transducer is slowly angled superiorly so that the structures seen later in the sweep are more anterior and superior than those seen initially. In this view, the true right-left orientation of structures is maintained, therefore allowing assessment of the anatomy in three planes.

Despite the immense information that can be obtained from echocardiography, DORV is considered on the spectrum of "complex" congenital heart disease. The variation in anatomy from patient to patient makes it challenging to approach surgical repair in a uniform manner. This is the ideal scenario in which the technique of 3D printing can be applied to increase understanding of the anatomic spatial relationships in a more straightforward manner.

## Common Surgical Approaches to DORV

Surgical approaches to DORV are highly dependent on variations of the patient anatomy [4, 5]. The relationship between the aorta or pulmonary artery, VSD, and left ventricle is essential in determining whether a straightforward baffle from the left ventricle to one of the great arteries may be created (without or with an arterial switch procedure). This would allow rerouting the oxygenated blood to the aorta using a patch to direct the blood from the left ventricle. The use of this technique assumes that multiple factors precluding such a surgical approach are not present. There must be an unobstructed pathway which is not hindered by atrioventricular valve tissue. The VSD must be in such a position that it is at least closely related to the aorta or pulmonary artery. This would avoid the need for a long baffle pathway utilizing a significant amount of right ventricular volume. Both left and right ventricles must be of adequate size to support the systemic and pulmonary circulations, respectively. A ventricle with inadequate size or systolic function could possibly fail after a biventricular surgical repair. In the case where none of these precluding factors are present, a biventricular repair with a baffle from the left ventricle to the aorta may be possible. In the case in which the pulmonary artery is stenotic or the baffle from the left ventricle to the aorta obstructs the flow to the pulmonary artery, a conduit from the right ventricle to the pulmonary artery may be used. In patients with a DORV, atrioventricular discordance, ventricular inversion, a subpulmonary VSD, and an anterior aorta that is far from the left ventricle, a double switch procedure, involving both an atrial and arterial switch procedure, may be considered. The right atrial flow is directed to the left-sided right ventricle. The left ventricle is baffled to the nearest outflow tract, which, in this case, is the pulmonary artery. The great arteries are then switched by disconnecting them at the root and bringing the posterior pulmonary artery more anteriorly and the aorta more posteriorly [6].

In the presence of anatomic variables that would preclude a biventricular repair, however, the patient would undergo a single-ventricle palliation [2]. The initial surgery for such a patient would depend on the specific inadequacy of the neonatal anatomy, i.e., insufficient pulmonary versus systemic blood flow. The first common surgical intervention, the bidirectional Glenn anastomosis, would be performed at approximately 4 months of age, involve attaching the superior vena cava to a branch pulmonary artery, and unload the single systemic ventricle. The final stage, or Fontan completion, would occur at approximately 3–4 years of age and consist of attaching the inferior vena cava to the pulmonary artery, thereby rerouting all systemic venous return passively to the pulmonary arteries. Given the complexity in anatomy and the critical decision that must be made between a

one- or two-ventricle repair, the utility of a 3D printed cardiac model becomes readily apparent.

## Imaging

Once a patient is identified for model creation, consideration must be given to the imaging modality to be used as the source dataset: 3D echocardiography, cardiac MRI, or cardiac CT.

The advantages of 3D echocardiography include having the study performed in the office on the same day as the office visit. There may or may not be a need for sedation depending on the age and level of cooperation of the child. The major limitation of 3D echocardiographic images is that they only partially represent the anatomy. The field of view from the ultrasound probe represents a pyramidal volume. Although the width of the pyramid can be adjusted up to angles of $110° \times 110°$ using ECG gating, an image dataset inclusive of the whole heart is usually not available. In addition, use of ECG gating can introduce "stitch" artifact due to images from different phases being integrated into one volume. The presence of such artifact significantly reduces the quality of the 3D dataset and any 3D model created from it. Additionally, it can be challenging to filter from 3D echocardiographic images the background "noise" that can degrade the blood–tissue border that, in turn, is crucial in delineating the structures needed for segmentation. Specifically for patients with a DORV, it would be a challenge to acquire the full anatomy with a proposed pathway from the ventricle through the VSD to the aorta in one dataset. However, valvular structures are well represented in echocardiographic images. If there is a question of valvular tissue obstructing a baffle pathway, echocardiographic images obtained of that specific area and the resultant 3D virtual or printed file may be able to provide additional data regarding this anatomy.

A cardiac MRI study offers whole-heart imaging with good spatial resolution. When good quality images are obtained, a 3D model can reliably capture the full anatomy needed to plan a baffle from the left ventricle to the aorta. Good blood pool-to-tissue contrast can be obtained with (magnetic resonance angiography) or without (balanced steady-state free precession) administration of an intravenous contrast agent. CMR studies are typically long, however, and they require either sedation or general anesthesia for the large majority of pediatric cases. For this reason, the studies must be scheduled in advance.

Cardiac CT has the advantage of providing images with good spatial resolution in a short period of time. Whereas a cardiac MRI study may take an hour to complete, a cardiac CT study can be completed in a matter of minutes. However, nephrotoxic intravenous contrast must be administered to establish good blood pool-to-tissue contrast, a significant consideration in patients with impaired renal function. In addition, the radiation exposure of CT is a disadvantage, especially in pediatric patients.

Therefore, if whole-heart imaging is needed, echocardiographic images should not be the modality of choice. Cardiac MRI is typically preferred over CT in the pediatric population because of lack of radiation exposure. However, if the length of the cardiac MRI study is a limitation, a cardiac CT can alternatively be performed.

## Considerations in Post-processing and Planning

Once the image dataset has been acquired, careful attention must be given to the method of segmentation and appearance of the final 3D virtual model. The quality of the final 3D printed model is highly dependent on the quality of the source 3D image dataset. A source dataset with good blood pool-to-myocardium contrast will be simpler to post-process. Details of the anatomy of interest will guide the post-processing so that it is clearly represented.

## Segmentation Method

Post-processing of a 3D image dataset involves a process called segmentation. This entails highlighting, or thresholding, an area of interest based on variations in radiodensity among the structures. An upper and lower limit (threshold) in gray

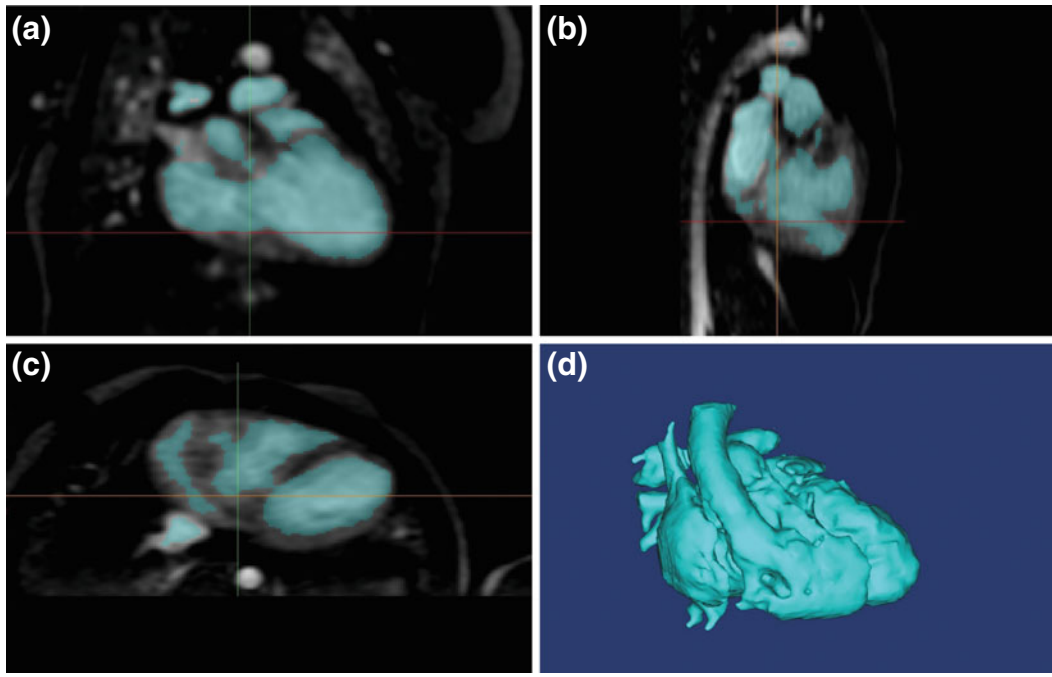


**Fig. 9.1** Segmentation. The blood pool is highlighted using "thresholding" based on gray values in orthogonal views (**a**–**c**). An "offset" layer is created on the surface of this model (**d**) which is then hollowed, leaving a representation of the intracardiac anatomy

values is set to optimally isolate specific parts of the anatomy, such as the blood pool or myocardium (Fig. 9.1). The method of segmentation that produces the best 3D model, involving either the myocardium versus the blood pool, also varies depending on the specific anatomy of interest for each patient. In one method, the myocardium and vessel walls are targeted for segmentation, and the blood pool is left intentionally nulled. The resulting 3D model usually requires a significant amount of post-processing because the thoracic pulmonary vasculature and liver are often highlighted and must be painstakingly separated from myocardium. However, in cases in which the specific thickness of the myocardium and perhaps epicardial details are important, this method of post-processing should be used. For example, this approach is useful when evaluating multiple complex VSDs. Blood pool segmentation entails highlighting the blood volume, creating a 3D object from this segmentation, and subsequently creating a layer that is offset from the resulting 3D mass. The offset layer, whose caliber can be arbitrarily assigned, is then hollowed so that the intracardiac anatomy can be appreciated. Although this method does not give one a sense of the actual dimensions of the vessel wall or myocardium, the intracardiac anatomy is well demonstrated with good detail. There is often much less post-processing involved because the bright blood pool is easier to isolate from the other tissues. Blood pool segmentation is particularly useful in patients with complex intracardiac anatomy that must be delineated for presurgical planning.

## Optimization of a 3D Virtual Model

Once an initial version of a 3D model has been created, multiple steps may be undertaken for virtual model optimization. These steps will ensure a good quality 3D printable model. The 3D virtual model represents a polygonal mesh structure that consists of a collection of vertices, edges, and faces defining the shape of the object.

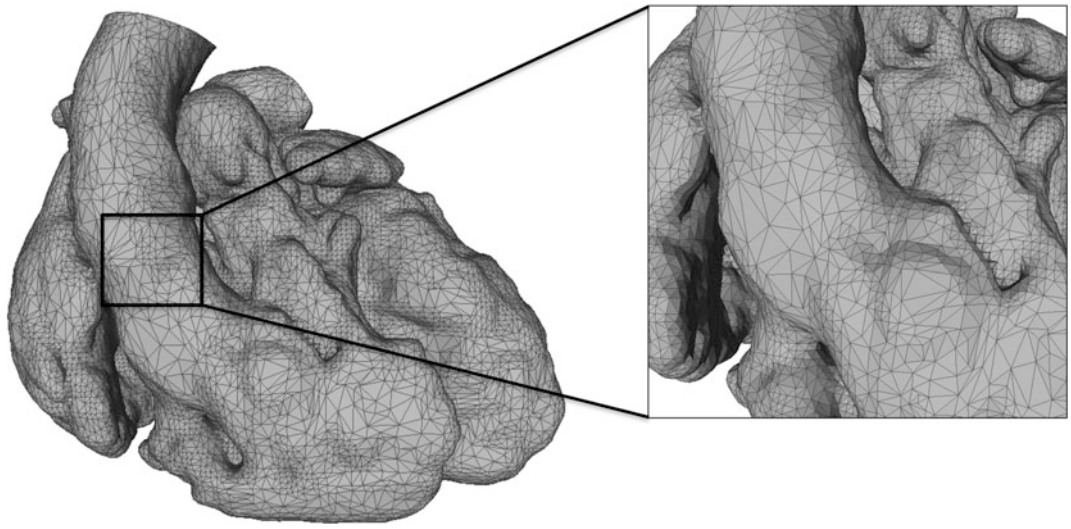

**Fig. 9.2** Polygonal mesh. The structure of the 3D virtual model is comprised of a triangular mesh

In a triangular mesh, the polygons are triangles of different shapes and sizes organized to create the surfaces of the cardiac model (Fig. 9.2). A high-quality mesh consists of the least of number of triangles needed to define the topology of the 3D structure. In order to simplify the mesh, the number of triangles can be reduced by merging, and the sizes and shapes of the triangles are made more consistent throughout the surface. The final optimization of the 3D model consists of multiple steps, such as cropping, smoothing, and removal of free-floating parts.

## Cropping

After a gross 3D virtual file has been created, it must be cropped so that the anatomy of interest is best visualized. In order to create a more "true-to-life" model, the end of the vessels can be cropped to represent the patent vessel lumen. This can be done for the systemic and pulmonary veins, systemic and pulmonary arteries, and any other accessory vessels in a whole-heart model, and this approach results in a more realistic appearing 3D cardiac model. In a patient with a DORV, the most significant relationships that can be demonstrated on a 3D model for presurgical planning are those between the VSD, great arteries, and ventricles (Fig. 9.3). The plane with which these relationships can be simultaneously demonstrated will vary from patient to patient. It is not necessarily true that this can be done using a single plane which simply cuts through the heart along one angle, but instead there may be a combination of planes at different angles used to reveal the anatomy from various aspects. The goal of visualizing these spatial relationships is to assess whether the patient is a candidate for a two-ventricle repair or for a single-ventricle palliation. Although this determination rests on multiple factors, one of the most important considerations is whether oxygenated blood flow can be rerouted to the aorta in an unobstructed manner. In patients with a subaortic VSD, the distance between the tricuspid valve and the pulmonary valve predicts the feasibility of a two-ventricle repair, as this is the region through which a LV to aortic baffle pathway will be created. [7–9]. As 3D models become more commonly used in patients with a DORV, it may be possible that 3D quantification using 3D printed cardiac models will improve and help to predict the optimal surgical approach for a given patient.

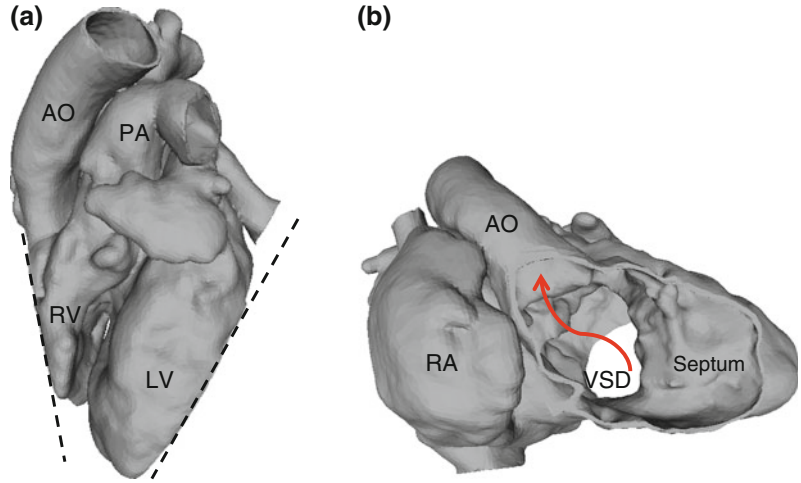


**Fig. 9.3** Cropping. The virtual model is cropped to best demonstrate the internal anatomy of interest. **a** The right and left ventricular free walls have been removed (*dotted lines*). **b** The model is rotated to allow viewing from the RV aspect with the VSD en face. The pathway from the left ventricle through the VSD to the aorta is of importance for presurgical planning (*red arrow*)

## Smoothing

Smoothing of the virtual 3D model allows for an improvement in the overall appearance of the model. The surface of the virtual model is made less coarse without changes in the representation of the 3D anatomy. Laplacian smoothing is one algorithm by which a triangular mesh can be smoothed. It entails reassigning the position of each vertex in a mesh based on the surrounding points (Fig. 9.4). This step can often be completed with commercially available 3D post-processing imaging software or with an open-source software such as Meshlab® (Pisa, Italy). In order to complete this task in Meshlab®, the 3D file should first be imported, using the "Import Mesh" function under the File menu. Once the file has been imported, the Laplacian smooth function should be utilized under the "Smoothing, Fairing, and Deformation" option from the Filters menu. The smoothing steps auto-fills to 3 but can be changed based on preference. It is advisable to start with one smoothing step as one of the drawbacks of using the Laplacian smoothing function is that the model shrinks with each additional iteration.

## Free-Floating Parts

In addition to smoothing, any free-floating parts that may have been left over from segmentation must be removed, as the printer will not be able to process the file if such parts are present. Free-floating parts usually result from the segmentation process in which some artifact is highlighted in the orthogonal imaging planes. This results in 3D pieces that are not representative of the actual anatomy or physically connected to the 3D model. They often float in a cavity or may be present in a vessel lumen (Fig. 9.5). Meshlab may also be used to remove such pieces. Once a 3D virtual file has been imported as detailed above, the "Cleaning and Repairing" option can be used under the Filters menu. The "Remove Isolated Pieces" option allows specification of the size under which all free-floating pieces should be removed from a file. A maximum diameter, using an absolute measurement (world units), can be used to set the limit of pieces to be removed. All the floating pieces with sizes less than the specified one will be removed.

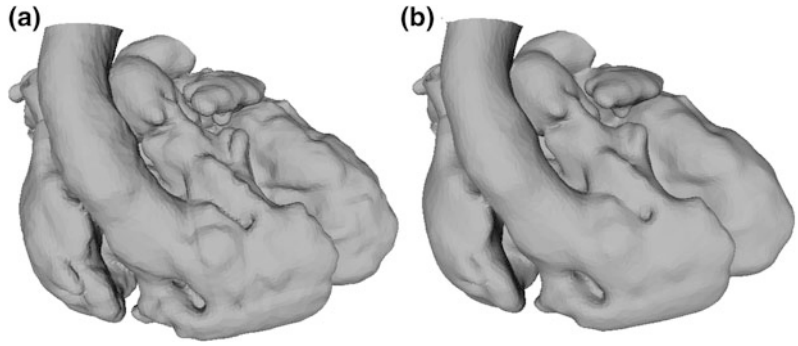


**Fig. 9.4** Smoothing. The Laplacian smoothing function results in a virtual model with a less coarse surface, contributing to its optimization prior to printing. The original virtual file is demonstrated on the *left* (**a**), with the post-processed model, after the smoothing function has been applied, on the *right* (**b**)

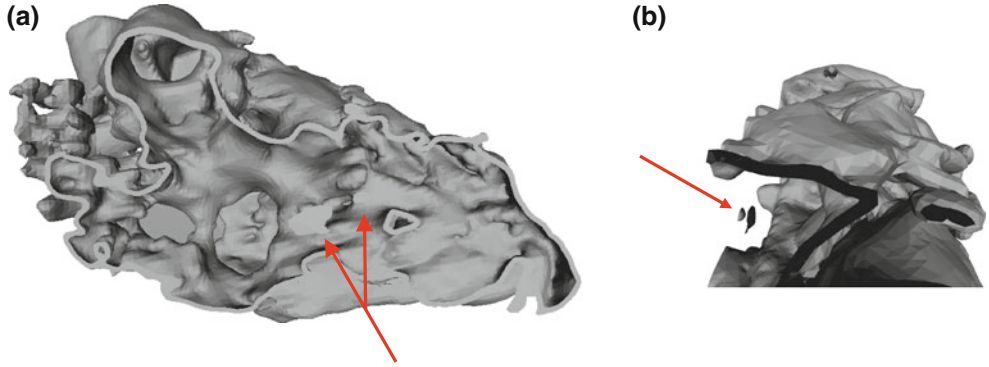


**Fig. 9.5** Removal of free-floating pieces. In preparation for 3D printing, any free-floating pieces present in the cavity of the models must be removed. The red arrows indicate the position of the two free-floating pieces. **a** The virtual model is viewed from the rightward aspect with the right ventricular free wall cropped out. The two free-floating pieces are seen en face as indicated by the *arrows*. **b** The model is rotated to allow appreciation of the two pieces which are completely disconnected from the main model and floating in the cavity

## Virtual Versus 3D Printed Model

Once a virtual 3D cardiac model has been optimized and cropped appropriately, it can clarify the relevant 3D relationships to the surgeon. Whether the 3D virtual model should then be translated into a physical model may be considered a matter of preference. Viewing of the virtual model allows manipulation of the 3D file so that it is viewed from any dimension. The limitation is that a 3D object is being viewed on a 2D screen. There is an advantage with viewing the anatomic relationships in three dimensions. Certain applications such as use of the printed models to practice surgical procedures highlight the value of a printed model. Teaching parents about their child's congenital heart disease is likely more effective with a physical model, given the general lack of familiarity with cardiac anatomy in the lay population. In an effort to conserve resources such as print material and support material, one must determine whether transitioning from a virtual to a physical model will add any information based on the details of each case.

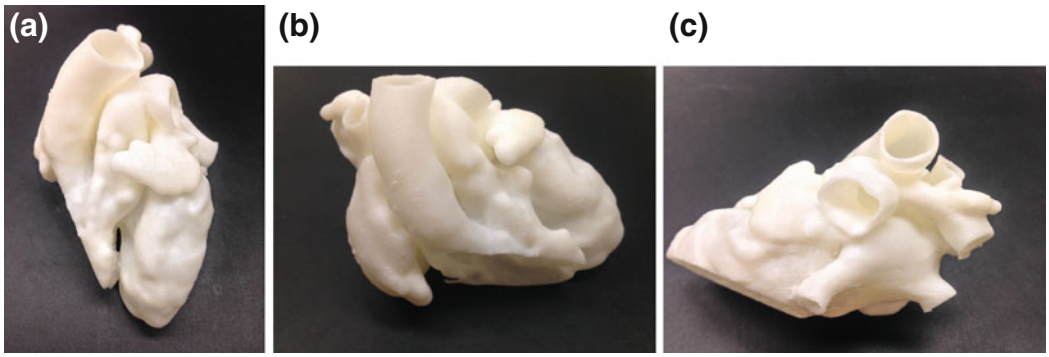


**Fig. 9.6** Physical model. The virtual model is transformed into a physical object using a 3D printer. The printed model is viewed from the superior aspect (**a**), rightward aspect (**b**), and from posteriorly (**c**)

## Choice of 3D Printer

The 3D virtual file that is created after post-processing can be used to create a physical model on any 3D printer with the technical capability to process the complex 3D structure (Fig. 9.6). The virtual file can be saved in a number of different 3D file formats. More commonly used formats include a stereolithography file (.stl) or polygonal file format (.ply). The choice of which printer to use depends on the complexity of the model, the material and color preferences of the cardiac team, the time in which the model is needed for presurgical planning, and material costs. Models which have fine structures such as small vessels should involve a printer which has supports that are easily removable and do not have to be manually removed. There are multiple desktop printers which have soluble supports. Once the print is complete, it is put into a warm water bath, sometimes with a basic solution, to dissolve the supports away. This method helps to remove support material within the lumens of vessels or other crevices present in the model. As an example, the Makerbot replicator 2X® (Brooklyn, New York) is a desktop printer which prints models with a reasonably good resolution. The printer uses a polylactic acid or PLA material for the model and supports. Once the model is complete, the supports must be broken off manually, often using fine plyers to allow removal within smaller structures and curvatures of the model. Another desktop printer, the Mojo (Stratasys, Eden Prairie, MN), prints in ABS plastic with soluble supports. Once the print is complete, the model is placed in a warm bath of a basic solution with an agitator allowing for faster dissolution of the support material. The models' internal and external surfaces are rendered clean of support material. When printing models of complex congenital heart disease, printers utilizing support dissolution are recommended because of the ease with removing the supports. Printers which use a powder, such as sandstone, as the material for the model, utilize high-velocity air for support removal. This blows away the powder present in the cavity of the heart.

Another consideration in choosing the printer involves the team preference for softer, more pliable material versus harder, more solid material. The former allows for visualization of the anatomy as well as the potential for simulated repair of the defect on the model itself, such as using sewing material on the model to repair a septal defect.

## References

1. Van Praagh R. Terminology of congenital heart disease. Glossary and commentary. Circulation. 1977;56(2):139–43.
2. Fontan F, Baudet E. Surgical repair of tricuspid atresia. Thorax. 1971;26(3):240–8.
3. Serraf Pfammatter JP, Berdat P, Hammerli M, Carrel T. Pediatric cardiac surgery after exclusively

echocardiography-based diagnostic work-up. Int J Cardiol. 2000;74:185–90.
4. Kleinert S, Sano T, Weintraub RG, et al. Anatomic features and surgical strategies in double-outlet right ventricle. Circulation. 1997;96:1233–9.
5. Bradley TJ, Karamlou T, Kulik A, Mitrovic B, Vigneswaran T, Jaffer S, Glasgow PD, Williams WG, Van Arsdell GS, McCrindle BW. Determinants of repair type, reintervention, and mortality in 393 children with double-outlet right ventricle. J Thorac Cardiovasc Surg. 2007;134(4):967–73.
6. Farooqi KM, Nielsen JC, Uppu SC, Srivastava S, Parness IA, Sanz J, Nguyen K. Use of 3-dimensional printing to demonstrate complex intracardiac relationships in double-outlet right ventricle for surgical planning. Circ Cardiovasc Imaging. 2015;8(5).
7. Lecompte Y, Batisse A, Di Carlo D. Double-outlet right ventricle:a surgical synthesis. Adv Cardiac Surg. 1993;4:109–36.
8. Sakata R, Lecompte Y, Batisse A et al. Anatomic repair of anomalies of ventriculoarterial connection associated with ventricular septal defect. I. Criteria of surgical decision. J Thorac Cardiov Surg. 1988;95: 90–5.
9. Castaneda AR, Jonas RA, Mayer JE, Hanley FL. Double-outlet right ventricle. In: Cardiac surgery of the neonate and infant. Philadelphia: WB Saunders, 1994;445–59.

# Pulmonary Valve Placement

10

Alistair B.M. Phillips, MD and Evan M. Zahn, MD

## Introduction

There are currently over 100,000 patients with tetralogy of Fallot alive in the USA. A majority of these patients have some degree of pulmonary regurgitation. Indications for requiring pulmonary valve replacement (PVR) are continually being redefined, as more is understood about right ventricular (RV) failure as a result of chronic volume load from the pulmonary regurgitation. It was once believed that a patient with repaired tetralogy of Fallot would not need another operation. However, congenital heart specialists began realizing that a portion of these patients would require placement of a pulmonary valve in order to prevent the negative effects of chronic regurgitation of blood into the RV and symptom-free survival [1]. Chronic regurgitation is a result of resection of the abnormal pulmonary valve and, in most cases, involves placing a patch to increase the size of the RV outflow tract (RVOT). Depending on the extent of main pulmonary artery hypoplasia, some patients may require a RV to pulmonary artery conduit placement. As the conduit does not grow with the patient, it will develop stenosis over time and may be stented to relieve this obstruction. While stenting of the RV to pulmonary artery conduit results in a decrease in RV pressure, it is still associated with increased risk of regurgitation [2]. Negative long-term effects of chronic regurgitation include exercise intolerance, arrhythmias, RV dilation and dysfunction, heart failure, and even sudden cardiac death [3]. Congenital heart specialists are now finding that much greater numbers of patients with repaired tetralogy of Fallot and significant pulmonary insufficiency will benefit from placement of a competent valve for better clinical outcome and less adverse events [4–7]. Figure 10.1 is a literature representation from different years, by different authors, showing the change in indication for PVR over the last 10 years.

## Pulmonary Valve Replacement

There are two primary approaches to placement of a pulmonary valve. The "gold standard" is a surgical replacement of the valve. The main benefits of a surgical approach are that the valve can be placed with very little morbidity and mortality but requires open-heart surgery, and placement on cardiopulmonary bypass. Additionally, surgically placed pulmonary valves may require subsequent reintervention in certain patients [8]. Surgical intervention allows other anatomic issues to be addressed, such as pulmonary artery stenosis and closure of residual shunts. Batlivala and colleagues have illustrated that surgical PVR is associated with low mortality rates, demonstrating a 5-year mortality rate of 1.3% among 254 patients [9]. Alternatively, surgical PVR requires longer hospitalization

A.B.M. Phillips (✉) · E.M. Zahn
Cedars Sinai Medical Center, Los Angeles, CA, USA
e-mail: alistair.phillips@me.com


K.M. Farooqi (ed.), *Rapid Prototyping in Cardiac Disease*,
DOI 10.1007/978-3-319-53523-4_10

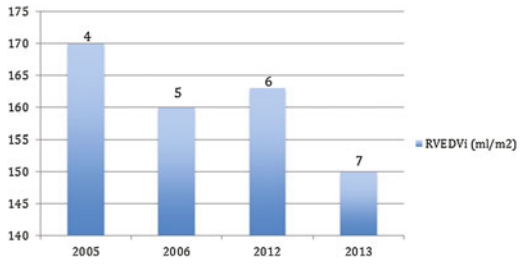


**Fig. 10.1** Literature representation from different years, by different authors; references are above the *bars*. Over the last 10 years, there has been in change in the indication for pulmonary valve replacement from 170 ml/m$^2$ in 2005 to 150 ml/m$^2$ in 2013

periods and increased rates of blood transfusion in comparison with other PVR techniques [10].

Recently, there has been the development of percutaneous pulmonary valve replacement (PPVR), with the benefit of not requiring open-heart surgery [11]. Patients are able to be discharged the next day and do not typically have to undergo surgical reintervention. Additionally, this approach to valve placement maintains the valvular competency and is associated with very low rates of mortality [12]. However, this approach is only for patients with previous conduit placement during their repair, approximately 15% of all tetralogy of Fallot patients. In PPVR, the device currently in use cannot be used in patients with an outflow tract that has a diameter greater than 22 mm [12]. This approach can be limited by patient size, complex anatomy, and vascular access. It is reserved for simpler cases as other anatomic issues cannot be simultaneously addressed. Overall PPVR is minimally invasive and reduces the risk of postsurgical complications, decreases hospital stay, and improves outflow hemodynamics in patients [13].

To address the limitations of both surgical valve placement and PPVR, adapting a "perventricular" approach (placing a large sheath via the apex of the right ventricle) has been developed. In the last few years, perventricular access has been widely accepted and used for muscular ventricular septal defect (VSD) closures [14–16]. As the largest study to date, Xing and colleagues reported on VSD closures in 408 pts with a success rate of 96.3% and a complication rate of less than 4%. Complications included trivial pulmonary regurgitation and incomplete right bundle branch block [16]. Though this approach is not currently being widely used for pulmonary valve implantation, much success has been reported in the literature [17–19]. The mainstay of this less invasive approach is the avoidance of cardiopulmonary bypass with minimal or no complications, providing direct access to the RVOT without compromising the tricuspid valve, sustaining injury to a femoral vessel, or risking damage to the valve [20].

3D printing using additive manufacturing to produce anatomically correct models of the RVOT helps to plan both the surgical approach and catheter-based approach. Dr. Charles Hull in the mid-1980s invented stereolithography (STL) [21] to produce solid objects from digital files using a process involving curing of liquid photopolymer using ultraviolet laser [22]. From this initial work, the field of 3D printing or rapid prototyping began.

Rapid prototyping in medicine has had great success and is a rapidly growing field. It has been very valuable for the planning of procedures. Armillotta et al [23] reported using rapid prototyping models in the planning of percutaneous pulmonary valves. They reported that the three specific applications were (1) diagnostic visualization, (2) surgical planning, and (3) implant fabrication [23]. The use of 3D printing to aid complex surgical planning has been gaining popularity in particular for congenital heart disease [24, 25]. The biggest limitations in early reports of cardiac modeling are the lack of detail related to thin mobile structures such as the atrial septum and valve tissue [24], and the challenge of demonstrating improved clinical outcomes using rapid prototyping [26]. With the improvement in 3D printing techniques and the materials used, surgical and interventional planning can be greatly improved [27].

## 3D Printing for Pulmonary Valve Replacement

The 3D printed RVOT and proximal branch pulmonary arteries allow for interventional staging. We reported our experience using a 4-step approach for planning of replacement of the pulmonary valve [28]. The algorithm we use involves the 3D printed outflow tract and aids in interventional planning, giving us the ability to decide between a percutaneous or perventricular approach.

The perventricular approach combines the skills of both the interventional cardiologist and the surgeon in what is referred to as the "hybrid" approach. This technique has been proven to be safe, effective, and beneficial [15].

We reviewed all patients referred to us for PVR, for suitability, for trancatheter, for surgical, or for perventricular valve placement. The evaluation included echocardiography and magnetic resonance imaging (MRI). In all patients, the MRI data were used to produce a 3D model of the RVOT using postprocessing software (Materialise®). One representative model is shown in Fig. 10.2.

All patients were treated in the "hybrid" catheterization laboratory with cardiopulmonary bypass on standby. Patients underwent right and left heart catheterization with balloon sizing of the outflow tract, 3D rotational angiography, and coronary evaluation during balloon sizing.

**Fig. 10.2** Using the data from CT or MRI scans, 3D printed outflows are created. Using different printers and materials allows for either more rapid prototyping, or printing in different materials. The different materials allow for translucent printing on the *left*, and printing can be done in different materials of different compliance

Patients underwent routine surgical preparation that included preparing for a full sternotomy. In all patients, a perventricular approach was used, via a subxiphoid incision and accessing the RV diaphragmatic surface. For the perventricular approach, a micropuncture needle [Cook Medical Micropuncture Introducer Set: 21 g/7 cm: 5.0 fr/10 cm: 0.018/40 cm wire (Ref #: G43870)] was then placed and a wire placed into the RVOT under transesophageal guidance. After confirming the location, two 4-0 polypropylene sutures with felt pledgets purse strings were placed around the wire with approximately a 1 cm diameter. A six-French sheath [Terumo Pinnacle introducer sheath 6 fr/10 cm 0.038 guidewire (Ref #: RSS602)] was placed over the wire, and the wire was exchanged. A delivery sheath was placed over the wire into the RV, and RV outflow stent(s) were placed to produce an appropriate landing zone for stented valve placement. Heparin was administered to an ACT >200.

Postdeployment angiography and pull back were performed to determine angiographic regurgitation and valve stenosis. Intracardiac echocardiography was performed to determine degree of pulmonary regurgitation and stented valve instability. In the first 2 patients, no chest tubes were used. The remaining 6 patients had 24 Blake drains placed.

## Results

Demographic information for our patients is summarized in Table 10.1. Eight patients were treated with perventricular pulmonary valve placement. Table 10.2 reviews the catheterization information for the patients. There were two complications that occurred. One patient developed a preperitoneal collection that needed to be drained by interventional radiology, and another patient developed a pericardial effusion that required drainage. Three patients had disruption of secondary chordae that lead to mild tricuspid

**Table 10.1** Patient demographic information and MRI data for the first 8 consecutive patients treated with a perventricular hybrid pulmonary valve replacement

| Patient | Age (years) | Weight (kg) | BSA | LV EF ($) | RV EF (%) | RVEDV index (ml/m$^2$) | PRF (%) | Minimum RVOT diameter (mm) |
|---|---|---|---|---|---|---|---|---|
| 1 | 15.4 | 64 | 1.79 | 65 | 55.7 | 180.2 | 45 | 22 |
| 2 | 12.5 | 36 | 1 | 62.9 | 48.3 | 179 | 41 | 22 |
| 3 | 19.8 | 82.6 | 1.75 | 69.1 | 57.1 | 153.8 | 36 | 24 |
| 4 | 31.5 | 85.9 | 2.01 | 29.9 | 30.1 | 149.7 | 52 | 27 |
| 5 | 23.8 | 53.6 | 1.53 | 59.8 | 49.9 | 156.7 | 49 | 27 |
| 6 | 10 | 26.4 | 0.97 | 56 | 50 | 166 | 46 | 24 |
| 7 | 25 | 90 | 2 | [a] | [a] | [a] | [a] | 28 |
| 8 | 62 | 69 | 1.9 | [a] | [a] | [a] | [a] | 27 |

*BSA* Body surface area, *EF* Ejection fraction, *RVEDV* Right ventricular ejection fraction, *PRF* Pulmonary regurgitant fraction, *RVOT* Right ventricular outflow tract
[a]No MRI performed, only CT scan secondary to indwelling pacemaker

regurgitation. There was dramatic improvement in pulmonary artery diastolic blood pressure postimplant, 10.2 ± 2.0 mm Hg compared to RV diastolic pressure preimplant, 3.8 ± 1.8 mm Hg ($p = 0.003$). All patients had severe regurgitation, preimplant. There was no significant gradient from RV to pulmonary artery with a mean gradient of 2.3 ± 1.0 mm Hg post-implant.

Median length of stay was 2 days, no patient had device migration, and all patients had significant improvement of regurgitation. Figure 10.3a–c reviews the steps of the procedure, in the 3D printed model of the RV outflow tract, and on the right panel shows the corresponding catheterization images.

## Conclusions

The hybrid approach to congenital heart surgery provides for less invasive treatment, avoidance of cardiopulmonary bypass, and decreased risk of complications and is a great alternative for selected groups of patients who are not candidates for surgery or percutaneous approaches [29, 30]. Though not much research has been published on perventricular access for pulmonary valve placements with the hybrid approach, it is an ideal maneuver for surgeons and patients. No procedural complications have been reported thus far [17, 19, 31]. While there are many advantages to this kind of hybrid approach, it is difficult to place a valve in the pulmonary position due to the variability and complexity in anatomy of the RVOT, especially in patients with tetralogy of Fallot. The use of 3D models can help guide preoperative planning and decision making.

We have used 3D models in pulmonary valve placements via hybrid procedure to guide planning, visualize unforeseen complications, provide personalized treatment, and help educate patient and families. There are an increasing number of groups reporting on their experience using this technology. Schmauss and colleagues used a 3D model in decision making when replacing an aortic arch and demonstrated that the model provided a better understanding of the disease, anticipating problems prior to surgery, and simulation of the procedure [32]. Similar to our work, Armillotta and colleagues used 3D models in percutaneous pulmonary valve placements for planning of the procedure as well as to assess the "feasibility" of valve implantation [33]. Schievano et al. built 3D models of RVOTs and pulmonary trunk anatomy to evaluate how helpful models were in selecting patients for PPVI. Using the models demonstrated increased accuracy in selecting patients for PPVI when

**Table 10.2** Catheterization data for the first 8 consecutive patients treated with a perventricular hybrid pulmonary valve replacement

| Patient | Fluoroscopy time (min) | Radiation exposure (mGy) | Minimum angiographic RVOT diameter (mm | Minimum static balloon size RVOT (mm) | Prestent-type/RVOT modification | Prestent balloon diameter (mm) | tPVR used | Concomitant procedure |
|---|---|---|---|---|---|---|---|---|
| 1 | 36 | 2122 | 21 | 28.4 | Palmaz 5110<br>iCast × 38 mm | 30 | Melody (mounted on a 24 BIB balloon) | |
| 2 | 32.1 | 894 | 23.9 | 24.6 | Palmaz 5010 | 25 | Melody (mounted on a 24 BIB balloon) | |
| 3 | 36.9 | 1265 | 24 | 24.7 | Palmaz 4010 | 30 | Sapien XT 29 mm | |
| 4 | 51.7 | 3703 | 25.5 | 29 | Palmaz 5110<br>iCast 10 × 38 mm | 30 | Sapien XT 29 mm | ASD closure |
| 5 | 51.1 | 3051 | 24.2 | 26.5 | Palmaz 4010 | 28 | Sapien XT 29 mm | LPA stent |
| 6 | 32 | 216 | 25.2 | 27.2 | Palmaz 3110<br>iCast 9 × 38 mm<br>iCast 10 × 38 | 28 | Sapien XT 29 mm | |
| 7 | 53.3 | 5849 | 26.8 | 33 | Palmaz 4010<br>iCast 9 × 38 mm<br>iCast 10 × 38 mm | 30 | Sapien XT 29 mm | |
| 8 | 59.7 | 2748 | 23.5 | 26.5 | Palmaz 5010 | 30 | Sapien XT 29 mm | |

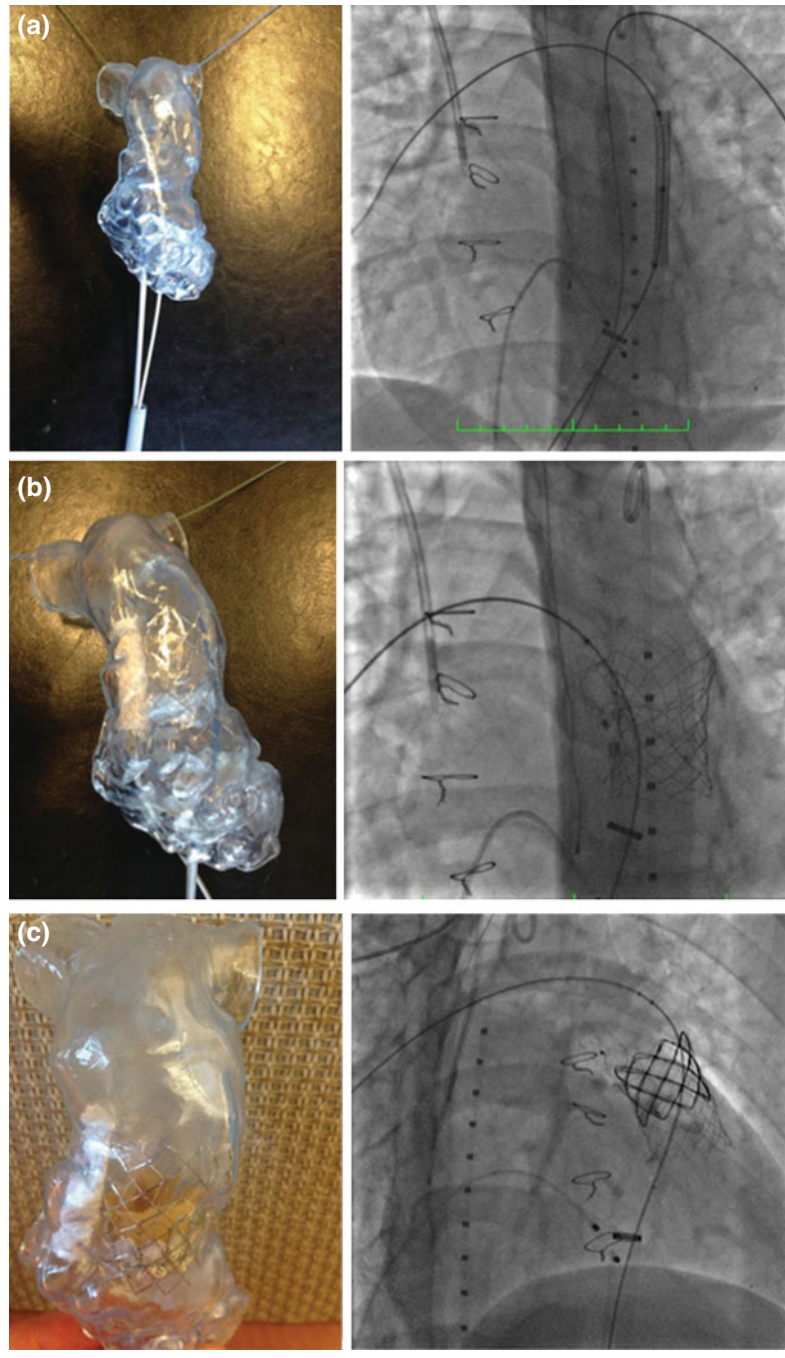


**Fig. 10.3** **a** The 3D printed model (*left*) is used to accurately place the wire for the best positioning of the stents (10-mm covered stent and 30-mm Palmaz) to reduce the size of the right ventricular outflow. The intraoperative angiogram (*right*) showing the exact wire and stent position used in the model. **b** Stents placed in the model on *left* and intraoperative angiogram showing the placement of the stents in the patient, exactly mimicking the simulation in the model. **c** The final result in the model (*left*) and in the patient. The placement of the stents was accurately predicted by using the model

compared to conventional MRI data [34]. This particular study highlights the importance of using 3D models to achieve maximal accuracy in decision making. In addition to preoperative planning, these models also help surgeons intraoperatively, allowing them to actively manipulate the orientation of an implantable valve to determine the best positioning for a specific patient's anatomy. Sodian and colleagues reported on the benefits of intraoperative

orientation by taking the sterilized model into the operating room, which offered the surgeon additional insight at the time of implantation [35]. Such models have been reported to reduce operating time [36].

Given the clear and accurate representation of a patient's anatomy, 3D models aid physicians in explaining the procedure to the patient and his or her family. They can also serve as an invaluable teaching tool for other physicians, colleagues, and nurses. Overall, 3D models have value in decision-making, patient-specific surgical planning, demonstrating anatomic orientation, and providing greater understanding of the defect to the physician and patient. Applying these novel techniques of perventricular access, stented valve, and 3D models to pulmonary valve implantation has proven to be effective and beneficial for patients to achieve better clinical outcomes at our institution.

## References


1. Shimazaki Y, Blackstone EH, Kirklin JW. The natural history of isolated congenital pulmonary valve incompetence: surgical implications. Thorac Cardiovasc Surg. 1984;32:257–9.
2. Aggarwal S, Garekar S, Forbes TJ, et al. Is stent placement effective for palliation of right ventricle to pulmonary artery conduit stenosis? J Am Coll Cardiol. 2007;49:480–4.
3. Babu-Narayan S, Diller GP, Gheta R, Bastin A, Karonis T, Li W, Pennell D, Uemera H, Sethia B, Gatzoulis M, Shore D. Clinical outcomes in surgical pulmonary valve replacement after repair of tetralogy of fallot and potential prognostic value of preoperative cardiopulmonary exercise testing. Circulation. 2014;129:18–27.
4. Therrien J, Provost Y, Merchant N, Williams W, Colman J, Webb G. Optimal timing for pulmonary valve replacement in adults after tetralogy of fallot repair. Am J Cardiol. 2005;95:779–82.
5. Geva T. Indications and timing of pulmonary valve replacement after tetralogy of fallot repair. Semin Thorac Cardiovasc Surg Pediatr Card Surg Ann. 2006;9:11–22.
6. Lee C, Min Kim Y, Lee C, Kwak J, Soo Park C, Young Song J, Shim W, Young Choi E, Yun Lee S, Suk Baek J. Outcomes of pulmonary valve replacement in 170 patients with chronic pulmonary regurgitation after relief of right ventricular outflow tract obstruction implications for optimal timing of pulmonary valve replacement. J Am Coll Cardiol. 2012;60:1005–14.
7. Geva T. Indications for pulmonary valve replacement in repaired tetralogy of fallot the quest continues. Circ. 2013;128:1855–7.
8. Lee C, Lee CH, and Kwak JG. Surgical pulmonary valve insertion. Cardiol Young. 2013;23:915–20.
9. Batlivala SP, Emani S, Mayer JE, McElhinney DB. Pulmonary valve replacement function in adolescents: a comparison of bioprosthetic valves and homograft conduits. Ann Thorac Surg. 2012;93:2007–16.
10. McKenzie E, Khan M, Dietzmann T, Guzman-Pruneda F, Samayoa A, Liou A, Heinle J, Fraser C. Surgical pulmonary valve replacement: a benchmark for outcomes comparisons. J Thorac Cardiovasc Surg. 2014;pii:S0022–5223(14)00267-0.
11. Zahn E, Hellenbrand W, Lock J, McElhimmey D. Implantation of the melody transcatheter pulmonary valve in patients with a dysfunctional right ventricular outflow tract conduit early results from the u.s. clinical trial. J Am Coll Cardiol. 2009;54:1722–9.
12. Lurz P, Gaudin R, Taylor A, Bonhoeffer P. Percutaneous pulmonary valve implantation. Semin Thorac Cardiovasc Surg Pediatr Card Surg Ann. 2009:112–117.
13. Lurz P, Coats L, Khambadkone S, Nordmeyer J, Boudjemline Y, Schievano S, Muthurangu V, Lee TY, Parenzan G, Derrick G, Cullen S, Walker F, Tsang V, Deanfield J, Taylor AM, Bonhoeffer P. Percutaneous pulmonary valve implantation: impact of evolving technology and learning curve on clinical outcome. Circulation. 2008;117(15):1964–72.
14. Bacha EA, Cao QL, Galantowicz ME, Cheatham JP, Fleishman CE, Weinstein SW, Becker PA, Hill SL, Koenig P, Alboliras E, Abdulla R, Starr JP, Hijazi ZM. Multicenter experience with perventricular device closure of muscular ventricular septal defects. Pediatr Cardiol. 2005;26(2):169–75.
15. Amin Z, Gu X, Berry JM, Titus JL, Gidding SS, Rocchini AP. Perventricular [correction of Periventricular] closure of ventricular septal defects without cardiopulmonary bypass. Ann Thorac Surg. 1999;68(1):149–53.
16. Xing Q, Pan S, An Q, Zhang Z, Li J, Li F, Wu Q, Zhuang Z. Minimally invasive perventricular device closure or perimembranous ventricular septal defect without cardiopulmonary bypass: multicenter experience and mid-term follow-up. J Thorac Cardiovasc Surg. 2010;139(6):1409–15.
17. Simpson KE, Huddleston CB, Foerster S, Nicholas R, Balzer D. Successful subxyphoid hybrid approach for placement of a Melody percutaneous pulmonary valve. Catheter Cardiovasc Interv. 2011;78(1):108–11.
18. Holoshitz N, Ilbawi MN, Amin Z. Perventricular Melody valve implantation in a 12 kg child. Catheter Cardiovasc Interv. 2013;82(5):824–7.
19. Cubeddu RJ, Hijazi ZM. Bailout perventricular pulmonary valve implantation following failed

percutaneous attempt using the EdwardsSapien transcatheter heart valve. Catheter Cardiovasc Interv. 2011;77(2):276–80.
20. Bacha E, Marshal A, McElhinney D, del Nido P. Expanding the hybrid concept in congenital heart surgery. Semin Thorac Cardiovasc Surg Pediatr Card Surg Ann. 2007:146–50.
21. Hull C. Apparatus for production of three-dimensional object by stereolithography. U.S. Patent 4,575,330, 1986.
22. Schubert C, van Langeveld MC, Donoso LA. Innovations in 3D printing: a 3D overview from optics to organs. Br J Ophthalmol. 2014;98:159–61.
23. Armillotta A, Bonhoeffer P, Dubini G, Ferragina S, Migliavacca F, Sala G, S Schievano. Use of rapid prototyping models in the planning of percutaneous pulmonary valved stent implantation. J. Eng Med. 2005;221(H):407–16.
24. Mottl-Link S, Hübler M, Kühne T, Rietdorf U, Krueger JJ, Schnackenburg B, De Simone R, Berger F, Juraszek A, Meinzer H-P, Karck M, Hetzer R, Wolf I. Physical models aiding in complex congenital heart surgery. Ann Thorac Surg. 2008;86:273–7.
25. Schrot Janelle, Pietila Todd, Sahu Anurag. State of the art: 3D printing for creating compliant patient-specific congenital heart defect models. J Cardiovasc Magn Reson. 2014;16(Suppl 1):W19.
26. Kim Michael S, Hansgen Adam R, Wink Onno, Quaife Robert A, Carroll John D. Rapid prototyping: a new tool in understanding and treating structural heart disease. Circulation. 2008;117:2388–94.
27. Schrot J, Pietila T, Sahu A. State of the art: 3D printing for creating compliant patient-specific congenital heart defect models. J Cardiovasc Magn Reson. 2014;16(Suppl 1):W19.
28. Phillips AB, Nevin P, Shah A, Olshove V, Garg R, Zahn EM. Development of a novel hybrid strategy for transcatheter pulmonary valve placement in patients following transannular patch repair of tetralogy of fallot. Catheter Cardiovasc Interv. 2016;87(3):403–10. doi:10.1002/ccd.26315 (Epub 2015 Nov 3).
29. Phillips AB, Green J, Bergdall V, Yu J, Monreal G, Gerhardt M, Cheatham JP, Galantowicz M, Holzer RJ. Teaching the "Hybrid Approach": a novel swine model of muscular ventricular septal defect. Pediatr Cardiol. 2009;30(2):114–8.
30. Bacha EA, Hijazi ZM, Cao QL, Starr JP, Waight D, Koenig P, Agarwala B. New therapeutic avenues with hybrid pediatric cardiac surgery. Heart Surg Forum. 2004;7(1):33–40.
31. Holoshitz N, Kenny D, Hijazi ZM. Hybrid interventional procedures in congenital heart disease. Methodist Debakey Cardiovasc J. 2014;10(2):93–8.
32. Schmauss D, Juchem G, Weber S, Gerber N, Hagl C, Sodian R. Three-dimensional printing for perioperative planning of complex aortic arch surgery. Ann Thoracic Surg. 2014;97(6):2160–3.
33. Armillotta A, Bonhoeffer P, Dubini G, Ferragina S, Migliavacca F, Sala G, Schievano S. Use of rapid prototyping models in the planning of percutaneous pulmonary valved stent implantation. Proc Inst Mech Eng H. 2007;221(4):407–16.
34. Schievano S, Migliavacca F, Coats L, Khambadkone S, Carminati M, Wilson N, Deanfield J, Bonhoeffer P, Taylor A. Percutaneous pulmonary valve implantation based on rapid prototyping of right ventricular outflow tract and pulmonary trunk from MR data. Radiology. 2007;242:490–7.
35. Sodian R, Schmauss D, Markert M, Weber S, Nikolaou K, Haeberle S, Vogt F, Vicol C, Lueth T, Reichart B, Schmitz C. Three-dimensional printing creates models for surgical planning of aortic valve replacement after previous coronary bypass grafting. Ann Thorac Surg. 2008;85(6):2105–8.
36. Ngan EM, Rebeyka IM, Ross DB, Hirji M, Wolfaardt JF, Seelaus R, Grosvenor A, Noga ML. The rapid prototyping of anatomic models in pulmonary atresia. J Thorac Cardiovasc Surg. 2006;132(2):264–9.

# Adult Congenital Heart Disease

# 11

Shafkat Anwar, MD, Gautam K. Singh, MD,
Orlando Petrucci, MD, Pirooz Eghtesady, MD, PhD,
Pamela K. Woodard, MD and Joseph J. Billadello, MD

## Scope of Adult Congenital Heart Disease and Role of 3D Printing

Congenital heart disease (CHD) is the most common birth defect, diagnosed in about 1% of births in the USA. Advances in medical and surgical care have dramatically improved the survival rate of these patients. Approximately 85–90% of neonates born with CHD will reach adulthood, a percentage which is likely to further increase in the next two decades [1]. This has caused a demographic shift in which adults now outnumber children with CHD [2]. Two-thirds of the CHD population consists of patients 18 years of age or older with an estimated 1.5 million adult survivors in the USA alone. This population includes not only those with mild and moderate forms of CHD but also those with severe pathology [3]. Despite advances in the field, death rates among patients over 20 years old with CHD (ACHD) exceed that of the general population by 2–7 times [4].

Many ACHD patients arrive at the adult centers with few medical records or with records from various providers with conflicting reports on the original diagnosis and surgical procedures performed. Although cardiac surgery for CHD began in the 1950s, it was often performed on older children and adults, with multiple staged procedures. Complex cardiac defects were not approached until the mid to late 1970s when infant cardiopulmonary bypass was in common use [4]. Aside from the large number of patients with previously diagnosed CHD, there exists a population of adults whose CHD was not diagnosed during childhood. These adults may be asymptomatic or become symptomatic later in life and therefore escaped detection until adulthood [4]. Such defects include atrial septal defects, bicuspid aortic valve, variants of tetralogy of Fallot, congenitally corrected transposition of the great vessels, and coronary artery anomalies [4].

The standard transthoracic echocardiogram performed on the ACHD patient with complex anatomy may not provide suitable information because of poor acoustic windows. In these cases, cardiac magnetic resonance imaging (MRI) or computed tomography (CT) are invaluable techniques to better delineate cardiac anatomy and physiology. In addition to confirmation of the original diagnosis and clarification of the surgical procedures performed, we have

S. Anwar (✉) · G.K. Singh
Division of Cardiology, Department of Pediatrics, Washington University in St. Louis School of Medicine, St. Louis, MO, USA
e-mail: anwar_s@kids.wustl.edu

O. Petrucci · P. Eghtesady
Division of Cardiothoracic Surgery, Department of Surgery, Washington University in St. Louis School of Medicine, St. Louis, MO, USA

P.K. Woodard
Mallinckrodt Institute of Radiology, Washington University in St. Louis School of Medicine, St. Louis, MO, USA

J.J. Billadello
Division of Cardiovascular Medicine, Department of Internal Medicine, Washington University in St. Louis School of Medicine, St. Louis, MO, USA


K.M. Farooqi (ed.), *Rapid Prototyping in Cardiac Disease*,
DOI 10.1007/978-3-319-53523-4_11

occasionally found unexpected residual lesions amenable to intervention by either percutaneous or operative techniques that have improved the patient's functional status. Cardiac MRI when coupled with 3-dimensional (3D) printing has aided our ACHD surgeons in planning operations and has become a teaching tool for trainees and patients alike.

Advanced support of the failing systemic right ventricle (RV) and bridging to cardiac transplantation for ACHD patients who underwent the atrial switch procedure for D-transposition of the great vessels or who have congenitally corrected transposition poses unique challenges as does support of the patient with a failing univentricular heart treated with the Fontan palliation. Ventricular assist devices (VADs) are underutilized in ACHD patients in part because of their complex anatomy and physiology. 3D printing offers individualized structural models that would enable pre-surgical planning of cannula and device placement in ACHD patients with heart failure who are candidates for such therapies [5]. Surgical myectomy is performed in patients with hypertrophic cardiomyopathy and severe disabling symptoms due to left ventricular outflow tract (LVOT) obstruction. A complex LVOT anatomy and limited visualization of the left ventricular cavity in the surgical field may increase the risk and technical challenge of the surgery. 3D printing may provide information on left ventricular geometry allowing preoperative simulation of surgical repair [6].

## Challenges of Conventional Imaging in ACHD and 3D Printing from Echocardiography

ACHD patients often require complex and intricate cardiac surgery or catheterization requiring 3D spatial conceptualization of defects to achieve optimal repair and outcome. 3D visualization of the heart is integrated into today's image guided diagnosis and intervention but is limited on 2D display systems. Current conventional imaging modalities such as 2D transthoracic echocardiography and transesophageal echocardiography may not reveal spatial relationships of cardiac lesions adequately. 3D printing can overcome these limitations by producing 3D replicas of exact proportions to the native anatomy. Lesions in ACHD that can benefit from 3D modeling include but are not limited to: inflow or outflow obstructions, baffle and conduit stenosis, residual shunts, and complex intracardiac anatomy.

While conventional 2D echocardiography has limitations in ACHD, it is important to note that it should be used to complement MRI and CT datasets in 3D printing, as it provides superior visualization of certain cardiac structures. Given its high temporal and spatial resolution for thin, mobile structures, it can resolve structures such as atrioventricular (AV) valves and the atrial septum better than MRI or CT. Early investigations with 3D echocardiography have shown promising feasibility and accuracy for 3D printing [7, 8].

As with MRI and CT, 3D modeling from echocardiography is contingent on a high-quality source dataset to avoid inaccuracies in the printed model [9]. This may be achieved with a high frame rate image acquisition, optimization of settings, and meticulous post-processing [8]. For highly accurate models of the valve apparatus, a combination of a high spatial resolution image dataset, robust image post-processing software, and a multimaterial 3D printer are needed. As the technology advances, 3D printing from echocardiography may facilitate novel transcatheter and surgical valve intervention and replacement strategies [10, 11]. By co-registering echocardiographic, MRI and CT datasets it may be possible to produce models that utilize the strengths of complementary imaging modalities.

## CT and MRI Techniques for 3D Printing

MRI or CT image datasets can be used to 3D print whole heart models. In either case, image quality must be of the highest available resolution and be free of motion artifacts. For cardiac 3D printing, the study must be electrocardiogram (EKG) gated to suppress cardiac motion. For CT, the study should be performed during a

breathhold, and for MRI, the study should be respiratory gated to compensate for respiratory motion. For 3D printing, 3D MRI contrast-enhanced volumetric techniques are preferred to contrast-enhanced CT due to the ability to acquire images with a homogenous blood-pool signal. With CT, contrast enhancement is dynamic resulting in variation in intensity at different anatomic locations. However, CT provides high-resolution rapid imaging, which can be advantageous for patients unable to undergo MRI or for specific diagnoses (ex. tetralogy of Fallot with pulmonary atresia and multiple aorto pulmonary collaterals).

### Cardiac CT

Standard volumetric breathheld EKG-gated cardiac CT imaging is suitable for 3D printing. The study may be EKG-gated either retrospectively or prospectively. Prospective gating results in decreased radiation dose at the expense of reconstruction options being more limited. For cardiac CT imaging, the injection rate for contrast should be relatively high to provide optimal contrast. Unlike imaging for coronary CT angiography, when cardiac CT is performed for CHD, a saline "chaser" should not be administered, allowing contrast opacification of both the left and right heart. As for coronary CT angiography, using standard 64-slice CT scanners, the heart rate should be 65 beats per minute or less to reduce cardiac motion artifact. Beta-blockers, administered either intravenously or orally, should be used with caution in ACHD patients, especially in those with pulmonary hypertension, severe sinus bradycardia, second and third degree heart block, bronchial asthma or chronic obstructive pulmonary diseases. Images should be reconstructed at 1.0 mm slice thickness or less.

### Cardiac MRI

Contrast-enhanced, EKG-gated, respiratory navigated, volumetric gradient recalled echo (GRE) imaging is an ideal dataset for making 3D prints. The dataset should be both isotropic and high resolution with both slice thickness and in-plane resolution at 1.3 mm or less. In addition, the dataset should be obtained with both spectral fat saturation and inversion recovery at approximately 200–250 ms to completely suppress soft tissue. The intravenous contrast agent administered could be either an intravascular agent such as ferumoxytol or a high-relaxivity MR contrast agent such as gadobenate dimeglumine administered via a slow (0.1 mL/sec) infusion of 0.2 mmol/Kg [12]. The infusion should be started at the beginning of an interleaved data acquisition to provide uniform enhancement for both peripheral and central *k*-space [12]. A disadvantage of this technique is the length of acquisition of the sequence, which is both dependent upon temporal resolution and heart rate, and has the potential to run as long as 20 minutes in bradycardic patients.

## Surgical Perspective on 3D Printing in ACHD

Detailed visualization and comprehension of the cardiac anatomy is of ultimate importance in surgical management of ACHD patients. In addition to echocardiography, imaging modalities such as CT angiography and MRI provide complementary spatial information. The methods for 3D reconstruction such as volume or surface rendering are helpful for understanding complex anatomical relationships. However, this information is limited in that it is viewed on a two-dimensional screen, lacking depth perception and other valuable spatial information. 3D printing in CHD has gained prominence in the recent years, used as part of the diagnostic process and for surgical planning [13, 14]. This technology allows better diagnosis comprehension and deeper discussion with a multidisciplinary team for all potential options of treatment [10, 15]. Furthermore, it provides a versatile tool for discussion with the patient and caregivers regarding the details of the procedure, particularly apt for complex procedures.

## Surgical Planning

Stepwise mental visualization of the planned procedure including surgical approach and type of incision, as well as the manner of conduct of bypass are all possible applications of 3D printing. Nearly all ACHD patients have undergone multiple prior procedures resulting in dense adhesions that may preclude an extensive dissection during the case. Conversely, unnecessary dissection must be avoided due to the potential for excessive bleeding. A 3D model can reveal what areas may need to be dissected and options for exposure of the relevant anatomy during the procedure. For cases that require intracardiac baffles or aortic arch reconstruction, a model can aid in understanding the potential size and shape of the reconstructive patches, prior to surgery [16]. Given that the heart is a dynamic structure, with changes in dimensions with the cardiac cycle, our practice is to review models along with dynamic (cine) imaging and conventional 2D images. Models with pliable materials allow conduction of a mock procedure before the planned intervention. 3D models can also provide valuable understanding of key relationships of great vessels and the heart to surrounding structures. Our group uses these models for unifocalization procedures, given that standard angiography fails to show the relationship of the major aortopulmonary collateral arteries (MAPCAs) to important airway structures. Furthermore, 2D MR or CT or digital 3D reconstructions don't have the same utility as a model. The surgeon can rotate the model in his or her hand, examining details of the vessels that will need to be disconnected from the aorta, and reimplanted.

About one quarter of adults with CHD will progress to heart failure by 30 years of age [17]. VADs have been an essential tool in the armamentarium for treatment of heart failure [18]. However, the utilization of VADs in patients with CHD remains less frequently employed due to the highly variable anatomy and complex physiology in this population [19]. Once again, 3D models offer powerful tools for this planning with VAD juxtaposition to the model to help identify optimal placement for the patients. This valuable application is discussed in detail in a separate chapter in this textbook.

## 3D Models for Surgical Training

With the improvement in survival of ACHD patients, higher numbers of sicker patients are undergoing surgery and percutaneous interventional procedures later in life. Teaching junior surgeons or fellows during these cases is challenging, and a pre-surgical discussion of the case with a 3D model is quite helpful for this purpose. As those interventions that are not very frequently performed, using 3D models is one way of giving close to a "real world" experience for the surgeon in training. The precise definition of spatial relationships between structures is crucial in the development of medical skills and to avoid inadvertent complications during the real case. Furthermore, with soft flexible models it is now possible to practice the surgery on an exact replica of the case, a valuable pre-operative simulaiton experience.

## Patient Counseling

Counseling a patient or caregiver with complex CHD can be challenging. There is an "expert to non-expert" interaction, further complicated by the complexity of the procedure or abnormal anatomy and the emotional nature of the conversation. In this challenging scenario, the 3D model can help improve communication with the patient and patient's family, increasing their comprehension of the disease [13].

## Applications of 3D Printing in ACHD

Cardiac MRI and CT are powerful imaging modalities that provide important information in the management of ACHD patients. Applications include visualization of complex anatomy, tissue characterization, and precise assessment of physiology including volumes, function, and

flow [20–24]. 3D printing adds value in the evaluation of ACHD patients with heart disease of "moderate" or "great" complexity [25]. As discussed in the preceding section, in complex patients an exact replica of the patient's anatomy in the form of a 3D model offers several benefits, which include: enhanced understanding of complex spatial relationships, precise pre-surgical planning, trainee education and simulation, and patient and family counseling [14, 26, 27]. The ACHD literature has identified risk factors that increase morbidity and mortality in ACHD patients undergoing heart surgery. These include complex anatomy, prior surgeries, and length of time spent on cardiopulmonary bypass [28–30]. These added benefits of 3D printing may have important effects on outcomes [26, 31–33]. Table 11.1 shows utilization and benefits of some cases with 3D printing from our institution. Adult patients (>18 years old) underwent cardiac CT or MRI (CMRI) for clinical evaluation. CMRI was performed on a 1.5 T scanner with a 3D respiratory navigated inversion recovery FLASH sequence after 0.03 mmol/kg blood-pool gadolinium contrast, gadofosveset trisodium. We have had similar success in 3D printing using a slow infusion of a high-relaxivity MR contrast agent such as gadobenate dimeglumine. Contrast-enhanced cardiac CT was performed on a 128 slice dual-source CT scanner using high-pitch spiral mode.

The following cases show specific applications of 3D printing in ACHD patients.

## Case 1

A twenty-nine-year-old (121 kg) male with history of double outlet right ventricle (DORV) underwent a two ventricle repair with a Rastelli procedure, ventricular septal defect (VSD) closure with baffling of left ventricle (LV) to aorta, and RV to pulmonary artery (PA) conduit placement in early life. He presented with exercise intolerance. Cardiac MRI showed complex LVOT obstruction, a small residual VSD, dilation of aortic root (sinus of Valsalva), and aortic regurgitation. A 3D model was printed to aid in surgical planning. Figure 11.1 shows complex obstruction under the aortic valve with muscle bundles in the LVOT. Note the small VSD and buckling of the VSD patch into the LVOT. A catheter crosses the VSD from the RV with the tip in the LV. A ridge of muscle crosses the LVOT. Figure 11.1b shows a second model, created to simulate the "surgeon's view." Corresponding anatomy from the operating room is shown in Fig. 11.1c.

## Case 2

A sixteen-year-old male with history of heterotaxy syndrome, single ventricle anatomy with a systemic RV, had undergone a total cavo-pulmonary connection (aka Fontan) palliation with an extracardiac fenestrated conduit. He subsequently underwent percutaneous device closure of the Fontan fenestration. A surveillance MRI was performed to evaluate single ventricle anatomy and physiology. A 3D model was printed for teaching purposes. The model (Fig. 11.2) shows a dilated and hypertrophied RV, the aorta as the only outflow from the functional single ventricle and the Fontan conduit and superior vena cava connecting to the pulmonary arteries. The fenestration occlusion device is shown in green.

## Case 3

A thirty-six-year-old male (86 kg) with history of d-transposition of the great arteries (d-TGA) underwent an atrial switch operation (Senning technique) in infancy with an interatrial baffle. He underwent surveillance MRI to evaluate the atrial baffle, ventricular function, and systemic and pulmonary venous pathways. A 3D model was printed for education and counseling purposes. The 3D model (Fig. 11.3) shows a dilated and hypertrophied systemic RV and a more slender and thin-walled pulmonic LV, reflecting the ventricular remodeling that occurs in older d-TGA patients following atrial switch. The interatrial baffle is clearly shown and channels blood flow (catheter course) from the pulmonary

**Table 11.1** ACHD cases of cardiac 3D printing

| Diagnosis | Age at imaging study (years) | Weight at study (kg) | Reason for printing | Modality | Did 3D model add value over prior imaging? | Pre-intervention cases: Did the 3D model aid in making management decisions? |
|---|---|---|---|---|---|---|
| Bicuspid aortic valve, severe dilation of aortic root and ascending aorta, moderate AR, dilated LV, mild LV dysfunction | 20 | 83 | Patient counseling<br>Trainee education | CT | Yes | N/A |
| Coarctation of aorta, s/p repair | 21 | 55 | Trainee education | MRI | No | N/A |
| DORV, s/p VSD closure (Rastelli) and RV-PA conduit. Complex LVOT obstruction | 30 | 121 | *Pre-intervention planning*<br>Patient counseling<br>Trainee education | MRI | Yes | Yes |
| Dextrocardia, DORV, right-sided IVC, extracardiac Fontan baffle to LPA, left SVC to left-sided superior cavo-pulmonary connection | 31 | 64 | Patient counseling<br>Trainee education | MRI | Yes | N/A |
| D-transposition of the great arteries, s/p atrial switch (Senning) | 36 | 86 | Patient counseling<br>Trainee education | MRI | Yes | N/A |
| DORV, D-malposition of the great arteries. H/o Blalock-Hanlon procedure (atrial septectomy), PA band in infancy. Followed by classic Glenn (SVC to RPA anastomosis), PA band takedown and modified Mustard procedure (IVC baffled to left atrium). Cyanosis and atrial arrhythmia | 40 | 54 | *Pre-intervention planning*<br>Patient counseling<br>Trainee education | MRI | Yes | Yes |
| DORV, s/p repair followed by RVOT reconstruction, SubAS resection. Recurrent LVOT obstruction | 45 | 65 | *Pre-intervention planning*<br>Patient counseling<br>Trainee education | MRI | Yes | Yes |
| Unbalanced AV canal, left dominant, superior-inferior atria, DORV, Taussig bing type, L-malposed great arteries, sub-PS, PS. Increasing cyanosis | 45 | 67 | *Pre-intervention planning*<br>Patient counseling<br>Trainee education | MRI | Yes | Yes |

*AR* Aortic regurgitation, *LV* Left ventricle, *DORV* Double outlet right ventricle, *VSD* Ventricular septal defect, *RV-PA* Right ventricle to pulmonary artery, *LVOT* Left ventricular outflow tract, *IVC* Inferior vena cava, *SVC* Superior vena cava, *D* Dextro, *RVOT* Right ventricular outflow tract, *subAS* Sub-aortic stenosis, *AV canal* Atrioventricular canal, *L* Levo, *PS* Pulmonary stenosis

Reproduced from Anwar et al. [14]; http://dx.doi.org/10.1016/j.jcmg.2016.03.013, with permission of Elsevier

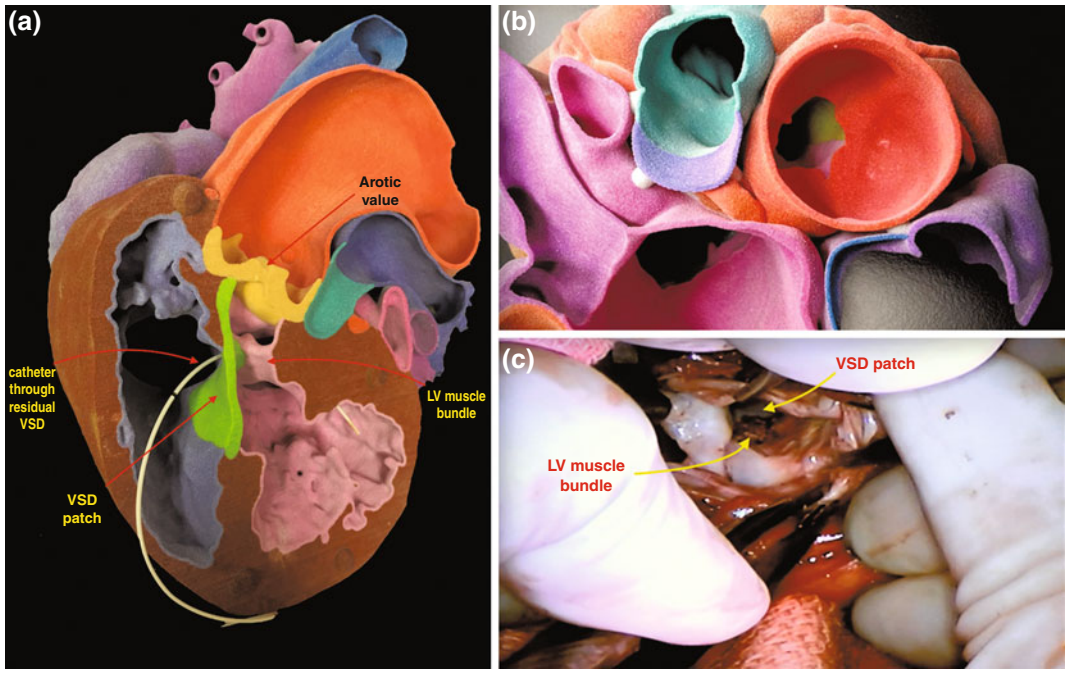


**Fig. 11.1** **a** Complex obstruction under the aortic valve with muscle bundles in the LVOT. Note the small VSD and buckling of the VSD patch into the LVOT. A catheter crosses the VSD from the RV with the tip in the LV. A ridge of muscle crosses the LVOT. **b** Shows a second model, created to simulate the "surgeon's view." Corresponding anatomy from the operating room is shown in (**c**)

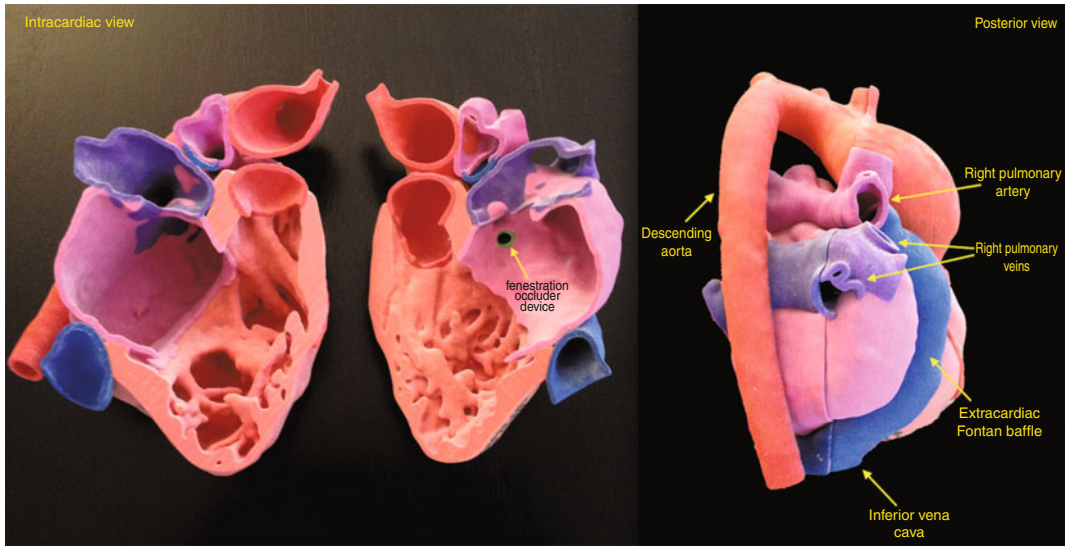


**Fig. 11.2** Dilated and hypertrophied RV, the aorta as the only outflow from the functional single ventricle and the Fontan conduit and superior vena cava connecting to the pulmonary arteries. The fenestration occlusion device is shown in *green*

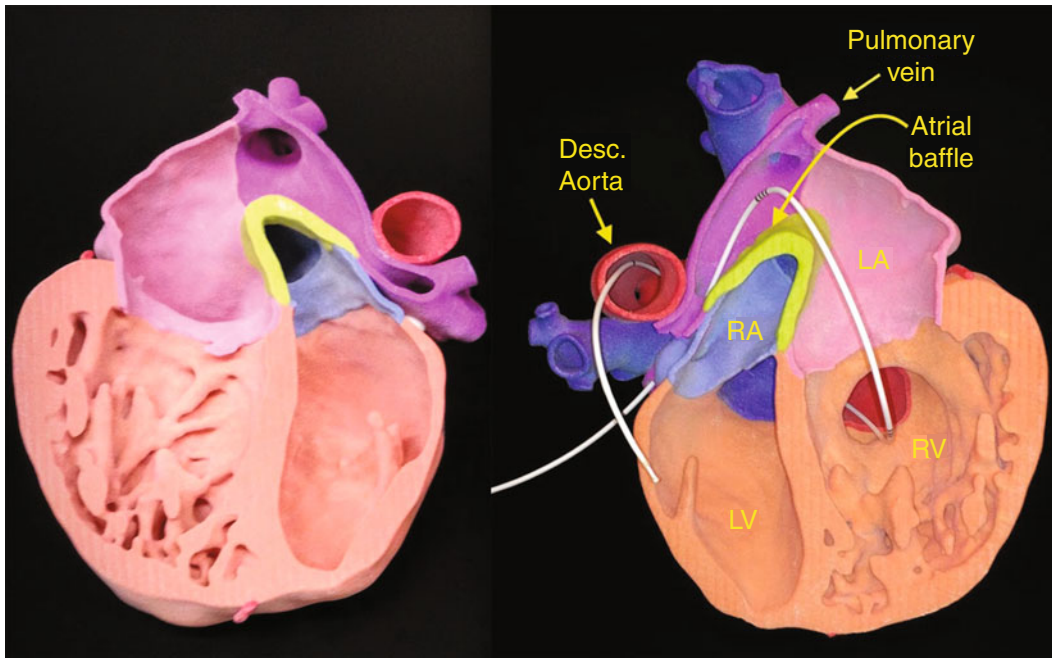


**Fig. 11.3** Dilated and hypertrophied systemic RV and a more slender and thin-walled pulmonic LV, reflecting the ventricular remodeling that occurs in older d-TGA patients following atrial switch. The interatrial baffle is clearly shown and channels blood flow (catheter course) from the pulmonary veins and left atrium (*LA*) to the RV and aorta. Likewise, the baffle directs systemic venous return from the right atrium (*RA*) to the LV and pulmonary arteries

veins and left atrium (LA) to the RV and aorta. Likewise, the baffle directs systemic venous return from the right atrium (RA) to the LV and pulmonary arteries.

## Case 4

A 3D virtual cardiac model of a thirty-one-year-old male with dextrocardia, DORV (Fig. 11.4a) demonstrates the intracardiac anatomy. The extracardiac Fontan is seen coursing from the right-sided inferior vena cava (IVC) to the left PA. A left-sided superior vena cava (SVC) joins the superior cavo-pulmonary connection (Glenn).

## Case 5

A 3D model (Fig. 11.4b) of a nineteen-year-old male with bicuspid aortic valve and suspected connective tissue disorder is depicted. The model shows a severely dilated aortic root and ascending aorta. A prominent coronary artery is also seen.

## Case 6

A cardiac model is demonstrated of a forty-year-old female with DORV, D-malposition of the great arteries, s/p multiple surgeries, concluding with a classic Glenn (SVC to RPA anastomosis), and modified Mustard procedure (IVC baffled to LA). The 3D model (Fig. 11.4c) shows the anatomy of DORV, two VSDs, classic Glenn connection, and a calcified IVC to LA conduit. Severe left PA dilation was also seen, not shown in this image.

## Case 7

A forty-five-year-old female with left dominant unbalanced AV canal, DORV presented with

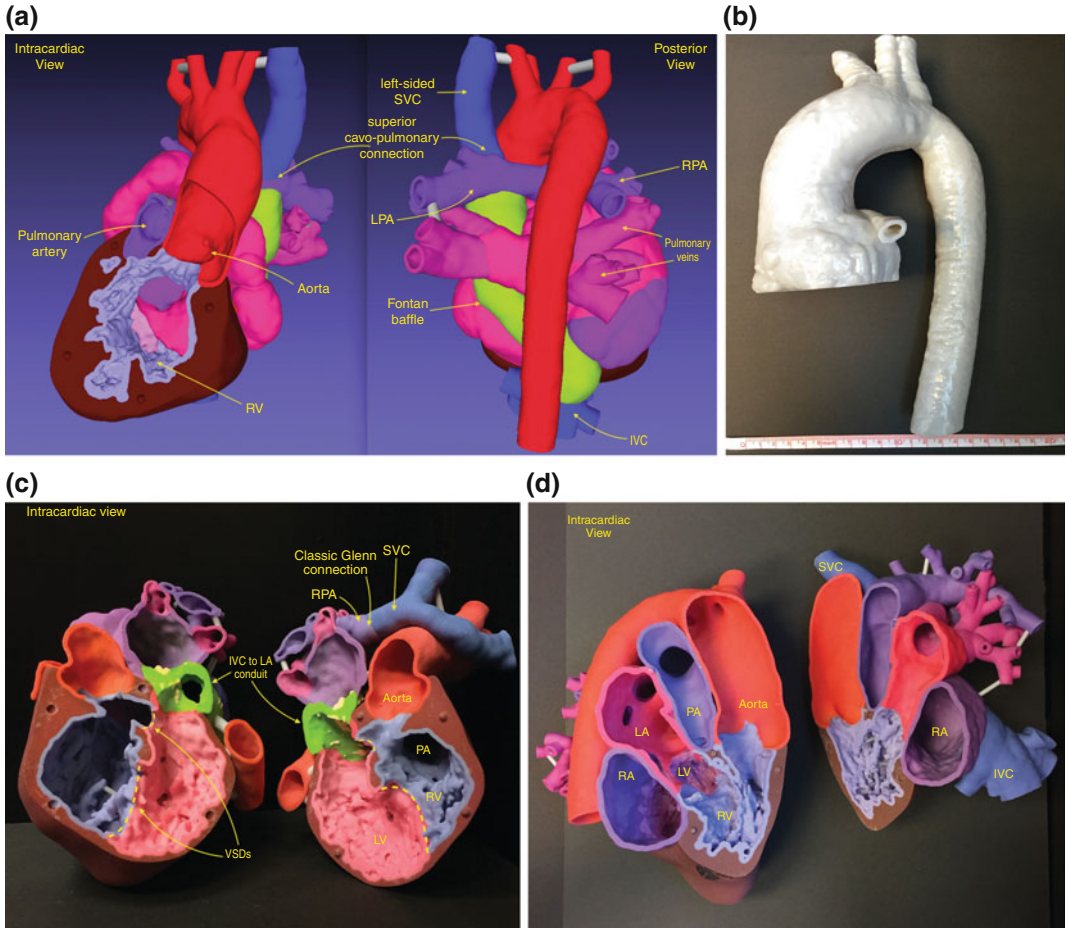


**Fig. 11.4** **a–d** 3D models of patients with adult congenital heart disease

cyanosis. She had been previously diagnosed as a "criss-cross" heart. The 3D model (Fig. 11.4d) shows AV concordance (non criss-cross) and significant right ventricular outflow tract obstruction and pulmonary stenosis, likely the etiology of the patient's progressive cyanosis.

## Conclusion

3D printing is a transformative technology with the potential to substantially improve the care of complex adult congenital patients with high morbidity. While cardiac 3D printing has been made possible by sophisticated technology, the human element remains the most crucial component in creating a model. Each step in the printing process, from image acquisition to segmentation, design and printing may introduce inaccuracies that can lead to deviation from anatomic "truth." Thus, involvement of an expert imager with intimate knowledge of cardiac anatomy and physiology is essential during the entire 3D printing process, making this a time and labor intensive process. Ultimately, its long-term viability will depend upon the impact it has on improving patient outcomes. Early experience suggests a promising future for cardiac 3D printing.

## References


1. Warnes CA, Liberthson R, Danielson GK, Dore A, Harris L, Hoffman JI, et al. Task force 1: the changing profile of congenital heart disease in adult life. JAC. 2001;37(5):1170–5.
2. Gurvitz M, Burns KM, Brindis R, Broberg CS, Daniels CJ, Fuller SMPN, et al. Emerging research directions in adult congenital heart disease: a report from an NHLBI/ACHA working group. J Am Coll Cardiol. 2016;67(16):1956–64.
3. Warnes CA, Bhatt AB, Daniels CJ, Gillam LD, Stout KK. COCATS 4 Task force 14: training in the care of adult patients with congenital heart disease. JAC. 2015;65(17):1887–98.
4. Bhatt AB, Foster E, Kuehl K, Alpert J, Brabeck S, Crumb S, et al. Congenital heart disease in the older adult: a scientific statement from the American heart association. Circ Am Heart Assoc J. 2015;131(21): 1884–931.
5. Farooqi KM, Saeed O, Zaidi A, Sanz J, Nielsen JC, Hsu DT, et al. 3D printing to guide ventricular assist device placement in adults with congenital heart disease and heart failure. JACC Heart Failure. 2016; 4(4):301–11.
6. Yang DH, Kang J-W, Kim N, Song J-K, Lee J-W, Lim T-H. Myocardial 3-dimensional printing for septal myectomy guidance in a patient with obstructive hypertrophic cardiomyopathy. Circulation. 2015;132(4):300–1.
7. Mahmood F, Owais K, Taylor C, Montealegre-Gallegos M, Manning W, Matyal R, et al. Three-dimensional printing of mitral valve using echocardiographic data. J Am Coll Cardiol (JCMG). 2015;8(2):227–9.
8. Olivieri LJ, Krieger A, Loke Y-H, Nath DS, Kim PCW, Sable CA. Three-dimensional printing of intracardiac defects from three-dimensional echocardiographic images: feasibility and relative accuracy. YMJE. 2015;28(4):392–7.
9. Mahmood F, Owais K, Montealegre-Gallegos M, Matyal R, Panzica P, Maslow A, et al. Echocardiography derived three-dimensional printing of normal and abnormal mitral annuli. Ann Card Anaesth. 2014;17(4):279–83.
10. Gosnell J, Pietila T, Samuel BP, Kurup HKN, Haw MP, Vettukattil JJ. Integration of computed tomography and three-dimensional echocardiography for hybrid three-dimensional printing in congenital heart disease. J Digit Imaging. 2016.
11. Vukicevic M, Puperi DS, Jane Grande-Allen K, Little SH. 3D printed modeling of the mitral valve for catheter-based structural interventions. Ann Biomed Eng. 2016.
12. Zheng J, Bae KT, Woodard PK, Haacke EM, Li D. Efficacy of slow infusion of gadolinium contrast agent in three-dimensional MR coronary artery imaging. J Magn Reson Imaging. 1999;10(5):800–5.
13. Biglino G, Capelli C, Wray J, Schievano S, Leaver LK, Khambadkone S, et al. 3D-manufactured patient-specific models of congenital heart defects for communication in clinical practice: feasibility and acceptability. BMJ Open. 2015;5(4):e007165.
14. Anwar S, Singh GK, Varughese J, Nguyen H, Billadello JJ, Sheybani EF, et al. 3D Printing in complex congenital heart disease: across a spectrum of age, pathology, and imaging techniques. JACC Cardiovasc Imaging. 2016.
15. Jacobs S, Grunert R, Mohr FW, Falk V. 3D-Imaging of cardiac structures using 3D heart models for planning in heart surgery: a preliminary study. Interact Cardiovasc Thorac Surg. 2008;7(1):6–9 (Oxford University Press).
16. Kiraly L, Tofeig M, Jha NK, Talo H. Three-dimensional printed prototypes refine the anatomy of post-modified Norwood-1 complex aortic arch obstruction and allow presurgical simulation of the repair. Interact Cardiovasc Thorac Surg. 2016;22(2): 238–40 (Oxford University Press).
17. Norozi K, Wessel A, Alpers V, Arnhold JO, Geyer S, Zoege M, et al. Incidence and risk distribution of heart failure in adolescents and adults with congenital heart disease after cardiac surgery. Am J Cardiol. 2006;97(8):1238–43.
18. Ryan TD, Jefferies JL, Zafar F, Lorts A, Morales DLS. The evolving role of the total artificial heart in the management of end-stage congenital heart disease and adolescents. ASAIO J. 2015;61(1):8–14.
19. Ross HJ, Law Y, Book WM, Broberg CS, Burchill L, Cecchin F, et al. Transplantation and mechanical circulatory support in congenital heart disease. Circ Am Heart Assoc Inc. 2016;133(8):802–20.
20. Knobelsdorff-Brenkenhoff von F, Trauzeddel RF, Schulz-Menger J. Cardiovascular magnetic resonance in adults with previous cardiovascular surgery. Eur Heart J Cardiovasc Imaging. 2013.
21. Partington SL, Valente AM. Cardiac magnetic resonance in adults with congenital heart disease. Methodist Debakey Cardiovasc J. 2013;9(3):156–62 (Methodist DeBakey Heart & Vascular Center).
22. Saremi F. Cardiac CT and MR for Adult Congenital Heart Disease. 2013.
23. Kilner PJ, Geva T, Kaemmerer H, Trindade PT, Schwitter J, Webb GD. Recommendations for cardiovascular magnetic resonance in adults with congenital heart disease from the respective working groups of the European Society of Cardiology. Eur Heart J. 2010;31(7):ehp586–805 (The Oxford University Press).
24. Marcotte F, Poirier N, Pressacco J, Paquet É, Mercier L-A, Dore A, et al. Evaluation of adult congenital heart disease by cardiac magnetic resonance imaging. Congenital Heart Disease. 2009;4(4):216–30 (Blackwell Publishing Inc).
25. Warnes CA, Williams RG, Bashore TM, Child JS, Connolly HM, Dearani JA, et al. ACC/AHA 2008

guidelines for the management of adults with congenital heart disease: a report of the American College of Cardiology/American Heart Association task force on practice guidelines (writing committee to develop guidelines on the management of adults with congenital heart disease): developed in collaboration with the american society of echocardiography, heart rhythm society, international society for adult congenital heart disease, society for cardiovascular angiography and interventions, and society of thoracic surgeons. Circulation. 2008;118(23):e714–833.

26. Farooqi KM, Uppu SC, Nguyen K, Srivastava S, Ko HH, Choueiter N, et al. Application of virtual three-dimensional models for simultaneous visualization of intracardiac anatomic relationships in double outlet right ventricle. Pediatr Cardiol. 2015;37(1):90–8 (US:Springer).
27. Ejaz F, Ryan J, Henriksen M, Stomski L. Color-coded patient-specific physical models of congenital heart disease. Rapid Prototyping. 2014;20(4):336–43.
28. Giamberti A, Chessa M, Abella R, Butera G, Carlucci C, Nuri H, et al. Morbidity and mortality risk factors in adults with congenital heart disease undergoing cardiac reoperations. Ann Thorac Surg. 2009;88(4):1284–9.
29. Holst KA, Dearani JA, Burkhart HM, Connolly HM, Warnes CA, Li Z, et al. Risk factors and early outcomes of multiple reoperations in adults with congenital heart disease. Ann Thorac Surg. 2011; 92(1):122–30.
30. Holst KA, Dearani JA, Burkhart HM, Connolly HM, Warnes CA, Li Z, et al. Reoperative multivalve surgery in adult congenital heart disease. Ann Thorac Surg. 2013;95(4):1383–9.
31. Costello JP, Olivieri LJ, Su L, Krieger A, Alfares F, Thabit O, et al. Incorporating three-dimensional printing into a simulation-based congenital heart disease and critical care training curriculum for resident physicians. Congenital Heart Dis. 2015; 10(2):185–90.
32. Ryan JR, Moe TG, Richardson R, Frakes DH, Nigro JJ, Pophal S. A novel approach to neonatal management of tetralogy of Fallot, with pulmonary atresia, and multiple aortopulmonary collaterals. 2015;8(1):103–4.
33. Hu A, Wilson T, Ladak H, Haase P, Fung K. Three-dimensional educational computer model of the Larynx: voicing a new direction. Arch Otolaryngol Head Neck Surg. 2009;135(7):677–81 (American Medical Association).

# Part III
# Structural Heart Disease

# Transcatheter Aortic Valve Replacement

12

Marija Vukicevic, PhD, Eleonora Avenatti, MD and Stephen H. Little, MD, FRCPC, FACC, FASE

## Aortic Valve Stenosis

Calcific aortic stenosis (AS) is the most common type of valvular heart disease in the developed world, affecting 2–5% of older adults in Western countries [1]. With a rapid rise in prevalence in patients aged 65 years or older, the global burden of aortic stenosis is expected to increase as developed countries realize an increase in life expectancy [2].

In AS, thickened, calcified valve leaflets lose their normal mobility, turning a functional valve into a small, fixed orifice that creates a barrier to the left ventricle (LV) outflow. This obstructive physiology is the later, terminal phase of a broader pathological entity, known as calcific aortic valve disease (CAVD), an active process involving complex biologic pathway and cellular interactions [3].

M. Vukicevic · E. Avenatti · S.H. Little (✉)
Department of Cardiology, Houston Methodist DeBakey Heart and Vascular Center, Houston, TX, USA
e-mail: shlittle@houstonmethodist.org

M. Vukicevic
e-mail: mvukicevic@houstonmethodist.org

E. Avenatti
e-mail: eavenatti@houstonmethodist.org


K.M. Farooqi (ed.), *Rapid Prototyping in Cardiac Disease*,
DOI 10.1007/978-3-319-53523-4_12

## Transcatheter Aortic Valve Replacement

As researchers have delved into molecular and cellular aspect of the disease, parallel efforts have been put into development of new therapeutic strategies. End-stage CAVD-AS represents a mechanical problem that requires a mechanical solution. Until recently, the only option for an affected individual was an open heart surgery for aortic valve replacement (SAVR), with its considerable burden of risks and complications. With the advent of transcatheter aortic valve replacement (TAVR), a prosthetic valve is guided in a retrograde fashion from the femoral artery to the aortic root and deployed across the native aortic valve using either balloon expansion or self-expanding nitinol strategies. Alternative access to the aortic root can also be achieved with direct aortic puncture, transapical puncture, or less commonly via subclavian artery catheterization.

This new technology was first applied to a patient in France in 2002, and initial clinical studies demonstrated that for patients with symptomatic severe AS, TAVR was superior to medical treatment for very prohibitive surgical candidates and comparable to SAVR for patients deemed to be at high risk for SAVR [4–6]. Today, TAVR represents the new treatment standard for patients with symptomatic severe AS with high or prohibitive surgical risk [7]. Based on good initial and midterm outcome data [5, 7–9], ongoing trials are evaluating the use of

TAVR for patients with a lower predicted risk for SAVR [10].

## Current Knowledge Gaps and Clinical Challenges

New technologies bring new challenges, and the TAVR revolution has left many questions yet unanswered. The technical challenges for this catheter-based therapy are multiple, but current research and development are largely focused on device design features to reduce the occurrence and severity of paravalvular regurgitation (PVR), to allow more control during device deployment, and to allow total repositionability of the device [11]. Additional challenges include the creation and validation of noninvasive imaging methods to provide a functional evaluation of both the acute and chronic valve performances [12].

The bigger of these challenges, which has indeed been referred to as the Achilles' heel of TAVR, is occurrence of PVR after valve deployment. PVR is a clinical, procedural, and diagnostic challenge. Clinically, the presence of significant PVR is associated with an increased incidence of rehospitalization and death [13]. From a procedural viewpoint, it is the final result of multiple possible contributing factors including suboptimal prosthesis sizing, incorrect implant depth, and the patient-specific amount and distribution of calcium within the aortic root. The presence of significant calcification around the valve is necessary for anchoring the prosthetic valve; however, a bulk of calcium or an asymmetric calcium distribution may prevent the ideal positioning of the prosthesis or the sealing of the prosthesis to the native root annulus. Not only is the occurrence of PVR difficult to predict, but the accurate quantification of PVR severity remains one of the most challenging tasks of contemporary noninvasive cardiology. The considerable range of incidence of PVR reported in large clinical trials, between 4 and 12%, reflects the difficulties in quantifying PVR severity, created by the presence of ultrasound artifacts, eccentric and/or multiple regurgitant jets, complex and calcified aortic root anatomy, and as yet unclear reference standards for PVR severity [13].

## Imaging for Transcatheter Aortic Valve Replacement

Aortic valve stenosis has long been evaluated with echocardiography. Today, ultrasound evaluation remains a fundamental tool for the diagnosis of severe AS, patient selection for TAVR, procedural guidance, and postprocedural follow-up [7, 14, 15]. Two-dimensional (2D) echocardiography offers a high temporal resolution, with the opportunity to evaluate function over time coupled with structure. Lower temporal resolution of volumetric acquisition with 3D echocardiography has long been a limiting factor, but recent technological developments are overcoming it, so that real-time volumetric evaluation with echocardiography is becoming a reliable option.

The other key technology in TAVR planning is contrast-enhanced computed tomography (CT) with electrocardiogram (ECG)-gated sequences and high spatial resolution. Clinically, CT datasets are crucial in establishing suitability of the peripheral access vessels to accommodate the relatively large valve delivery systems. The complete geometry of the proximal aorta—i.e. diameters of ascending aorta, aortic root, and annulus—can be reliably obtained with CT, and these measures are the reference standard used to determine the valve size for every patient [16].

The very same imaging modalities, 3D echocardiography and CT, can be used as source of data for 3D stereolithographic printing to obtain physical models accurately reproducing patient-specific features. Such models are being applied in multiple different contexts and with different aims for clinical care [17–21].

# 3D Printing Advances

In 2002, the first experimental work was performed using a functional and rather simplified AS model. The models were manufactured using

stereolithography technology and investigated the effect of 3D valve shape on hemodynamic pressure loss across the left ventricular outflow tract [17]. Most of the initial AS models were used primarily as an additional visualization tool before surgical procedures, granting better comprehension of complex anatomic geometries [18, 19]. Recent advancements in image acquisition and software for image postprocessing, along with rapid progress in 3D printing techniques, permit the manufacturing of a highly accurate replica of the most complex patient-specific geometry. The ongoing challenge has been to fabricate multisegmental anatomic constructs, in which the aortic valve, left ventricle outflow tract (LVOT), ascending aorta, and calcific structures can be 3D-printed with a multimaterial technology to replicate not only the geometry, but the pathologic valve function as well.

## Patient-Specific Aortic Stenosis Modeling

### Clinical imaging methods and models

Reconstruction of each patient-specific model starts with an acquisition of high-quality medical images that will be used for the identification and reconstruction of the target anatomy. Different imaging modalities can be used for 3D reconstruction, depending on the structure of interest. Magnetic resonance (MR) or CT images are suitable for modeling larger vessels or ventricular structures, while echocardiographic images can be used for heart valve replication. Software advancements now allow for a fusion of imaging from CT and echocardiography and their integration into a single model. For the aortic root, CT imaging alone is typically sufficient, but for other reconstruction targets such as the mitral valve apparatus, both echocardiographic images (depicting the leaflet tissue) with CT images (best depicting the subvalvular chordae tendineae) may be optimal.

There are multiple steps involved in the development process of functional patient-specific 3D AS models (Fig. 12.1). Volumetric CT imaging data used for AS model reconstruction are typically part of the preprocedural patient evaluation. This imaging dataset can be exported to segmentation software in Digital Imaging and Communication in Medicine (DICOM) format. Within the segmentation software, it is possible to identify a target anatomy and differentiate the calcific structures, soft tissue, and blood volume at each imaging slice based on the threshold intensity of pixels. Reconstruction of each model starts with creation of a segmentation mask, which is performed manually or semiautomatically by detecting the anatomic structures in 2D imaging planes based on the pixel color intensity (Fig. 12.1, Step 2). After segmentation of the region of interest in three 2D orthogonal planes, the target anatomy is transformed into a virtual 3D model of blood volume and soft tissue constructs (Fig. 12.1, Step 3). The rendered 3D virtual models are saved as stereolithographic files (.stl) and exported to design software for further adjustments and optimization. Within the design software, the blood volume of the aortic root and ventricular chamber is hollowed, model walls representing the aortic and ventricular tissue added, and the 3D geometry is transformed into functional models (Fig. 12.1, Step 4). From the .stl file, the 3D virtual model can be printed with additional coupling elements to allow it to be then incorporated into a flow phantom (Fig. 12.1, Step 5).

Manufacturing a complex, multimaterial model is possible using PolyJet technology. This technique uses additive manufacturing, a process in which a 3D printer (Objet500 Connex 3) sprays fine layers of liquid photopolymers, 16 μm thick, along with a support material onto a platform, while a UV light instantaneously cures each layer. At the end of the 3D printing process, the support material is dissolved, leaving only the anatomic structures of interest. A schematic outline of the development process of transforming the volumetric CT data into a physical model is shown in Fig. 12.1.

PolyJet technology is capable of fabricating a wide range of AS geometries including bicuspid valves and various arrangements of calcific depositions. Morphological accuracy of replicated anatomic models is analyzed by comparing

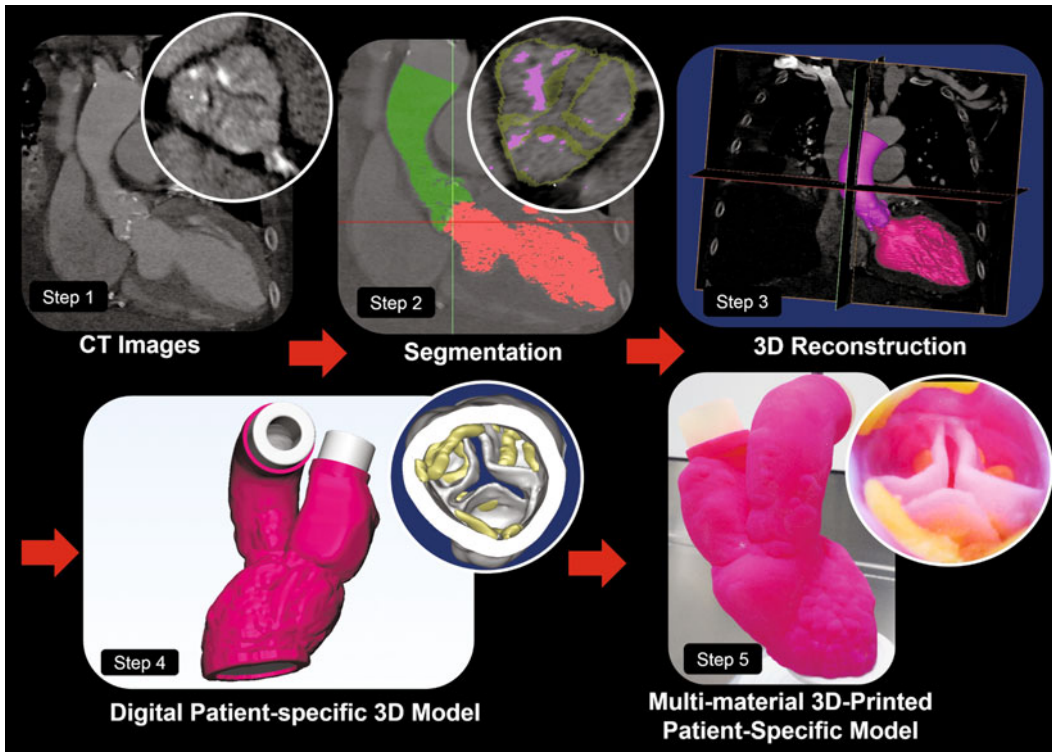


**Fig. 12.1** Development process of a multimaterial, patient-specific model of aortic stenosis. *Step 1* CT imaging dataset converted into DICOM format. *Step 2* Segmentation process includes identification of target anatomic geometry and creation of segmentation mask. *Step 3* Reconstruction of 2D segments into 3D virtual model. *Step 4* Digital patient-specific model adjusted for coupling within a flow loop. *Step 5* Multimaterial 3D-printed patient-specific model. Modified with permission from Vukicevic et al. [22]

the CT scans of the AS models to the patients' CT scan or echocardiographic images. An example of a CT scan comparison of a patient with the model created from the image dataset is shown in Fig. 12.2, while the echocardiographic images of the patient and the corresponding model are shown in Fig. 12.3a, b.

## Functional Modeling

Aortic stenosis is particularly well suited for functional replication with 3D modeling. This is because the relatively fixed valve that characterizes calcific aortic valve disease demonstrates little motion throughout the cardiac cycle. As such, the replicated aortic cusps do not need to demonstrate normal cusp motion throughout the cardiac cycle, although a subtle expansion of the stenotic valve orifice with augmented flow volume has recently been demonstrated [20]. This flow dependency of the 3D-printed valve area is consistent with the behavior of native AS cusps [20].

Maragiannis et al. [20, 21] reconstructed the first functional, multimaterial, patient-specific AS models and replicated the clinical hemodynamic conditions of aortic stenosis using an in vitro environment. The obtained models have been coupled to a custom-designed flow loop shown in Fig. 12.3, replicating the hemodynamics of aortic stenosis. The flow loop consists of compliance and resistance elements tuned to physiological values and a pulsatile mock ventricle pump that ejects the fluid through the model. Quantification of forward flow and AS stroke volume is achieved using in-line flow transducers. Peak pressure gradient across the 3D-printed valve is measured using high-fidelity pressure

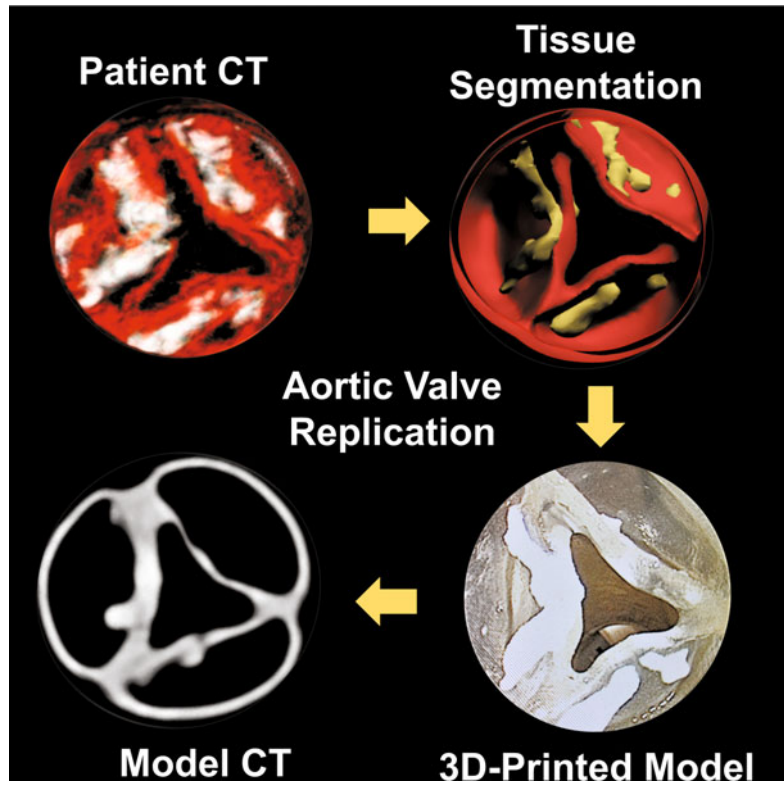


**Fig. 12.2** Fabrication of patient-specific models. Short-axis images of each model are shown in the three steps of the model fabrication process. First, CT-DICOMs are converted into STL files in computer-aided design (CAD) software and then 3D-printed using two different materials simultaneously. Note the correspondence of calcific nodules (*bright white* and *yellow*) and leaflet geometry throughout the model creation process. Images adapted with permission from Maragiannis et al. [21]

transducers positioned proximal and distal to the modeled valve.

The final step before 3D printing each model is to design and affix coupling segments onto the patient-specific geometry to allow incorporation of the model into the flow phantom. This typically consists of designing appropriate tubing connectors. Within the software environment, the continuity of the model surface and elimination of intersections between segmented geometries are assured [18, 21].

Experimental evaluation of patient-specific AS hemodynamics has been performed using both echocardiography and cardiac MR techniques. Doppler analysis of velocity profiles across the AS model under varied flow conditions has been reported (Fig. 12.3). Transvalvular peak and mean Doppler-derived pressure gradients were comparable to those measured in a 3D-printed model using high-fidelity pressure transducers. Flow estimates from clinical study of Doppler stroke volume were compared against flow volume as calculated using calibrated ultrasonic flowmeters positioned upstream and downstream to the 3D-printed AS model. 2D Doppler quantification of systolic flow based on continuous-wave Doppler peak and mean gradient in the 3D-printed phantoms was compared to the actual clinical data of the patient (Fig. 12.3). These studies confirmed the reproducibility of clinical hemodynamic parameters using functional 3D-printed AS models. Key hemodynamic features of the AS, including aortic valve area and peak and mean flow velocity, were accurately replicated with good agreement between clinical patient data and the 3D patient model within the flow phantom (Fig. 12.3c, d).

## 3D Printing Material for Aortic Stenosis

Multimaterial 3D printing allows for accurate replication of complex 3D models integrating multiple anatomic structures. Printing the regional

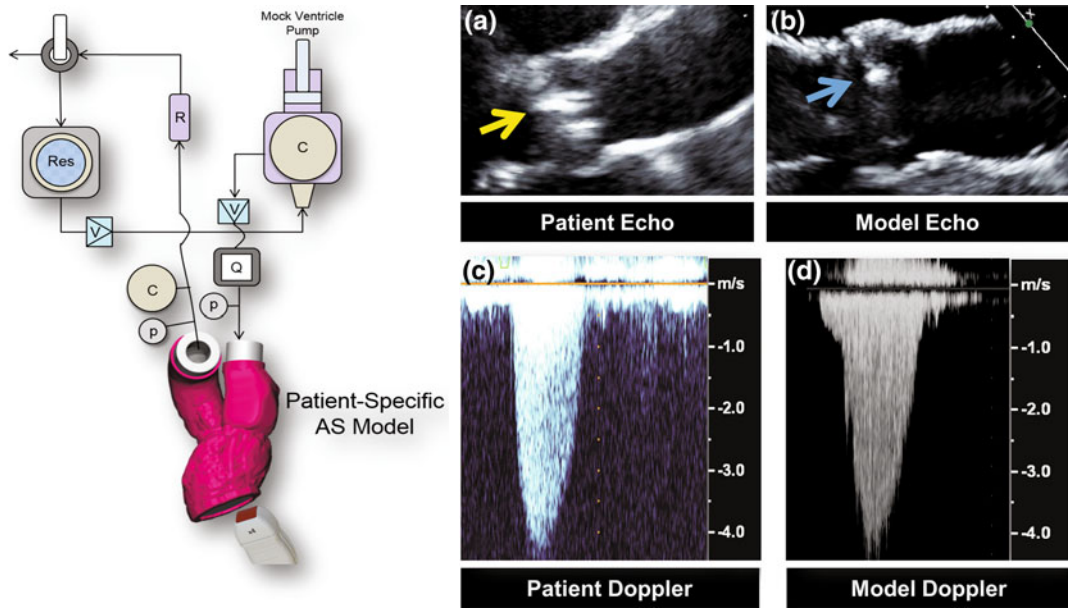


**Fig. 12.3** A typical flow loop setup for functional replication of aortic stenosis. Flow loop contains mock ventricle, compliance elements (*c*), resistance elements (*R*), reservoir (*Res.*), valves (*V*), pressure, and flow transducers (*p* and *Q*, respectively). **a** Echocardiographic image of the aortic valve in patient; **b** echocardiographic image of the model of aortic stenosis of the same patient; **c** patient Doppler interrogation of the flow through a stenotic aortic valve; and **d** Doppler velocity profile recorded in the patient-specific aortic stenosis model. Modified with permission from Maragiannis et al. [21]

material properties of tissue and calcific structures integrated in the same 3D model requires careful selection of materials. Patient-specific models are typically manufactured from Sylgard (Dow Corning), TangoPlus (Stratasys), or HeartPrint Flex (Materialise) materials, of which the TangoPlus material has mechanical properties most similar to select human tissue [23].

PolyJet technology represents a 3D printing technique that permits the use of a wide range of liquid photopolymers with different elastic properties, from rubber-like to rigid, transparent, translucent, or opaque, and with a wide spectrum of available colors. The choice of 3D printing material is based on the mechanical properties of the anatomic structure that is being replicated. Fused material selection is a pivotal step in the modeling process and has required preliminary definition of soft tissue and hard calcium characteristics [24, 25]. Aortic root, ascending aorta, and aortic valve cusps can be printed using a flexible material (TangoPlus, Stratasys), while the calcium is usually 3D-printed from a rigid material (VeroPlus, Stratasys). Elastic properties of rubber-like TangoPlus material are expressed by Young's modulus or elastic modulus and calculated as stress-to-strain ratio. The print material frequently used for the noncalcified anatomic regions (TangoPlus) has a manufacturer-reported elastic modulus of 0.146 MPa at 20% strain. The print material used for the calcified anatomic region (VeroWhitePlus) has a manufacturer-reported elastic modulus of 2000–3000 MPa. In the study by Maragiannis et al., tensile testing of the replicated aortic root tissue material was 0.4 MPa, that is comparable to the biaxial testing result of human aorta root tissue reported as $1.24 \pm 0.563$ MPa [25]. Other recent studies showed that the flexible TangoPlus material is suitable to accurately replicate AS geometry and functional properties of aortic valve leaflets under small deformations [26].

## Applications

Translating 3D imaging information into 3D digital anatomy and 3D print multimaterial, anatomically accurate models of the aortic valve complex, with all functional parts, represents a significant advancement in postprocessing of medical images. Replicating the biomechanics of aortic structures allows for highly accurate evaluation of diseased patient-specific physiology and represents a potentially very powerful new tool for assessment of acute hemodynamics that are difficult to quantify using current noninvasive imaging methods. In addition, such models facilitate accurate testing of novel medical devices and their design improvements such as those used for TAVR.

Being able to 3D print patient-specific geometry before an interventional cardiac procedure and to explore different interventional techniques could save time in the procedure room, increase efficiency of the procedure, and decrease the risk of unpredicted outcomes.

Besides the advantages as a visualization tool for better understanding of complex anatomic cases, 3D-printed models can also be used for educational purposes and to improve cardiologist–surgeon communication. In addition, these models can assist in delivering anatomic information to patients and their families and to help them better understand their clinical condition.

Moreover, as mentioned, 3D-printed patient-specific models are capable of simulating the functional performance of calcific aortic valve disease under pressurized flow conditions. Indeed, although these patient-specific models reflect realistic anatomic reconstruction of only a single moment within the cardiac cycle, they nonetheless demonstrate that the relatively immobile valve condition of AS can be replicated accurately [20, 21].

## Aortic Regurgitation

At the other end of the spectrum of aortic valve disease, chronic aortic regurgitation (AR) accounts for approximately 10% of aortic valve disease that requires surgical intervention. In the Western world, AR develops as a consequence of primary valve disease, i.e., bicuspid morphology, calcific degeneration, or aortopathies [27]. However, iatrogenic AR, especially paravalvular AR (PVR) in the TAVR era, remains a significant clinical concern.

Although not yet referenced in current clinical guidelines [1], percutaneous technology developed for AS has been applied to AR in recent years [28]. TAVR use in this setting requires specific adjustments due to the differences in anatomic features from AS. Regurgitant valves usually lack the extensive calcification that is used as an anchoring point for the deployed prosthesis in AS, raising the concerns of prosthesis malpositioning. There is also a need for significant oversizing of the transcatheter valve, which increases the risk of periprocedural annular rupture. Replication of regurgitant flow with functional 3D-printed models can give insight into the dynamics of primary AR, guiding technical development of device design and understanding of post-TAVR paravalvular regurgitation.

Functional patient-specific models of AR can be manufactured using multimaterial 3D printing technology and reconstructed in the same fashion as AS models. One example of a patient-specific AR model reconstructed from CT images and 3D-printed using multimaterial technology is shown in Fig. 12.4. The principle of developing the AR 3D printed model is analogous to the AS model reconstruction previously described. It starts with the selection of an appropriate CT dataset, acquired during diastole, which is exported in DICOM format and then postprocessed using segmentation software. Identification and segmentation of anatomic structures of interest will lead to a patient-specific virtual model which is then converted into a physical multimaterial model using 3D printing technology (Fig. 12.4, top panel).

### Replicating AR and Doppler Evaluation

Coupling a 3D-printed model of AR into a flow phantom (Fig. 12.3) allows for experimental

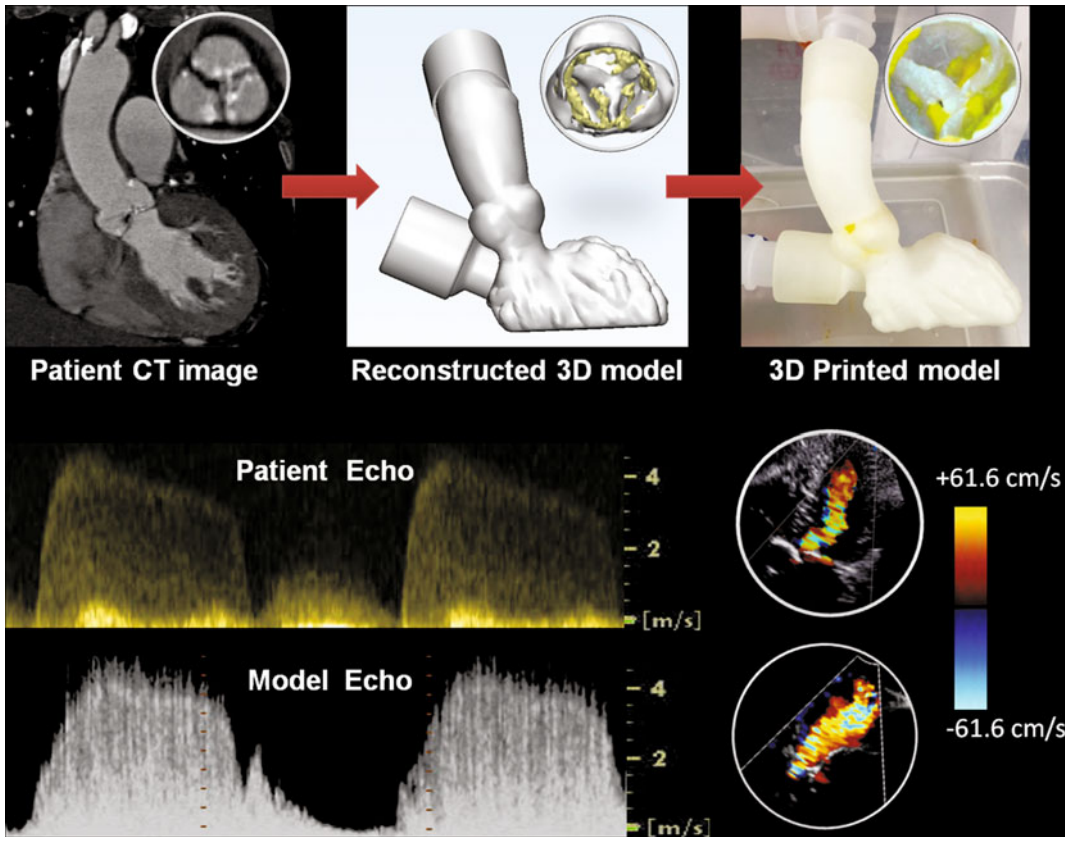


**Fig. 12.4** Development of aortic regurgitation model. Doppler velocity profile and color Doppler flow features in a patient and in the corresponding 3D-printed model

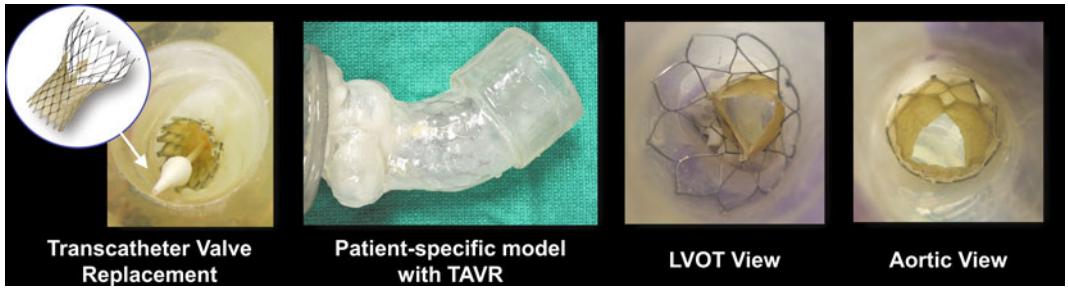


**Fig. 12.5** Tabletop transcatheter aortic valve implantation. Patient-specific interaction of the prosthetic valve with replicated calcium is depicted. Modified with permission from Vukicevic et al. [22]

testing and replication of AR hemodynamics applicable to either primary valve disease or post-TAVR paravalvular regurgitation. Accurate reconstruction of AR geometry along with appropriate design of the imaging chamber is central for the correct replication of regurgitant volume and successful imaging analysis. If transvalvular hemodynamic conditions of the clinical echocardiogram are appropriately reproduced, and the experimental setup permits good-quality Doppler

image acquisition, then the similarity between the clinical and modeled Doppler parameters can be remarkably good. Examples of highly comparable spectral and color Doppler characteristics acquired in the functional AR model are shown in Fig. 12.4.

For the specific purpose of replicating paravalvular regurgitation after TAVR, the in vitro system can be used for deployment of a transcatheter aortic valve within the 3D-printed patient-specific model. An evaluation of the final confirmation of a self-expanding nitinol stent is evident in Fig. 12.5. Incompressible calcified structures prevent the full stent expansion and the ideal sealing of the deployed valve against the aortic wall. Such benchtop modeling of TAVR could aid in better procedural planning and device selection. In addition, patient-specific PVR modeling could offer an ideal in vitro setting for the testing of noninvasive methods for the demanding task of PVR severity quantification.

## Future Efforts

The ability to create patient-specific functional models of aortic root geometry may now allow the modeling of other aortic valve conditions. For example, functional models of noncalcified bicuspid aortic valves could assist in understanding modes of aortic root dilation. Models may be designed to study the interaction of the ascending aorta with a left ventricular assist device (LVAD) outflow cannula.

For TAVR, these modeling efforts can help to identify possible correlations between annular calcification, annular size, variable implant depth, and the acute function of a deployed transcatheter aortic valve and severity of PVR. If employed on a more routine basis, these models may be studied to mitigate PVR by choosing a nonstandard implant depth that takes advantage of the hourglass contour of the valve prosthesis to supply greater radial force along the region in the greatest contact with the modeled root or valve calcification.

In vitro quantification of post-TAVR PVR within the 3D printed model could determine if 3D color Doppler can be used to quantify the regurgitation around a deployed valve. PVR can be captured within a 3D color Doppler dataset and the flow area representing the paravalvular orifice area measured. Anatomically, the paravalvular defect is often a crescent-shaped orifice with an eccentrically directed regurgitant jet. Such geometry and flow characteristics limit the accuracy of 2D Doppler quantification methods. For this particular problem, 3D color Doppler represents an attractive alternative, since flow quantification does not rely on assumptions of orifice geometry or flow direction. However, like 2D Doppler, the Doppler imaging angle limits the accurate assessment of flow velocity by 3D color Doppler methods. For the assessment of these complex flows, four-dimensional phase-contrast MR may be the best-suited quantification tool. As the utility of 3D printing in TAVR deployment and postprocedural assessment becomes more common, we can expect to see more new and innovative applications of this technology in combination with other advanced imaging modalities.

## References

1. Nishimura RA, Otto CM, Bonow RO, Carabello BA, Erwin JP, Guyton RA, et al. AHA/ACC guideline for the management of patients with valvular heart disease: executive summary: a report of the American college of cardiology/american heart association task force on practice guidelines. Circulation. 2014; Jun 10;129(23):2440–92.
2. Nkomo VT, Gardin JM, Skelton TN, Gottdiener JS, Scott CG, Enriquez-Sarano M. Burden of valvular heart diseases: a population-based study. Lancet. 2006;368(9540):1005–11.
3. Rajamannan NM, Evans FJ, Aikawa E, Grande-Allen KJ, Demer LL, Heistad DD, et al. Calcific aortic valve disease: not simply a degenerative process: a review and agenda for research from the national heart and lung and blood institute aortic stenosis working group. Executive summary: calcific aortic valve disease-2011 update. Circulation. 2011;124 (16):1783–91.
4. Cribier A, Eltchaninoff H, Bash A, Borenstein N, Tron C, Bauer F, et al. Percutaneous transcatheter

implantation of an aortic valve prosthesis for calcific aortic stenosis: first human case description. Circulation. 2002;106(24):3006–8.
5. Leon MB, Smith CR, Mack M, Miller DC, Moses JW, Svensson LG, et al. Transcatheter aortic-valve implantation for aortic stenosis in patients who cannot undergo surgery. N Engl J Med. 2010;363(17):1597–607.
6. Smith CR, Leon MB, Mack MJ, Miller DC, Moses JW, Svensson LG, et al. Transcatheter versus surgical aortic-valve replacement in high-risk patients. N Engl J Med. 2011;364(23):2187–98.
7. Adams DH, Popma JJ, Reardon MJ, Yakubov SJ, Coselli JS, Deeb GM, et al. Transcatheter aortic-valve replacement with a self-expanding prosthesis. N Engl J Med. 2014;370(19):1790–8.
8. Reardon MJ, Adams DH, Kleiman NS, Yakubov SJ, Coselli JS, Deeb GM, et al. 2-year outcomes in patients undergoing surgical or self-expanding transcatheter aortic valve replacement. J Am Coll Cardiol. 2015;66(2):113–21.
9. Mack MJ, Leon MB, Smith CR, Miller DC, Moses JW, Tuzcu EM, et al. 5-year outcomes of transcatheter aortic valve replacement or surgical aortic valve replacement for high surgical risk patients with aortic stenosis (PARTNER 1): a randomised controlled trial. Lancet. 2015;385(9986):2477–84.
10. Thyregod HG, Steinbrüchel DA, Ihlemann N, Nissen H, Kjeldsen BJ, Petursson P, et al. Transcatheter versus surgical aortic valve replacement in patients with severe aortic valve stenosis: 1-year results from the all-comers notion randomized clinical trial. J Am Coll Cardiol. 2015;65(20):2184–94.
11. Kheradvar A, Groves EM, Goergen CJ, Alavi SH, Tranquillo R, Simmons CA, et al. Emerging trends in heart valve engineering: Part II. Novel and standard technologies for aortic valve replacement. Ann Biomed Eng. 2015;43(4):844–57.
12. Hamm CW, Arsalan M, Mack MJ. The future of transcatheter aortic valve implantation. Eur Heart J. 2016 Mar 7;37(10):803–10.
13. Little SH, Paravalvular regurgitation after TAVR: a Doppler dilemma. JACC Cardiovasc Imaging. 2015;8(9):1004–6.
14. Holmes DR, Mack MJ, Kaul S, Agnihotri A, Alexander KP, Bailey SR, et al. 2012 ACCF/AATS/SCAI/STS expert consensus document on transcatheter aortic valve replacement. J Am Coll Cardiol. 2012;59(13):1200–54.
15. Hahn RT, Little SH, Monaghan MJ, Kodali SK, Williams M, Leon MB, Gillam LD. Recommendations for comprehensive intraprocedural echocardiographic imaging during TAVR. JACC Cardiovasc Imaging. 2015;8(3):261–87.
16. Achenbach S, Delgado V, Hausleiter J, Schoenhagen P, Min JK, Leipsic JA. SCCT expert consensus document on computed tomography imaging before transcatheter aortic valve implantation (TAVI)/transcatheter aortic valve replacement (TAVR). J Cardiovasc Comput Tomogr. 2012;6(6):366–80.
17. Gilon D, Cape EG, Handschumacher MD, Song JK, Solheim J, VanAuker M, et al. Effect of three-dimensional valve shape on the hemodynamics of aortic stenosis: three-dimensional echocardiographic stereolithography and patient studies. J Am Coll Cardiol. 2002;40(8):1479–86.
18. Schmauss D, Schmitz C, Bigdeli AK, Weber S, Gerber N, Beiras-Fernandez A, et al. Three-dimensional printing of models for preoperative planning and simulation of transcatheter valve replacement. Ann Thorac Surg. 2012;93(2):e31–3.
19. Farooqi KM, Sengupta PP. Echocardiography and three-dimensional printing: sound ideas to touch a heart. J Am Soc Echocardiogr. 2015;28(4):398.
20. Maragiannis D, Jackson MS, Igo SR, Chang SM, Zoghbi WA, Little SH Functional 3D printed patient-specific modeling of severe aortic stenosis. JACC. 2014;64(10):1066–70.
21. Maragiannis D, Jackson MS, Igo SR, Schutt RC, Connell P, Grande-Allen J, et al. Replicating patient-specific severe aortic valve stenosis with functional 3D modeling. Circ Cardiovasc Imaging. 2015 Oct;8(10):e003626.
22. Vukicevic M, Mosadegh B, Min JK, Little SH. Cardiac 3D printing and its future direction. JACC Cardiovasc Imaging. 2017 Feb;10(2):171–84.
23. Cloonan AJ, Shahmirzadi D, Li RX, Doyle BJ, Konofagou EE, McGloughlin TM. 3D-printed tissue-mimicking phantoms for medical imaging and computational validation applications. 3D Printing Addit Manufact. 2014;1(1):14–23.
24. Ionita CN, Mokin M, Varble N, Bednarek DR, Xiang J, Snyder KV, et al. Challenges and limitations of patient-specific vascular phantom fabrication using 3D polyjet printing. Proc SPIE Int Soc Opt Eng. 2014;9038:90380M.
25. Martin C, Pham T, Sun W. Significant differences in the material properties between aged human and porcine aortic tissues. Eur J Cardiothorac Surg. 2011;40(1):28–34.
26. Wang K, Zhao Y, Chang Y-H, Qian Z, Zhang C, Wang B, et al. Controlling the mechanical behavior of dual-material 3D printed meta-materials for patient-specific tissue-mimicking phantoms. Mater Des. 2016;90:704–12.
27. Iung B, Baron G, Butchart EG, Delahaye F, Gohlke-Bärwolf C, Levang OW, et al. A prospective survey of patients with valvular heart disease in Europe: the euro heart survey on valvular heart disease. Eur Heart J. 2003;24(13):1231–43.
28. Seiffert M, Bader R, Kappert U, Rastan A, Krapf S, Bleiziffer S, et al. Initial german experience with transapical implantation of a second-generation transcatheter heart valve for the treatment of aortic regurgitation. JACC Cardiovasc Interv. 2014;7(10):1168–74.

# Valvular Heart Disease

13

Mario Montealegre-Gallegos, MD,
Jelliffe Jeganathan, MBBS
and Feroze Mahmood, MD, FASE

## Introduction

Valvular heart disease (VHD) affects all age-groups. It can occur in the setting of congenital heart disease affecting children, as rheumatic heart disease affecting young adults or as degenerative heart disease during old age. Degenerative VHD is becoming increasingly prevalent in industrialized countries due to an aging population and results in significant healthcare costs and decreased quality of life. VHD's impact on quality of life is considerable when compared to other cardiac conditions because it affects all age-groups. It is unlike coronary artery disease, associated with subsequent ventricular dysfunction, which predominantly affects elderly patients. There is a significant increase in the prevalence of VHD in older individuals, with the incidence rising sharply after 64 years of age [1, 2]. The natural course of VHD can result in a range of hemodynamic derangements, many of which can be prevented with appropriate surgical intervention (Table 13.1) [3].

M. Montealegre-Gallegos ·
J. Jeganathan · F. Mahmood (✉)
Department of Anesthesia, Critical Care and Pain Medicine, Beth Israel Deaconess Medical Center, Harvard Medical School, Boston, MA, USA
e-mail: fmahmood@bidmc.harvard.edu

M. Montealegre-Gallegos
e-mail: mmonteal@bidmc.harvard.edu

J. Jeganathan
e-mail: jjeganat@bidmc.harvard.edu


K.M. Farooqi (ed.), *Rapid Prototyping in Cardiac Disease*,
DOI 10.1007/978-3-319-53523-4_13

The increase in the prevalence and incidence of VHD underscores the importance of screening and early diagnosis. While there are detailed guidelines addressing indications for surgical intervention in VHD, precise classification of patients according to the severity of disease will help to identify patients who may be managed medically without the need for surgery (Table 13.2) [3].

The most common VHDs that warrant surgical repair or replacement include [1] the following:

1. Mitral regurgitation
2. Aortic stenosis
3. Aortic regurgitation
4. Mitral stenosis

## Mitral Regurgitation

When a structural defect in the mitral valve leads to regurgitation, it is known as primary or organic mitral regurgitation (MR). Mitral valve prolapse is the most common cause of primary MR in developed countries. While rheumatic heart disease is the second most common cause overall, it remains the most common etiology in developing countries. Congenital heart disease and infective endocarditis are other causes of primary MR. Remodeling of the left ventricle resulting in incomplete closure of a structurally normal mitral valve is known as secondary or functional MR. Patients with MR due to left ventricular dysfunction usually present at an advanced stage of heart failure leading to an underestimation of MR [4]. Prognosis of patients

**Table 13.1** Consequences of valvular heart diseases

| Consequences of valvular heart diseases |
|---|
| **Aortic stenosis**<br>• 5-year survival rate of symptomatic severe AS is from 15–50%<br>*Results in*<br>• Left ventricular dysfunction<br>• Left ventricular hypertrophy<br>• Pulmonary hypertension |
| **Aortic regurgitation**<br>• Aortic root diameter and family history of acute cardiac events are strong predictors of mortality in AR<br>*Results in*<br>• Left ventricular dilatation (LVESD > 50 mm)<br>• Left ventricular systolic dysfunction<br>• Decreased LVEF (<50%) |
| **Mitral stenosis**<br>• Asymptomatic pt survival is up to 10 years<br>• Poor prognosis for symptomatic patients without treatment<br>*Results in*<br>• Left atrial enlargement |
| **Mitral regurgitation**<br>• Poor prognosis<br>• Untreated chordal rupture can lead to pulmonary hypertension<br>*Results in*<br>• Left atrial enlargement<br>• Left ventricular enlargement in severe MR<br>• Pulmonary hypertension in severe MR |
| **Severe tricuspid stenosis or regurgitation**<br>*Results in*<br>• Right atrial enlargement<br>• Inferior vena cava dilation |

with functional MR depends on the severity of left ventricular dysfunction.

## Aortic Stenosis

The prevalence of aortic stenosis (AS) in adults is approximately 2% for patients aged 70–80 and increases to 3–9% after 80 years of age. Atherosclerosis and AS have common risk factors, such as age, hypertension, and smoking [4]. The rate of progression from moderate to severe AS significantly varies between individuals and is unpredictable. In the USA, bicuspid aortic valve is the most common congenital anomaly leading to AS. Unfortunately, bicuspid aortic valve may be difficult to detect in the outpatient setting, leading to an underestimation of the prevalence of the condition. The majority of patients with bicuspid aortic valve progress to AS after age 50, which highlights the importance of early diagnosis of this condition [5].

**Table 13.2** Surgical indications for different valvular heart lesions

| Valvular lesion | Surgical indication |
|---|---|
| **Mitral regurgitation** | **Symptomatic patients**<br>• With severe MR<br>• EROA $\geq$ 0.2 $cm^2$<br>• LVEF > 30%<br>**Asymptomatic patients**<br>• With severe MR<br>• Left ventricular dysfunction<br>• EROA $\geq$ 0.2 $cm^2$<br>• LVEF = 30–60%<br>• LVESD $\geq$ 40 mm |
| **Mitral stenosis** | **Symptomatic patients**<br>• PMBC when MVA $\leq$ 1.5 $cm^2$ without any contraindications<br>• MV repair when MVA $\leq$ 1.5 $cm^2$ with contraindications for PMBC and without high risk for surgery<br>**Asymptomatic patients**<br>• Severe MS with MVA $\leq$ 1.5 $cm^2$ undergoing other cardiac surgery |
| **Aortic stenosis** | **Symptomatic patients**<br>• Severe high-gradient AS<br>• Severe leaflet calcification<br>• Congenital stenosis with AVA $\leq$ 1.0 $cm^2$<br>**Asymptomatic patients**<br>• Severe AS<br>• LV dysfunction<br>• Severe leaflet calcification<br>• Congenital stenosis |
| **Aortic regurgitation** | **Symptomatic patients**<br>• Severe AR<br>• Severe valve calcification<br>• Congenital abnormality like bicuspid valve<br>• Valvular damage due to rheumatic disease<br>**Asymptomatic patients**<br>• Severe AR<br>• Abnormal LV systolic function<br>• LVEF < 50%<br>• Severe LV dilatation |

## Aortic Regurgitation

Degenerative valve disease is the leading cause of aortic regurgitation (AR) in developed countries, while rheumatic heart disease is the most common etiology in developing countries. Bicuspid aortic valve is the most common cause of AR in patients under 50 [4]. Aortic root dilation and calcific valve disease are other etiologies [6]. Factors such as old age, hypertension, dyslipidemia, smoking, and diabetes lead to aortic dilation that can cause secondary AR. Trace AR is common and has been found in up to 13% of men before 50 years of age. The prevalence of mild AR increases from 3.7% in the sixth decade to 12.2% in the eighth decade, whereas that of moderate-to-severe AR increases from 0.5 to 2.2% [7].

## Mitral Stenosis

Mitral stenosis (MS) is the least common VHD in the USA and other developed countries. This is due to the fact that MS is most commonly caused by rheumatic heart disease. In the last decade, the proportion of mitral valve surgeries dedicated to correcting mitral stenosis has decreased from 30 to 14% in the USA [1]. Other rare causes of MS are mitral annular calcification, radiation exposure, and certain congenital metabolic conditions [8, 9].

## Other Causes of Valvular Heart Disease

Systemic inflammatory conditions such as systemic lupus erythematosus (SLE) can cause fusion of valve commissures and thickening of the leaflets. Drug-induced VHD, postradiation VHD, endocarditis, and device implantation are some other reasons for increased burden of VHD. Isolated tricuspid and pulmonic valve lesions are very rare.

## Challenges for Rapid Prototyping in Valvular Heart Disease

Rapid prototyping (RP) is a promising and rapidly growing technology for the evaluation and management of VHD [10]. Potential uses of RP in VHD include ex vivo valve analysis, hemodynamic testing, surgical planning, teaching, and design of patient-specific prostheses. However, despite all these uses, there are currently no clear guidelines for application of RP for VHD; therefore, it is a technology awaiting specific indications.

There are several limitations that may make RP difficult to apply in VHD (Table 13.3). First, cardiac valves are thin and mobile structures, which require a high spatial and temporal resolution to obtain adequate 3D datasets for segmentation and modeling [11]. These high temporal and spatial resolutions usually require electrocardiogram (ECG) gating and reconstructive imaging, so that absence of patient motion and a stable cardiac rhythm are necessary. Second, imaging artifacts and inadequate image optimization (e.g., high-ultrasound gain settings, acoustic shadowing, blurring, and blooming) may decrease the accuracy of the structure's 3D representation.

**Table 13.3** Limitations for rapid prototyping in valvular heart disease

| |
|---|
| – Image with high spatial resolution required |
| – High temporal resolution necessary to select appropriate part of the cardiac cycle |
| – Imaging artifacts may affect dataset quality |
| – Optimal imaging settings (e.g., gain and compression) necessary to visualize adequate tissue–blood interface |
| – Variations of preload, afterload, rhythm, etc., also determine valve function |
| – Dynamic component of valve opening and closure during the cardiac cycle is not represented |
| – Time-consuming |
| – Postprocessing of dataset and printed models is necessary |

Third, associated conditions (e.g., calcification and prosthetic material) may hinder adequate visualization of the leaflet tissue [12]. This is an important concern for degenerative VHD such as AS, which is frequently associated with significant valve leaflet calcification. Fourth, although the anatomic structure of the valve leaflets is important for adequate valve function, the functional valve apparatus (i.e., valve annulus, papillary muscles, sinuses of Valsalva, and loading conditions) is equally important. Replicating these structures is challenging with currently available methods. Fifth, cardiac valves are dynamic structures that need adequate closure to avoid regurgitation and adequate opening to avoid stenosis. Although imaging-derived RP of valves is currently possible, these models are generated during a specific part of the cardiac cycle and may not be completely representative of the structural changes that the valve undergoes during the systolic and diastolic phases [13.]. Sixth, although feasible with new technologies, so far it has not been possible to create exact models that replicate the heterogeneous thickness and flexibility of the different valvular components. Lastly, the use of RP at the point of care is still limited by the timely availability of models. Imaging data acquisition, exporting Cartesian-type Digital Imaging and Communications in Medicine (DICOM) files, segmentation, generation, and refinement of a stereolithography (.stl) file are all time-consuming processes. Furthermore, commonly used RP modalities such as fused deposition modeling and stereolithography require at least some level of postprocessing. Removal of supports, ultraviolet curing of resin, and print soaking in water or alcohol can significantly increase the time required for model availability at the point of care (e.g., operating room and interventional suite).

In this section, we will discuss the different imaging modalities used to evaluate VHD, the use of 3-dimensional (3D) transesophageal echocardiography (TEE) to assess VHD in the perioperative period and the potential applications of RP in patients with VHD.

## Imaging Modalities Used to Evaluate Valvular Heart Disease

Imaging is essential for evaluating patients suffering from VHD. In these patients, imaging is used to identify the type of valve dysfunction and quantify its severity, evaluate the repercussions of the underlying VHD in cardiac function, establish a prognosis, and select the appropriate management (surgical, interventional, or medical) [14]. Imaging modalities may also be used for preoperative surgical planning, intraoperative procedural guidance, and postoperatively for patient follow-up.

Imaging modalities that can be used to assess VHD include MRI, computerized tomography (CT), and echocardiography [14, 15]. Despite great improvements in MRI and CT technology, echocardiography is the imaging modality of choice to evaluate VHD. The reasons for this are its increased portability, low risk, low comparative cost, its ability to image valve tissue with high temporal and spatial resolutions and to provide reliable qualitative and quantitative information regarding transvalvular flows. Furthermore, in order to produce high-quality reconstructions, CT and MRI usually require intravenous contrast, sedation, and use of ionizing radiation [16]. 3D TEE is a particularly useful imaging modality in VHD and will be discussed during the next section.

In recent years, the combination of imaging techniques (i.e., multimodality imaging) has increasingly been used in patients with VHD, particularly to guide and plan percutaneous interventions for structural heart disease [17].

## Rapid Prototyping from Three-Dimensional Transesophageal Echocardiographic Data

Echocardiography is the most frequently used imaging modality for evaluating VHD in the clinical setting. Transthoracic echocardiography

and TEE may be used for assessing VHD, with both modalities having their own advantages and disadvantages. Although transthoracic echocardiography (TTE) is noninvasive, obtaining high-quality 3D datasets may be more difficult due to patient movement, respiration, and artifacts associated with the ribs and lungs. TEE is minimally invasive and has a low rate of severe complications. If 3D TEE is performed under general anesthesia, the patient can be paralyzed and made apneic, thus reducing motion artifacts. Furthermore, the relative closeness of the TEE transducer to the mitral valve and their perpendicular relationship allow generation of high-quality images. There are well-established indications for TEE in cardiac surgery [18], and this imaging modality is used for most cardiac procedures in a large number of institutions. Recent developments in 3D TEE have made it the imaging modality of choice for assessment of mitral valve disease [19], particularly in the perioperative period. In this setting, 3D TEE provides high-quality dynamic imaging under physiological conditions, which may be superior to surgical visualization of the valve in an empty, arrested heart [20]. However, 3D TEE suffers from the inherent limitation of visualizing 3D images on a flat two-dimensional screen [11]. Although manufacturers have significantly improved volume-rendering algorithms, visualization of the data in the clinical setting is still limited and may be inaccurate (e.g., due to parallax error) in some cases [21]. For this reason, RP of 3D TEE or TTE-generated valve models may provide a better alternative to visualization of a volume-rendered image.

## Overview of 3D Printing a Mitral Valve Model from Transesophageal Echocardiography

Here, we describe a brief overview of a workflow for steps involved in printing a three-dimensional valve model from transesophageal echocardiography. High-quality TTE images may also be substituted into the workflow, if available. The workflow can be divided into the following five steps:

1. Acquisition of high-resolution 3D images
2. Converting imaging data from DICOM to Cartesian DICOM format
3. Segmentation of mitral valve structure to develop a 3D mitral valve model
4. Optimization of the 3D model
5. 3D printing

A high-resolution 3D TEE dataset is required for 3D printing a valve model. R-wave gated imaging has both high temporal and spatial resolutions and is ideal in patients with regular cardiac rhythm (Fig. 13.1a). Wide-angle "live" zoom mode or single-beat full-volume acquisition can be used in patients with arrhythmias. The 3D image dataset thus acquired from the echo machine will be in a DICOM format that can be exported to a digital video disc (DVD) or a universal serial bus (USB). The DICOM files are then converted into "Philips Cartesian DICOM" format using QLAB (Philips Medical Systems, Andover, MA), which makes the 3D images readable by segmentation software programs (Fig. 13.1b). Of note, currently only Philips (Amsterdam, Netherlands), 3D datasets can be converted into Cartesian DICOM format and segmented. The Cartesian DICOM file can then be imported into any available segmentation software such as Mimics Innovation Suite (Materialise, Leuven, Belgium), ITK-SNAP (http://www.itksnap.org), or 3D Slicer (http://www.slicer.org), where the region of interest, a mitral valve in this case, is segmented from the 3D echocardiographic data (Fig. 13.1c). The process of segmentation is largely a semiautomated procedure. The segmented file is then saved as a stereolithography (.stl) file and can be further edited and refined using specific software programs such as 3Matic (Materialise, Leuven, Belgium), Blender (Blender Foundation, Amsterdam, Netherlands), or Meshlab (Visual Computing Lab, National Research Council of Italy) (Fig. 13.1d). When the final model of the mitral valve is ready in a 3D printable format (.stl, .amf, .ply, etc.), it can then be printed using a suitable 3D printer or can be outsourced to a 3D printing company (Fig. 13.1e). Alternatively, a 3D echocardiographic dataset of the mitral valve may be imported into TomTec software (Image Arena,

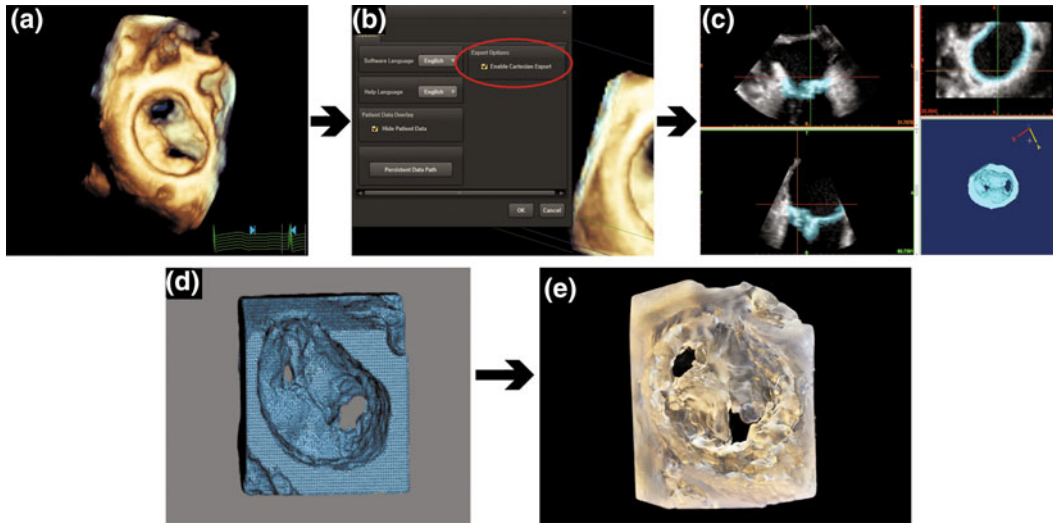


**Fig. 13.1** A high-quality 3D TEE image of the mitral valve is obtained in DICOM format (**a**). The image is then converted into Cartesian DICOM format via QLAB software (**b**). The mitral valve is then segmented from the Cartesian DICOM to generate a 3D model using Mimics (**c**). The 3D model thus generated is further refined and optimized in 3Matic (**d**) and finally printed with a suitable 3D printer (**e**)

TomTec GmbH, Munich, Germany). This workflow involves identifying anatomic landmarks of the mitral valve annulus from different two-dimensional views. Once this is complete, a 3D rendering of the mitral valve is created with a relatively clean outline of the annulus. This file can then be exported as a 3D file, i.e., STL, and be processed on a 3D printer for physical model creation [20]. This process is less labor-intensive than the manual segmentation of the valve leaflets. In addition, the borders of the annulus are more succinctly defined, albeit derived from a limited number of points identified on 2D images.

## Rapid Prototyping in Valvular Heart Disease: Current Uses and Future Directions

### Surgical Planning

The examination of heart valves for surgical repair/replacement is a challenging endeavor. During heart surgery, valves are examined on an empty, noncontractile, and relaxed heart (i.e., under the effect of cardioplegia). In these procedures, surgical planning is challenging and usually needs to be modified "on the spot" depending on specific findings.

Additionally, an increasing number of patients with VHD are undergoing percutaneous interventional procedures (e.g., MitraClip and transcatheter aortic valve replacement). Initially indicated only in high-risk patients, these procedures are now chosen by patients or physicians as a primary treatment option. Interventional procedures are particularly challenging due to a lack of direct visualization of the heart valves during the procedure. 3D printing could help the surgeon or interventionalist perform an "ex vivo" examination of valvular anatomy (Fig. 13.2). There are some reports of use of 3D printing for this purpose with encouraging results [22–25].

### Hemodynamic Testing

Our current understanding of valvular hemodynamics is primarily derived from fluid dynamic models, in vivo Doppler studies performed under unstable and changing circumstances (e.g., surgery), and extrapolation of animal data

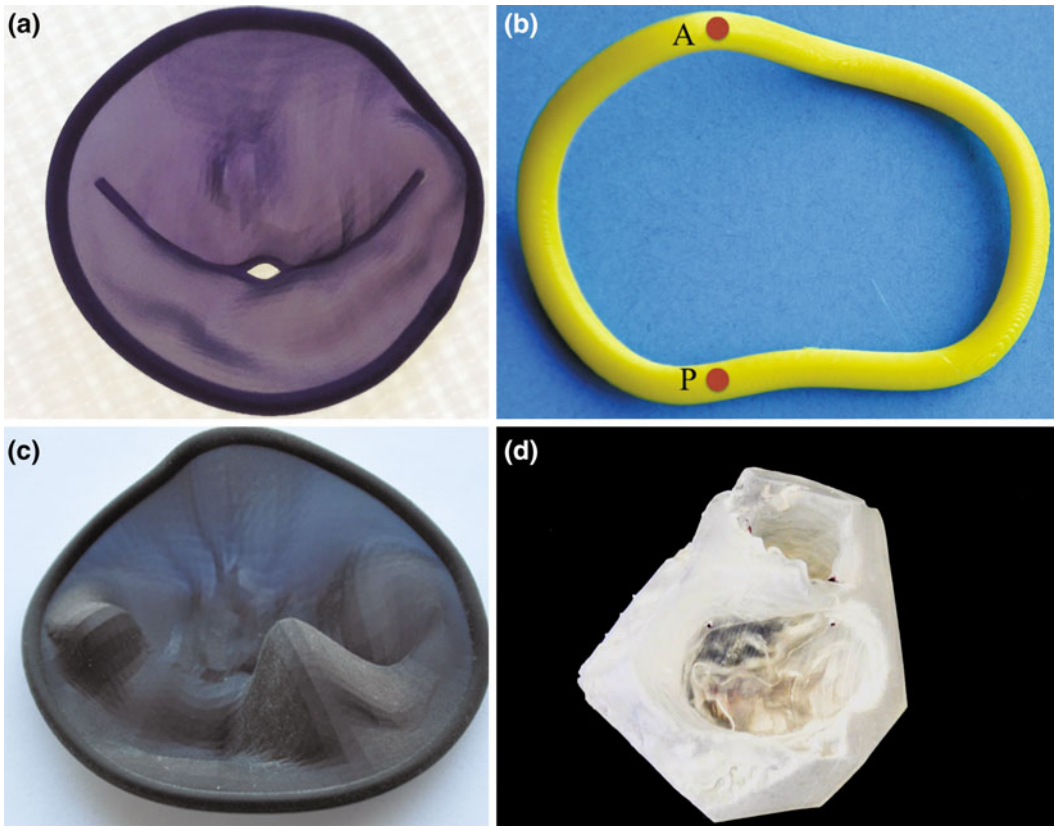


**Fig. 13.2** **a** Normal 3D-printed mitral valve, **b** 3D-printed mitral annulus obtained from a patient with Barlow's disease showing significant dilation with labeled anterior (*A*) and posterior (*P*) points, **c** 3D-printed mitral valve from a patient with myxomatous disease, with dilated mitral annulus and posterior leaflet prolapse, and **d** 3D-printed aortic–mitral complex. The precise relationship between the aortic and mitral valves is observed

[26]. The ability to test physiological parameters of patient-specific anatomic models in pulsatile flow chambers (i.e., pulse duplicators) is a potential application of RP [27]. Current 3D printing technology allows for these models to be developed from multiple materials and therefore has different properties. In our experience, we have developed flexible silicone molds derived from rigid 3D-printed mitral valve models. These molds can be adapted to a pulsatile chamber (Fig. 13.3) to simulate diastole. We have used these models to study echocardiographic Doppler parameters commonly used for mitral valve assessment such as pressure half-time [27]. Other models could be adapted to other types of chambers that simulate the systolic phase.

## Communication with Patients and Medical Training

The utility of RP in VHD extends beyond direct clinical application and can be applied toward communication with patients and for medical training. Patient-specific models can be used in the preoperative period to explain the anatomy to patients with VHD and discuss the possible treatment options. RP also has the potential of creating relatively low-cost, open-access simulators for cardiac surgery and percutaneous interventions [10, 20]. One of the main disadvantages of simulation training is that modern simulators can be associated with significant purchase and maintenance costs. Use of RP may help to make simulation more accessible for medical training.

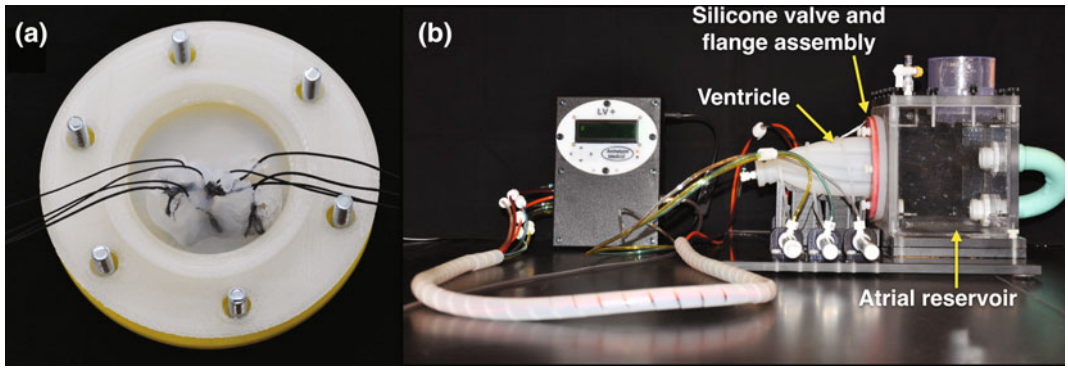


**Fig. 13.3** **a** Silicone model of the mitral valve is adapted to a flange and **b** silicone model of the mitral valve and flange adapted to a pulse duplicator system (Archetype Medical Inc., Ontario, Canada)

## Design of Patient-Specific Prostheses

Perhaps, one of the most exciting future applications of RP in VHD is the design of patient-specific prostheses. These prostheses could be created based on the patients' own 3D imaging data and adapted to suit their specific needs. This has been shown to be successfully applied in other types of pathologies [28]. The development of biocompatible, sterile materials is a requirement for these models. Recently, 3D-printed silk materials have been described for the treatment of bone fractures [29]. These materials show great potential for designing annuloplasty rings for treatment of mitral and tricuspid valve disease. These prostheses could be designed to be reabsorbed once the initial problem (e.g., MR) resolves. There have also been promising studies on the use of RP for the development of scaffolds for tissue-engineered heart valves [30] and even bioprinting of valve conduits [31, 32].

## Conclusion

In conclusion, RP is a developing technology with multiple potential applications for VHD, including surgical planning, hemodynamic testing, surgical training, and design of patient-specific prostheses. 3D TEE is particularly well suited for 3D printing of heart valves, due to its availability, logistic advantages, relatively low cost, and high temporal and spatial resolution. However, many obstacles still need to be addressed so that echocardiographically derived 3D-printed models can be used for patient diagnosis and management at the point of care.

## References

1. Vahanian A, Iung B, Himbert D, Nataf P. Changing demographics of valvular heart disease and impact on surgical and transcatheter valve therapies. Int J Cardiovasc Imaging. 2011;27(8):1115–22.
2. Nkomo VT, Gardin JM, Skelton TN, Gottdiener JS, Scott CG, Enriquez-Sarano M. Burden of valvular heart diseases: a population-based study. Lancet. 2006;368(9540):1005–11.
3. Nishimura RA, Otto CM, Bonow RO, Carabello BA, Erwin JP, Guyton RA, et al. AHA/ACC guideline for the management of patients with valvular heart disease: a report of the American College of Cardiology/American Heart Association task force on practice guidelines. J Thorac Cardiovasc Surg. 2014;148:e1–132.
4. Iung B, Vahanian A. Epidemiology of valvular heart disease in the adult. Nat Rev Cardiol. 2011;8(3):162–72.
5. Roberts WC, Ko JM. Frequency by decades of unicuspid, bicuspid, and tricuspid aortic valves in adults having isolated aortic valve replacement for aortic stenosis, with or without associated aortic regurgitation. Circulation. 2005;111(7):920–5.
6. Enriquez-Sarano M, Tajik AJ. Clinical practice. Aortic regurgitation. N Engl J Med. 2004;351(15):1539–46.
7. Singh JP, Evans JC, Levy D, Larson MG, Freed LA, Fuller DL, et al. Prevalence and clinical determinants

of mitral, tricuspid, and aortic regurgitation (the Framingham Heart Study). Am J Cardiol. 1999;83 (6):897–902.
8. Olson LJ, Subramanian R, Ackermann DM, Orszulak TA, Edwards WD. Surgical pathology of the mitral valve: a study of 712 cases spanning 21 years. Mayo Clin Proc. 1987;62(1):22–34.
9. Horstkotte D, Niehues R, Strauer BE. Pathomorphological aspects, aetiology and natural history of acquired mitral valve stenosis. Eur Heart J. 1991;12 (Suppl B):55–60.
10. Owais K, Pal A, Matyal R, Montealegre-Gallegos M, Khabbaz KR, Maslow A, et al. Three-dimensional printing of the mitral annulus using echocardiographic data: science fiction or in the operating room next door? J Cardiothorac Vasc Anesth. 2014;28 (5):1393–6.
11. Olivieri LJ, Krieger A, Loke Y-H, Nath DS, Kim PCW, Sable CA. Three-dimensional printing of intracardiac defects from three-dimensional echocardiographic images: feasibility and relative accuracy. J Am Soc Echocardiogr. 2015;28(4):392–7.
12. Faletra FF, Ramamurthi A, Dequarti MC, Leo LA, Moccetti T, Pandian N. Artifacts in three-dimensional transesophageal echocardiography. J Am Soc Echocardiogr. 2014;27(5):453–62.
13. Jiang L, Owais K, Matyal R, Khabbaz KR, Liu DC, Montealegre-Gallegos M, et al. Dynamism of the mitral annulus: a spatial and temporal analysis. J Cardiothorac Vasc Anesth. 2014;28(5):1191–7.
14. Pibarot P, Larose É, Dumesnil J. Imaging of valvular heart disease. Can J Cardiol. 2013;29(3):337–49.
15. Choo WS, Steeds RP. Cardiac imaging in valvular heart disease. Br J Radiol. 2011;84(Spec No 3): S245–57.
16. Rengier F, Mehndiratta A, von Tengg-Kobligk H, Zechmann CM, Unterhinninghofen R, Kauczor H-U, et al. 3D printing based on imaging data: review of medical applications. Int J Comput Assist Radiol Surg. 2010;5(4):335–41.
17. Gaemperli O, Delgado V, Habib G, Kaufmann PA, Bax JJ. The year in cardiology 2015: imaging. Eur Heart J. 2016;37(8):667–75.
18. Hahn RT, Abraham T, Adams MS, Bruce CJ, Glas KE, Lang RM, et al. Guidelines for performing a comprehensive transesophageal echocardiographic examination: recommendations from the american society of echocardiography and the society of cardiovascular anesthesiologists. J Am Soc Echocardiogr. 2013;26(9):921–64.
19. Mahmood F, Matyal R. A quantitative approach to the intraoperative echocardiographic assessment of the mitral valve for repair. Anesth Analg. 2015;121(1):34–58.
20. Mahmood F, Owais K, Taylor C, Montealegre-Gallegos M, Manning W, Matyal R, et al. Three-dimensional printing of mitral valve using echocardiographic data. JACC Cardiovasc Imaging. 2015;8(2):227–9.
21. Mahmood F, Jeganathan J, Saraf R, Shahul S, Swaminathan M, Mackensen GB, et al. A practical approach to an intraoperative three-dimensional transesophageal echocardiography examination. J Cardiothorac Vasc Anesth. 2016;30(2):470–90.
22. Ripley B, Kelil T, Cheezum MK, Goncalves A, Di Carli MF, Rybicki FJ, et al. 3D printing based on cardiac CT assists anatomic visualization prior to transcatheter aortic valve replacement. J Cardiovasc Comput Tomogr. 2016 Jan;10(1):28–36 (Figure 4 (A–D): 3D models of patients with adult congenital heart disease).
23. Gallo M, D'Onofrio A, Tarantini G, Nocerino E, Remondino F, Gerosa G. 3D-printing model for complex aortic transcatheter valve treatment. Int J Cardiol. 2016;1(210):139–40.
24. Dankowski R, Baszko A, Sutherland M, Firek L, Kałmucki P, Wróblewska K, et al. 3D heart model printing for preparation of percutaneous structural interventions: description of the technology and case report. Kardiol Pol. 2014;72(6):546–51.
25. Sodian R, Schmauss D, Markert M, Weber S, Nikolaou K, Haeberle S, et al. Three-dimensional printing creates models for surgical planning of aortic valve replacement after previous coronary bypass grafting. Ann Thorac Surg. 2008;85(6):2105–8.
26. Eskesen K, Olsen NT, Dimaano VL, Pinheiro A, Sogaard P, Fritz-Hansen T, et al. New approach to intracardiac hemodynamic measurements in small animals: echo-guided percutaneous apical puncture. J Ultrasound Med. 2012;31(8):1233–8.
27. Mashari A, Knio Z, Jeganathan J, Montealegre-Gallegos M, Yeh L, Amador Y, et al. Hemodynamic testing of patient-specific mitral valves using a pulse duplicator: a clinical application of three-dimensional printing. J Cardiothorac Vasc Anesth (in press).
28. Zopf DA, Hollister SJ, Nelson ME, Ohye RG, Green GE. Bioresorbable airway splint created with a three-dimensional printer. N Engl J Med. 2013;368 (21):2043–5.
29. Perrone GS, Leisk GG, Lo TJ, Moreau JE, Haas DS, Papenburg BJ, et al. The use of silk-based devices for fracture fixation. Nat Commun. 2014;5:3385.
30. Sodian R, Loebe M, Hein A, Martin DP, Hoerstrup SP, Potapov EV, et al. Application of stereolithography for scaffold fabrication for tissue engineered heart valves. ASAIO J. 2002;48(1):12–6.
31. Duan B, Kapetanovic E, Hockaday LA, Butcher JT. Three-dimensional printed trileaflet valve conduits using biological hydrogels and human valve interstitial cells. Acta Biomater. 2014;10(5):1836–46.
32. Duan B, Hockaday LA, Kang KH. 3D bioprinting of heterogeneous aortic valve conduits with alginate/gelatin hydrogels. J Biomed. 2013.

# Assessment of Ventricular Assist Device Placement and Function

14

Omar Saeed, MD, Kanwal Majeed Farooqi, MD and Ulrich P. Jorde, MD

## Heart Failure in Congenital Heart Disease

Congenital heart disease (CHD) is reported to occur with an incidence between 3 and 20 for every 1000 live births, and the majority of cases are related to structural malformations [1, 2]. With remarkable improvements in surgical approaches and postoperative management, survival has dramatically improved to over 90% after the first year of life [3]. The majority of morbidity is now noted to occur in adults with CHD with 76% of deaths occurring in those who survived their first year after the age of 18. Overall, in patients with CHD, the median age of survival has increased from 37 years in 2002 to 57 years in 2007 [4].

Since patients with CHD are surviving for longer periods of time, there has been an increase in the burden of heart failure (HF) in this growing population. The major structural etiologies of HF in patients with CHD stem from failure of a systemic right ventricle, residual cardiopulmonary abnormalities, and from sequela of palliative surgical interventions such as the Fontan procedure. Although the overall prevalence of HF in all CHD patients is uncertain, approximately 50% of those who undergo a Fontan procedure develop HF as adults. Once HF develops, it becomes the leading cause of death accounting for 26% of all deaths in adults with CHD. Despite such a lethal burden from HF, only 3% of patients that undergo heart transplantation have CHD, leading to a dire need for alternative methods of circulatory support [5–7].

## The Role of Mechanical Circulatory Support in HF from CHD

During the past two decades, there has been remarkable progress in the development and implementation of durable mechanical circulatory support (MCS) with left ventricular assist devices (LVADs) for patients with end-stage HF. The current generation of smaller and more durable continuous flow (CF) LVADs have replaced the preceding generation of pulsatile devices. At the moment, the most commonly utilized CF LVADs are HeartMate II (HM II), (Thoratec Corp., Pleasanton, CA, USA) and the HeartWare Ventricular Assist Device (HVAD, Heartware Inc., Framingham, MA, USA). HM II is an axial flow device which is placed in a sub-diaphragmatic pocket and has been implanted in over 20,000 patients. HVAD is a smaller

O. Saeed (✉) · U.P. Jorde
Department of Medicine, Division of Cardiology, Montefiore Medical Center, Albert Einstein College of Medicine, New York, NY, USA
e-mail: osaeed@montefiore.org

U.P. Jorde
e-mail: ujorde@montefiore.org

K.M. Farooqi
Department of Pediatrics, Division of Pediatric Cardiology, Rutgers New Jersey Medical School, Newark, NJ, USA
e-mail: kanwal.farooqi@rutgers.edu


K.M. Farooqi (ed.), *Rapid Prototyping in Cardiac Disease*,
DOI 10.1007/978-3-319-53523-4_14

pump in which blood flows in a centrifugal fashion and is implanted in the intra-pericardial space. Both devices are approved for patients awaiting cardiac transplantation, and HM II is also available as DT for patients not eligible for cardiac transplantation.

The Interagency Registry for Mechanically Assisted Circulatory Support (INTERMACS) is the largest registry of patients supported by MCS, encompassing over 150 centers across the United States. From 2006 to 2014, there were 111 adult patients with CHD supported by MCS reported to INTERMACS. Of these patients, 63 were reported to have great complexity lesions. D-TGA status post-atrial switch with failure of the systemic ventricle was the most prevalent great complexity lesion at 44%, followed by palliated single ventricle circulation (25%). Following any durable VAD placement, patients with CHD ($n$ = 89) had similar survival in comparison with those with no CHD ($n$ = 13,554; CHD: 6 months 82%, 24 months 65%; no CHD: 6 months 87%, 24 months 69%, $p$ = *ns*) [8].

Outcomes of heart transplantation after MCS in patients with CHD have been reported. An analysis from the Scientific Registry of Transplant Recipients (SRTR) spanning from 1987 to 2012 showed that MCS was utilized in 83 out of 1213 (6.8%) patients with CHD. Those who underwent MCS were sicker, with greater renal dysfunction (creatinine 1.7 ± 0.9 vs. 1.3 ± 0.9. $p < 0.001$), more likely to be on mechanical ventilation (9.6% vs. 3.8%, $p = 0.019$) and in the ICU in comparison with the non-MCS group. Despite presence of more end organ dysfunction and a higher baseline risk profile in patients who underwent MCS, both groups showed similar 30 day (MCS: 10.8%, no MCS 13.5%, $p = 0.62$) and 1 year survival (MCS: 64%, no MCS 67%, $p = 0.57$) after heart transplantation [9].

Although MCS by VAD placement can be a viable tool in bridging carefully selected patients with CHD to heart transplantation, it is utilized less frequently in those with CHD (6.8%) in comparison with patients with acquired heart disease (18.8%) [9]. The major barriers that have been reported in the placement of a VAD are related to complex anatomical arrangements, inflow cannula positioning, excessive trabeculations in the systemic right ventricle leading to inflow cannula occlusion, and lack of a receiving venous chamber in patients with a single ventricle and Fontan circulation. There is also critical need for accurate assessment of great vessels and shunts and collateral vessels [10]. Such barriers may become more amenable to VAD insertion if complex anatomical arrangements are presented by a preoperative model in a three-dimensional landscape.

## Three-Dimensional Printing

Three-dimensional printing, also known as rapid prototyping, enables creation of physical anatomical models from data sets derived from patient's imaging studies such as cardiac CT scan and MRI. After image segmentation, a virtual 3D model is created which can be printed by a 3D printer into a physical 3D model. This 3D model allows direct visualization of the patient's cardiac anatomy to assist with preoperative planning for VAD placement. Next, we will review the specific anatomy of various complex CHD lesions, the existing experience and challenges with MCS utilization, and the potential of 3D models to assist in overcoming barriers to VAD placement [11].

## D-Transposition of the Great Arteries (D-TGA)

In patients with D-TGA, there is ventriculoarterial discordance meaning that the aorta arises from the right ventricle (RV) and the pulmonary artery arises from the left ventricle (LV) [12]. Since deoxygenated venous blood is pumped from the RV to the systemic circulation, neonates are cyanotic at birth and usually require an atrial septostomy to allow mixing of two otherwise separate and parallel circuits. This mixing of blood allows an improvement in cyanosis, but ultimately, an atrial switch operation is now performed within the first few weeks after birth to

correct ventriculoarterial discordance. The atrial switch operation involves disconnecting the pulmonary artery and aorta superior to the semilunar valves and re-anastomosing them to the RV and LV, respectively [13].

Before the atrial switch operation became standard of care, patients with D-TGA routinely underwent an atrial switch operation. This involved creation of inter-atrial baffles to redirect deoxygenated systemic blood to the LV and oxygenated pulmonary blood to the RV. Autologous tissue was used to create the baffle in the Senning procedure while synthetic material is used in the Mustard procedure [14]. Although the atrial switch provides a durable solution to cyanosis, the major long-term complication of this operation is HF due to the RV functioning as the systemic ventricle. The morphologic spongy and heavily trabeculated make-up of the RV, along with the relative inefficiency of the tricuspid valve apparatus, results in ventricular failure when chronically subjected to high systemic pressures. In addition, there may be impaired myocardial blood flow and coronary flow reserve to meet the higher demands of supporting systemic circulation. It is estimated that about 30% of patients who have undergone atrial switch will develop HF by age 40, at which point their 1 year mortality can reach 50% [15–17].

## L-Transposition of the Great Arteries (L-TGA)

In patients with L-TGA, also known as congenitally corrected TGA (CCTGA), there is both atrioventricular and ventriculoarterial discordance. Systemic venous deoxygenated blood leaves the right atrium to enter the right-sided left ventricle which then leads to the pulmonary artery. Oxygenated pulmonary venous return enters the left atrium and then moves to the leftward systemic right ventricle which pumps to the aorta [18]. Similar to D-TGA, in L-TGA, the RV is the systemic ventricle and in adulthood can lead to HF in 25–67% of patients [19].

## CF LVAD Implantation in D-TGA and L-TGA

Implantation of both pulsatile and continuous flow devices has been reported in patients with D-TGA who have undergone an atrial switch operation. Since CF LVADs are now the mainstay of MCS, we will further discuss the experience with such devices in TGA. Maly and colleagues reported a case series of 5 patients with D-TGA with systemic RV failure 28–32 years after a Mustard operation who underwent HeartMate II implantation. Three of the five patients were successfully bridged to heart transplantation while the other 2 patients died on postoperative days 502 and 34 from progressive HF and pump thrombosis, respectively. The authors described using real time 3D transesophageal echocardiography (TEE) to assess if the inflow cannula was directed toward the tricuspid valve and noted that RV trabeculations and the moderator band were resected to prevent cannula obstruction [20]. In another series of cases, significantly better flows were achieved when the inflow cannula was placed posterior to the moderator band in comparison with anterior placement. This could be contrary to a tendency to place the inflow cannula at the palpable apical dimple which leads to anterior placement and subsequent low flows due to interference by the moderator band and anterior papillary muscles [21]. Implantation of the smaller HVAD has also been reported in patients with TGA, including 1 case in which there was a reduction in pulmonary hypertension leading to successful cardiac transplantation [22].

There are a few reports that describe placement of CF LVADs in patients with L-TGA. Joyce and colleagues reported implantation of the DeBakey VAD (MicroMed, Technology, Houston TX). In their description, the systemic RV was found in the anterior chest, and the inflow cannula was placed in the RV apex after excision of trabeculae to the papillary muscles. As cardiopulmonary bypass was weaned, there were low flows of 0.5 L/min noted in the LVAD, which improved to 2.5 L/min after manipulation

of the device by 180° toward the left chest [21]. In a case reported by Menachem et al., a patient with L-TGA and situs inversus underwent HM II placement. During this case, the cardiac apex was noted at the right axillary line, requiring rotation of the anterior aspect of the VAD by 180°. This rotation allowed for placement of the inflow cannula successfully in the systemic RV. An HVAD has also been described to be placed in a patient with L-TGA with a leftward aorta, requiring anastomoses of the outflow graft toward the leftward pleural space [23].

## Challenges to CF VAD Placement in D-TGA and L-TGA

The preceding reports demonstrate both feasibility and utility of CF LVAD placement in patients with D-TGA and L-TGA and also highlight challenges to device placement in this population. These challenges are centered on appropriate inflow cannula placement and positioning to achieve optimal flows during device operation. As opposed to routine placement of the inflow cannula in the LV apical region marked by a dimple, the RV apex can be ill-defined leading to difficultly in locating the appropriate site of cannula insertion. Once an apical core is removed, care must be taken to identify and remove nearby anatomical structures in the RV such as trabeculae, moderator band, and papillary muscles which can obstruct blood flow into the inflow cannula. To overcome these barriers, most groups perform aggressive resection of these structures and place the cannula in a posterior location [20, 21]. 3D models can reveal the spatial arrangements of such intra-cardiac structures in the preoperative setting which may assist in surgical planning and optimal cannula positioning. Although such a strategy has not been tested in a prospective method, Figs. 14.1 and 14.2 show how virtual and printed 3D models can display intra-cardiac structures that may interfere with flow into the cannula. It is foreseeable to virtually simulate cannula positioning in various orientations to achieve minimal interference and achieve optimal circulatory support.

In addition to cannula positioning, surgical approach may need modification due to the variation in the location of the RV in patients with D-TGA and L-TGA. In patients with D-TGA, the RV is anterior and rightward similar to normal anatomy, whereas in L-TGA, it is leftward, in the usual LV position. In these patients, placement of a VAD in the right abdomen instead of the left can cause compression of right-sided structures which requires close monitoring in the postoperative setting. This global arrangement of cardiac chambers and other nearby organs is notable by routine cardiac CT or MRI but can be spatially enhanced by 3D modeling to add to preoperative surgical approach.

## Fontan Palliation

Patients born with a severely underdeveloped ventricle in whom the circulation is only supported by a single ventricle are currently palliated with a Fontan procedure. This palliative strategy involves creation of a pathway from the inferior vena cava to the pulmonary artery and leaves the sole functioning ventricle to supply the systemic circulation [24]. The major forms of CHDs that typically require the Fontan palliation include hypoplastic left heart syndrome, tricuspid atresia, and double inlet LV. During the Fontan palliation, venous blood flows passively to the pulmonary arteries. In the long term, this circulation is associated with an approximate failure rate of 30% in a 20-year follow-up [25]. The major co-morbidities of the Fontan palliation include protein losing enteropathy (PLE), plastic bronchitis, thromboembolism, bleeding diathesis, atrial arrhythmias, and liver cirrhosis [26, 27].

Adults with a failing Fontan circulation are commonly poor candidates for heart transplantation due to chronic malnutrition, major co-morbidities, and significant end organ dysfunction. For such patients, VAD placement may be an option to reach hemodynamic stability, rehabilitate end organ function, and possibly regain candidacy for heart transplantation. There is only limited experience with VAD implantation in patients with the Fontan circulation in

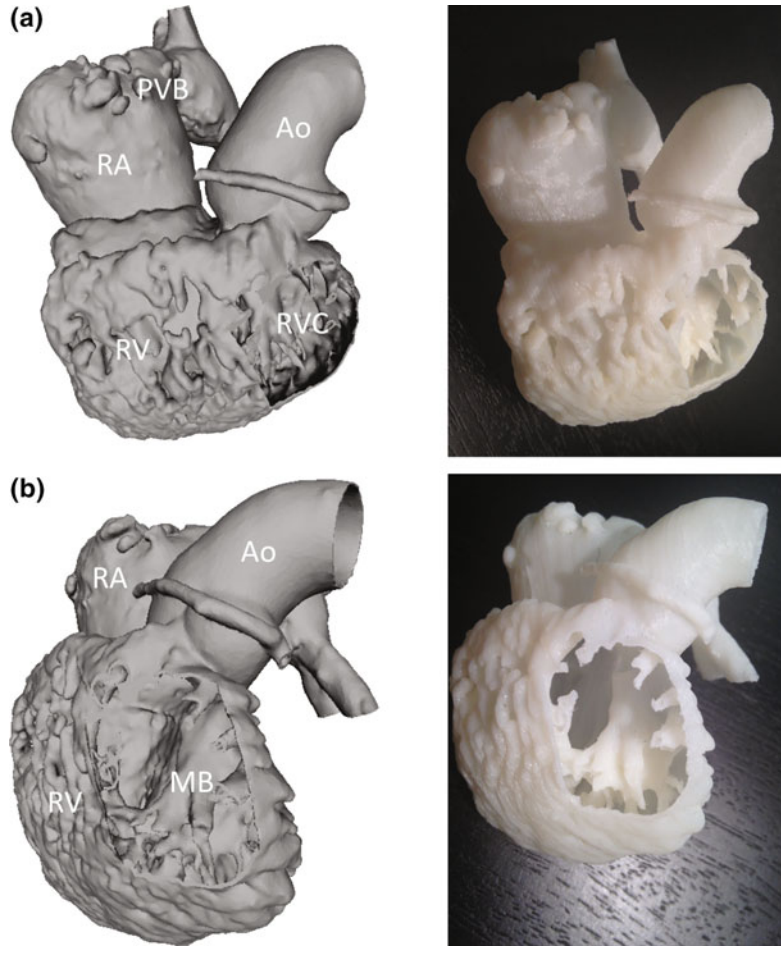


**Fig. 14.1** D-TGA 3D virtual model (*left*) and corresponding printed model (*right*) of the pulmonary venous baffle (*PVB*) to the systemic right ventricle (*RV*) in a 36 yo patient with D-TGA s/p Mustard procedure in HF. The model is viewed from the anterior aspect (**a**) and leftward aspect (**b**). The anatomic landmarks of interest, i.e., the prominent trabeculations of the systemic *RV* and the moderator band (*MB*) were well reproduced. This would allow presurgical planning of cannula placement as to avoid possible inflow obstruction due to these trabeculations. Right atrium (*RA*), right ventricular cavity (*RVC*), aorta (*Ao*)

either the right-sided circulation or the failing systemic ventricle. Pretre et al. reported a case of insertion of a Berlin Heart in a patient with a failing Fontan after a conversion procedure with a normal functioning systemic ventricle. The cavopulmonary anastomosis was taken down, and chambers were created for inflow and outflow cannulation. The outflow cannula to the pulmonary artery was implanted in the proximal stump of the Fontan conduit. A capacity chamber was created with anastomosis to the superior vena cava with an enlargement patch of xenopericardium and to the inferior vena cava. The inflow venous cannula was inserted in this capacity chamber. Both cannulas were externalized and connected to a 60-ml paracorporeal ventricle. Postoperatively, the patient had marked recovery of end organ function and went on to receive cardiac transplantation after 13 months of mechanical circulatory support [28]. Newcomb et al. described a case of ventricular failure after Fontan conversion which needed VAD implantation. In this report, VAD cannulation was done through the apex of the heart and ascending aorta, and the patient was eventually bridged to cardiac transplantation [29].

## Challenges to VAD Placement in the Fontan Circulation

Although the cases above demonstrate feasibility of VAD implantation in patients with a failing Fontan circulation, there remains a paucity of reported experience of successful bridging of such patients to cardiac transplantation. In cases

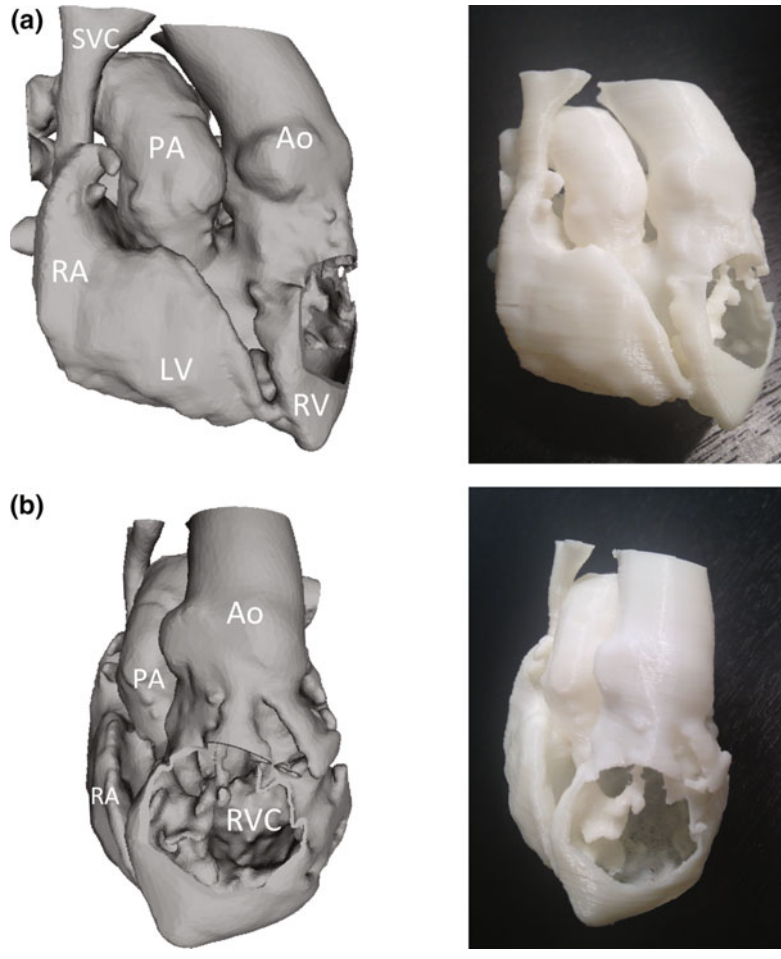


**Fig. 14.2** L-TGA 3D virtual model (*left*) and corresponding printed model (*right*) in a 51 yo patient with L-TGA in HF. The model is viewed from the anterior aspect (**a**) and leftward aspect (**b**). The prominent systemic right ventricular (*RV*) trabeculations and an anterior and leftward aorta are clearly identified, allowing accurate presurgical planning. Superior vena cava (*SVC*), right atrium (*RA*), left ventricle (*LV*), pulmonary artery (*PA*), right ventricular cavity (*RVC*)

of right-sided circulatory failure with preserved function of the systemic ventricle, the cavopulmonary anastomosis may require deconstruction prior to creation of pathways for the VAD cannulas. A major challenge is to accomplish simultaneous drainage of systemic venous blood from superior and inferior vena cava into the VAD inflow cannula. As reported above, after takedown of the cavopulmonary anastomosis, systemic venous drainage is possible by creation of a capacity chamber between the superior and inferior vena cava, which is connected to the VAD inflow cannula. Prior to takedown of the cavopulmonary anastomosis, it is imperative to preoperatively assess for leaks and stenosis within the Fontan and to comprehend the spatial relationship between major vascular structures and collaterals to prevent adverse hemorrhagic complications. In cases, where the systemic ventricle is failing, several precautions are noteworthy during implantation of the VAD. These include precisely localizing the apex which may be displaced or not in communication with the major ventricular chamber and delineation of the surface coronary anatomy [28, 29]. Preoperative 3D modeling of the Fontan circulation, Fig. 14.3, may further aid in comprehending the anatomical arrangement of the cavopulmonary anastomosis, global orientation of the systemic ventricle, and the spatial orientation of nearby vascular structures for optimal preoperative surgical approach and planning.

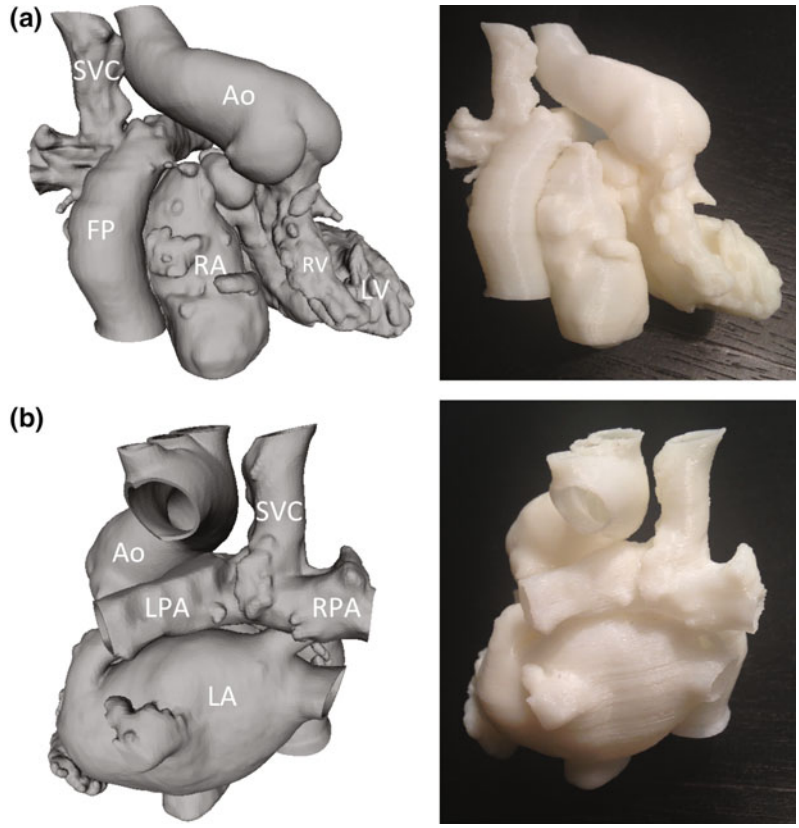


**Fig. 14.3** Fontan A 3D virtual model (*left*) and corresponding printed model (*right*) in a 37-year-old patient with tricuspid atresia, D-transposed great vessels s/p Fontan procedure with persistent ascites and atrial arrhythmias. The model is viewed from the anterior aspect (**a**) and from the posterior aspect (**b**). The Fontan pathway (*FP*) and its spatial relationship with the rest of the anatomy are well represented on the 3D model and can be used to plan *VAD* placement using any of the techniques mentioned earlier. Superior vena cava (*SVC*), right atrium (*RA*), right ventricle (*RV*), left ventricle (*LV*), right pulmonary artery (*RPA*), left pulmonary artery (*LPA*), left atrium (*LA*), aorta (*Ao*)

## Inflow Cannula Malposition

In patients with advanced HF, not related to CHD, the inflow VAD cannula is placed in the left ventricle at the apical dimple. To ensure optimal unloading, the cannula is set and fixed in place to face the inflow across the mitral valve. On occasion, alarming low flows may be noticed from the device. To uncover the etiology of reduced flow, it becomes essential to evaluate inflow cannula position for misalignment. Figure 14.4, shows CT images of a HM II in a patient who presented with new onset low flow alarms eleven months after implantation. Non rotated images (Fig. 14.4a) appear to show that the inflow cannula is facing the mitral annulus. However, manipulation of virtual 3D images (Fig. 14.4b) revealed that the inflow cannula was directed toward the apical septum rather than the mitral valve. The patient opted to defer reparative surgery, but this case demonstrates that 3D modeling may be able to show spatial intricacies of the inflow cannula orientation not viewable by two dimensional imaging.

In summary, in a growing adult population of CHD patients with HF, 3D modeling may aid in preoperative planning prior to VAD placement through tangible manipulation of atypical intracardiac structures and enhanced comprehension of

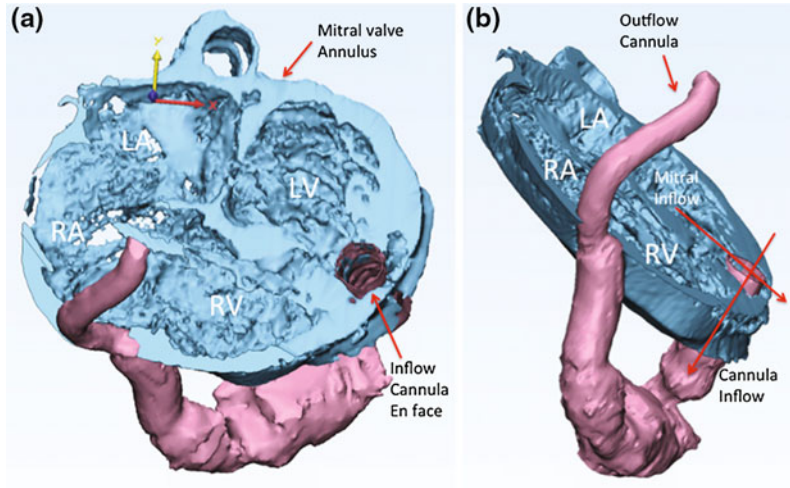


**Fig. 14.4** Cannula malposition. The myocardium was segmented to create this virtual model. A virtual three-dimensional model showing the same HM II inflow cannula in a four chamber (**a**) and rotated view (**b**) to demonstrate malposition. In this virtual model, it is apparent that the inflow cannula is misaligned toward the apical septum instead of the correct alignment toward the mitral annulus. Right atrium (*RA*), right ventricle (*RV*), left atrium (*LA*), left ventricle (*LV*)

unusual anatomical arrangements. Closer spatial assessment of the inflow is also enhanced through 3D imaging. Further prospective evaluation to assess the added utility of 3D modeling in preoperative planning and assessing optimal inflow cannula alignment is warranted.

## References


1. Hoffman JI, Kaplan S, Liberthson RR. Prevalence of congenital heart disease. Am Heart J. 2004;147 (3):425–39.
2. Stout KK, et al. Chronic heart failure in congenital heart disease a scientific statement from the American Heart Association. Circulation. 2016;133(8):770–801.
3. Wren C, O'sullivan J. Survival with congenital heart disease and need for follow up in adult life. Heart 2001;85(4):438–43.
4. Van Der Bom T, et al. The changing epidemiology of congenital heart disease. Nat Rev Cardiol. 2011;8 (1):50–60.
5. Verheugt CL, et al. Mortality in adult congenital heart disease. Eur Heart J. 2010;ehq032.
6. Oechslin EN, et al. Mode of death in adults with congenital heart disease. Am J Cardiol. 2000;86 (10):1111–6.
7. Zomer AC, et al. Circumstances of death in adult congenital heart disease. Int J Cardiol. 2012;154 (2):168–72.
8. VanderPluym C, et al. Utilization and outcomes of ventricular assist device support in adult congenital heart disease: an analysis of the interagency registry for mechanically assisted circulatory support (INTERMACS). J Heart Lung Transplant. 2016;35 (4):S151–2.
9. Maxwell BG, et al. Heart transplantation with or without prior mechanical circulatory support in adults with congenital heart disease. Eur J Cardio-Thorac Surg. 2013;ezt498.
10. Ross HJ, et al. Transplantation and mechanical circulatory support in congenital heart disease a scientific statement from the American Heart Association. Circulation. 2016;133(8):802–20.
11. Farooqi KM, et al. 3D printing to guide ventricular assist device placement in adults with congenital heart disease and heart failure. JACC Heart Fail. 2016;4(4):301–11.
12. Van Praagh R. The importance of segmental situs in the diagnosis of congenital heart disease. In Seminars in roentgenology. WB Saunders; 1985.
13. Jatene A, et al. Successful anatomic correction of transposition of the great vessels. A preliminary report. Arq Bras Cardiol. 1975;28(4):461–4.
14. Mustard W, et al. The surgical management of transposition of the great vessels. J Thorac Cardiovasc Surg. 1964;48:953–8.

15. Piran S, et al. Heart failure and ventricular dysfunction in patients with single or systemic right ventricles. Circulation. 2002;105(10):1189–94.
16. Turina M, et al. Late functional deterioration after atrial correction for transposition of the great arteries. Circulation. 1989;80(3 Pt 1):I162–7.
17. Poirier NC, et al. Long-term results of left ventricular reconditioning and anatomic correction for systemic right ventricular dysfunction after atrial switch procedures. J Thorac Cardiovasc Surg. 2004;127(4):975–81.
18. Van Praagh R. What is congenitally corrected transposition? N Engl J Med. 1970;282(19):1097–8.
19. Graham TP, et al. Long-term outcome in congenitally corrected transposition of the great arteries: a multi-institutional study. J Am Coll Cardiol. 2000;36(1):255–61.
20. Maly J, et al. Bridge to transplantation with long-term mechanical assist device in adults after the Mustard procedure. J Heart Lung Transplant. 2015;34(9):1177–81.
21. Joyce DL, et al. Mechanical circulatory support in patients with heart failure secondary to transposition of the great arteries. J Heart Lung Transplant. 2010;29(11):1302–5.
22. Stokes MB, et al. Successful bridge to orthotopic cardiac transplantation with implantation of a HeartWare HVAD in management of systemic right ventricular failure in a patient with transposition of the great arteries and previous atrial switch procedure. Heart Lung Circ. 2016;25(5):e69–71.
23. Menachem JN, et al. Initial experience of left ventricular assist device support for adult patients with transposition of the great vessels. Congenital Heart Dis. 2015;10(5):382–6.
24. Fontan F, Baudet E. Surgical repair of tricuspid atresia. Thorax. 1971;26(3):240–8.
25. d'Udekem Y, et al. The Fontan procedure contemporary techniques have improved long-term outcomes. Circulation 2007;116(11 suppl):I-157–4.
26. d'Udekem Y. et al. Redefining expectations of long-term survival after the Fontan procedure twenty-five years of follow-up from the entire population of Australia and New Zealand. Circulation 2014;130(11 suppl 1):S32–8.
27. Nakano T, et al. Results of extracardiac conduit total cavopulmonary connection in 500 patients. Eur J Cardiothorac Surg. 2015;48(6):825–32.
28. Prêtre R, et al. Right-sided univentricular cardiac assistance in a failing Fontan circulation. Ann Thorac Surg. 2008;86(3):1018–20.
29. Newcomb AE, et al. Successful left ventricular assist device bridge to transplantation after failure of a Fontan revision. J Heart Lung Transplant. 2006;25 (3):365–7.

# Cardiac Tumors

15

Ryan A. Moore, MD and Michael D. Taylor, MD, PhD

## Introduction to Cardiac Tumors

Primary cardiac tumors are rare in children, with a reported incidence of less than 0.1% [1]. The majority of primary tumors in children are benign, with rhabdomyomas comprising 40–60%, teratomas 15–19%, and fibromas 12–16% [2]. The remaining tumors include vascular, myxomas, fibroelastomas, pleuropericardial cysts, Purkinje cell tumors, lipomas, and primary malignancies, the majority of which are sarcomas. Interestingly, in adults, metastases to the heart from other primary cancers are 30 times more common than primary cardiac tumors [3]. Additionally, a mural or intraluminal thrombus is always in the differential diagnosis when a cardiac mass is present and should be thoroughly evaluated [1].

The majority of pediatric cardiac tumors do not need surgical intervention. However, even histologically, benign tumors can become problematic due to their size and location. Benign cardiac tumors causing inflow or outflow obstruction or compression of cardiac structures often require surgical removal [4]. Additionally, benign cardiac tumors can lead to arrhythmias requiring ablation. Using image-guided catheter ablation planning may lead to improved results. While malignant primary cardiac tumors are rarer than their benign counterparts, they should always be considered for surgical removal given the 1-year survival rate of ~10% without resection [5, 6]. While many patients are asymptomatic, arrhythmias and heart failure due to inflow or outflow obstruction can be consequences of large or invasive tumors. Cardiac tumors are often complex 3-dimensional (3D) structures within or around the heart. Using 3D printing in procedural planning can be a valuable tool to improve targeted approaches and ultimately outcomes.

## Current Imaging of Cardiac Tumors

Cardiac magnetic resonance (CMR) has emerged as the primary diagnostic modality for cardiac tumor characterization [7]. Utilizing different CMR sequences, the multi-parametric tissue characteristics of a cardiac tumor can be defined. Additionally, CMR provides clear definition of tumor location and extent. Echocardiography is the conventional screening method for intracardiac masses and tumors. It is the primary modality for characterizing well-defined rhabdomyomas that often do not require any further imaging. 3D echocardiography can provide additional detail related to tumor location and extent, particularly when atrioventricular or semilunar valves are involved. Computed tomographic (CT) imaging can also assist with tumor

R.A. Moore, MD (✉) · M.D. Taylor, MD, PhD
The Heart Institute, Cincinnati Children's Hospital Medical Center, 3333 Burnet Avenue, MLC 2003, Cincinnati, OH 45229, USA
e-mail: ryan.moore@cchmc.org

M.D. Taylor, MD, PhD
e-mail: michael.taylor1@cchmc.org


K.M. Farooqi (ed.), *Rapid Prototyping in Cardiac Disease*,
DOI 10.1007/978-3-319-53523-4_15

location and extent although it provides limited tissue characterization for assisting with diagnosis.

## Value Added by 3D Printed Models of Cardiac Tumors

Cardiac tumors are often complex 3D structures that can distort normal cardiac anatomy. Visualizing the tumor size and location relative to pertinent cardiac structures is critical to a successful operation. Additionally, understanding how the cardiac geometry may change after tumor debulking or resection is important during procedural planning. For the rare malignant tumors that require surgical excision, 3D printing may provide benefit in defining the tumor borders during surgical planning.

## Cardiac Tumor Model Creation and Post-processing

As discussed above, CMR is the primary modality for defining cardiac tumor type, location, extent, and size [7]. The distinct MR signal characteristics of cardiac tumors and the surrounding muscle and soft tissue provide imaging data needed to perform high-level 3D reconstruction. For 3D printing, a post-contrast respiratory-navigated, cardiac-gated 3D-free-breathing steady-state free precession or inversion recovery gradient echo angiogram is best to define cardiac tumors. To optimize resolution for 3D reconstruction and segmentation, the 3D whole heart imaging should be acquired with $\sim$1 mm isotropic voxels. Various tumors will have differences in appearance based on their signal properties. Attention to detail for segmentation is critical in defining the borders and extent of the mass. In our experience, segmenting the entire heart is of great value for cardiac tumors because it gives the best sense of the tumor's location relative to pertinent structures. When considering 3D printing cardiac tumors, attention should be paid to the type of material (flexible vs. hard) needed in relation to the cardiac structures. We have typically printed the tumor in a separate material and color from the surrounding myocardium. For intracardiac tumors, a hard, opaque material is best visualized within a flexible, clear shell denoting the cardiac structures. For external tumors, the cardiac structures may need to be printed in a more rigid material to support the large tumor. For simulation cases, 3D printing a flexible model is best with various colors to separate tumor for pertinent cardiac structures.

## Case Examples

The authors report two cases of cardiac tumors where 3D printing was crucial to decision making related to procedural planning.

### Large Cardiac Fibroma Causing Right Ventricular Outflow Tract Obstruction

#### Case Summary

An infant was found to have a large tumor compressing and replacing the anterior wall of the right ventricular outflow tract (RVOT), encasing the left anterior descending coronary artery (LAD), and causing outflow obstruction. A 3D model facilitated surgical planning, particularly guiding the extent of tumor resection while avoiding coronary artery injury.

#### Clinical Details

A previously healthy infant presented to the emergency department for inconsolable fussiness. A chest X-ray revealed an enlarged cardiac silhouette. A bedside transthoracic echocardiogram demonstrated a large pericardial effusion with no evidence of tamponade. Pericardiocentesis was performed, and a total of 150 ml of fluid was drained. The echocardiogram showed a large heterogeneous mass in the right ventricle (RV), measuring approximately 6 $\times$ 4 $\times$ 3 cm. The RVOT was narrowed to <3 mm at the level of the mass. CMR confirmed the presence of a large mass on the epicardial surface of the RV producing significant compression of the RVOT,

with findings characteristic of a cardiac fibroma (Fig. 15.1a). Analysis of the pericardial fluid did not reveal malignant cells. The decision was made to attempt surgical resection or debulking of the mass, with the primary goal of relieving RVOT obstruction and obtaining definitive tissue diagnosis. Based on the CMR, a virtual 3D model of the heart and great vessels was created and subsequently 3D-printed to guide surgical planning (Figs. 15.2 and 15.3). The model showed the extent of the tumor and delineated how it wrapped around the right lateral aspect of the main pulmonary artery. The anatomic position of the mass placed the left anterior descending (LAD) artery at risk for damage during resection and posteriorly displaced the right coronary artery.

Figure 15.1d shows the tumor, which completely covered the anterior surface of the heart. The tumor filled the mediastinum making it difficult to visualize its total extent or move the heart as needed. Therefore, intraoperatively, the patient was placed on cardiopulmonary bypass. The resection was continued to relieve RVOT obstruction, with immense care taken to avoid putting the LAD at risk. The tumor was separated from the right coronary artery, and further dissection clearly revealed it arose from the myocardium. The majority of muscle of the RV free wall and the RVOT was very thin or had been completely replaced by tumor. Most of the anterior free wall from the atrioventricular groove to the interventricular septum up to the annulus of the main pulmonary artery was removed. Further lateral resection of the mass was not possible due to its intimate involvement with the LAD. After debulking as much of the tumor as deemed to be safe, the RVOT was reconstructed using CorMatrix patch (CorMatrix Cardiovascular, Inc., Roswell, GA). An intraoperative transesophageal echocardiogram showed the RV systolic function to be mildly depressed with severe hypokinesis of the anterior free wall, and no RVOT obstruction, or tricuspid or pulmonary valve insufficiency. The final pathology demonstrated that the tumor was a fibroma with foci of myxoid changes, consistent with the preoperative CMR findings. The patient was discharged home on postoperative day 17 and will be followed by oncology and cardiology to ensure no regrowth of the tumor or recurrent RVOT obstruction.

Because the LAD was covered for much of its length by the tumor, identifying its course intraoperatively was not possible. However, the 3D model clarified the relationship of the tumor, main pulmonary artery, and the LAD, prior to and during surgery, allowing us to plan a safe surgical approach and extent of resection.

## Large Residual Cardiac Rhabdomyoma Causing Refractory Ventricular Tachycardia

### Case Summary

The second patient was an adolescent with tuberous sclerosis and multiple cardiac rhabdomyomas with associated accelerated ventricular rhythm. He had one large residual

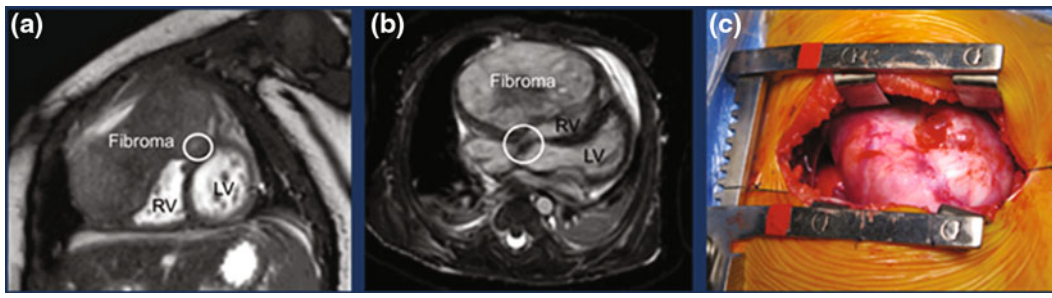


**Fig. 15.1** Case 1: Cardiac MRI **a**, **b** showing the tumor compressing the RVOT (*circle*), and an intraoperative photograph showing the large fibroma on the anterior surface of the heart (**c**)

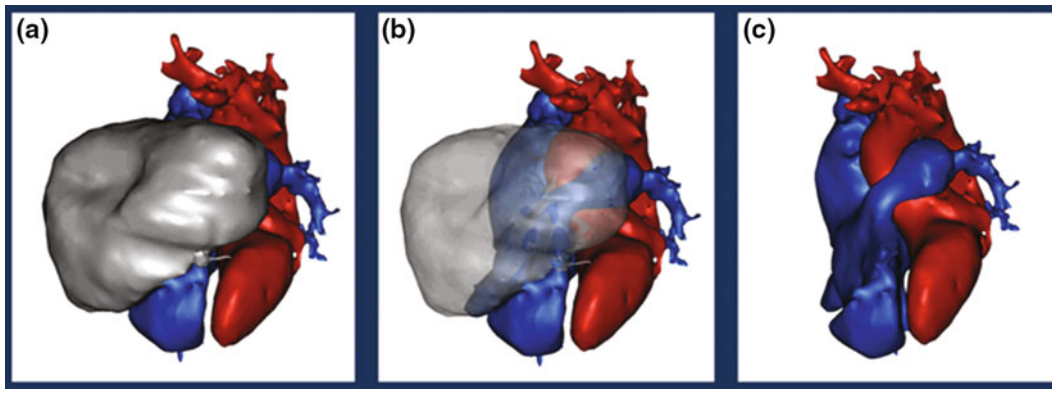


**Fig. 15.2** Case 1: 3D modeling demonstrating the cardiac tumor (*gray*) compressing the RV (*blue*). The tumor is shown opaque (**a**), transparent (**b**), and after removal from RV surface (**c**). The 3D reconstruction assisted with assessing the extent of RV compression, which ultimately required surgical reconstruction after tumor debulking

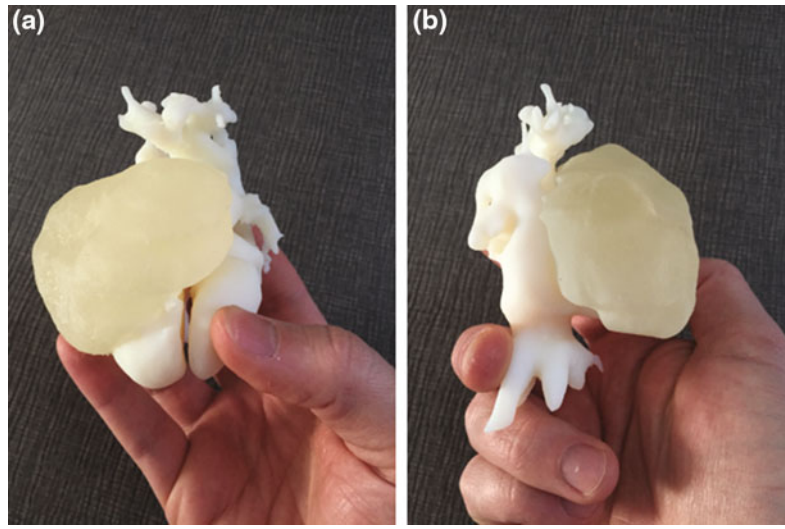


**Fig. 15.3** Case 1: 3D printed heart model demonstrating the fibroma in a clear, flexible rubber printed material on the anterior surface of the heart demonstrated in an opaque, hard plastic printed material. The 3D model assisted with determining the extent of RV compression, as well as defining the left coronary course within a portion of the tumor

rhabdomyoma in the basal left ventricular free wall that was causing mild left ventricular outflow tract obstruction and thought to be the focus for his recurrent ventricular arrhythmias. A 3D model facilitated electrophysiology study planning and discussion related to potential surgical resection.

## Clinical Details

An adolescent with a history of tuberous sclerosis and multiple cardiac rhabdomyomas, most of which had resolved, except for one large residual tumor in the left ventricular outflow tract, presented with episodic palpitations. An electrocardiogram was performed, which demonstrated a

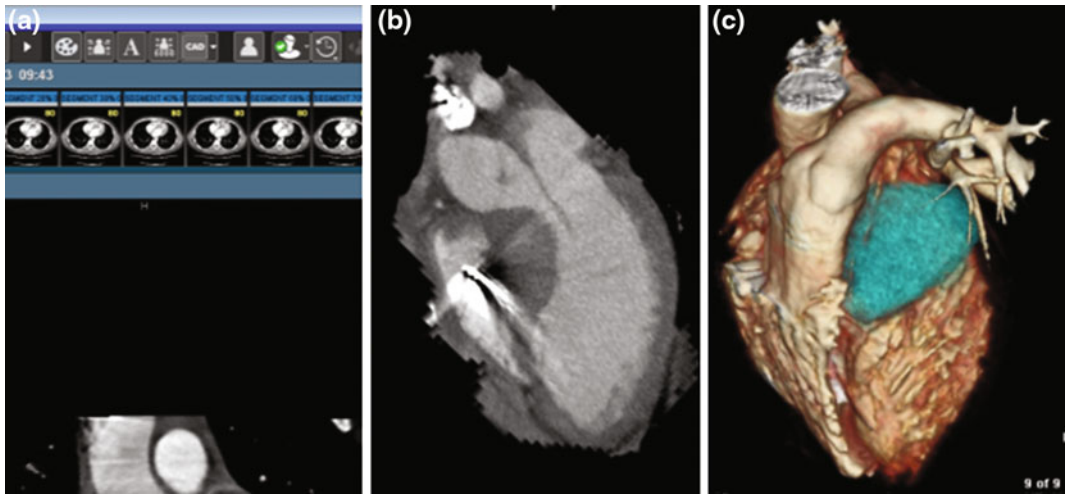


**Fig. 15.4** Case 2: Large cardiac rhabdomyoma causing partial left ventricular outflow tract obstruction and malignant ventricular arrhythmias. Coronal projection (**a**). Reformatted 3-chamber demonstrating rhabdomyoma in the left ventricular outflow trace (**b**). Volume-rendered 3D reconstruction with large rhabdomyoma denoted in *blue* (**c**)

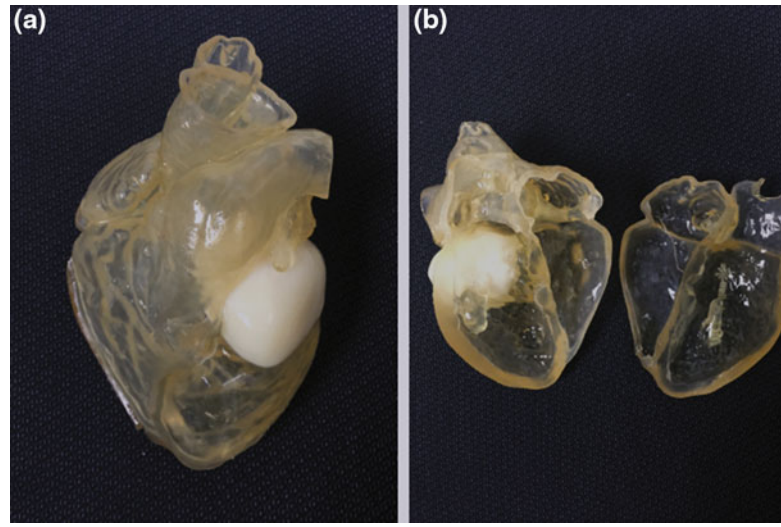


**Fig. 15.5** Case 2: 3D printed model of large cardiac rhabdomyoma in the basal lateral wall of the left ventricle. The tumor was causing mild left ventricular outflow tract obstruction and refractory ventricular arrhythmias

wide QRS complex tachycardia with right bundle branch block morphology and leftward inferior QRS axis. Atrial activity was not definitively seen. Adenosine was administered without apparent affect. Intravenous diltiazem was given and the heart rate slowed. During the episode, the patient became anxious but maintained consciousness. An invasive cardiac electrophysiology study showed monomorphic ventricular tachycardia originating near the rhabdomyoma. Radiofrequency lesions placed at the site of earliest ventricular activation did not have any effect on the tachycardia. Tachycardia termination was not achieved, and the patient left the laboratory with continued tachycardia which was resulting in hemodynamically instability. On one occasion, a short burst of ventricular pacing converted the tachycardia to ventricular fibrillation. An implanted cardioverter-defibrillator (ICD) was placed approximately 1 month later.

A few years later, the patient presented to an outside hospital in unstable ventricular tachycardia, and after failing conversion with adenosine, he was given intravenous amiodarone resulting in a possible allergic reaction. His echocardiogram at the time showed severe ventricular dysfunction requiring a left ventricular assist device. There was significant concern that his arrhythmias were not manageable with medication alone and plans were made to attempt another ablation. For this ablation, the electrophysiology service requested a 3D printed heart model to assist them with the exact location of the tumor, so that circumferential radiofrequency lesions could be applied around its full extent. Given the previously placed ICD, a cardiac CT angiogram was performed to assess the tumor size and location. The CT images were used as a source dataset for 3D virtual model reconstruction and 3D printing (Fig. 15.4). The 3D printed heart model demonstrated a large rhabdomyoma positioned within the mid-myocardium with extension into the left ventricular outflow tract and causing partial obstruction (Fig. 15.5). Using the 3D model as a guide during the EP procedure, the patient underwent successful ablation with marking of the model at each individual lesion. The patient did well after the procedure for several months; however, the ventricular arrhythmias returned. Discussion at that time included the possibility of removing the tumor. Utilizing the 3D model for surgical discussion, it was felt that the tumor was intercalated into such a large part of the left ventricular mass, removal would likely lead to significant cardiac dysfunction, and heart transplant would have to be considered. Tumor resection was therefore deferred. After the final ablation, a different antiarrhythmic was used and was successful in controlling the ventricular arrhythmias.

## Conclusion

Cardiac tumors in pediatrics are rare and often benign. However, even benign tumors can have significant hemodynamic affects related to tumor type, size, and potential for mass effect or inflow/outflow obstruction. CMR is the leading modality for characterizing cardiac tumors in pediatrics. Each CMR tumor case should be approached with the foresight to obtain an adequate imaging dataset for possible 3D reconstruction with subsequent 3D model printing. As demonstrated above, 3D reconstructions and 3D printed heart models of cardiac tumors better demonstrate tumor extent and potential interactions with nearby cardiac structures than 2D imaging alone. Utilizing 3D printed models for cardiac tumors aids in surgical and procedural planning and ultimately may improve outcomes by providing an anatomic blueprint for approaching surgical debulking, resection, or other necessary interventions.

## References

1. Leja MJ, Shah DJ, Reardon MJ. Primary cardiac tumors. Tex Heart Inst J. 2011;38:261–2.
2. Gunther T, Schreiber C, Noebauer C, Eicken A, Lange R. Treatment strategies for pediatric patients with primary cardiac and pericardial tumors: a 30-year review. Pediatr Cardiol. 2008;29:1071–6.
3. Padalino MA, Reffo E, Cerutti A, Favero V, Biffanti R, Vida V, Stellin G, Milanesi O. Medical and surgical management of primary cardiac tumours in infants and children. Cardiol Young. 2014;24:268–74.
4. Freedom RM, Lee KJ, MacDonald C, Taylor G. Selected aspects of cardiac tumors in infancy and childhood. Pediatr Cardiol. 2000;21:299–316.
5. Uzun O, Wilson DG, Vujanic GM, Parsons JM, De Giovanni JV. Cardiac tumours in children. Orphanet J Rare Dis. 2007;2:11.
6. Cho JM, Danielson GK, Puga FJ, Dearani JA, McGregor CG, Tazelaar HD, Hagler DJ. Surgical resection of ventricular cardiac fibromas: early and late results. Ann Thorac Surg. 2003;76:1929–34.
7. Beroukhim RS, Prakash A, Buechel ER, Cava JR, Dorfman AL, Festa P, Hlavacek AM, Johnson TR, Keller MS, Krishnamurthy R, Misra N, Moniotte S, Parks WJ, Powell AJ, Soriano BD, Srichai MB, Yoo SJ, Zhou J, Geva T. Characterization of cardiac tumors in children by cardiovascular magnetic resonance imaging: a multicenter experience. J Am Coll Cardiol. 2011;58:1044–54.

# Part IV
# Management Strategies

# Establishing a Cardiovascular Rapid Prototyping Service

16

Kevin A. Gralewski, MSE, Yoav Dori, MD, PhD and Kevin K. Whitehead, MD, PhD

## Introduction

The roots of additive manufacturing, or 3D printing, can be traced to the early 1980s. This technology was born out of the concept of creating prototypes by which to test and verify design iterations for mass production before committing to the expensive elements of mass production, such as casting molds or milling processes. As resolution and available materials for 3D printed products improved over the ensuing 30 years, its application has expanded across many fields [1]. Today, 3D printing is widely used to manufacture finished products in many industries. As with most technologies, the confluence of advancements in 3D printers themselves, along with the growing awareness of the technology, beyond the first adopter audience, has led to a marked expansion of application [2].

The medical community has also adopted this technology and its use has been significantly increasing in recent years. The ability of 3D printers to quickly produce one-off unique designs with sub-millimeter resolution lends itself well to patient-specific anatomical modeling. In fact, this medical application has been used since the mid-2000s [3] with the recent rapid advancements in imaging and printer technology, 3D printed anatomical models have been used to improve planning for surgery, cardiac catheterization, and education of medical trainees and patients/families alike [4, 5].

Creating patient-specific anatomical models with sufficient fidelity on which to base clinical decisions or educate is not simple. Expertise is required at various steps along the process, which can be as multidisciplinary as the clinical intervention itself. The purpose of this chapter is to provide the reader with perspective on this process and the required resources necessary to establish a 3D modeling service within their institution.

For completeness and clarity, the discussion will begin with an outline of the process. Each project will likely have their own unique elements, but the general workflow in creating a patient-specific model is as follows:

1. Image acquisition of the anatomy by a 3D imaging modality such as Computed Tomography (CT) or Magnetic Resonance Imagining (MRI).
2. Segmentation, or partitioning of the of the 3D image dataset according to desired regions of interests (ROI).
3. Adding specific design features such as wall thickness, identifying labels, access ports for

K.A. Gralewski · Y. Dori · K.K. Whitehead (✉)
Department of Cardiology, The Children's Hospital of Philadelphia, Philadelphia, PA, USA
e-mail: whiteheadk@email.chop.edu

K.A. Gralewski
e-mail: gralewskik@email.chop.edu

Y. Dori
e-mail: doriy@email.chop.edu


K.M. Farooqi (ed.), *Rapid Prototyping in Cardiac Disease*,
DOI 10.1007/978-3-319-53523-4_16

intervention, or attachment points for assembly of multiple pieces.
4. Printing of the segmented volume renderings, which will include material selection as defined by the printer, that can vary by both mechanical properties and/or color.
5. Post-processing, which might involve cleaning of the print run to finish quality and assembly of any subunits into the final model.

## Image Acquisition

Each level of the workflow can introduce a new opportunity for error or at least a limitation to meeting the design goals. However, the most significant part of the process is without question, image acquisition. For obvious reasons, models or design prototypes can never exceed the resolution or fidelity of the original dataset. For this reason, image acquisition must be planned with modeling in mind. Segmentation (discussed in the following section) requires cardiac gating, and consensus among the medical team should be reached regarding the most appropriate portion of the cardiac cycle to capture for modeling. In general, surgical planning will be aided by models acquired in diastole, but there may be instances where systolic gating is more appropriate, such as in defining a ventricular septum defect (VSD) pathway if baffling through the VSD is part of the proposed intervention. For images obtained via MRI, some form of respiratory compensation is also generally required. This has traditionally been performed using respiratory navigation, which tracks diaphragm motion and excludes acquisitions outside of a pre-determined window near end-expiration. Newer techniques using motion correction rather than traditional navigator promise improved scan times, especially in patients who are free breathing and have inconsistent respiratory patterns. For either CT or MRI modalities, scan resolution should be isotropic and near 1 mm resolution if possible. Similarly, effort should be made to capture the entire ROI in a single image sequence. While image registration algorithms can align inter-sequence images, the error inherit to the process can distort the anatomy beyond usability.

Our institution routinely uses contrast-enhanced MRI sequences acquired with a blood pool contrast agent. Acquisition time is around 2–8 min, and we normally use a cardiac gated, respiratory navigated 3D-FLASH (Fast Low Angle Shot) acquisition with a non-selective inversion pulse timed to null non-enhanced extravascular tissue. Some have reported good success with non-contrast-enhanced sequences, usually a steady-state free precession sequence with a T2-preparatory pulse. This sequence can provide excellent resolution and contrast, but is more subject to artifacts from flow and metal.

## Segmentation

Once the desired image sequences are acquired, the files, typically formatted as Digital Imaging and Communications in Medicine (DICOM) format, are imported to a software program capable of segmentation, which is the process of partitioning particular region(s) of the image sequence according to some defined common parameter. When this parameter is a range of voxel intensity, specifically, Hounsfield units (HU) in the case of CT datasets, the segmentation method is referred to as thresholding. Threshold-based segmentation is the simplest of the segmentation algorithms and in many ways is quite rudimentary, although when coupled with a cropping tool, is sufficient to isolate many different ROIs. There are a number of open-source and commercially available software packages with thresholding and cropping tools. It is left to the reader to determine which software works best for their particular application and budget. Some of the most widely run programs include: 3DSlicer from the National Alliance for Medical Image Computing and Insight Segmentation and Registration Toolkit (ITK) from Kitware which are both open sources, and the Mimics/3-matic® package commercially available through Materialise®.

It is highly recommended that the segmentation program, along any corresponding design

software (i.e., CAD programs), be run on its own designated machine for multiple reasons. First, the minimum technical specifications required to run such computationally intensive programs can be restrictive to the type of machine. Second, the time required to complete segmentation can be prohibitive if the program is run on the same computer as the image acquisition workstation. Also worth consideration is the time commitment to image processing. At this time, preceding the era of fully automated segmentation, modeling cannot be completed on the order of a single clinical visit. The segmentation required for modeling is more detailed and intensive than direct volume rendering functions common to many modern image acquisition workstations. This also implies that the process will require a new skill set with an associated learning curve to master the process. This will of course vary by operator and their natural aptitude, but in general, segmentation processing can be learned over the course of a few training days. Institutions are encouraged to identify or hire-in a designated technician to complete segmentation and the greater modeling processes, as opposed to adding the responsibilities to a clinician. Again, the time requirements for the entire process are likely to be too prohibiting for the latter.

While hiring new dedicated staff may incur more cost, there are several benefits to having a dedicated, non-clinician responsible for segmentation. The learning curve for the technician, if not already trained through previous experience, will be steeper. Also, once they are fully trained and operational, their full commitment to the process will prevent any atrophy of skills, as is a common occurrence with part-time effort. Image processing technicians may also bring to the project other technical or engineering skills not necessarily found among clinicians that can improve final designs or their efficiency. Also, as the scope of the modeling service grows, the dedicated technician should, by definition, have available time to scale with operation. The challenge of having the process completed by a non-clinician is that they often lack medical expertise. This can result in an inability to relate the model to the actual clinical scenario. This may be overcome with direct consultation with the ordering or supervising physician. While this may seem counterproductive, it is certainly unavoidable given that no individual will hold the expertise to create all model types. The only alternative to avoiding the physician–technician consultation would be to train all physicians interested in modeling which would be completely impractical for reasons already discussed.

## Including Manufactured Design Elements

Once segmentation of all ROIs is complete, design features may be added to bring the segmented volumes into their "model" form. Some of the more widely incorporated features include unique cut planes through the model with accompanying attachment hardware which allows one to bind the split pieces together; direct labeling of features with ambiguous location or orientation (i.e., left femur); added vessel wall thickness around previously segmented blood volumes to create luminal spaces; and color coding volumes in a single print to provide contrast across the model (i.e., assigning contrasting colors to the pulmonary arteries and veins of a full thoracic cardiac model to delineate between the vessels running into and out of the lung parenchyma). Of note, the ability to perform these post-processing steps is dependent on the resources available to a center. For example, printing in different colors would require a printer with the ability to run single prints with multiple materials.

Incorporating features that alter the structure of the model require advanced design tools. Their necessity for any planned applications should be included in the selection criteria for the segmentation software package. Some of the programs have these functions built-in, to varying degrees, while others will require a stand-alone supplemental program. To convey the potential importance and degree to which such design algorithms may be called upon take, as an anecdote, the process for creating a luminal model.

After segmentation of the patient vessel blood volume from the image stack, the user has isolated the luminal space. To create a model vessel, the general strategy is to create a second volume with the gross shape of the originally segmented ROI but larger in general cross-sectional area. A common practice is to create a new volume by sweeping out an increased radius orthogonal to the lumen volume centerline by approximately 2 mm. By convention, this larger volume is usually referenced as a wrapped or region growing volume. The vessel model is then created by subtracting the original segmented blood volume ROI from the resultant wrapped volume by the use of a Boolean operator (specifically an "A not B" function, where "A" = wrapped volume, and "B" = original blood volume). Such a function will remove volume "A" wherever it is coincident to volume "B", thereby rendering a hollow vessel with a thickness equal to the increasing factor for the radius used to define the wrapped volume, in the example above, 2 mm.

To summarize, the common design process of reconstructing luminal spaces for vessel modeling requires the following algorithms: thresholding, cropping, region growing/wrapping, and Boolean operators. Given this number of unique functions, users may wish to invest through capital or programing effort in software packages that streamline this process to increase model making efficiency.

## Printing and Material

As previously mentioned, some final design features, mainly model color and material durometer, or hardness, will be a function of the printer. Many inexpensive commercially available 3D printers rely on a fused deposition modeling (FDM) technology. This method generally limits the print run to a single material, mostly thermoplastic materials such as Acrylonitrile Butadiene Styrene (ABS), PolyEtherEtherKetone (PEEK), and other polycarbonate (PC) plastics [6]. These printers are inexpensive but often have lower resolution than other 3D printers.

Polyjet printers are another common technology capable of depositing multiple materials in a single run; however, their cost can be multiple orders of magnitude higher than the lower end FDM machines. It is also important to note, while the polyjet technology allows for finished printer materials of various durometers, many of materials currently available cannot match the biological compliance of elastic arteries such as the aorta. This is certainly an area of active development by material venders and has had many recent advancements [7]. While the lower durometer materials struggle to match biological compliance behaviors, they do offer utility in surgical and catheterization planning, mainly because they are capable of being punctured. This is important when planning catheter access routes, such as transseptal or transapical approaches, and other surgical incision planning. This feature should be considered against the higher operational cost for such materials as they are considerably more expensive to run.

Polyjet printers require higher start-up capital and overhead cost given the consumables are more expensive than the alternative FDM technology. However, the polyjet technology does offer benefit for its investment. Polyjet printers provide better print resolution, measured on the order of microns, and better print quality consistency, both within large single print runs and across runs over time. Polyjet printers also have greater reliability. In general, final print products can still be salvaged if they incur minor issues during the print process on polyjet machines. Polyjet machines are also more amenable to printing single runs in multiple colors, though the most capable printer type for creating photo-realistic color patterns is a colorjet printing machine, a type of powder bed fusion printing technology.

If compliance of the printing material is a necessity, the best current approach is to use casting with non-printing commercially available products with more appropriate bulk moduli. In this process, instead of the 3D printer creating the finished model, it is used to create a mold of the desired anatomy for lost-wax casting procedures or simply as the direct mold for the final casting

material. Such modeling practices require additional resources and facilities, such as a fume hood and general laboratory space for material preparation, but also expand the scope of the service. Our institutional has routinely used such molding procedures to create compliant aortas. This can be critical in hemodynamic studies or catheterization planning, as in stenting a coarctation.

## Post-Processing

Nearly all printing technologies require some post-processing cleaning before the model can be deemed finish quality. This involves the removal of support material that was laid down during the print process to make the 3D volume possible. This post-processing can be time-consuming, but is necessary to remove excess material from the model, and therefore, it should not be neglected when scheduling prints against hard deadlines.

Physical removal of the support material varies by printer technology. Cleaning is simplest for powder bed fusion printing wherein the finished print is simply removed from a bed of unused powder material and brushed clean. Typically, the unused powder material can be recycled for subsequent prints. Other printer technologies require more involved post-processing to yield the final model. Many of the FDM machines, for instance, lay down finish material in the form of struts formed in model cavities to buttress material that is deposited in subsequent layers of the print. These struts, or pillars, have to be cut or broken away from the finished model. Some printers lay down soluble support materials which can be dissolved after the model is complete by immersing it in a solution. Conversely, some polyjet machines lay down a unique support material. It forms a solid support matrix, but is deposited in such a way that requires less force to shear it away from the finish material. A high-pressure water jet is usually packaged with the printer to facilitate this cleaning. This additional equipment leads to further consideration for the service setup. Water-soluble support materials are being developed for polyjet printers and promise easier cleaning, especially in flexible or complex models.

The facilities to house and support this machinery should be discussed before investing in any technology. Most of the print materials are non-hazardous with publicly available material safety data sheets (MSDS). Reviewing these documents and the intentions of the print service with institutional facilities and safety management is certainly beneficial. The equipment will require obvious space, but may also require specialized ventilation and a fire suppression system to comply with local and federal occupational regulations [8]. Electrical backup to the printer would also be beneficial from a safety and practical standpoint. Many larger printers can run for over 10 h, which naturally leads to prints running overnight, unstaffed. Returning to a printer the following day to a failed/incomplete job due to a power outage is clearly undesirable. Mitigating this with uninterruptible power supplies (UPS) is strongly advised. The selection of the specific UPS should be deferred to the printer manufacturer and budgeted appropriately. Waste disposal should also be planned with institutional facilities before start-up of the service.

## Cost

For all the factors outlined above, the cost of initiating an in-house printing service can range from several thousand dollars to several hundred thousand with an annual budget to match. The disparity in cost depends on the scope of the service. Larger scale programs may be worth the higher investment on the basis of improved clinical decision making and research/educational advancements. Currently, there is limited ability to recoup the costs of 3D printing for clinical cases, though as research advances, and if improved outcomes can be shown, this may change. For current operational management, it is suggested the financial investment should be handled on an institutional department level. Such services typically have the discretionary spending capabilities to support

**Fig. 16.1** 3D printer laboratory space for Stratasys/Objet Connex 500 polyjet printer complete with post-processing facilities including an Underhill Powerblast high-flow, self-contained, water cleaning unit and manual cleaning supplies. Not shown is the workstation to perform segmentation and run the printer software

the demands of 3D printing, especially at larger academic institutions.

The scale of the printing service will also determine the optimal workflow. Smaller services with limited personnel work best with a personal consultation between those completing the modeling tasks outlined above and the ordering physician. For such an arrangement, covering the cost of manufacturing is often easiest by determining the cost of the material used as well as quantifying the time and effort dedicated to image and model post-processing. Such smaller purchases often can be funded by the ordering physician's research money or home department. Larger scale services require a more robust system. Interdepartmental agreements may be needed to set up billing and payment methods. Ordering procedures will still ultimately require personnel consultation given the uniqueness of each case, but the initiating event can be automated. Given there is no current mechanism for billing the service of creating a 3D printed model to the patient and/or their insurance in clinical cases, it is not yet appropriate for such an ordering mechanism to be built into the electronic medical record. As further research is conducted and this process becomes more commonplace, there will surely be movement toward a quantification of effort and therefore an assessment of appropriate reimbursement.

Figure 16.1 shows a 3D printer laboratory space for Stratasys/Objet Connex 500 polyjet printer complete with post-processing facilities including an Underhill Powerblast high-flow, self-contained, water cleaning unit and manual cleaning supplies. Not shown is the workstation to perform segmentation and run the printer software.

## References

1. Gao W, Zhang YB, Ramanujan D, Ramani K, Chen Y, Williams CB Wang CCL, Shin YC, Zhang S, Zavattieri PD. The status, challenges, and future of additive manufacturing in engineering. Comput Aided Des. 2015;69:65–89.
2. Schubert C, van Langeveld MC, Donoso LA. Innovations in 3D printing: a 3D overview from optics to organs. Br J Ophthalmol. 2014;98:159–61.
3. Knox K, Kerber CW, Singel SA, Bailey MJ, Imbesi SG. Rapid prototyping to create vascular replicas from CT scan data: making tools to teach,

rehearse, and choose treatment strategies. Cathet Cardiovasc Interv. 2005;65:47–53.
4. Valverde I, Gomez G, Coserria JF, Suarez-Mejias C, Uribe S, Sotelo J, Velasco MN, de Soto JS, Hosseinpour AR, Gomez-Cia T. 3D printed models for planning endovascular stenting in transverse aortic arch hypoplasia. Cathet Cardio Interv. 2015;85:1006–12.
5. Naftulin JS, Kimchi EY, Cash SS. Streamlined, inexpensive 3D printing of the brain and skull. PLoS ONE. 2015;. doi:10.1371/journal.pone.0136198.
6. Ventola CL. Medical applications for 3D printing: current and projected uses. Pharm Ther. 2014;39: 704–11.
7. Gaynor AT, Meisel NA, Williams CB, Guest JK. Multiple. J Manuf Sci E-T ASME. 2014; 136:SI.
8. Kim Y, Yoon C, Ham S, Park J, Kim S, Kwon O, Tsai PJ. Emissions of nanoparticles and gaseous material from 3D printer operation. Enrivon Sci Technol. 2015;20:12044–53.

# Utility of a 3D File Database

17

Matthew Bramlet, MD
and Meghan Coakley McCarthy, MS, PhD

## Introduction

While the concept of digital three-dimensional (3D) data has been around for decades, the inability to interact with the content in a meaningful manner has prevented its full utilization. The impact of the rapid emergence of consumer 3D printing has made the potential applications in the medical field much more apparent.

## 3D Data for Improved Understanding in Medicine

Medical imaging scans produce two-dimensional (2D) representations of anatomy or 3D renderings presented on a 2D screen. Despite technological enhancements, complete understanding of 2D information is limited to the brain's capability to translate these images into an accurate 3D representation in the mind's eye [1–3]. This visuospatial skill is highly variable among individuals, regardless of their general aptitude [4–7]. In the current "apprenticeship-based" model of medical training, this ability is not explicitly assessed or challenged on a routine basis. While one must rely heavily on this ability in fields such as surgery or radiology, it is less critical in internal medicine or psychiatry. It is possible that individuals' visuospatial abilities influence career path [8–10]. Recent literature has described the assessment of visuospatial skills in candidate selection for surgical or radiologic specialties [11–13]. Ultimately, this selection bias could exacerbate the disparity in visuospatial skills across disciplines.

## 3D Modeling for Interdisciplinary Communication

When complex 3D concepts influence medical decision making, variations in visuospatial abilities can be a hidden barrier to communication among individuals in a treatment team. The purpose of 3D modeling is to minimize or even eliminate this barrier through direct visualization and therefore improved understanding of the anatomy. Utilizing this technique, the key structural aspects of the congenital heart disease are demonstrated clearly to all. For the medical team, this becomes a valuable tool for communication, ultimately leading to better collaborative decision making.

M. Bramlet, MD (✉)
Advanced Imaging and Modeling, Jump Trading Simulation and Education Center, Children's Hospital of Illinois, University of Illinois College of Medicine, Peoria, IL, USA
e-mail: matthew.bramlet@jumpsimulation.org
URL: http://www.jumpsimulation.org

M.C. McCarthy, MS, PhD
Bioinformatics and Computational Biosciences Branch, Office of Cyber Infrastructure and Computational Biology, National Institute of Allergy and Infectious Diseases, National Institutes of Health, Bethesda, MD, USA
e-mail: meghan.coakley@nih.gov


K.M. Farooqi (ed.), *Rapid Prototyping in Cardiac Disease*,
DOI 10.1007/978-3-319-53523-4_17

## Development of a High-quality Anatomical Database

The category of congenital heart disease includes innumerable lesions with sometimes complex anatomic arrangements. Such complicated anatomy can be difficult to conceptualize and learn without representative 3D models. Although the majority of anatomical defects can be found in congenital heart disease pathologic libraries, the case studies are outdated, sometimes in poor condition, and are not being replenished. The paucity of modern case descriptions and the lack of good quality anatomical representations leave an emerging gap in congenital heart disease education.

## Origin of the 3D Heart Library

To bridge this gap, we are working on providing an online repository of digital 3D models of case studies representing normal cardiac anatomy as well as congenital heart lesions. The purpose of the 3D Heart Library Collection is to serve as a source of digital reproductions of human anatomic hearts ranging from infant to adult, simple to complex, with a focus on congenital heart disease.

The Heart Library emerged as a collaborative effort with the National Institutes of Health (NIH). Researchers realized how useful 3D printing technology could be when evaluating complex 3D structures. They also recognized that most researchers and clinicians had little or no experience using the software required to generate such models. In response, a team led by the National Institute of Allergy and Infectious Diseases (NIAID) created the NIH 3D Print Exchange: an online, open-source resource dedicated to the discovery, sharing, and creation of 3D-printable models related to bioscience and medicine. The Heart Library is one of the several "special collections" on the Web site, which are curated by external collaborators. It is the first of any such collection where models will be rigorously and independently reviewed by a panel of subject-matter experts.

## Open-Source Data Sharing and Community Development

A main goal of the Heart Library is to improve the understanding of congenital heart disease through sharing of heart models and ideas. This is in line with the community-driven nature of the NIH 3D Print Exchange [14]. The entirety of the 3D Print Exchange database, including the Heart Library, is free to use. Any site visitor can create an account, free of charge, and download content. In addition, by eliminating restrictions on who can contribute, the Exchange provides opportunities for models to come from sources around the world.

The site relies on open-source standards and software to provide value-added features, including custom Web-based tools for converting raw experimental data or medical imaging scans into ready-to-print 3D file formats. The Exchange features an in browser interactive 3D viewer that supports color content for 3D print files. It also provides application program interfaces (APIs) to allow greater access to the database, provide for batch submissions, and connect users to other 3D printing services.

Registered users are able to rate models with one to five stars, and add comments to each model page to provide feedback on the quality and utility of the models, or their own experience using it. In addition to the community-based contribution design, the Heart Library will also foster collaboration, to create a community of specialists who work together to advance the utility of these models in medical practice. As evidence of the Exchange's value and innovative design, it received the 2015 HHS Innovates Award from the US Department of Health and Human Services.

## Heart Library Content

The simple act of sharing a 3D model, accompanied by details about the case, becomes a key part of how we hope to advance the collective knowledge about congenital heart disease through the use of this online database. When a

model is generated as part of medical decision making, its value is primarily focused on improving communication within a medical treatment team. Once it is shared in the database, its value extends from medical decision making to medical education. Furthermore, models designed specifically for educational purposes will no longer be restricted to an institution or region. More generally, the database provides a means to disseminate this valuable content worldwide, so that practitioners, students, educators, and patients can utilize the content.

## 3D Models as Peer-Reviewed Case Study Reports

With each heart model that is created to solve a clinical question, there are associated clinical facts surrounding the case that provide context and more of a complete clinical picture. To preserve this value in a large database, we decided to consider each 3D model submission similar to a case report. The purpose of a case report is to describe a rare or unusual clinical scenario that can be cataloged for future reference. We believe that including 3D representations of congenital heart disease, along with the 2D image datasets from which they are derived, will bring significant value to the case reports. Each model published in the Heart Library can stand on its own as a short case report and be cited in a publication by referencing the unique database accession code.

**Table 17.1** Database content

| Content | |
|---|---|
| Keywords | Clinical description |
| Age (see Table 17.2) | Height |
| Weight | BSA |
| Diagnosis | Previous surgeries |
| Imaging source | Segmentation method |
| Units of measure | Scale |
| Institution | Submitting author |

## Clinical Case Study Data Requirements

The content to be included for each case pertains to clinically relevant information as well as workflow-related details including image acquisition information and method of segmentation (Table 17.1). The diagnosis, as compiled from the STS database, and a list of surgical procedures which the patient has undergone, will also be entered for each case. A short description to outline the clinical question can also be included to give the learner a sense of the relevant discussion points.

## 3D Model File

The digital model (.stl file or other acceptable formats) should accurately represent source DICOM data. Segmentation techniques are categorized into one of the three methodology types as described below. Poorly rendered models that deviate too far from the source image will be rejected.

## DICOM Data

De-identified image datasets in the Digital Imaging and Communications in Medicine (DICOM) format are required to be submitted with the model, both for the peer-review process as well as to provide a reference for segmentation analysis. A 3D imaging dataset which is free of artifact with resolution between 1 and 1.5 mm isovoxels is ideal. Datasets with resolution or artifacts that do not allow for accurate reproduction of anatomy will not be accepted due to the increased risk of false data transmission to the digital model.

## Protecting Patient Information

Sharing case study details and raw medical image data is critical to the Library. Extra care must be taken to protect patient privacy when making clinical data available to the public. Concern for HIPAA compliance may create a barrier for clinicians who wish to submit their 3D case reports. We have extensively evaluated

HIPAA requirements to ensure that contributions to the library do not violate patient privacy. If no Personal Health Information (PHI) is included in the data, then the data does not fall under the HIPAA Privacy Rule [15]. All content contributed to the Heart Library will not contain PHI. The submitting clinician is responsible for reviewing and removing any PHI prior to uploading data for peer review. Two methods to de-identify PHI are the "Safe Harbor" method and/or the use of a statistician to limit risk. The former requires removal of all 18 identifiers enumerated at section 164.514(b)(2) of the regulation (Table 17.2) and for the purposes of the Heart Library is the only acceptable method for submission.

Utmost care must be taken by the submitting physician or organization in de-identifying DICOM data. The NIH 3D Print Exchange also has tools in place to automatically remove PHI that is named in the HIPAA Privacy Rule (see Table 17.2). Having redundancy in checking for privacy data will significantly minimize liability.

**Table 17.2** 18 PHI identifiers of the HIPAA Privacy Rule

| |
|---|
| 1. Names |
| 2. All geographic subdivisions smaller than a state, except for the initial three digits of the ZIP code if the geographic unit formed by combining all ZIP codes with the same three initial digits contains more than 20,000 people |
| 3. All elements of dates except year, and all ages over 89 or elements indicative of such age |
| 4. Telephone numbers |
| 5. Fax |
| 6. E-mail addresses |
| 7. Social security numbers |
| 8. Medical records numbers |
| 9. Health plan beneficiary numbers |
| 10. Account numbers |
| 11. Certificate or license numbers |
| 12. Vehicle identifiers and license plate numbers |
| 13. Device identifiers and serial numbers |
| 14. URLs |
| 15. IP addresses |
| 16. Biometric identifiers |
| 17. Full-face photographs and any comparable images |
| 18. Any other unique, identifying characteristic or code, except as permitted for re-identification in the Privacy Rule |

## 3D Rendering Quality, Methods, and Review

The peer-review aspect of the Library is essential to providing verification that a digital 3D model is a true representation of the source 2D medical image series. In the field of congenital heart disease, expertise in both congenital heart imaging and 3D model creation is not well-established. It is therefore difficult to define quality in an emerging field such as this. In collaboration with recognized leaders in 3D printing and modeling of cardiac anatomy, we established standards and methods for model creation and evaluation.

### Defining "Quality"

The aim of this part of the process was to build a high-quality assessment method that would be reproducible and quantifiable, yet also adaptable. This difficult task involved defining the segmentation method and the assessment process itself. As has been described in previous chapters, the current postprocessing technology involves creating a "mask" over 2D images to identify the structures to be printed. Therefore, the current set of methodologies and peer-review processes are tied to visual interpretation of a 2D image in a 3D dataset and manual translation into the 3D form.

### Methodologies

An expert panel identified the various methods of segmentation currently used to generate 3D cardiac models and created categorical definitions. The quality of the source image data is also evaluated. Color coding of anatomic models is recommended to follow the convention laid out

by Frakes et al. [16] Based on current techniques, segmentation has been separated into 3 methods: (1) solid blood pool (2) blood pool/myocardial border, and (3) myocardium and vessel wall.

Solid blood pool segmentation involves highlighting the intracardiac and intravascular structures to create a 3D model which represents the blood pool. This method is typically utilized for extracardiac vascular assessment.

Blood pool/myocardial border segmentation starts with the 3D product of method 1. A layer of predetermined thickness is subsequently applied to the outside of the model. The internal 3D model representing the blood pool is then subtracted, leaving a cast which can be cropped to view the intracardiac anatomy. This method is the most commonly utilized method for rendering hearts currently and is useful for both extracardiac and intracardiac evaluation.

The goal of myocardium and vessel wall segmentation is to highlight the myocardium, vascular walls, and intracardiac structures directly, maintaining their actual caliber and thickness. This method is currently the most time-consuming method because of the extensive postprocessing that is needed to create a "clean" 3D model. This method is useful, for example, in cases in which an accurate representation of the thickness of the myocardium is important to have in the final printed model. Final verification of segmentation using any method involves comparing the final segmentation with the source image dataset.

As new techniques of postprocessing emerge, the methods of assessment will be adjusted accordingly. The utility of the peer-review process is that adaptability can be built into a scoring system. Furthermore, due to the limited expertise in this field, the peer-review system becomes necessary as a means to create a community of individuals holding themselves accountable to the assessment of quality.

## Peer Review

The primary purpose of the peer-review process in medicine is to verify the accuracy of information through a community of experts. The benefit of establishing the peer-review process through the NIH Heart Library is that as the technology continues evolving, a standard for quality assessment will have been set. For complete adaptation of 3D printing technology, there has to be broad acceptance of its utility. The Gartner hype cycle is a curve representing the maturity, adoption, and social application of specific technologies. It divides this progression into 5 phases. 3D printing in medicine has mirrored the emergence of consumer 3D printing. It is currently perceived to be following consumer 3D printing down into the trough of disillusionment of the Gartner hype cycle for 2015 as illustrated in Fig. 17.1 [17].

At this stage, the technology has been demonstrated as possible, but not necessarily useful. Although some physicians and surgeons may be at a stage of skepticism toward 3D printing technology, this will likely improve with evidence and/or personal experience. With the low prevalence of congenital heart disease, it is difficult to gather evidence over a short period of time that will change these attitudes. Therefore, a focus on experience may be a critical route toward initial acceptance. The peer-review process tied to the Heart Library will help to guide those interested in this technology down a "high-quality" path to increase the chances that a positive experience is associated with its use.

An editorial board is in place to direct the development and refinement of guidelines for assessment. Keeping with the case report model, authorship will be assigned to the submitting author as well as the final peer reviewer to provide academic incentive for participation both from the submission standpoint and the review standpoint. A scoring system will be in place to provide a quantifiable value to the models. This scoring system is based on similar subjective scoring systems used in medical image assessment but will focus on the 3D cardiac model [18].

Initial assessments will focus on source image assessment and accuracy of the segmentation. The peer-review workflow is being designed to allow for collaborative communication between experts where information regarding 3D modeling including image acquisition, segmentation,

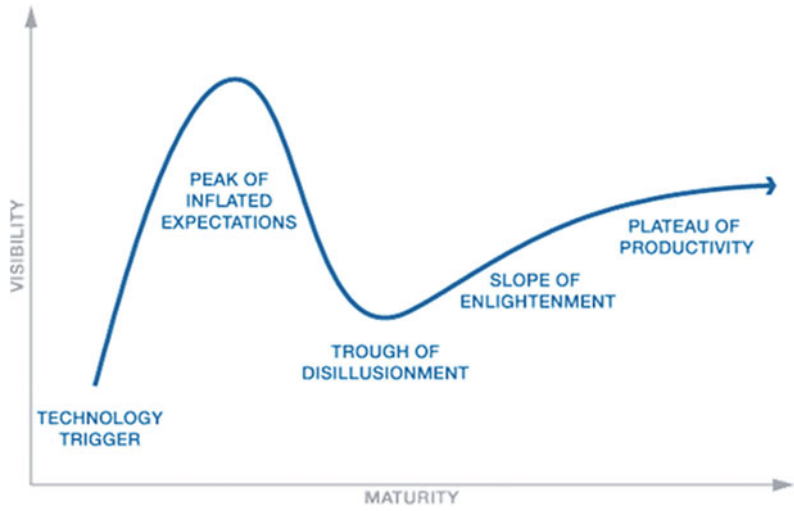


**Fig. 17.1** The Gartner hype cycle

file transfer, and current research can be shared and advanced collectively.

## Impact and Future

By creating a high-quality database with built-in tools that allow users to easily query and integrate content into their Web sites, the 3D Print Exchange eliminates barriers to creativity and understanding. The Heart Library peer-review workflow is designed around collaboration and harnessing collective expertise. The NIH-supported database, along with the quality assurance processes and editorial board oversight, increases the academic value assigned to authorship, as each case can be cited in journal publications via the database accession code. The most exciting discovery to come from the 3D Heart Library has yet to be conceived, but we hope that the design of this database will help foster its ideation.

**Acknowledgements** We gratefully acknowledge the support and encouragement of the NIH 3D Print Exchange co-founder, Dr. Darrell Hurt of the Bioinformatics and Computational Biosciences Branch, Office of Cyber Infrastructure and Computational Biology, National Institute of Allergy and Infectious Diseases. The NIH 3D Print Exchange (html://3dprint.nih.gov) is a collaborative effort owned by the National Institute of Allergy and Infectious Diseases. It was founded in collaboration with the Eunice Kennedy Shriver National Institute for Child Health and Human Development and the National Library of Medicine, with funding and support from the HHS Idea Lab, part of the US Department of Health and Human Services. Further we acknowledge Jump Trading Simulation and Education Center (html://www.jumpsimulation.org) for sponsoring the peer-review workflow component of the 3D Heart Library as well as Brent Cross and Aleem Zafar for their assistance in preparation of this manuscript.

## References

1. Wu B, Klatzky RL, Stetten GD. Mental visualization of objects from cross-sectional images. Cognition. 2012;123(1):33–49. doi:10.1016/j.cognition.2011.12.004.
2. Wu B, Klatzky RL, Stetten G. Visualizing 3D objects from 2D cross sectional images displayed in-situ versus ex-situ. J Exp Psychol Appl. 2010;16(1):45–59.
3. Provo J, Lamar C, Newby T. Using a cross section to train veterinary students to visualize anatomical structures in three dimensions. J Res Sci Teach. 2002;39(1):10–34.
4. Peters M, Laeng B, Latham K, Jackson M, Zaiyouna R, Richardson C. A redrawn Vandenberg and Kuse mental rotations test: different versions and factors that affect performance. Brain Cogn. 1995;28:39–58.
5. Kaufman HH, Wiegand RL, Tunick RH. Teaching surgeons to operate—principles of psychomotor skills training. Acta Neurochir (Wien). 1987;87(1–2):1–7.
6. Fleishman EA, Bartlett CJ. Human abilities. Annu Rev Psychol. 1969;20(1):349–80.

7. Sadideen H, Alvand A, Saadeddin M, Kneebone R. Surgical experts: born or made? Int J Surg. 2013;11 (9):773–8.
8. Langlois J, Wells GA, Lecourtois M, Bergeron G, Yetisir E, Martin M. Spatial abilities of medical graduates and choice of residency programs. Anat Sci Educ. 2015;8(2):111–9.
9. Brandt MG, Wright ED. Medical student career choice and mental rotations ability. Clin Invest Med. 2005;28(3):112.
10. Harris CJ, Herbert M, Steele RJC. Psychomotor skills of surgical trainees compared with those of different medical specialists. Br J Surg. 1994;81 (3):382–3.
11. Birchall D. Spatial ability in radiologists: a necessary prerequisite? Br J Radiol. 2015;88(1049):20140511.
12. Maan ZN, Maan IN, Darzi AW, Aggarwal R. Systematic review of predictors of surgical performance. Br J Surg. 2012;99(12):1610–21.
13. Tansley P, Kakar S, Withey S, Butler P. Visuospatial and technical ability in the selection and assessment of higher surgical trainees in the London deanery. Ann R Coll Surg Engl. 2007;89(6):591–5.
14. Coakley MF, Hurt DE, Weber N, Mtingwa M, Fincher EC, Alekseyev V, Chen DT, Yun A, Gizaw M, Swan J, Yoo TS. The NIH 3D print exchange: a public resource for bioscientific and biomedical 3D prints. 3D Printing Addit Manuf. 2014;1(3):137–140.
15. U.S. Department of Health and Human Services National Institutes of Health. Research Repositories, Databases, and the HIPAA Privacy; 2004. https://privacyruleandresearch.nih.gov/research_repositories.asp. Accessed 26 Feb 2016.
16. Ejaz F, Ryan J, Henriksen M, Stomski L, Feith M, Osborn M, Pophal S, Richardson R, Frakes D. Color-coded patient-specific physical models of congenital heart disease. Rapid Prototyping J. 2014;20 (4):336–43.
17. Gartner. Gartner's 2015 hype cycle for emerging technologies identifies the computing innovations that organizations should monitor; 2015. http://www.gartner.com/newsroom/id/3114217. Accessed 26 Feb 2016.
18. Greil GF, Powell AJ, Gildein HP, Geva T. Gadolinium-enhanced three dimensional magnetic resonance angiography of pulmonary and systemic venous anomalies. J Am Coll Cardiol. 2002;39 (2):335–41.

# 3D Bioprinting for Cardiovascular Tissue Engineering

18

Mitchell Kuss, BS and Bin Duan, PhD

## Introduction

Cardiovascular disease (CVD) is one of the leading causes of worldwide morbidity and mortality. This number is nearing 20 million deaths annually [1]. The late stages of CVD usually end in the need for replacement of cardiovascular tissue such as heart valves, arteries, and myocardium. This is due to the fact that these tissues are fully differentiated and load bearing, which does not allow for effective healing on their own. Current treatments for CVD include autografts (e.g., coronary artery bypass graft with autologous vein, Ross procedure), allografts (donor valve or heart valve transplants), and xenografts (bovine or porcine heart valves, arteries, etc.). There are more than 80,000 heart valve replacements and over 600,000 vascular implantations annually performed in the USA [2, 3]. These procedures result in the expenditure of $200 billion [4]. The current treatments have major drawbacks that cause problems during implementation. These include donor tissue shortage, immune rejection, anticoagulation therapy, and limited durability [5]. The emerging field of tissue engineering and regenerative medicine holds great promise as an alternative treatment option by creating engineered tissue to repair congenital defects, such as aortic valve stenosis and coarctation of the aorta, and for the repair of diseased cardiovascular tissue [6, 7].

3D printing is an advanced fabrication technique that is often referred to as additive manufacturing (AM) or solid-free form fabrication. It is characterized by the use of precisely detailed computer-aided designs, along with automated processes and standardized materials, to create specific 3D objects [8, 9]. Cardiovascular surgeons have already utilized 3D printing to generate individualized models of patients so that they can visualize anatomical structures before proceeding with the surgery [10, 11]. These models allow them to better understand structural abnormalities and to choose better surgical approaches than previously able when using artificial or cadaveric heart models. The National Institutes of Health (NIH) have launched a 3D printing exchange, in which users can share, download, and edit 3D print files related to health and science. Most of these models, and the ones used by surgeons, are made of plastics and are not applicable for tissue engineering.

The field of tissue engineering has adopted the 3D printing approach by using biodegradable polymers for building complex scaffolds and

M. Kuss · B. Duan (✉)
Mary & Dick Holland Regenerative Medicine Program, University of Nebraska Medical Center, Omaha, NE, USA
e-mail: bin.duan@unmc.edu

M. Kuss · B. Duan
Division of Cardiology, Department of Internal Medicine, University of Nebraska Medical Center, Omaha, NE, USA

B. Duan
Department of Surgery, College of Medicine, University of Nebraska Medical Center, Omaha, NE, USA


K.M. Farooqi (ed.), *Rapid Prototyping in Cardiac Disease*,
DOI 10.1007/978-3-319-53523-4_18

tissue constructs [12]. Printable biomaterials can be used for 3D printing scaffolds with post-cell seeding, conditioning, and in vivo implantation [8, 13–15]. 3D printing with biological materials usually requires surface cell seeding. This strategy has certain limitations due to difficulties in incorporating multiple cell types along with bioactive molecules [16, 17]. A possible fix for this problem is combining additive manufacturing with cells and biological factors. This technique is called bioprinting [18, 19]. Bioprinting is defined as the use of computer-aided layer-by-layer deposition for patterning and assembling living cells and biologics within a 2D or 3D construct [20]. When compared to other biofabrication techniques, bioprinting allows for the production of 3D constructs with more precisely controlled architecture, is able to incorporate multiple cells types, and can create a more physiologically relevant microenvironment [21].

In this chapter, we provide an overview of implementation of 3D bioprinting techniques for cardiovascular tissue engineering. First, we briefly introduce some background about bioprinting working principles, bioink materials development, and process configurations. Then, we focus on recent advances in the bioprinting of vascularized constructs, blood vessels, myocardium and heart valves, and the potential applications for pediatric patients. Finally, we discuss current major challenges and technological hurdles and potential solutions and future directions.

## Background

3D bioprinting is similar to additive manufacturing (AM); in that they both produce complex objects from a 3D design file by decomposing the shape into a series of 2D layers. A major difference is that bioprinting uses bioinks, which are mixtures or spheroids containing cells and/or biomaterials, rather than plastics used in AM. In bioprinting, a structure is built in a stepwise process in which each layer is bonded with the previous layer to build 3D constructs based on the given design [18, 22]. Bioprinting technology can be used to fabricate biomimetic structures, as well as specific anatomical 3D structures, by using images of patients obtained using medical imaging technologies, such as computed tomography (CT) or magnetic resonance imaging (MRI) [21, 23].

## Different Bioprinting Techniques

The types of bioprinting that are currently commonly used are inkjet, laser/light, and extrusion-based. Inkjet bioprinting implements different mechanisms, such as thermal [24], a piezoelectric actuator [25], laser-induced forward transfer [26], and pneumatic pressure [27], to deposit tiny bioink droplets onto a substrate. This technique is able to produce a relatively high resolution and is suited to generate thin layers [28, 29] or patterned structures [30] for soft tissue regeneration or for cell manipulation. Laser/light based bioprinting, or stereolithography/projection bioprinting, uses laser or other light sources, such as UV, to scan the surface of a photocurable polymer solution as the stage incrementally lowers [31]. This allows the layers to be polymerized on top of each other, creating a 3D structure in a bottom-up manner [32]. Extrusion-based bioprinting (EBB) utilizes a mechanical force driven by either air pressure or motor to extrude biomaterials, cell aggregates, or microcarriers through a nozzle to build a 3D structure. The nozzle diameter is normally large enough to minimize the cell damage as the material is extruded [33].

## Bioinks

A variety of bioinks can be used for bioprinting. These include cell suspensions, cell-laden hydrogels, microcarriers, cell/tissue spheroids, and decelluralized matrix components [34–36]. Each bioink has different properties, works best with certain types of bioprinting, and can have different functions. The choices for bioinks to be used in inkjet and laser bioprinting are limited due to the process in which bioinks are

deposited. EBB on the other hand utilizes a variety of bioinks. Inkjet and laser bioprinters require very fluid bioinks, while EBB can use bioinks with a range of viscosities.

Hydrogels are the most widely used bioinks for EBB. This is partially due to the ability to be extruded and partially due to the fact that hydrogels can be tuned to have properties similar to specific types of tissue. For example, for cartilage bioprinting, biostable hydrogels with limited or slow biodegradability and higher mechanical properties, such as poly(ethylene glycol) (PEG), alginate, agarose, and methylcellulose, are often used [37–39]. Bioactive hydrogels, such as gelatin, collagen, fibrin, and peptides, have the capacity to support cell adhesion and can be implemented in cardiovascular bioprinting [40–44]. Microcarriers have a large surface area and a bioactive environment and encourage quick cell attachment and proliferation. Microcarriers can be used to encapsulate cells and then be incorporated into other hydrogel-based bioinks. Scaffold-free spheroids for bioprinting can be fabricated via biofabrication approaches, such as hanging drop, micromolding, microfluidics, and spinner flasks. When deposited, spheroids can fuse together and quickly generate more complex constructs with heterogeneous cell populations and better biomimicry. This enables the co-culture of endothelial cells, smooth muscle cells, fibroblasts, cardiomyocytes, and other related cardiovascular cell types. As with other types of bioinks, the bioprinting process using spheroids is limited. This is due to the need to produce a large number of spheroids, load the spheroids, deposit them, and handle the constructs, which causes the whole process to be very time-consuming and labor-intensive [45]. In addition, the constructs made from the scaffold-free spheroids require a long time to remodel and fully mature, and are still mechanically weak and may not hold their shape under certain conditions.

New materials are constantly being tested for their printability and usability in bioprinting applications. One material being considered as a valid bioink source is extracellular matrix (ECM) from various native tissues. The ECM is first decellularized, then dissolved into a paste-like bioink via chopping and smashing [46]. Using ECM allows the production of native tissue-like microenvironments from an almost unlimited source. The decellularization process must be standardized for each specific tissue source, so that the results create consistent and component controllable bioinks. To improve the mechanical properties and increase printability, ECM bioinks can be combined with hydrogel bioinks or be deposited around a printed frame. These hybrid printing processes increase the complexity of the bioinks and printing process, and often require specific software and hardware control that may not be readily available.

## 3D Bioprinting of Microvasculatures and Vascularized Constructs

Many tissues and organs, such as cardiovascular, bone, liver, and pancreas, are highly vascularized and require a functional vascular network to aid in the regeneration of the tissue [47, 48]. For decades, tissue engineering has aimed to create functional tissues and organs. This has been limited because current methods still cannot generate fully vascularized tissue constructs. The evolution of 3D printing has allowed the adoption of vascularization strategies from general tissue engineering and combined them with its own abilities to produce in vitro vasculature and vascular constructs. These approaches include (a) vascular constructs generation by self-assembly of cells; (b) microvasculature generation by inkjet-based bioprinting; (c) bioprinted constructs generation with growth factor delivery; and (d) generation of channel-based vascularized constructs.

Cell self-assembly is the autonomous organization of cells with similar adhesive properties into a stable pattern or structure without external intervention [49]. This is utilized in the production of vasculature. Cell spheroids prepared from cell suspensions can be deposited so that they fuse together into vascular-like constructs (Fig. 18.1a) [50]. Branching patterns can be

achieved by adding agarose rods as templates and fusing them with multicellular spheroids. This creates tubular structures with controllable diameters, wall thicknesses, as well as branching patterns (Fig. 18.1b, c) [51]. Alternatingly depositing multicellular cylinders composed of human smooth muscle cells (HSMC) and human skin fibroblasts (HSF) will allow for the formation of double-layered vascular walls with specific patterns (Fig. 18.1d) [51]. A downfall of this process is that it can be very time-consuming and requires a lot of manual work to produce large amounts of these building blocks [52]. Kucukgul et al. used optimized computer-aided algorithms and support hydrogels to bioprint mouse embryonic fibroblast (MEF) cell aggregates [53] to form an aortic tissue construct. While this approach to cardiovascular tissue bioprinting is relatively more efficient than other methods, the overall resolution and controllability is somewhat lacking.

Inkjet printing can also be used to bioprint vascular structures. A commercial inkjet printer has been modified to do just this. It was modified to simultaneously deposit human microvascular endothelial cells (HMEC) and fibrin to form microvasculature (Fig. 18.1e) [54]. The printed fibrin scaffold retained its proper printed shape (Fig. 18.1f), while the endothelial cells proliferated around it to form a tubular structure. The printed ring-shaped microvasculature had much better integrity after a 21-day culture, excluding Texas Red-conjugated dextran from the printed structure (Fig. 18.1g). This strategy shows that inkjet bioprinting has the ability to bioprint multiple cell types together, and that the use of mesenchymal stem cells (MSC) or smooth muscle cells can help support the formation and maturation of microvasculature. A problem with the method of inkjet bioprinting is that the cell deposition is performed on a substrate (biopaper) to support the weak cell layer(s).

Angiogenic growth factors play an important role in neovascularization. They signal cells to perform certain functions crucial to blood vessel generation. Angiogenic growth factors can activate endothelial (progenitor) cells and regulate their migration. They also promote cell assembly, vessel formation, and maturation [55]. The correct processes must be used to deliver the growth factors properly. For the best results, special delivery strategies, such as using nanoparticles and microspheres, are used instead of direct addition in vitro and injection in vivo. The controlled release of vascular endothelial growth factor (VEGF) from gelatin microparticles (GMP) within 3D bioprinted scaffolds and the effects on subsequent vascularization have been

**Fig. 18.1** Strategies to generate microvasculatures and vascularized constructs. **a–d** Self-assembly of cells for vascular grafts generation. **a** Sequential steps of cell fusion of vascular tissue spheroids in collagen I hydrogel [50]; **b** Bioprinted tubular structures with cellular cylinders [51] (*a*) design template, (*b*) bioprinter with two vertically moving print heads, (*c*) printed construct; **c** Fusion pattern of multicellular spheroids assembled into branched structure [51] (*a*) built of 300-μm spheroids with branches of 1.2 mm (*solid arrow*) and 0.9 mm (*broken arrows*), (*b*) fused branched construct after 6 days of deposition; **d** Built of a double-layered vascular wall [51] (*a*, *e*) multicellular cylinders assembled by SMC (*green*) and fibroblasts (*red*), (*b*, *f*) H&E staining, (*c*, *g*) α smooth muscle actin (*brown*), (*d*, *h*) Caspase-3 (*brown*). **e–g** Generation of microvasculatures by inkjet-based bioprinting [54]. **e** Schematic drawing of simultaneous deposition of HMEC and fibrin channel scaffold using modified thermal inkjet printer; **f** Printed fibrin scaffold; **g** Printed ring-shaped microvasculature, (*a*) cultured for 21 days (calcein AM, *green*), (*b*) improved integrity after 21-day culture with all dextran molecules (*red*) excluded from the printed structure. **h–j** Generation of bioprinted constructs with growth factor delivery [56]. **h** Cumulative release of VEGF. Fast (directly incorporated in Matrigel) and slow release (application of gelatin microspheres) of VEGF; **i** Bioprinted hydrogel mixture and tubulogenesis assay; **j** Vessel formation in EPC seeded scaffolds after one-week subcutaneous implantation in mice: (*a*) fast release showed less CD31 (*brown*) than (*b*) slow release of VEGF in the bioprinted hydrogels (Matrigel:alginate = 3:1). Blood vessels are indicated with arrows. **k–n** Coaxial nozzle-assisted 3D bioprinting of vasculature. **k** Schematic of fabrication of a 3D alginate structure with built-in microchannels [37]; **l** 3D construct fabricated based on hollow alginate filaments [37] (*a*) printed construct, (*b*) longitudinal section, (*c*) cross section, (*d*) SEM image of the cross section; **m** Formation of printed carbohydrate–glass filament architecture and vascular lumen with endothelial monolayer after removing sacrificial filament and perfusion [59]; **n** (*a*) Formation of dual channel by bioprinting sacrificial gelatin within fibrin, (*b*) GFP-HUVEC (*green*) within fibrin showed tube structure and capillary network after 12-day culture and RFP-HUVEC (*red*) in the channel-developed lumen structure [60]

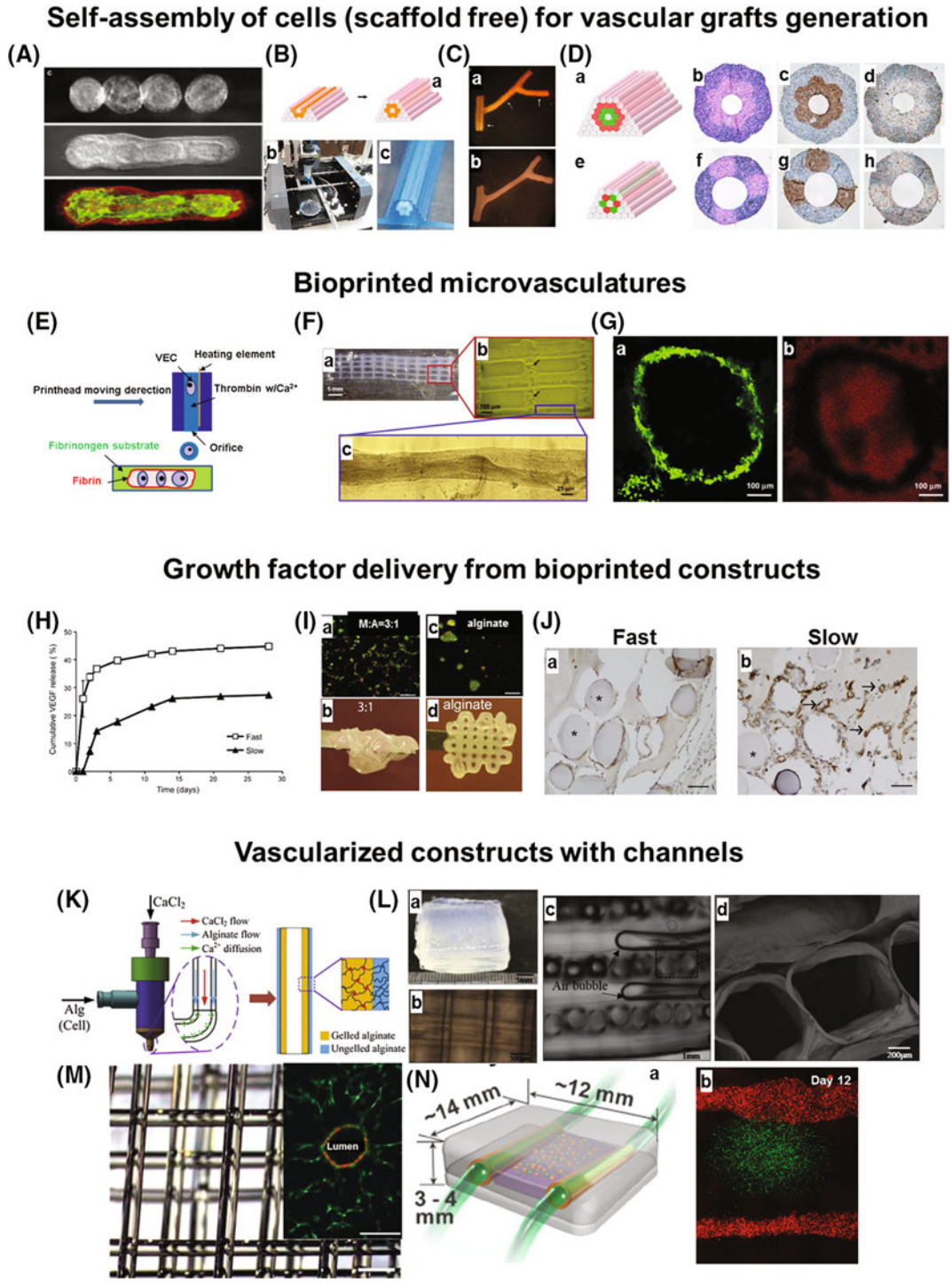


investigated [56]. VEGF was incorporated into Matrigel for fast release, or was put into GMP, which was then dispersed throughout Matrigel plugs for slow release. The application of GMP embedded in Matrigel plugs showed a significant, prolonged release of VEGF (Fig. 18.1h).

Alginate was added to the Matrigel to enhance the mechanical properties and 3D printability. The problem with this addition was that large cell aggregates were induced and there was reduced tubulogenesis of endothelial progenitor cells (EPC) (Fig. 18.1i). A working combination of Matrigel and alginate mixture was found to be Matrigel/alginate = 3/1 with VEGF-incorporated. Heterogeneous 3D bioprinted scaffolds made of this mixture were subcutaneously implanted in mice. During this experiment, it was found that the slowly released VEGF promoted more vessel formation with more CD31 expression than the fast release VEGF (Fig. 18.1j). Nano-/microparticle delivery strategies influence the effectiveness of growth factors. The delivery strategies can enable dual or even multiple therapeutic reagents and angiogenic factors to be released in a synergistic way within bioprinted constructs [57].

All cardiovascular tissue requires a vascular network to maintain cell viability and to meet the oxygen and nutrient demands of the tissue. This is true of both micro- and macro-engineered tissue. The large, clinically relevant cardiovascular constructs must have flow throughout the entire construct. As useful as they are, angiogenic factors and endothelial cells are not able to provide immediate flow channels or generate perfusable constructs within a short time period [58]. This is where 3D bioprinting can help. 3D bioprinting provides the opportunity and ability to produce controlled vascular networks with clinically relevant size, perfusable channels, and multiple cells types. A coaxial nozzle-assisted 3D bioprinting system to fabricate hollow calcium alginate filaments has been implemented [36]. A sodium alginate solution, which can be cellular or acellular, is dispensed through the outer tube of the coaxial nozzle. This solution becomes cross-linked when it comes in contact with calcium chloride that is dispensed through the inner channel of the nozzle. The combination forms a filament with a hollow channel (Fig. 18.1k). The hollow alginate filaments were then used as the building blocks for further printing (Fig. 18.1l). Scanning electron microscopy image (SEM) confirmed the formation of a hollow structure and the uniform fusion section between adjacent hollow filaments (Fig. 18.1l). Other than directly printing the channel, it is also possible to create channel networks within engineered tissue constructs by printing sacrificial materials.

This sacrificial material process involves 3D printing networks out of an easily soluble material inside of a bulk material. This bulk material can be bioprinted or casted, and would typically be made of cell-laden hydrogels. The channel network is then dissolved or discarded by the method that best gets rid of the material chosen. For example, Miller et al. printed rigid 3D filament networks of carbohydrate glass. These were put inside of a fibrin hydrogel and then were sacrificed. The carbohydrate glass networks were used as cytocompatible sacrificial templates to generate cylindrical networks (Fig. 18.1m) [59]. Sugar-glass networks are compatible with many types of cell-laden matrices. The channel networks formed after removing the sugar-glass is able to support endothelial cells and withstand the pulsatile flow of human blood. They even have intervessel junctions to support branched fluid flow (Fig. 18.1m). A bioprinted template of agarose fibers has been utilized to fabricate perfusable microchannel networks within gelatin-based hydrogel constructs [39, 40]. The fabricated networks improved mass transport, cellular viability, and differentiation of cells within the cell-laden constructs. A process has also been developed in which two fluidic vascular channels are deposited with a fibrin-cell mixture in the middle (Fig. 18.1n) [60]. Human umbilical cord vascular endothelial cells (HUVEC) transfected with green fluorescent protein (GFP, green) and mCherry (red) were separately cultured and used for fibrin gel and fluidic channels, respectively (Fig. 18.1n). The HUVECs began to form tubular structures after a 1-week culture, and the capillary network became denser, creating more branches with a lumen. Both Pluronic F127 and methacrylated gelatin cell-laden hydrogels have been printed as sacrificial materials to form perfusable networks [61]. Four print heads were used in this process: first, a PDMS border was printed, then the sacrificial Pluronic F127 with

two different Gel-MA inks containing fluorescent labeled fibroblasts. Pluronic was removed, and the microchannels were endothelialized with RFP HUVEC.

## 3D Bioprinting of Myocardium

Within the realm of CVD, ischemic disease (e.g., myocardial infarction (MI) or a "heart attack") is the leading cause of death. Ischemia is the lack of oxygen delivery to the heart. Heart attacks represent 42% (7.3 million) of all CVD deaths [62]. An acute heart attack is normally caused by the blockage of one of the coronary arteries, which results in a lack of blood flow and ischemia. When deprived of oxygen, cardiomyocytes (CM) die and a vigorous inflammatory response is incited. This causes fibroblasts and endothelial cells to migrate to the area and form noncontracting fibrotic scars. Scars contain little myocardial tissue and reduce the contractile function of the heart, ultimately leading to heart failure. During injury, a great number of CM die. Due to the relative inability of CM to divide, these lost cells are not replaced [63]. In severe cases of heart failure, heart transplantation is often the next consideration in treatment. This strategy is complicated and not always ideal due to a shortage of donor organs and the risk of organ rejection by the body. Cellular cardiomyoplasty, or cell-based cardiac repair, has made remarkable progress in myocardial tissue regeneration [64]. This approach involves injecting cells into the myocardium, a less invasive procedure than other treatments. This technique has been limited by the low viability and difficulty the injected cells have in integrating with the host cells.

Tissue engineering and bioprinting might be able to help with cell survival and growth. Myocardial tissue engineering (MTE) requires the use of a high density of CM and other supporting cells, along with proper vascularization and efficient oxygen exchange, in order to generate synchronous contractions [65]. 3D bioprinting can be used to pattern and assemble cells with high density, defined organization, and defined spatial distribution. It also allows the creation of multilayered constructs with multiple cells types within each layer. Laser-induced inkjet bioprinting has been used to pattern HUVEC and human mesenchymal stem cell (hMSC) on a polyester urethane urea cardiac patch (Fig. 18.2a) [66]. It is possible to generate specific vascular patterns with HUVEC (green) and hMSC (red) arranged in a capillary-like pattern (Fig. 18.2b). Some patches with patterned cells and some with randomly seeded cells were transplanted in vivo to the infarcted zone of rat hearts after left anterior descending (LAD) ligation (Fig. 18.2c). EBB has been used to bioprint alginate and RGD-modified alginate scaffold with human fetal CM progenitor cells (hCMPC) (Fig. 18.2d) [67]. It was demonstrated that within the 3D culture, the printed hCMPCs had high cell viability (Fig. 18.2e). This group further implanted the bioprinted patch composed of an hCMPC HA/Gel matrix in a mouse model of myocardial infarction [68]. In this test, the hCMPCs retained their cardiogenic phenotype in the bioprinted constructs for up to one month (Fig. 18.2f, g). The patch was able to preserve heart function by reducing LV remodeling and improving myocardial viability.

As in standard MTE approaches, it is essential for 3D bioprinting of thick muscle-like tissues to generate synergistic contractile force. This is essential for the adequate repair or replacement of damaged heart tissue. One problem is the difficulty to functionally integrate the graft and the host tissue. This problem is due to both electromechanical and vascular connections. The cells being used in the 3D bioprinting of vascular tissue are stem cells, such as embryonic stem cells (ESC) and induced pluripotent stem cells (iPSC). Autologous cells, such as skeletal myoblasts and mesenchymal stromal cell (MSC), are also being utilized yet are not very successful at integrating with host cardiovascular tissue. The ideal cell source does not seem to exist [69]. This means that different strategies will need to be developed to use the cell sources available in a more effective manner. 3D bioprinting has the

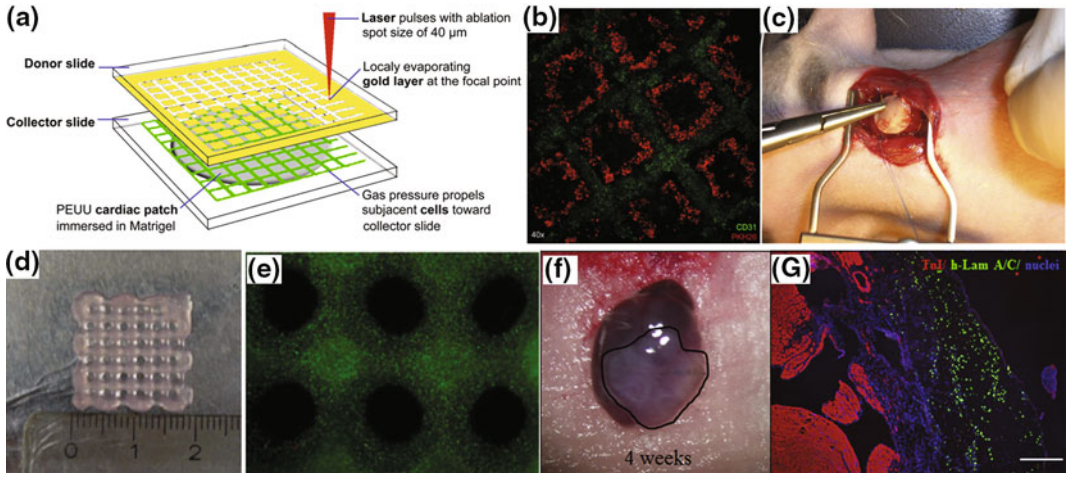


**Fig. 18.2** 3D bioprinting of myocardium. **a**–**c** Inkjet-based bioprinting of cardiac patch [66]. **a** Schematic bioprinting setup, **b** Patterned cells, **c** Patch implantation in vivo in a rat model. **d**–**g** Extrusion-based bioprinting of scaffolds with hCMPC **d**, **e** [67], **f**, **g**, [68]; **d** Bioprinted scaffolds, **e** High cell viability of hCMPC, **f** in vivo engraftment of the printed patch on the infarcted area of the ventricular wall for 4 weeks, **g** Presence of human Lamin A/C

ability to control the micro- and macro-architecture as well as the pore size/porosity, but the challenge of vascularizing thick tissue constructs has not been able to be overcome as of yet.

## 3D Printing of Heart Valves

The human heart has four valves that ensure unidirectional flow of blood. There are two atrioventricular/inflow valves, known as the mitral and tricuspid valves, and two semilunar/outflow valves, known as the aortic and pulmonary valves. Each valve is composed of leaflets that are attached to a fibrous annulus wall or root wall. Both the leaflets and root wall are biomechanically and structurally anisotropic [70, 71]. Leaflets and root walls are made up of mostly valve interstitial cells (VIC) and smooth muscle cells (SMC), respectively. They have valvular endothelial cells (VEC) covering the surfaces. The pathophysiology of valve disease is broad. One of the most common heart valve abnormalities is calcific aortic valve disease (CAVD) [72]. CAVD is commonly treated with surgical or interventional repair or replacement. The options for these replacements are mechanical or bioprosthetic valves [73]. Tissue engineering has great potential to address current limitations of nonliving prosthetics by providing living constructs that can grow, remodel, and integrate into the patients.

3D bioprinting, mainly EBB, has been implemented in the fabrication of tissue-engineered heart valves. The advantages of using 3D bioprinting techniques over traditional tissue engineering approaches are the ability to generate anatomically accurate trileaflet valves, mechanically heterogeneous valve conduits, and living engineered valves with correct spatial and temporal valve cells (VIC and SMC) distribution.

There are several different valve models and designs that have been used for 3D bioprinting. Duan et al. implemented a flat model with bioprinted trileaflet valve conduits. They used a combination of methacrylated hyaluronic acid and methacrylated gelatin to accommodate human aortic VIC (Fig. 18.3a, b) [74]. Control of the hydrogel viscosity and construct stiffness was created by optimizing the polymer ratio and concentration. The encapsulated cells were shown to have high viability and matrix remodeling ability with sulfated GAG deposition

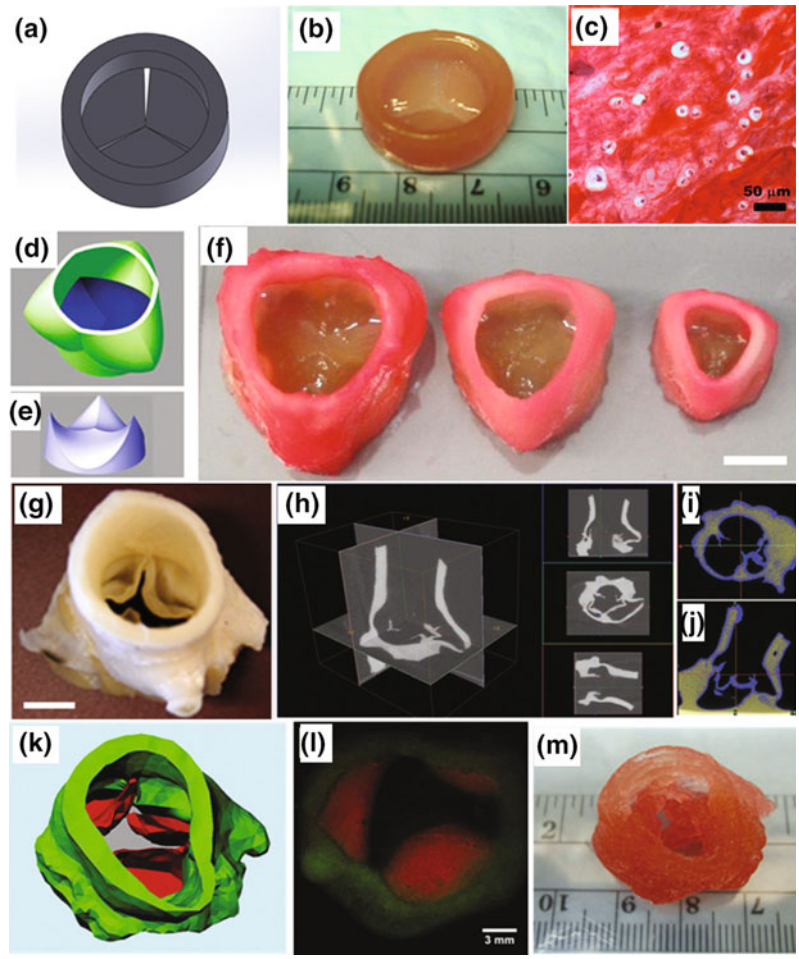


**Fig. 18.3** 3D bioprinting of heart valve. **a–c** Flat valve [74]; **d–f** Axisymmetric valve [75]; **g–m** Anatomical valve [77]. **a**, **d**, **e**, **k** Valve model; **b**, **f**, **m** Bioprinted valve; **c** Safranin-O staining showed GAG deposition; **h** µCT scan slices and their reconstruction; **i**, **j** The valve scans were viewed, thresholded, and segmented into separate STLs for the leaflet and the root; **l** Fluorescent image of first printed two layers of aortic valve conduit

(Fig. 18.3c). This testing model did not contain any sinuses, which are the widenings between root wall and leaflets. Both of these structures are needed to relieve abnormal stress and prevent blood back flow. Hockaday et al. used an improved design with an axially symmetric shape (Fig. 18.3d, e) and a combination of 700 and 8000 MW poly(ethylene glycol) diacrylate (PEGDA) to print valve conduits with biomechanical heterogeneity. In this design, the leaflets were more flexible while the root remained relatively rigid [75]. Axially symmetric heart valve scaffolds can be printed with various dimensions, showing that they can be made to fit adults and children, as well as varying heart sizes (Fig. 18.3f). The same group also was able to create an aortic valve geometric model using a µCT of a porcine aortic valve that was freshly obtained (Fig. 18.3g) [76]. When used with the scan, the model was able to maintain the normal anatomical characteristics of native valves, such as the ostium and sinus (Fig. 18.3h–j). For heterogeneous bioprinting, the valve root, made of SMC laden hydrogel, was deposited first and subsequently, the leaflet region of the layer, made of VIC-laden hydrogel, was extruded along its print paths (Fig. 18.3k) [77]. The same steps were repeated with aortic valve conduits with SMC and VIC encapsulated in the root and leaflet tissues, respectively. These exhibited geometry comparable to the original image of the derived valve (Fig. 18.3l, m) [77].

Tissue-engineered valve size and geometry play important roles in maintaining functionality

and stability under hemodynamic loading conditions [78, 79]. Computer simulations show that incorrect valve design may result in radial compression and eventually reduces leaflet size [80]. It is not known yet how valve geometry influences hemodynamic properties or how cells in the bioprinted valve conduits respond to such changes and remodel the matrix.

## 3D Bioprinting for Pediatric Applications

Deaths in children due to congenital heart disease, structural or electrical cardiac abnormalities, rank sixth in causes of death in 1- to 19-year-olds [81]. Cardiovascular repair or regeneration for children poses numerous challenges due to the small patient size, the risk of thromboembolism, the highly dynamic environment, and immature cell populations present in pediatric patients. In addition, the cardiovascular tissues in young patients are growing and remodeling much faster than in adults. Therefore, many prosthetic devices are suboptimal options because they cannot grow, remodel, or integrate with the host tissue [82]. 3D bioprinting allows for more precise fabrication of living constructs than traditional techniques. Hydrogel valves have been printed to span a range of clinically relevant sizes, as small as 12 mm inner diameter, which is approximately the size of a 6-month infant aortic valve, up to 22 mm inner diameter, which is an adult size [75]. The shape fidelity of printed valves was characterized using surface deviation analysis through micro-CT imaging in comparison with the design (Fig. 18.4a). In general, the accuracy of the design decreased with the decrease in the valve size, but the overall shape fidelity was decent even for pediatric valve printing. Recently, a whole heart structure was created using a thermoreversible support bath to enable bioprinting of freeform reversible embedding of suspended hydrogels [83]. This process allowed the printing of embryonic hearts with mechanical robustness and complex 3D internal and external anatomical architectures at a resolution of ~200 μm (Fig. 18.4b–f). Several groups have been using decellularization techniques to decellularized embryo or fetal tissues

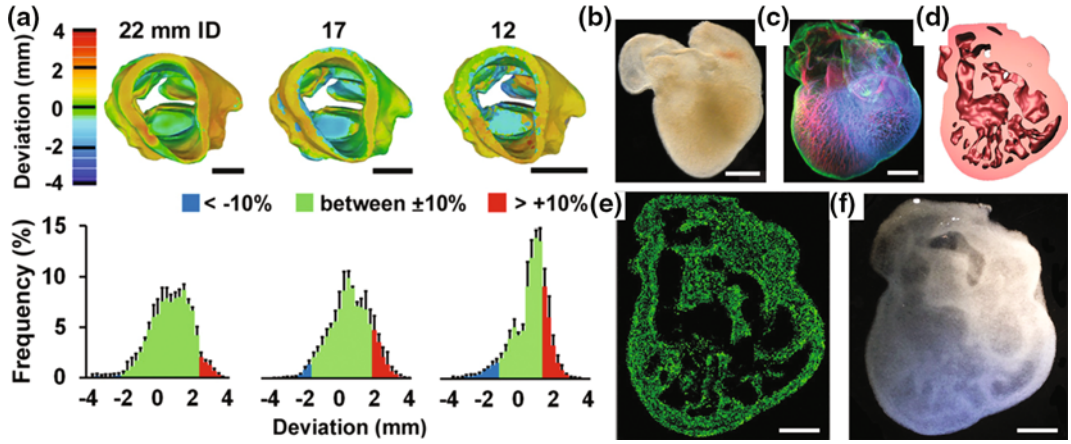


**Fig. 18.4** 3D bioprinting for pediatric applications. **a** Heat maps and average % frequency histograms representing surface deviations between printed porcine scaffolds with different sizes versus model geometries [75], **b**–**f** Printed whole heart based on 3D imaging data from chick embryo [83]; **b** Image of explanted embryonic chick heart; **c** 3D image of the embryonic chick heart stained for fibronectin (*green*), nuclei (*blue*), and F-actin (*red*); **d** Cross section of the 3D CAD model of the embryonic heart; **e** Cross section of the 3D printed heart (fluorescent alginate green); **f** 3D printed heart with internal structure visible through the translucent heart wall

[84, 85]. It has been demonstrated that fetal cardiac ECM significantly promoted the adhesion and expansion of neonatal cardiomyocytes compared with neonatal ECM and adult ECM [86]. Therefore, decellularized fetal or neonatal cardiovascular tissues have great potential to be further processed into bioinks for bioprinting.

## Challenges and Future Perspectives

3D bioprinting is a promising technique for the generation of cardiovascular tissue due to its ability to print heterogeneous and clinically relevant-sized tissue constructs. Despite the great progress and promise, there are still many challenges that hinder its further applications.

### Development of High-Performance Bioinks and High-Resolution Bioprinter

Although there are a large variety of bioinks to choose from, the challenge remains to develop the ideal bioink which is capable of printing biologically functional and mechanically robust tissue constructs. There are also many different tissue types, with varying properties, which makes finding the best bioink very difficult. The ideal bioink should be bioprintable, support cardiovascular cell functions, have comparable mechanical properties to native tissue/organs, and be affordable and commercially available with regulatory guidelines for clinical use [43]. One of the major hurdles in currently available hydrogel-based bioinks is to balance the cell functions and mechanical properties of cross-linked hydrogels. A high concentration of hydrogel results in stable mechanical properties, but causes low mobility and less spreading of the encapsulated cells. To get past this problem, bioinks that are crosslinkable in situ with spatially and temporally controllable cross-link rates and degrees are being developed [87, 88]. In addition, advanced biofabrication techniques are desirable to fabricate scaffold-free cell aggregation-based bioinks in high throughput to decrease the fusion time and enhance the mechanical properties and maturation.

Currently, a number of bioprinters, mainly extrusion-based, have been developed and commercialized. The commercialization of some bioprinters is limited due to the inadequate bioinks available. The ideal bioprinter should have at least a submicron resolution. It needs to have the ability to bioprint a matrix with an orientation which can induce the alignment of cardiovascular cells, such as cardiomyocytes and VIC. The bioprinter should also have multiple printing cartridges available to be used at the same time. This would allow the bioprinter to utilize multiple bioinks toward the bioprinting of one heterogeneous construct. This is especially significant for the bioprinting of the whole heart. More powerful and easy-to-use software would be needed to control the small resolution and multiple printing cartridges needed for the ideal bioprinter.

### Bioprinting of Functional Cardiovascular Constructs

With 3D bioprinting being in its infancy, so are most of its applications, especially in the cardiovascular realm. A major problem with bioprinted constructs is the lack of mechanical strength and integrity. This is mostly due to weak mechanical properties of the hydrogel-based bioinks that are being used [89]. For heart valves, the tensile and compressive properties of different bioprinted constructs were found to be much smaller than the peak moduli of native valve tissue [74]. However, healthy valve cells are subjected to physiological strain range rather than failure strain. Within a normal physiological strain range ($\sim$15% strain), valve cells can behave and function normally. The stiffness and moduli of bioinks are tunable and quite comparable to those of pulmonary valve leaflets in the physiological strain range. Although hydrogel bioinks may not meet the full mechanical strength range of native valve tissue initially, the tissue-engineered constructs may be strengthened through further hemodynamic conditioning via

collagen deposition and scaffold remodeling. Full characterization of the mechanical properties and functions of the constructs is crucial to produce the constructs that will withstand the complex hemodynamic pressures and flows of the cardiac environment [90, 91]. These properties and functions include electrophysiological functions, hydrodynamic response, compliance, and remodeling. In addition to having proper anatomical architecture and mechanical support, the bioprinted cardiovascular tissues should avoid thrombogenesis and be resistant to calcification after implantation. This is of particular importance for in vivo and pre-clinical applications. Avoiding these unfavorable developments often relies heavily on choosing and/or developing appropriate bioinks [92]. Another major point of importance for bioprinting cardiac tissue is to regulate the microenvironment, including matrix components, stiffness, and physiochemical stimuli. Regulating the microenvironment allows the control of the differentiation of stem cells and other cell sources toward the desired cardiovascular phenotypes [93].

### Whole Heart Bioprinting

Bioprinted cardiac and valve tissue constructs are used as patches or conduits for infarcted myocardium and for valve tissue engineering. They do not have an intact 3D structure with heart geometry [94]. The whole heart, as an organ, is complex, making it extremely difficult to bioprint cardiac tissue with full functions comparable to the native cardiovascular tissue. This is due to the tissues being composed of multiple cell types, ECM, and multiscale structures for pumping blood. Although matching all of the functions of the tissue types is difficult, the general structure of the whole heart can be bioprinted. One of the biggest hurdles in creating a fully functioning heart construct is generating multiscale vascularization with high enough density and branching networks. To achieve this, the bioink and bioprinter resolutions need to be improved. The ability to prevascularize the construct in vitro or in vivo would promote the formation of vascular networks. Currently, miniature organs with partial functions can be considered to be a future trend in organ printing. This is a practical strategy to use as a stepping stone to transition toward generating fully functioning organs.

## Conclusions

3D bioprinting has gained enormous attention as a technique for fabricating biological products, especially cardiovascular tissue. This is largely due to early successes and promising results of this process. Various bioinks, containing multiple cell types, biomaterials, and biomolecules can be bioprinted using several different printing mechanisms. This leads to major promise in using bioprinting for engineering cardiovascular constructs. Cardiovascular constructs, i.e., vascularized constructs, myocardium, and heart valve conduits, have been successfully bioprinted with decent resolution, similar architecture, and some of the normal functions of native tissue. 3D bioprinting techniques are helping to answer complex questions in cardiovascular disease and to generate engineered constructs for cardiovascular regeneration in both pediatric and adult patients. However, this group of techniques is still in its infancy and many challenges remain before we can generate tissue/organ analogs with full biological functions and complex microarchitectures. To advance the bioprinting techniques, efforts are being made to develop high-performance bioinks and high-resolution bioprinters. 3D bioprinting, combined with other tissue engineering, biofabrication, and biological strategies, shows a lot of promise in enabling significant improvements in cardiovascular tissue engineering and further clinical applications.

**Acknowledgements** This work has been supported by Mary & Dick Holland Regenerative Medicine Program start-up grant and Nebraska Research Initiative funding. The author has no financial disclosures.

## References


1. Go AS, Mozaffarian D, Roger VL, Benjamin EJ, Berry JD, Blaha MJ, Dai SF, Ford ES, Fox CS, Franco S, Fullerton HJ, Gillespie C, Hailpern SM, Heit JA, Howard VJ, Huffman MD, Judd SE, Kissela BM, Kittner SJ, Lackland DT, Lichtman JH, Lisabeth LD, Mackey RH, Magid DJ, Marcus GM, Marelli A, Matchar DB, McGuire DK, Mohler ER, Moy CS, Mussolino ME, Neumar RW, Nichol G, Pandey DK, Paynter NP, Reeves MJ, Sorlie PD, Stein J, Towfighi A, Turan TN, Virani SS, Wong ND, Woo D, Turner MB, Comm AHAS, Subcomm SS. Heart disease and stroke statistics-2014 update a report from the american heart association. Circulation. 2014;129:E28–292.
2. Lundberg MS. Cardiovascular tissue engineering research support at the national heart, lung, and blood institute. Circ Res. 2013;112:1097–103.
3. Schmidt CE, Baier JM. Acellular vascular tissues: natural biomaterials for tissue repair and tissue engineering. Biomaterials. 2000;21:2215–31.
4. Wong ND. Epidemiological studies of chd and the evolution of preventive cardiology. Nat Rev Cardiol. 2014;11:276–89.
5. Bouten CVC, Dankers PYW, Driessen-Mol A, Pedron S, Brizard AMA, Baaijens FPT. Substrates for cardiovascular tissue engineering. Adv Drug Deliv Rev. 2011;63:221–41.
6. Haraguchi Y, Shimizu T, Yamato M, Okano T. Concise review: cell therapy and tissue engineering for cardiovascular disease. Stem Cells Transl Med. 2012;1:136–41.
7. Spadaccio C, Chello M, Trombetta M, Rainer A, Toyoda Y, Genovese JA. Drug releasing systems in cardiovascular tissue engineering. J Cell Mol Med. 2009;13:422–39.
8. Duan B, Wang M. Selective laser sintering and its application in biomedical engineering. MRS Bull. 2011;36:998–1005.
9. Melchels FPW, Domingos MAN, Klein TJ, Malda J, Bartolo PJ, Hutmacher DW. Additive manufacturing of tissues and organs. Prog Polym Sci. 2012;37:1079–104.
10. Gerstle TL, Ibrahim AMS, Kim PS, Lee BT, Lin SJ. A plastic surgery application in evolution: three-dimensional printing. Plast Reconstr Surg. 2014;133:446–51.
11. Sodian R, Schmauss D, Markert M, Weber S, Nikolaou K, Haeberle S, Vogt F, Vicol C, Lueth T, Reichart B, Schmitz C. Three-dimensional printing creates models for surgical planning of aortic valve replacement after previous coronary bypass grafting. Ann Thorac Surg. 2008;85:2105–9.
12. Peltola SM, Melchels FPW, Grijpma DW, Kellomaki M. A review of rapid prototyping techniques for tissue engineering purposes. Ann Med. 2008;40:268–80.
13. Williams JM, Adewunmi A, Schek RM, Flanagan CL, Krebsbach PH, Feinberg SE, Hollister SJ, Das S. Bone tissue engineering using polycaprolactone scaffolds fabricated via selective laser sintering. Biomaterials. 2005;26:4817–27.
14. Yang SF, Leong KF, Du ZH, Chua CK. The design of scaffolds for use in tissue engineering. Part ii. Rapid prototyping techniques. Tissue Eng. 2002;8:1–11.
15. Zein I, Hutmacher DW, Tan KC, Teoh SH. Fused deposition modeling of novel scaffold architectures for tissue engineering applications. Biomaterials. 2002;23:1169–85.
16. Duan B, Wang M, Zhou WY, Cheung WL, Li ZY, Lu WW. Three-dimensional nanocomposite scaffolds fabricated via selective laser sintering for bone tissue engineering. Acta Biomater. 2010;6:4495–505.
17. Woodfield TBF, Malda J, de Wijn J, Peters F, Riesle J, van Blitterswijk CA. Design of porous scaffolds for cartilage tissue engineering using a three-dimensional fiber-deposition technique. Biomaterials. 2004;25:4149–61.
18. Derby B. Printing and prototyping of tissues and scaffolds. Science. 2012;338:921–6.
19. Ozbolat IT, Yu Y. Bioprinting toward organ fabrication: challenges and future trends. IEEE Trans Biomed Eng. 2013;60:691–9.
20. Guillemot F, Mironov V, Nakamura M. Bioprinting is coming of age: report from the international conference on bioprinting and biofabrication in bordeaux (3b'09). Biofabrication. 2010;2:010201.
21. Murphy SV, Atala A. 3d bioprinting of tissues and organs. Nat Biotechnol. 2014;32:773–85.
22. Mironov V, Reis N, Derby B. Bioprinting: a beginning. Tissue Eng. 2006;12:631–4.
23. Ozbolat IT. Bioprinting scale-up tissue and organ constructs for transplantation. Trends Biotechnol. 2015;33:395–400.
24. Cui XF, Boland T, D'Lima DD, Lotz MK. Thermal inkjet printing in tissue engineering and regenerative medicine. Recent Pat Drug Deliv Formulation. 2012;6:149–55.
25. Saunders RE, Derby B. Inkjet printing biomaterials for tissue engineering: bioprinting. Int Mater Rev. 2014;59:430–48.
26. Guillotin B, Souquet A, Catros S, Duocastella M, Pippenger B, Bellance S, Bareille R, Remy M, Bordenave L, Amedee J, Guillemot F. Laser assisted bioprinting of engineered tissue with high cell density and microscale organization. Biomaterials. 2010;31:7250–6.
27. Chang CC, Boland ED, Williams SK, Hoying JB. Direct-write bioprinting three-dimensional biohybrid systems for future regenerative therapies. J Biomed Mat Res Part B-Appl Biomat. 2011;98B:160–70.
28. Catros S, Guillemot F, Nandakumar A, Ziane S, Moroni L, Habibovic P, van Blitterswijk C, Rousseau B, Chassande O, Amedee J, Fricain JC. Layer-by-layer tissue microfabrication supports cell

proliferation in vitro and in vivo. Tissue Eng Part C-Methods. 2012;18:62–70.
29. Horvath L, Umehara Y, Jud C, Blank F, Petri-Fink A, Rothen-Rutishauser B. Engineering an in vitro air-blood barrier by 3d bioprinting. Sci Rep. 2015;5:7974.
30. Ali M, Pages E, Ducom A, Fontaine A, Guillemot F. Controlling laser-induced jet formation for bioprinting mesenchymal stem cells with high viability and high resolution. Biofabrication. 2014;6:045001.
31. Hribar KC, Soman P, Warner J, Chung P, Chen SC. Light-assisted direct-write of 3d functional biomaterials. Lab Chip. 2014;14:268–75.
32. Zhang AP, Qu X, Soman P, Hribar KC, Lee JW, Chen SC, He SL. Rapid fabrication of complex 3d extracellular microenvironments by dynamic optical projection stereolithography. Adv Mat. 2012;24:4266–4270 (ORCID VRa, MATERIALS A, 4266-+VIP, doi:10.1002/adma.201202024 D, 2012 PA).
33. Kang KH, Hockaday LA, Butcher JT. Quantitative optimization of solid freeform deposition of aqueous hydrogels. Biofabrication. 2013;5:035001.
34. Billiet T, Vandenhaute M, Schelfhout J, Van Vlierberghe S, Dubruel P. A review of trends and limitations in hydrogel-rapid prototyping for tissue engineering. Biomaterials. 2012;33:6020–41.
35. Levato R, Visser J, Planell JA, Engel E, Malda J, Mateos-Timoneda MA. Biofabrication of tissue constructs by 3d bioprinting of cell-laden microcarriers. Biofabrication. 2014;6:035020.
36. Pati F, Jang J, Ha DH, Kim SW, Rhie JW, Shim JH, Kim DH, Cho DW. Printing three-dimensional tissue analogues with decellularized extracellular matrix bioink. Nat Commun. 2014;5:3935.
37. Gao Q, He Y, Fu JZ, Liu A, Ma L. Coaxial nozzle-assisted 3d bioprinting with built-in microchannels for nutrients delivery. Biomaterials. 2015;61:203–15.
38. Jia J, Richards DJ, Pollard S, Tan Y, Rodriguez J, Visconti RP, Trusk TC, Yost MJ, Yao H, Markwald RR, Mei Y. Engineering alginate as bioink for bioprinting. Acta Biomater. 2014;10:4323–31.
39. Markstedt K, Mantas A, Tournier I, Avila HM, Hagg D, Gatenholm P. 3d bioprinting human chondrocytes with nanocellulose-alginate bioink for cartilage tissue engineering applications. Biomacromolecules. 2015;16:1489–96.
40. Bertassoni LE, Cardoso JC, Manoharan V, Cristino AL, Bhise NS, Araujo WA, Zorlutuna P, Vrana NE, Ghaemmaghami AM, Dokmeci MR, Khademhosseini A. Direct-write bioprinting of cell-laden methacrylated gelatin hydrogels. Biofabrication. 2014;6:024105.
41. Bertassoni LE, Cecconi M, Manoharan V, Nikkhah M, Hjortnaes J, Cristino AL, Barabaschi G, Demarchi D, Dokmeci MR, Yang YZ, Khademhosseini A. Hydrogel bioprinted microchannel networks for vascularization of tissue engineering constructs. Lab Chip. 2014;14:2202–11.
42. Billiet T, Gevaert E, De Schryver T, Cornelissen M, Dubruel P. The 3d printing of gelatin methacrylamide cell-laden tissue-engineered constructs with high cell viability. Biomaterials. 2014;35:49–62.
43. Loo YH, Lakshmanan A, Ni M, Toh LL, Wang S, Hauser CAE. Peptide bioink: self-assembling nanofibrous scaffolds for three-dimensional organotypic cultures. Nano Lett. 2015;15:6919–25.
44. Ozbolat IT, Hospodiuk M. Current advances and future perspectives in extrusion-based bioprinting. Biomaterials. 2016;76:321–43.
45. Williams SK, Touroo JS, Church KH, Hoying JB. Encapsulation of adipose stromal vascular fraction cells in alginate hydrogel spheroids using a direct-write three-dimensional printing system. BioRes Open Access. 2013;2:448–54.
46. Pati F, Ha DH, Jang J, Han HH, Rhie JW, Cho DW. Biomimetic 3d tissue printing for soft tissue regeneration. Biomaterials. 2015;62:164–75.
47. Horch RE, Kneser U, Polykandriotis E, Schmidt VJ, Sun JM, Arkudas A. Tissue engineering and regenerative medicine -where do we stand? J Cell Mol Med. 2012;16:1157–65.
48. Rouwkema J, Rivron NC, van Blitterswijk CA. Vascularization in tissue engineering. Trends Biotechnol. 2008;26:434–41.
49. Jakab K, Norotte C, Marga F, Murphy K, Vunjak-Novakovic G, Forgacs G. Tissue engineering by self-assembly and bio-printing of living cells. Biofabrication. 2010;2:022001.
50. Mironov V, Visconti RP, Kasyanov V, Forgacs G, Drake CJ, Markwald RR. Organ printing: tissue spheroids as building blocks. Biomaterials. 2009;30:2164–74.
51. Norotte C, Marga FS, Niklason LE, Forgacs G. Scaffold-free vascular tissue engineering using bioprinting. Biomaterials. 2009;30:5910–7.
52. Mehesz AN, Brown J, Hajdu Z, Beaver W, da Silva JVL, Visconti RP, Markwald RR, Mironov V. Scalable robotic biofabrication of tissue spheroids. Biofabrication. 2011;3:025002.
53. Kucukgul C, Ozler SB, Inci I, Karakas E, Irmak S, Gozuacik D, Taralp A, Koc B. 3d bioprinting of biomimetic aortic vascular constructs with self-supporting cells. Biotechnol Bioeng. 2015;112:811–21.
54. Cui XF, Boland T. Human microvasculature fabrication using thermal inkjet printing technology. Biomaterials. 2009;30:6221–7.
55. Novosel EC, Kleinhans C, Kluger PJ. Vascularization is the key challenge in tissue engineering. Adv Drug Deliv Rev. 2011;63:300–11.
56. Poldervaart MT, Gremmels H, van Deventer K, Fledderus JO, Oner FC, Verhaar MC, Dhert WJA, Alblas J. Prolonged presence of vegf promotes vascularization in 3d bioprinted scaffolds with defined architecture. J Control Release. 2014;184:58–66.
57. Park JY, Shim JH, Choi SA, Jang J, Kim M, Lee SH, Cho DW. 3d printing technology to control bmp-2 and vegf delivery spatially and temporally to promote

large-volume bone regeneration. J Mat Chem B. 2015;3:5415–25.
58. Paulsen SJ, Miller JS. Tissue vascularization through 3d printing: will technology bring us flow? Dev Dyn. 2015;244:629–40.
59. Miller JS, Stevens KR, Yang MT, Baker BM, Nguyen DHT, Cohen DM, Toro E, Chen AA, Galie PA, Yu X, Chaturvedi R, Bhatia SN, Chen CS. Rapid casting of patterned vascular networks for perfusable engineered three-dimensional tissues. Nat Mater. 2012;11:768–74.
60. Lee VK, Kim DY, Ngo HG, Lee Y, Seo L, Yoo SS, Vincent PA, Dai GH. Creating perfused functional vascular channels using 3d bio-printing technology. Biomaterials. 2014;35:8092–102.
61. Kolesky DB, Truby RL, Gladman AS, Busbee TA, Homan KA, Lewis JA. 3d bioprinting of vascularized, heterogeneous cell-laden tissue constructs. Adv Mater. 2014;26:3124–30.
62. Yeh RW, Sidney S, Chandra M, Sorel M, Selby JV, Go AS. Population trends in the incidence and outcomes of acute myocardial infarction. N Engl J Med. 2010;362:2155–65.
63. Murry CE, Wiseman RW, Schwartz SM, Hauschka SD. Skeletal myoblast transplantation for repair of myocardial necrosis. J Clin Invest. 1996;98:2512–23.
64. Reffelmann T, Kloner RA. Cellular cardiomyoplasty—cardiomyocytes, skeletal myoblasts, or stem cells for regenerating myocardium and treatment of heart failure? Cardiovasc Res. 2003;58:358–68.
65. Hirt MN, Hansen A, Eschenhagen T. Cardiac tissue engineering state of the art. Circ Res. 2014;114:354–67.
66. Gaebel R, Ma N, Liu J, Guan JJ, Koch L, Klopsch C, Gruene M, Toelk A, Wang WW, Mark P. Patterning human stem cells and endothelial cells with laser printing for cardiac regeneration. Biomaterials. 2011;32:9218–30.
67. Gaetani R, Doevendans PA, Metz CHG, Alblas J, Messina E, Giaccomello A, Sluijter JPG. Cardiac tissue engineering using tissue printing technology and human cardiac progenitor cells. Biomaterials. 2012;6(9):1782–90.
68. Gaetani R, Feyen DAM, Verhage V, Slaats R, Messina E, Christman KL, Giacomello A, Doevendans PAFM, Sluijter JPG. Epicardial application of cardiac progenitor cells in a 3d-printed gelatin/hyaluronic acid patch preserves cardiac function after myocardial infarction. Biomaterials. 2015;61:339–48.
69. Sui RQ, Liao XB, Zhou XM, Tan Q. The current status of engineering myocardial tissue. Stem Cell Rev Rep. 2011;7:172–80.
70. Butcher JT, Mahler GJ, Hockaday LA. Aortic valve disease and treatment: the need for naturally engineered solutions. Adv Drug Deliv Rev. 2011;63:242–68.
71. Hasan A, Paul A, Vrana NE, Zhao X, Memic A, Hwang YS, Dokmeci MR, Khademhosseini A. Microfluidic techniques for development of 3d vascularized tissue. Biomaterials. 2014;35:7308–25.
72. Chen JH, Simmons CA. Cell-matrix interactions in the pathobiology of calcific aortic valve disease critical roles for matricellular, matricrine, and matrix mechanics cues. Circ Res. 2011;108:1510–24.
73. Jana S, Tefft BJ, Spoon DB, Simari RD. Scaffolds for tissue engineering of cardiac valves. Acta Biomater. 2014;10:2877–93.
74. Duan B, Kapetanovic E, Hockaday LA, Butcher JT. Three-dimensional printed trileaflet valve conduits using biological hydrogels and human valve interstitial cells. Acta Biomater. 2014;10:1836–46.
75. Hockaday LA, Kang KH, Colangelo NW, Cheung PYC, Duan B, Malone E, Wu J, Girardi LN, Bonassar LJ, Lipson H, Chu CC, Butcher JT. Rapid 3d printing of anatomically accurate and mechanically heterogeneous aortic valve hydrogel scaffolds. Biofabrication. 2012;4:035005.
76. Hockaday LA, Duan B, Kang KH, Butcher JT. 3d printed hydrogel technologies for tissue engineered heart valves. 3D Printing Add Manuf. 2014;1:122–136.
77. Duan B, Hockaday LA, Kang KH, Butcher JT. 3d bioprinting of heterogeneous aortic valve conduits with alginate/gelatin hydrogels. J Biomed Mater Res, Part A. 2013;101A:1255–64.
78. Barannyk O, Oshkai P. The influence of the aortic root geometry on flow characteristics of a prosthetic heart valve. J Biomech Eng. 2015;137:051005.
79. Sanders B, Loerakker S, Fioretta ES, Bax DJP, Driessen-Mol A, Hoerstrup SP, Baaijens FPT. Improved geometry of decellularized tissue engineered heart valves to prevent leaflet retraction. Annals Biomed Eng. 2015. doi:10.1007/s10439-10015-11386-10434.
80. Loerakker S, Argento G, Oomens CWJ, Baaijens FPT. Effects of valve geometry and tissue anisotropy on the radial stretch and coaptation area of tissue-engineered heart valves. J Biomech. 2013;46:1792–800.
81. Vetter VL, Covington TM, Dugan NP, Haley DM, Dykstra H, Overpeck M, Iyer VR, Shults J. Cardiovascular deaths in children: general overview from the national center for the review and prevention of child deaths. Am Heart J. 2015;426–437.
82. Driessen-Mol A, Emmert MY, Dijkman PE, Frese L, Sanders B, Weber B, Cesarovic N, Sidler M, Leenders J, Jenni R, Grünenfelder J, Falk V, Baaijens FPT, Hoerstrup SP. Transcatheter implantation of homologous "off-the-shelf" tissue-engineered heart valves with self-repair capacity: long-term functionality and rapid in vivo remodeling in sheep. J Am Coll Cardiol. 2014;63:1320–9.
83. Hinton TJ, Jallerat Q, Palchesko RN, Park JH, Grodzicki MS, Shue HJ, Ramadan MH, Hudson AR, Feinberg AW. Three-dimensional printing of complex biological structures by freeform reversible embedding of suspended hydrogels. Sci Adv. 2015;1:e1500758.

84. Brennan EP, Tang XH, Stewart-Akers AM, Gudas LJ, Badylak SF. Chemoattractant activity of degradation products of fetal and adult skin extracellular matrix for keratinocyte progenitor cells. J Tissue Eng Regenerative Med. 2008;491–498.
85. Zhou P, Lessa N, Estrada DC, Severson EB, Lingala S, Zern MA, Nolta JA, Wu J. Decellularized liver matrix as a carrier for the transplantation of human fetal and primary hepatocytes in mice. Liver Transpl. 2011;418–427.
86. Williams C, Quinn KP, Georgakoudi I, Black III LD. Young developmental age cardiac extracellular matrix promotes the expansion of neonatal cardiomyocytes in vitro. Acta Biomaterialia. 2014;194–204.
87. Li C, Faulkner-Jones A, Dun AR, Jin J, Chen P, Xing YZ, Yang ZQ, Li ZB, Shu WM, Liu DS, Duncan RR. Rapid formation of a supramolecular polypeptide-DNA hydrogel for in situ three-dimensional multilayer bioprinting. Angew Chemie-Int Ed. 2015;54:3957–61.
88. Rutz AL, Hyland KE, Jakus AE, Burghardt WR, Shah RN. A multimaterial bioink method for 3d printing tunable, cell-compatible hydrogels. Adv Mat. 2015;27:1607–1614 (ORCID VRa, MATERIALS A, 1607-+VIP, doi:10.1002/adma.201405076 D, 2015 PM).
89. Seol YJ, Kang HW, Lee SJ, Atala A, Yoo JJ. Bioprinting technology and its applications. Eur J Cardiothorac Surg. 2014;46:342–8.
90. Jana S, Lerman A. Bioprinting a cardiac valve. Biotechnol Adv. 2015;33:1503–21.
91. Parvin NS, Blaser MC, Santerre JP, Caldarone CA, Simmons CA. Biomechanical conditioning of tissue engineered heart valves: too much of a good thing? Adv Drug Deliv Rev. 2016;96:161–75.
92. Zheng Y, Chen JM, Craven M, Choi NW, Totorica S, Diaz-Santana A, Kermani P, Hempstead B, Fischbach-Teschl C, Lopez JA, Stroock AD. In vitro microvessels for the study of angiogenesis and thrombosis. Proc Nat Acad Sci U S A. 2012;109:9342–7.
93. Duan B, Hockaday LA, Das S, Xu CY, Butcher JT. Comparison of mesenchymal stem cell source differentiation towards human pediatric aortic valve interstitial cells within 3d engineered matrices. Tissue Eng Part C-Methods. 2015;21:795–807.
94. Wang F, Guan JJ. Cellular cardiomyoplasty and cardiac tissue engineering for myocardial therapy. Adv Drug Deliv Rev. 2010;62:784–97.

# Past Developments and Future Directions of 3D Cardiac Printing: A Surgeon's Perspective

19

Khanh Nguyen, MD

## Introduction

As living organisms have evolved, optical perception of the environment in three dimensions (3D) has become more refined and complex. The ability to see in 3D is an essential component of human development, progressing alongside a higher level of brain and motor function as seen in primates and humans. These abilities enabled humanity to accurately assess their environment and contributed significantly to the establishment of civilization. In modern day medicine, one may consider the common task of envisioning a 3D mental construct from a two-dimensional (2D) echocardiographic image as the powerful demonstration of human brainpower at the top of the evolutionary tree. Nevertheless, through human history, we have searched for ways to assist our brains in processing 2D descriptions of structures in a more realistic 3D manner. The use of 3D imaging to help man comprehend and depict pathology predates the invention of the X-ray by Conrad Roentgen. This is well demonstrated in Florentine wax museum models that depict human anatomy and disease from the eighteenth and nineteenth centuries. During the industrial revolution, David Brewster invented the stereoscope to make 3D photographs, followed by the invention of the Kinematoscope in 1861 for 3D representation. Multiple other innovations for 3D depiction followed, leading to modern technologies such as 3D holographic modeling and 3D printing or additive manufacturing.

In 1938, Dr. Robert Gross, a surgeon at Harvard medical school, performed the ligation of a patient ductus arteriosus, ushering in an era of congenital cardiac surgery [1, 2]. Dr. Gross was then the chief resident of surgery under William E. Ladd, the surgeon-in-chief, at Boston Children's Hospital. He performed the dissection of numerous human cadavers to inspect the anatomy of the patent ductus arteriosus and practiced the operating steps on dogs. This preparation was akin to anatomic simulation, using cadaver hearts to provide a 3D road map to plan and practice the procedure. Such a road map may be considered analogous to a current day version of what would be a 3D printed cardiac model with a PDA. Dr. Gross, having thoroughly trained himself for the task, eventually set out to accomplish the actual operation with great success.

After Dr. Gross' monumental procedure, the establishment of the field of congenital heart surgery soon followed. As surgeons gained experience, more complex malformations were amenable to repair. However, the success of the field hinged ultimately on the simultaneous advancement of imaging technology to help make accurate diagnoses and plans for surgery. When Edler [3] invented M-mode echocardiography for evaluation of acquired mitral disease as

K. Nguyen, MD (✉)
Department of Cardiovascular Surgery,
Mount Sinai Hospital, 1190 Fifth Avenue,
PO Box 1028, New York, NY 10029-6574, USA
e-mail: khanh.nguyen@mountsinai.org


K.M. Farooqi (ed.), *Rapid Prototyping in Cardiac Disease*,
DOI 10.1007/978-3-319-53523-4_19

a guide for treatment, it paved the way for 2D, color Doppler, and transesophageal echocardiography which have become standard methods for evaluating congenital cardiac malformations.

## Cardiac Surgical Training

The field of congenital cardiac surgery involves performing surgery on some of the most complex congenital malformations. Congenital heart disease, with its critical and sometimes fragile physiology, combined with its complexity and rarity, makes the training of a congenital cardiac surgeon very demanding. Robust training requires repetitive demonstration of cardiac defects. The traditional apprenticeship model of teaching is based on the gradual accumulation of experience of the trainee, under the guide of a mentor, learning from both successes and failures. This learning continues well after completion of training and expertise is established not only by natural skill but also by practice and exposure. This learning curve has an impact on patient comfort, safety, surgical outcome, and cost [4, 5]. Healthcare institutions are becoming more aware of this issue and in an effort to circumvent this factor have turned to simulation technology. Surgical simulation has played an increasingly important role in training young surgeons working toward improving patient care and surgical outcomes. A simulation creates an artificial and safe environment for the apprentice to learn a new procedure without risking a patient's safety or comfort. Ideally, the surgical trainee would hone his or her skills in a virtual or a simulated setting until the technique was perfected. Only then would he or she be allowed to move on to real patients. Unfortunately, current medical simulators lack the fidelity to provide training beyond a basic skill level. It is predicted that with the refinement in simulation software and rapid growth of computing power, virtual simulation will soon provide advanced surgical training and possibly even result in some form of certification.

In the early 1990s, the medical industry began to see the impact of a novel form of surgical simulation, i.e., the application of 3D printed anatomic models in surgical training [6–8]. Its application was enthusiastically adopted in several surgical subspecialties including orthopedics, urology, plastic surgery, obstetrics, and gynecology as well as thoracic and cardiac surgery [9–11]. The use of 3D printed models of diseased body parts or organs as a preoperative road map is the most common application of this technology. Numerous reports of successful use reaffirm its role as a valuable tool for surgeons. Naturally, the field of congenital cardiac surgery has fully embraced 3D printing technology, which provides better understanding and allows management of complex malformations that can be accurately replicated in full-scale heart models [10]. More recently, surgical training courses have become available for congenital surgeons using 3D printed heart models. In 2015, such courses were offered at The Hospital for Sick Children, (Toronto, Canada) where surgeons and instructors worked on 3D printed models of congenital cardiac malformations such as transposition of the great arteries, hypoplastic left heart syndrome, and interrupted aortic arch. This method of training will eventually become routine for many training programs.

Although 3D printing technology is rapidly gaining momentum in the medical field, the process remains relatively costly and time-consuming. In cases of well-known or simple congenital heart diseases, 2D echocardiography usually provides most of the needed anatomic information one needs to formulate an effective treatment plan. However, when faced with rare or more complex conditions, echocardiography may not clearly demonstrate all of the relevant anatomic spatial relationships. In these cases, the congenital cardiac surgeon would typically perform an inspection intraoperatively to get a complete 3D picture of the anatomy. In less experienced hands, this could mean prolonged cardiopulmonary bypass, unnecessary myocardial ischemia, increased morbidity and mortality, and increased cost. This gap in spatial information is effectively addressed by cardiac 3D printing. It may in fact level the playing field and give the less experienced surgeon a tool to

become more efficient. A clear understanding of the complexity of anatomy with a well-planned procedure will likely reduce the risks for complications and shorten the duration of the operation.

## 3D Printing in Congenital Heart Disease

The application of 3D printing had been described in preoperative planning in various clinical scenarios in congenital heart surgery. Vodiskar et al. [11] reported the use of 3D printing in planning surgery in a 20-month-old patient who developed arch stenosis after arterial switch and aortic arch repair. The anatomic information gained from the cardiac model was used to simplify the surgical plan. In this case, the arch was repaired using descending aortic and antegrade cerebral perfusion with complete avoidance of deep hypothermic circulatory arrest, a surgical maneuver that is known for its associated morbidities. This technology was also applied for presurgical planning in another newborn with an interrupted aortic arch. The 3D cardiac model allowed the authors to opt for a simpler approach with aortic arch repair and pulmonary artery banding through a left thoracotomy, without the use of cardiopulmonary bypass, obviating the risks of a more extensive open-heart surgery through a sternotomy. In a third patient with double outlet right ventricle, the authors fashioned a patch for intracardiac baffle repair utilizing a 3D model. A similar patch was placed in the actual operation. The ventricular septal defect (VSD) was closed and the heart was septated successfully with no obstruction of the outflow tracts or interference with atrioventricular valve function.

As demonstrated in the last mentioned case, double outlet right ventricle is an ideal pathology for which 3D printing can greatly enhance surgical planning [12–14]. It is a congenital cardiac malformation that consists of a VSD and two ventricular outlets arising from the right ventricle. The surgical repair requires directing blood flow from the left ventricle through the septal defect to the aorta. The double outlet right ventricle diagnosis spans a spectrum of anatomic variations from the commonly known Tetralogy of Fallot to transposition of the great arteries. While surgical repair for these malformations has been quite successful, a subset of patients with double outlet right ventricle and a remote VSD, with or without straddling chordae, remains a technical challenge. The successful baffling of the left ventricle to the aorta depends on their anatomic relations, the size of the VSD and the presence of any straddling chordae. 2D echocardiography may not adequately delineate the 3D spatial relationship of the VSD to the aorta. Garekar et al. [13] used data from 5 patients with DORV and a remote VSD to create 3D models of the heart. The authors devised an assessment scale to quantify the information gained from the 3D models as compared to conventional imaging and concluded that the 3D printed hearts scored better in providing surface anatomy and spatial orientation, which are crucial in planning of an intracardiac baffle. Farooqi et al. [14] described the use of 3D printing in a 7-year-old with double outlet right ventricle and a non-committed VSD. Initially, a bidirectional Glenn shunt had been performed as a palliation to maintain the pulmonary circulation and allow the heart to grow until the decision between a single ventricular pathway or biventricular repair could be made. The 3D model indicated that the VSD could be closed for a two ventricular repair. He underwent placement of a VSD baffle, conal septal resection, take down of the Glenn shunt and reconstruction of a right ventricle to pulmonary artery conduit. His discharge echocardiogram showed a patent pathway with good biventricular function. A patient with similar anatomy may end up with a Fontan palliation, if the possible surgical options are unclear from 2D imaging. This may be a suboptimal option in the presence of two well-functioning ventricles.

It can be challenging to have a true and complete anatomic comprehension of complex cardiac malformations associated with anomalous pulmonary venous return. In lesions such as partial anomalous right pulmonary venous drainage, i.e., Scimitar syndrome [15], 3D printing

can demonstrate the location of the vein's entrance to the right atrium as well as its relation to the inferior vena cava (IVC) and the distance from the left atrial cavity and atrial septum, data which is crucial in planning a successful repair. Anomalous pulmonary venous drainage into a common atrium in heterotaxy syndrome [16] can also be difficult to precisely locate and atrial septation with a complex patch could be best planned using a 3D printed model.

For patients who have developed complications after previous cardiac operations, an accurate 3D printed model can help in planning a reoperation. Kiraly et al. [17] created a 3D aortic arch model in a patient with hypoplastic left heart syndrome who developed arch obstruction after a Norwood reconstruction. The surgical approach and steps of the operation were practiced on a hollowed, printed version of the aorta. The actual operation was performed in the same manner as the preoperative simulation. Similar applications were used in planning of an aortic translocation, the Nikaidoh procedure [18] in a patient with transposition of the great arteries, VSD, and pulmonary stenosis. 3D printing has also been used in pediatric patients with congenital heart disease undergoing cardiac transplantation, as described by Sodian et al. [19]. They reported two patients with single ventricle physiology who had previously undergone multiple corrective procedures and therefore had unpredictable anatomy for heart transplantation. The cardiac anatomy of each patient was well delineated by 3D printing before the transplantations and the procedural plans were determined based on the 3D models. These reports demonstrate that a patient-specific 3D printed model can be an excellent surgical planning and guidance tool in a wide variety of different surgical scenarios.

3D printing can also provide guidance in managing adult patients with congenital heart disease with heart failure requiring mechanical support. Farooqi et al. [20] proposed the application of 3D printing in planning placement of ventricular assist devices in patients with failing systemic right ventricles, such as patients with L-transposition of the great arteries or in those with D-transposition after an atrial switch. 3D printing can aid in cannula placement, which would be especially helpful due to the unique anatomic features of the right ventricle. Such models can also assist in cannula placement for a failing Fontan in either the pulmonary or systemic circulation depending on the clinical setting.

3D printing has also established a role in the management of cardiac tumors. The features of more advanced 3D printers allow the use of multicolor printing within the same model to delineate different tissues, which can be critical in tumor resections. Al Jabbari et al. reported the application of this technology in two adult patients [21]. The first patient was a 50-year-old male status-post left atrium osteosarcoma resection with tumor recurrence. Cardiac magnetic resonance image (MRI) showed multiple recurrent tumors with involvement of the pulmonary veins. A cardiac auto-transplantation (i.e., explantation and reimplantation of the heart for facilitation of the cardiac procedure and better exposure) was performed with excision of the entire posterior and anterior left atrium, part of the right pulmonary veins, and the pericardium. The veins were reconstructed with bovine pericardium. It is self-evident that a representative model would be extremely useful in such a complex case. The second patient was a 67-year-old male with recurrent renal cell carcinoma and IVC involvement. He underwent complete resection of the right atrium and IVC and reconstruction with bovine pericardium. Both patients did well with no recurrence after 6 months follow up. These cases underscore the effectiveness of 3D printing in accurately demonstrating the detailed encroachment of the tumors on cardiac structures and assuring complete tumor excision.

A similar concept which involves combining different imaging modalities is the use of hybrid 3D printing. Gillaspie et al. [22] fused MRI or computed tomography (CT) data with positron emission tomography (PET) scan data from pre- and post-induction therapy. They were able to delineate the response of tumors as well as identify tissues that appeared abnormal but were not actually involved with the malignancy. This

approach, which the authors termed "5D printing," allowed for more precise and complete removal of the tumor. The authors reported a 39-year-old female who was diagnosed with a left superior sulcus tumor that invaded the upper ribs, vertebral bodies, and nerve roots. After induction chemoradiation therapy, a "5D" printed model of the involved area was created for planning of resection. The patient underwent a staged en bloc resection of the involved structures together with a PET scan of active tumor areas and thoracic wall reconstruction. She did well at 4 months follow up with no evidence of tumor and required no further therapy. Superimposing different imaging data sets along with 3D printing is a powerful and effective tool in providing anatomic details that can greatly enhance the success of a challenging operation.

## Obstacles in Utility

As the use of 3D printing in cardiac surgery continues to grow, several issues have emerged that may necessitate a more systematic approach in utilizing the technology. It is likely that 3D printing will be limited to more complex congenital heart disease, in which its role is crucial in providing detailed anatomic information for the operative method. More common defects such as septal defects, Tetralogy of Fallot, or transposition of the great arteries can typically be imaged adequately using 2D echocardiography, cardiac MRI, and CT. It appears that the decision to use 3D printing to get a better demonstration of the anatomy rests on the expertise of the echocardiographer who detects subtle complex characteristics or suspects anatomic uncertainty that could affect the planning of the operation. It also depends on the comfort level of the operating surgeon who may prefer the reinforcement provided by having a physical model of the diseased heart in hand to plan the operation.

Not all structures are well represented with 3D printing technology, notably the cardiac valves and the sub-valvar apparatus. Cardiac MRI and CT often do not provide details of fine mobile structures, such as the chordae of the mitral valve. In these settings, the rendered images are the product of computerized assumptions and the specifics of the involved structure could be lost or inaccurate. For example, a minor cleft may not be recreated well on the image renderings but could have a significant impact on the outcome of a repair. A major chordal insertion, which may be difficult to pick up on imaging, can alter the placement of a patch or even make a heart impossible to septate. More refined software and powerful imaging may help to provide better accuracy in the future.

As an institution accumulates experience in cardiac 3D printing, issues of storage and keeping inventory may arise. Space is always a much-needed commodity in a busy medical center, and a large collection of printed models may pose a logistic issue of storage and retrieval. Depending on the material used for printing, it has been possible to recycle the printed material in an effort to reduce cost, waste, and help with managing of storage space. The models, once they have served their purpose, can be broken down and the printed material can be reclaimed. It is conceivable that due to the time-consuming process of preparing and printing the 3D models, one would be reluctant to dispose of models simply for the purpose of space management. It is likely, though, that as printing technology advances, that the production of a model may take minutes instead of hours or days. An organized storage inventory of 3D heart models can also serve as an effective educational tool for patients, medical students, and cardiac surgeons in training.

## Virtual Models

The virtual model which is created from post-processing of 3D imaging data sets and serves as the source file to create the physical model, may demonstrate its own utility. Virtual 3D imaging of cardiac malformations allows detailed examinations and virtual dissections of the heart. Farooqi et al. [23] created virtual cardiac 3D models of 6 patients with DORV and demonstrated that they effectively delineated the VSD's as well as the pathways for placement of a surgical baffle.

Indeed, 3D virtual imaging appears to be quite convenient and possibly equally effective. 3D virtual files can be easily sent and shared among team members. The surgeon can navigate him or herself within the cardiac cavity to learn about the anatomy and plan the repair. The ability to go inside the heart to view hard to reach locations makes virtual 3D modeling a very good pre-procedure planning tool. The benefit also lies in not having to deal with storage issues and being able to retrieve the imaging rapidly. On the other hand, a virtual model is neither tactile nor direct. For example, a sample of a VSD baffle patch based on a printed heart model would be easier to be fashioned. The produced patch could then be tested on the physical model, while this same process is not feasible on a virtual model viewed on a 2D monitor. The depth and distance perceptions from a printed model are real and palpable. Nevertheless, it would not be surprising to see virtual 3D imaging become more commonplace and perhaps the main advanced imaging modality used in preoperative planning in the near future.

The expansion of computational power continues to be the driving force for improving and advancing medical imaging and simulation technologies. Moore's law seems to work in our favor, as computing speed continues to increase. Clinically relevant dynamic virtual cardiac models will eventually be feasible [24]. We may have the ability to non-invasively assess hemodynamics of cardiac malformations before and after surgery. Dynamic cardiac models are produced with the construction of a virtual 3D cardiac model superimposed onto a simulation of blood flow using computational fluid dynamics. However, the requirement for computational power is enormous, and currently, the time needed to complete this simulation may take days. However, in a few years, Moore's law predicts a reduction of the time to just hours.

## Bioprinting

The progression from 3D printed heart models to printing biological heart components is inevitable. The rapid development of patient-specific bioprinting holds the promise of the next big step in medicine [25–29]. Much work has been done in creating patient-specific cardiac valve scaffolds and seeding them with patients' own cells. It is possible in the future that a patient can have his or her cardiac implants prepared before the actual operation. One can envision the great potential of 3D bioprinting in congenital heart surgery, which traditionally involves placement of vascular conduits, prosthetic patches, and valves. Current implantable surgical parts do not grow and are not patient specific. Appropriate and correctly sized conduits may not be available due to a wide range of patient sizes. Despite exploratory efforts in using bioprinting in clinical applications, the technology is still in its infancy. Future research and development will involve producing more physiologically suitable bioink materials to create functional and durable heart implants and possibly even full replacements.

## References

1. Gross Robert E. Surgical closure of the patent ductus arteriosus. J Pediatr. 1940;17(6):716–33.
2. Alexi-Meskishvili VV, Böttcher W. The first closure of the persistent ductus arteriosus. Ann Thorac Surg. 2010;90(1):349–56.
3. Singh S, Goyal A. The origin of echocardiography: a tribute to Inge Edler. Tex Heart Inst J. 2007;34 (4):431–8.
4. Ferraris VA, Harris JW, Martin JT, Saha SP, Endean ED. Impact of residents on surgical outcomes in high-complexity procedures. J Am Coll Surg. 2016.
5. Saliba AN, Taher AT, Tamim H, Harb AR, Mailhac A, Radwan A, Jamali FR. Impact of resident involvement in surgery (IRIS-NSQIP): looking at the bigger picture based on the American College of Surgeons-NSQIP database. J Am Coll Surg. 2016;222(1):30–40.
6. Satava RM. Surgical education and surgical simulation. World J Surg. 2001;25(11):1484–9.
7. de Visser H, Watson MO, Salvado O, Passenger JD. Progress in virtual reality simulators for surgical training and certification. Med J Aust. 2011;194(4).
8. Sørensen TS, Stawiaski J, Mosegaard J. Virtual open heart surgery: obtaining models suitable for surgical simulation. Stud Health Technol Inform. 2007;125:445–7.
9. Singhal AJ, Shetty V, Bhagavan KR, Ragothaman A, Shetty V, Koneru G, Agarwala M. Improved surgery

planning using 3-D printing: a case study. Indian J Surg. 2016;78(2):100–4.
10. Gerstle TL, Ibrahim AM, Kim PS, Lee BT, Lin SJ. A plastic surgery application in evolution: three-dimensional printing. Plast Reconstr Surg. 2014;133(2):446–51.
11. Vodiskar J, Kütting M, Steinseifer U, Vazquez-Jimenez JF, Sonntag SJ. Using 3D physical modeling to plan surgical corrections of complex congenital heart defects. Thorac Cardiovasc Surg. 2016.
12. Olivieri LJ, Krieger A, Loke YH, Nath DS, Kim PC, Sable CA. Three-dimensional printing of intracardiac defects from three-dimensional echocardiographic images: feasibility and relative accuracy. J Am Soc Echocardiogr. 2015;28(4):392–7.
13. Garekar S, Bharati A, Chokhandre M, Mali S, Trivedi B, Changela VP, Solanki N, Gaikwad S, Agarwal V. Clinical application and multidisciplinary assessment of three dimensional printing in double outlet right ventricle with remote ventricular septal defect. World J Pediatr Congenit Heart Surg. 2016;7(3):344–50.
14. Farooqi KM, Gonzalez-Lengua C, Shenoy R, Sanz J, Nguyen K. Use of a three dimensional printed cardiac model to assess suitability for biventricular repair. World J Pediatr Congenit Heart Surg. 2016;7(3):414–6.
15. Tsitouridis I, Tsinoglou K, Morichovitou A, Stratilati S, Siouggaris N, Kontaki T. Scimitar syndrome versus meandering pulmonary vein: evaluation with three-dimensional computed tomography. Acta Radiol. 2006;47(9):927–32 (Review).
16. Makhija Z, Marwah A, Mishra S, Kumar J, Goel A, Sharma R. Biventricular repair in heterotaxy patients. World J Pediatr Congenit Heart Surg. 2015;6(2):195–202.
17. Kiraly L, Tofeig M, Jha NK, Talo H. Three-dimensional printed prototypes refine the anatomy of post-modified Norwood-1 complex aortic arch obstruction and allow presurgical simulation of the repair. Interact CardioVasc Thorac Surg. 2016;22(2):238–40.
18. Valverde I, Gomez G, Gonzalez A, Suarez-Mejias C, Adsuar A, Coserria JF, Uribe S, Gomez-Cia T, Hosseinpour AR. Three-dimensional patient-specific cardiac model for surgical planning in Nikaidoh procedure. Cardiol Young. 2015;25(4):698–704.
19. Sodian R, Weber S, Markert M, Loeff M, Lueth T, Weis FC, Daebritz S, Malec E, Schmitz C, Reichart B. Pediatric cardiac transplantation: three-dimensional printing of anatomic models for surgical planning of heart transplantation in patients with univentricular heart. J Thorac Cardiovasc Surg. 2008;136(4):1098–9.
20. Farooqi KM, Saeed O, Zaidi A, Sanz J, Nielsen JC, Hsu DT, Jorde UP. 3D printing to guide ventricular assist device placement in adults with congenital heart disease and heart failure. JACC Heart Fail. 2016;4(4):301–11.
21. Al Jabbari O, Abu Saleh WK, Patel AP, Igo SR, Reardon MJ. Use of three-dimensional models to assist in the resection of malignant cardiac tumors. J Card Surg. 2016;31(9):581–3.
22. Gillaspie EA, Matsumoto JS, Morris NE, Downey RJ, Shen KR, Allen MS, Blackmon SH. From 3-dimensional printing to 5-dimensional printing: enhancing thoracic surgical planning and resection of complex tumors. Ann Thorac Surg. 2016;101(5):1958–62.
23. Farooqi KM, Uppu SC, Nguyen K, Srivastava S, Ko HH, Choueiter N, Wollstein A, Parness IA, Narula J, Sanz J, Nielsen JC. Application of virtual three-dimensional models for simultaneous visualization of intracardiac anatomic relationships in double outlet right ventricle. Pediatr Cardiol. 2016;37(1):90–8.
24. Mittal R, Seo JH, Vedula V, Choi YJ, Liu H, Huang HH, Jain S, Younes L, Abraham T, George RT. Computational modeling of cardiac hemodynamics: Current status and future outlook. J Comput Phys. 2016;305:1065–82.
25. Duan B. State-of-the-art review of 3D bioprinting for cardiovascular tissue engineering. Ann Biomed Eng. 2016.
26. Jana S, Lerman A. Bioprinting a cardiac valve. Biotechnol Adv. 2015;33(8):1503–21.
27. Cheung DY, Duan B, Butcher JT. Current progress in tissue engineering of heart valves: multiscale problems, multiscale solutions. Expert Opin Biol Ther. 2015;15(8):1155–72.
28. Beyersdorf F. Three-dimensional bioprinting: new horizon for cardiac surgery. Eur J Cardiothorac Surg. 2014;46(3):339–41.
29. Duan B, Kapetanovic E, Hockaday LA, Butcher JT. Three-dimensional printed trileaflet valve conduits using biological hydrogels and human valve interstitial cells. Acta Biomater. 2014;10(5):1836–46.

# Index

*Note*: Page numbers followed by *f* and *t* indicate figures and tables respectively.




K.M. Farooqi (ed.), *Rapid Prototyping in Cardiac Disease*,
DOI 10.1007/978-3-319-53523-4